UNIVERSITY OF BIRMINGHAM
University of Birmingham Research at Birmingham

Global Boundary Stratotype Section and Point (GSSP) for the Anthropocene Series:

Waters, Colin N.; Zalasiewicz, Jan; Summerhayes, Colin; Fairchild, Ian J.; Rose, Neil L.; Loader, Neil J.; Shotyk, William; Cearreta, Alejandro; Head, Martin J.; Syvitski, James P. M.; Williams, Mark; Wagreich, Michael; Barnosky, Anthony D.; Zhisheng, An; Leinfelder, Reinhold; Jeandel, Catherine; Gałuszka, Agnieszka; Ivar Do Sul, Juliana A.; Gradstein, Felix; Steffen, Will

DOI:
10.1016/j.earscirev.2017.12.016

License:
Creative Commons: Attribution-NonCommercial-NoDerivs (CC BY-NC-ND)

Document Version
Peer reviewed version

Citation for published version (Harvard):
Waters, CN, Zalasiewicz, J, Summerhayes, C, Fairchild, IJ, Rose, NL, Loader, NJ, Shotyk, W, Cearreta, A, Head, MJ, Syvitski, JPM, Williams, M, Wagreich, M, Barnosky, AD, Zhisheng, A, Leinfelder, R, Jeandel, C, Gałuszka, A, Ivar Do Sul, JA, Gradstein, F, Steffen, W, Mcneill, JR, Wing, S, Poirier, C & Edgeworth, M 2017, 'Global Boundary Stratotype Section and Point (GSSP) for the Anthropocene Series: Where and how to look for potential candidates', *Earth Science Reviews*. https://doi.org/10.1016/j.earscirev.2017.12.016

Link to publication on Research at Birmingham portal

Publisher Rights Statement:
DOI: 10.1016/j.earscirev.2017.12.016

General rights
Unless a licence is specified above, all rights (including copyright and moral rights) in this document are retained by the authors and/or the copyright holders. The express permission of the copyright holder must be obtained for any use of this material other than for purposes permitted by law.

•Users may freely distribute the URL that is used to identify this publication.
•Users may download and/or print one copy of the publication from the University of Birmingham research portal for the purpose of private study or non-commercial research.
•User may use extracts from the document in line with the concept of 'fair dealing' under the Copyright, Designs and Patents Act 1988 (?)
•Users may not further distribute the material nor use it for the purposes of commercial gain.

Where a licence is displayed above, please note the terms and conditions of the licence govern your use of this document.

When citing, please reference the published version.

Take down policy
While the University of Birmingham exercises care and attention in making items available there are rare occasions when an item has been uploaded in error or has been deemed to be commercially or otherwise sensitive.

If you believe that this is the case for this document, please contact UBIRA@lists.bham.ac.uk providing details and we will remove access to the work immediately and investigate.

Download date: 19. Apr. 2024

Accepted Manuscript

Global Boundary Stratotype Section and Point (GSSP) for the Anthropocene Series: Where and how to look for potential candidates

Colin N. Waters, Jan Zalasiewicz, Colin Summerhayes, Ian J. Fairchild, Neil L. Rose, Neil J. Loader, William Shotyk, Alejandro Cearreta, Martin J. Head, James P.M. Syvitski, Mark Williams, Michael Wagreich, Anthony D. Barnosky, An Zhisheng, Reinhold Leinfelder, Catherine Jeandel, Agnieszka Gałuszka, Juliana A. Ivar do Sul, Felix Gradstein, Will Steffen, John R. McNeill, Scott Wing, Clément Poirier, Matt Edgeworth

PII:	S0012-8252(17)30408-7
DOI:	https://doi.org/10.1016/j.earscirev.2017.12.016
Reference:	EARTH 2557
To appear in:	*Earth-Science Reviews*
Received date:	8 August 2017
Revised date:	14 December 2017
Accepted date:	21 December 2017

Please cite this article as: Colin N. Waters, Jan Zalasiewicz, Colin Summerhayes, Ian J. Fairchild, Neil L. Rose, Neil J. Loader, William Shotyk, Alejandro Cearreta, Martin J. Head, James P.M. Syvitski, Mark Williams, Michael Wagreich, Anthony D. Barnosky, An Zhisheng, Reinhold Leinfelder, Catherine Jeandel, Agnieszka Gałuszka, Juliana A. Ivar do Sul, Felix Gradstein, Will Steffen, John R. McNeill, Scott Wing, Clément Poirier, Matt Edgeworth , Global Boundary Stratotype Section and Point (GSSP) for the Anthropocene Series: Where and how to look for potential candidates. The address for the corresponding author was captured as affiliation for all authors. Please check if appropriate. Earth(2017), https://doi.org/10.1016/j.earscirev.2017.12.016

This is a PDF file of an unedited manuscript that has been accepted for publication. As a service to our customers we are providing this early version of the manuscript. The manuscript will undergo copyediting, typesetting, and review of the resulting proof before it is published in its final form. Please note that during the production process errors may be discovered which could affect the content, and all legal disclaimers that apply to the journal pertain.

ACCEPTED MANUSCRIPT

Global Boundary Stratotype Section and Point (GSSP) for the Anthropocene Series: Where and how to look for potential candidates.

Colin N. Waters[1], Jan Zalasiewicz[1], Colin Summerhayes[2], Ian J. Fairchild[3], Neil L. Rose[4], Neil J. Loader[5], William Shotyk[6], Alejandro Cearreta[7], Martin J. Head[8], James P.M. Syvitski[9], Mark Williams[1], Michael Wagreich[10], Anthony D. Barnosky[11], An Zhisheng[12], Reinhold Leinfelder[13], Catherine Jeandel[14], Agnieszka Gałuszka[15], Juliana A. Ivar do Sul[16], Felix Gradstein[17], Will Steffen[18], John R. McNeill[19], Scott Wing[20], Clément Poirier[21], Matt Edgeworth[22]

[1]*School of Geography, Geology and the Environment, University of Leicester, University Road, Leicester LE1 7RH, UK.*

[2]*Scott Polar Research Institute, Cambridge University, Lensfield Road, Cambridge CB2 1ER, UK.*

[3]*School of Geography, Earth and Environmental Sciences, University of Birmingham, Birmingham B15 2TT, UK.*

[4]*Environmental Change Research Centre, Department of Geography, University College London, Gower Street, London WC1E 6BT, UK.*

[5]*Department of Geography, Swansea University, Singleton Park, Swansea SA2 8PP, Wales, UK.*

[6]*Department of Renewable Resources, University of Alberta, 348B South Academic Building, Edmonton, Alberta T6G 2H1 CANADA.*

[7]*Departamento de Estratigrafía y Paleontología, Facultad de Ciencia y Tecnología, Universidad del País Vasco UPV/EHU, Apartado 644, 48080 Bilbao, Spain.*

[8]*Department of Earth Sciences, Brock University, 1812 Sir Isaac Brock Way, St. Catharines, ON, L2S 3A1 Canada.*

ACCEPTED MANUSCRIPT

[9]*University of Colorado-Boulder Campus, Box 545, Boulder CO, 80309-0545, USA.*

[10]*Department of Geodynamics and Sedimentology, University of Vienna, A-1090 Vienna, Austria.*

[11]*Jasper Ridge Biological Preserve, Stanford University, Stanford, CA 94305, USA.*

[12]*State Key Laboratory of Loess and Quaternary Geology, Institute of Earth Environment, Chinese Academy of Sciences, Xi'an 710061, China.*

[13]*Department of Geological Sciences, Freie Universität Berlin, Malteserstr. 74-100/D, 12249 Berlin, Germany.*

[14]*LEGOS, Université de Toulouse, CNRS/CNES/IRD/UPS), 14 avenue Edouard Belin, 31400 Toulouse, France.*

[15]*Geochemistry and the Environment Division, Institute of Chemistry, Jan Kochanowski University, 15G Świętokrzyska St, 25-406 Kielce, Poland.*

[16]*Leibniz Institute for Baltic Sea Research Warnemüende (IOW), Biological Oceanography Section, Seestrasse 15, 18119 Rostock - Germany.*

[17]*Natural History Museum, Postboks 1172, Blindern, 0318 Oslo, Norway.*

[18]*The Australian National University, Canberra ACT 0200, Australia.*

[19]*Georgetown University, Washington DC, USA.*

[20]*Smithsonian Institution, Washington DC, 20013 USA.*

[21]*Morphodynamique Continentale et Côtière, Université de Caen Normandie, CNRS; 24 rue des Tilleuls, F-14000 Caen, France.*

[22]*School of Archaeology and Ancient History, University of Leicester, University Road, Leicester LE1 7RH, UK.*

Corresponding author: Colin N Waters

School of Geography, Geology and the Environment, University of Leicester, University Road, Leicester LE1 7RH, UK. cw398@leicester.ac.uk

ACCEPTED MANUSCRIPT

ACCEPTED MANUSCRIPT

ABSTRACT

The Anthropocene as a potential new unit of the International Chronostratigraphic Chart (which serves as the basis of the Geological Time Scale) is assessed in terms of the stratigraphic markers and approximate boundary levels available to define the base of the unit. The task of assessing and selecting potential Global Boundary Stratotype Section and Point (GSSP) candidate sections, a required part of the process in seeking formalisation of the term, is now being actively pursued. Here, we review the suitability of different stratified palaeoenvironmental settings and facies as potential hosts for a candidate GSSP and auxiliary sections, and the relevant stratigraphical markers for correlation. Published examples are evaluated for their strengths and weaknesses in this respect. A marked upturn in abundance of radioisotopes of ^{239}Pu or ^{14}C, approximately in 1952 and 1954 CE respectively, broadly coincident with a downturn in δ^{13}C values, is applicable across most environments. Principal palaeoenvironments examined include: settings associated with accumulations of anthropogenic material, marine anoxic basins, coral reefs, estuaries and deltas, lakes at various latitudes, peat bogs, snow/ice layers, speleothems and trees. Together, many of these geographically diverse palaeoenvironments offer annual/subannual laminae that can be counted and independently dated radiometrically (e.g. by ^{210}Pb). Examples of possible sections offer the possibility of correlation with annual/seasonal resolution. From among such examples, a small number of potentially representative sites require the acquisition of more systematic and comprehensive datasets, with correlation established between sections, to allow selection of a candidate GSSP and auxiliary stratotypes. The assessments in this paper will help find the optimal locations for these sections.

ACCEPTED MANUSCRIPT

Keywords: Anthropocene; Global Boundary Stratotype Sections and Points; Chronostratigraphy; Palaeoenvironments

Contents

ABSTRACT 3

1. INTRODUCTION 13

2. KEY STRATIGRAPHIC MARKERS 16

2.1 Key markers 17

2.1.1 Novel materials 19

2.1.2 Geochemical markers 21

2.1.3 Biotic markers 28

2.2 Independent dating techniques 30

3. SUITABILITY OF PALAEOENVIRONMENTAL ARCHIVES FOR HOSTING POTENTIAL GSSP CANDIDATES 33

3.1 Anthropogenic deposits 33

3.1.1 Fresh Kills Landfill, New York 36

3.1.2 Teufelsberg, Berlin 36

3.1.3 Vienna, Austria 37

3.1.4 Gorrondatxe-Tunelboca beachrock, Spain 37

3.2 Marine anoxic basin deposits 39

3.2.1 Santa Barbara Basin, California 44

3.2.2 Black Sea 48

3.2.3 Saanich Inlet, Canada 49

3.2.4 Saguenay Fjord, Canada 51

3.2.5 Cariaco Basin, Venezuela 52

3.3 Coral bioherms, calcified sponges and marine bivalve shells 53

3.3.1 Caribbean ^{13}C Suess effect and heavy metal concentrations 56

3.3.2 Guam (Pacific Ocean) .v. Caribbean Pu radionuclide signals 60

3.3.3 ^{14}C, Pb and $\delta^{15}N$ signals in deep-water Atlantic gorgonian corals 62

3.3.4 Global temperature and pH proxies from corals in the Great Barrier Reef 64

ACCEPTED MANUSCRIPT

3.3.5 Plastics in the Great Barrier Reef 65

3.3.6 North Atlantic marine bivalves 65

3.4 Estuarine and deltaic deposits 66

3.4.1 Clyde Estuary, Scotland (Pb and organic compounds) 71

3.4.2 Urola Estuary, Spain 73

3.4.3 San Francisco Bay, USA 74

3.4.4 Indus Delta 77

3.5 Lake sediments 77

3.5.1 Crawford Lake, Canada 87

3.5.2 Lochnagar, Scotland 88

3.5.3 Lilla Öresjön, Sweden 92

3.5.4 Huguangyan Maar Lake, Guangdong, China 93

3.5.5 Maha'ulepu Lake of Kauai, Hawaii 94

3.6 Peat and peatlands (mires) 95

3.6.1 Pb, organic contaminants and radionuclide fallout deposition at Etang de la Gruère, Jura Mountains, Switzerland 102

3.6.2 Spheroidal carbonaceous particles and Pb in Malham Tarn Moss, England 104

3.7 Ice 105

3.7.1 Law Dome Ice Core, East Antarctica 117

3.8 Speleothems 120

3.8.1 Ernesto Cave, Italy 124

3.8.2 Urban speleothem, Paris 127

3.9 Trees 127

3.9.1 Tree rings and palaeoclimate signals 130

3.9.2 Stable carbon isotopic signal 133

3.9.3 Sulphur concentrations and isotopic ratios 135

3.9.4 The radiocarbon bomb spike and heavy metal concentrations 138

4 Summary 139

5 Conclusions 147

ACCEPTED MANUSCRIPT

Figures

Figure 1. [B&W] Primary and some secondary markers for the 65 GSSPs that have been ratified currently by IUGS. The four in the Cenozoic that deal with stable isotope events (base Eocene, Quaternary, Calabrian and Holocene) and the iridium anomaly (base Paleocene) provide models for choosing markers for the base of the Anthropocene.

Figure 2. [B&W] Cores through the Gorrondatxe-Tunelboca beachrock, Spain. A natural high-energy open beach sand deposit, pre-dating the discharges of iron slag, is overlain by cemented sandy and coarse beach deposits that are commonly conglomeratic with abundant slag clasts and incorporating littoral foraminifera. Three distinct foraminiferal assemblages are recognised (ranges for assemblages 1. 2 and 3 marked by arrows) Modified from Martínez-García et al. (2013).

Figure 3**.** [Colour] Location of marine dead zones (from NASA Earth Observatory https://earthobservatory.nasa.gov/IOTD/view.php?id=44677; Aquatic Dead Zones generated 17th July 2010). Red circles show the location and size of the dead zones. Black dots show where dead zones of unknown size have been observed. The distribution commonly occurs adjacent to populous land areas (shown by the brown scale), but not to upwelling zones (shown by concentration of particulate organic carbon, in blue scale).

Figure 4. [B&W] Key signals in marine cores from the Santa Barbara Basin, with a) Pu signal (Koide et al. 1975), b) variations in sedimentation rates (Krishnaswami et al. 1973), c) selected heavy metals (Schmidt and Reimers 1991) and d) planktonic foraminifera (Field et al. 2006).

Figure 5. [Colour] a) Distribution of shallow-water framework-building coral reefs (from NOAA: Where Are Reef Building Corals Found http://oceanservice.noaa.gov/education/tutorial_corals/coral05_distribution.html) and cold-water corals (from Freiwald et al. 2017) and b) the inventory of anthropogenic CO_2 (µmol CO_2/kg) in surface waters (from Swart et al. 2010).

ACCEPTED MANUSCRIPT

Figure 6. [Colour] a) Changes in $\delta^{13}C$ with respect to age for corals from the Atlantic and the Pacific/Indian oceans compared to published data from sclerosponges, averaged after removing the mean $\delta^{13}C$ value of the coral skeleton from 1900 CE to the present day and shown as a five-year running mean (Swart et al. 2010). This is compared with $\delta^{13}C$ data from Law Dome ice core (Rubino et al. 2013) which show a ~1955 CE inflection; b) $^{240+239}Pu$ concentrations in annual growth bands from *Porites lobata* in Guam (Lindahl et al. 2011) and *Orbicella (Montastrea) annularis* in the U.S. Virgin Islands (Benninger and Dodge 1986); dpm kg^{-1} = decays per minute per kilogram; mBq kg^{-1} = millibecquerel per kilogram.

Figure 7. [Colour] a) Plot of $\Delta^{14}C$ vs age for 7 different colonies of the deep-sea gorgonian coral *Primnoa resedaeformis* with spline fit through the data (Sherwood et al. 2005a), and for the bivalve *Arctica islandica* (Weidman and Jones 1993); b) $\delta^{15}N$-AA depletion in deep-sea gorgonian corals in the NW Atlantic (Sherwood et al. 2011) © (2011) National Academy of Sciences; c) Pb concentration; and d) $^{206}Pb/^{207}Pb$ in Bermuda corals (Kelly et al. 2009).

Figure 8. [Colour] Distribution of deltas and estuaries (from Tessler et al. 2015), major mud deposits (from Hanebuth et al. 2015) and areas where neobiota amenable to fossilization have recognizably altered coastal ecosystems (from: Major pathways and origins of invasive species infestations in the marine environment In UNEP/GRID-Arendal Maps and Graphics Library http://www.international-marine.com/invasivespecies/PublishingImages/invasive_vectors_001.png).

Figure 9. [B&W] Example of data from a single core from the Clyde Estuary showing a) Pb concentrations and $^{207/206}Pb$ isotope ratios, and b) PAH, TPH and PCB organic chemical signatures (Vane et al. 2011).

Figure 10. [Colour] Metal concentrations (Cu, Ni, Pb, Zn) versus foraminiferal density in the Urola estuary (northern Spain). FA1–FA3 represent three distinct foraminiferal assemblages referred to in the text. Modified from Goffard (2016).

Figure 11. [B&W] Chronology of selected invasive mollusc species into San Francisco Bay (for dates of invasion see: Carlton et al. 1990; Cohen 2004, 2011; Committee on Non-native Oysters in the Chesapeake Bay, Fofonoff et al. 2017, National Research Council 2004), and terrestrial invasive

ACCEPTED MANUSCRIPT

species in the Maha'ulepu sinkhole succession of Kauai, Hawaii (Burney et al. 2001). In both successions, cultural human changes are indicated by the lefthand column, and neobiota in the righthand column. Although the two successions developed nearly 4000 km apart, and in tropical and warm temperate zones respectively, by the mid-19th century some taxa present on the California coast (e.g. the bivalve *Crassostrea virginica*, see DeFelice et al. 2001) were also present in Hawaii, suggesting the possibility of correlation between remote successions.

Figure 12. [Colour] Location of the 365 sites recording lake hypoxia (Jenny et al. 2016). Recent hypoxia records onset of varves after 1700 CE, whereas naturally hypoxic lakes were taken to be those in which laminations persisted for at least 300 years.

Figure 13. [B&W] Radiogenic signature from Lake Victoria, Australia (Hancock et al. 2011). Profiles of ^{137}Cs (closed squares), $^{239+240}$Pu (open circles) and ^{238}Pu/$^{239+240}$Pu (triangles).

Figure 14. [Colour] Sediment δ^{15}N profiles from Northern Hemisphere lakes (from Holtgrieve et al. 2011). Lake ecotypes include: temperate/boreal (green circles), alpine (blue circles), and arctic (red circles), and the Greenland Summit ice core is indicated with a yellow circle. The solid lines are the median posterior fits to the observed data using the most parsimonious model, and the dotted lines are the 2.5 and 97.5% credible limits.

Figure 15. [B&W] Replacement of Holocene diatom assemblages by *Asterionella formosa* and/or *Fragilaria crotonensis* mainly in lake cores from US high-altitude sites, since ~1950 CE (Saros et al. 2005). Location of lakes shown on Figure 14.

Figure 16. [Colour] Stratigraphic signals of the last millennium in Crawford Lake, Canada. The horizontal red line near the top is the ~1950 CE level, marked by both lithological and biostratigraphic changes in available data. From Zalasiewicz et al. (2017a), modified after Ekdahl et al. (2004). DAR is diatom accumulation rate.

Figure 17. [Colour] Contamination record in Lochnagar sediments (Scotland) demonstrating appearances as post-mid-20th century markers: (a) Spheroidal carbonaceous particles (SCPs) (from Yang et al. 2002a); (b) Hg and Pb (from Yang et al. 2002a); (c) δ^{15}N (from Curtis and Simpson 2011); (d) the chlorinated pesticides DDT and toxaphene from core collected in 1997 CE related to emission

ACCEPTED MANUSCRIPT

data (from Muir and Rose 2007); (e) chlorobenzenes (from Muir and Rose 2007); (f) total PCBs related to global emissions (from Muir and Rose 2007); and (g) PDBEs related to UK emissions (from Muir and Rose 2007).

Figure 18. [B&W] Physical, chemical and biological trends from Lilla Öresjön (SW Sweden), a high-sulphate deposition area (from Renberg and Battarbee 1990).

Figure 19. [Colour] Historical variations of concentrations and mass accumulation rates (MARs) of black carbon (BC), char, and soot, parent-PAHs, oxygenated PAHs (OPAHs), and azaarenes (AZAs) in the Huguangyan Maar Lake (from Han et al. 2016).

Figure 20. [Colour] Global map of peatland regions with basal peat ages (black <8 ka, red 8-12 ka, and blue >12 ka) (from Yu et al. 2010).

Figure 21. [B&W] Core from Etang de la Gruère, Switzerland collected in 1991 CE: A) Pb Enrichment Factor (EF) calculated as the ratio of Pb/Sc in the peats, normalized to the background value (from Shotyk et al. 1998); B) Pb isotopic values (from Shotyk et al. 1998); C) ΣPCBs (from Berset et al. 2001); D) ΣPAHs (from Berset et al. 2001); E) ^{137}Cs (from Appleby et al. 1997). Succession dated using ^{210}Pb to 35 cm depth (Appleby et al. 1997) and ^{14}C yr BP from 35 cm to base (Shotyk et al. 1998).

Figure 22. [B&W] Spheroidal carbonaceous (fly ash) particles (SCPs), lead and iron concentrations from Malham Tarn Moss, England (from Swindles et al. 2015).

Figure 23. [Colour] Distribution of ice caps and glaciers (blue) and ice sheets (white) from NASA Earth Observatory Randall Glacier Inventory in 2014 CE http://earthobservatory.nasa.gov/IOTD/view.php?id=83918 (acquired 7th May 2014; produced by Jesse Allen and Robert Simmon). Inset maps showing the main polar drilling sites in Antarctica and Greenland mentioned in the text.

Figure 24. [Colour] δ^{18}O, δD and accumulation rates for the North Greenland Eemian Ice Drilling site (NEEM) (Masson-Delmotte et al. 2015).

Figure 25. [Colour] Ice core signals since 1700 CE (from Wolff 2014). CH_4 and CO_2 ice-core data (blue dots) are from Law Dome, Antarctica (MacFarling Meure et al. 2006), and recent atmospheric data (red lines) from Mauna Loa (CO_2) and Cape Grim (CH_4) observatories. The horizontal dashed lines are the highest values observed in ice cores of the last 800,000 years prior to the period shown. Beta

ACCEPTED MANUSCRIPT

radioactivity is from Coats Land, Antarctica (Wolff et al. 1999). Sulphate and nitrate are shown for two cores from Greenland: B16 (dashed red) and B21 (solid blue) (Fischer et al. 1998). The 18th- and 19th-century spikes in sulphate are signals of volcanic eruptions.

Figure 26. [B&W] Concentrations (5-year running means) in Greenland ACT2 ice core from 1772 to 2003 CE of sulphur (NssS), thallium (Tl), cadmium (Cd) and lead (Pb), compared to black carbon (BC), from McConnell and Edwards (2008). Sulphur peaks in 1817 and 1883 CE relate to the Tambora and Krakatoa volcanic eruptions, respectively. © (2008) National Academy of Sciences, U.S.A.

Figure 27. [Colour] a) Law Dome ice core and firn records for CO_2 concentration and $\delta^{13}C$ for atmospheric CO_2 for the past 1000 years (from Rubino et al. 2013); b) Law Dome ice core and firn records for CH_4 concentration and $\delta^{13}C$ for atmospheric CH_4 for the past 1000 years (from Ferretti et al. 2005); c) N_2O concentrations in the Law Dome ice core over the past 2000 years and 200 years (Wolff 2013).

Figure 28. [Colour] Extent of carbonate outcrops present across global landmass by Ulrichstill https://commons.wikimedia.org/w/index.php?curid=9412430 Created 6th February 2010. Karst landscapes and speleothems occur within these regions, and locations mentioned in the text are indicated.

Figure 29. [Colour] Ernesto Cave, Italy: a) Age model based on lamina counting related to local mean air temperature (Frisia et al. 2003); b) $\delta^{18}O$ and $\delta^{13}C$ profiles (Scholz et al. 2012); c) Radiocarbon profile and comparable European atmospheric emissions (Fohlmeister et al. 2011); d) S concentration and $\delta^{34}S$ (Frisia et al. 2005, Wynn et al. 2010).

Figure 30. [Colour] Forest map of the world with key locations mentioned in the text. © (2006) FAO.

Figure 31**.** [Colour] a) The 20-year smoothed Northern Hemisphere extratropics reconstruction of radial stem productivity in high elevation and high latitude forest environments since 800 CE (black) and two-tailed 95% bootstrap confidence intervals (blue) (from Esper et al. 2002); b) $\delta^{13}C$ variability from Loader et al. (2013) for the period 1500-2008 CE measured in tree-ring cellulose for a composite tree-ring stable isotope chronology developed using *Pinus sylvestris* trees from northern Fennoscandia. Fine line represents annually-resolved $\delta^{13}C$ variability, thick solid line presents the

ACCEPTED MANUSCRIPT

annual data smoothed with a centrally-weighted 51-year moving average. Dashed line represents the mean $\delta^{13}C$ value for the "pre-industrial" period 1500-1799 CE. Mean annual replication for the record is >13 trees. Analytical precision σ_{n-1} = 0.12 per mille n=951 which compares favourably with the analytical precision of the method typically reported (σ_{n-1} = 0.10 n=10) (Boettger et al. 2007, McCarroll and Loader 2004, Loader et al. 2013a).

Figure 32. [Colour] a) Tree rings (*Pinus sylvestris*) samples from 1960 to 2003 CE at Niepołomice (Poland) showing changes of radiocarbon concentration (from Rakowski et al. 2013) compared with Northern Hemisphere (Zone 1) atmospheric values (from Hua and Barbetti 2004); b) European S emissions; c) S concentrations; and d) $\delta^{34}S$ in *Abies alba* from NE Italy compared with European S emissions (Wynn et al. 2014).

Tables

Table 1. Requirements for establishing a Global Boundary Stratotype Section and Point (GSSP). Table modified from Gradstein et al. (2012, Table 2.1, p. 36), revised from Remane et al. (1996) according to current procedures and recommendations of the ICS.

Table 2. Potential palaeoenvironmental archives and facies and their stratigraphic markers for a candidate GSSP. ? – uncertain suitability of the specified signal.

Table 3. Reasons for and against using an anthropogenic deposit as a potential host for a GSSP.

Table 4. Reasons for and against using a marine anoxic basin deposit as a potential host for a GSSP.

Table 5. Reasons for and against using a coral or bivalve shell as a potential host for a GSSP.

Table 6. Reasons for and against using an estuarine or deltaic deposit as a potential host for a GSSP.

Table 7. Reasons for and against using a lake deposit as a potential host for a GSSP.

Table 8. Selected examples of the use of proxies for various types of atmospherically sourced environmental change.

Table 9. Reasons for and against using a peat deposit as a potential host for a GSSP.

ACCEPTED MANUSCRIPT

Table 10. Reasons for and against using an ice core as a potential host for a GSSP.

Table 11. Reasons for and against using a speleothem as a potential host for a GSSP.

Table 12. Reasons for and against using a tree ring as a potential host for a GSSP.

Table 13. Summary of key mid-20th century proxy signals and potential palaeoenvironments for a GSSP. The initial date represents the marked onset of the signal; the peak signal is shown in brackets. Reference numbers relate to main geographical locations mentioned in the text: (1) Santa Barbara, USA; (2) Caribbean; (3) Nova Scotia, Canada; (4) Clyde Estuary, Scotland; (5) Urola Estuary, Spain; (6) Lake Victoria, Australia; (7) North America; (8) China; (9) Lochnagar, Scotland; (10) Lilla Öresjön, Sweden; (11) Northern England; (12) Switzerland; (13) Antarctica; (14) Greenland; (15) Ernesto Cave, Italy; (16) Fenno-Scandinavia; (17) Poland; (18) Ontario, Canada.

ACCEPTED MANUSCRIPT

ACCEPTED MANUSCRIPT

1. INTRODUCTION

The Anthropocene Working Group (AWG), a working group of the Subcommission on Quaternary Stratigraphy (SQS) of the International Commission on Stratigraphy (ICS), is facilitating the process that will lead to the submission of formal proposals to define the Anthropocene as a chronostratigraphic unit. Such a unit comprises a body of strata formed during a specific interval of geological time. Units of the International Chronostratigraphic Chart (upon which the Geological Time Scale is based) are chronostratigraphic units, and each is defined by a synchronous base. The AWG is working towards a definition of the geological Anthropocene based on "the first appearance of a clear synchronous signal of the transformative influence of humans on key physical, chemical, and biological processes at the planetary scale. As such, it stands in contrast to various local or diachronous inscriptions of human influences on the Holocene stratigraphic record" (Zalasiewicz et al. 2017c). This working definition most closely aligns with the mid-20th century "Great Acceleration" in human population, resource consumption, global trade and technological evolution, proxy signals from which produce a distinctive stratigraphical boundary (Steffen et al. 2016). There are alternative interpretations of the definition of the Anthropocene, but these are generally grounded on a non-stratigraphical basis (e.g. the discussion on various geomorphological considerations of the start of the Anthropocene by Brown et al. 2017).

Within the Phanerozoic, the current internationally agreed method for defining chronostratigraphic boundaries is via selection of a Global Boundary Stratotype Section and Point (GSSP) as a physical reference level for a particular, and optimally correlatable, geological time boundary. The process of deciding on a GSSP, outlined by Remane et al.

ACCEPTED MANUSCRIPT

(1996) and Remane (1997, 2003) and summarised by Smith et al. (2014) is a complex process that normally requires: 1) an initial selection of a boundary level characterized by a marker event (the primary marker event) of optimal global correlation potential; 2) selection of a stratotype section from a number of potential sections, with the chosen stratotype section containing the best possible record of the primary marker event as well as other marker events that support global correlation, 3) ideally the selection of some auxiliary stratotypes in which the same level is represented by similar or other proxy signals in different parts of the world (Walker et al. 2009, in defining the Holocene Series, provided five auxiliary stratotypes as well as the GSSP); and, 4) definition of the precise point within stratified rock or sediment (or glacial ice in the case of the Holocene) that fixes the chronostratigraphic boundary with a precise moment of time. Formalisation of a GSSP is a careful procedure as, once ratified, it normally cannot be subsequently revised for at least ten years (Remane et al. 1996).

Table 1 provides a formal and comprehensive listing of the reasonable requirements for establishment of a GSSP, most of which will pertain also to a formal basis for the Anthropocene. It includes the requirement for stratigraphical completeness across the GSSP level, with adequate thickness of strata both above and below the boundary in order to demonstrate the transition. Therefore, the presence of an unconformity, marking a discontinuous succession, at or near the proposed boundary, would render it unsuitable. The selected section should also be accessible for subsequent investigations, ideally with provision for conservation and protection of the site.

The rank currently preferred by the AWG for the Anthropocene is that of series/epoch (Zalasiewicz et al. 2017c). The procedure leading to official acceptance of a GSSP for the

ACCEPTED MANUSCRIPT

Anthropocene Series/Epoch and its corresponding Age/Stage would require: 1) the selection by the AWG of a single GSSP candidate from one or more potential candidates, based on proposals submitted to it; 2) the recommendation of that proposal by the SQS; 3) its approval by the voting membership of the ICS; and 4) ratification by the Executive Committee of the International Union of Geological Sciences (IUGS). All voting within the ICS, and its constituent subcommissions and their working groups, requires a supermajority of 60% or more for a proposal to be approved.

1. Name and stratigraphic rank of the boundary
Including concise statement of GSSP definition
2. GSSP geographic and physical geology • Geographic location, including map coordinates • Geological setting (lithostratigraphy, sedimentology, palaeobathymetry, post-depositional tectonics, etc.) • Precise location and stratigraphic position of GSSP level and specific point • Stratigraphic completeness across the GSSP level • Adequate thickness and stratigraphic extent of section above and below • Accessibility, including logistics, national politics and property rights • Provisions for conservation and protection
3. Primary and secondary markers • Primary correlation marker (event) at GSSP level • Secondary markers – biostratigraphy, magnetostratigraphy, chemical stratigraphy, sequence stratigraphy, cycle stratigraphy, other event stratigraphy, marine–land correlation potential • Potential age dating from volcanic ash and/or orbital tuning • Demonstration of regional and global correlation
4. Summary of selection process • Relation of the GSSP to historical usage • References to historical background and adjacent (stage) units • Selected publications • Other candidates and reasons for rejection • Summary of votes and received comments • Other useful reference sections
5. Official publication • Summary for official documentation in IUGS journal *Episodes* • Digital stratigraphy (litho-, palaeo-, magneto-, and chemo-stratigraphic) images and graphic files submitted to ICS for public archive • Full publication in an appropriate journal

ACCEPTED MANUSCRIPT

Table 1. Requirements for establishing a Global Boundary Stratotype Section and Point (GSSP). Table modified from Gradstein et al. (2012, Table 2.1, p. 36), revised from Remane et al. (1996) according to current procedures and recommendations of the ICS.

Here we offer a preliminary assessment of palaeoenvironments and their depositional facies where potential GSSP candidate sections for defining the lower boundary of the Anthropocene may be located, based on the published literature. Few of these example sections were chosen with the specific purpose of defining the Anthropocene as a chronostratigraphic unit. Rather they show a range of proxy signals, analysed in published studies for varied (non-ICS) purposes. The palaeoenvironmental research illustrated in this review demonstrates the timing and processes through which these signals have been imprinted in strata, and the extent to which they allow stratigraphic correlation worldwide. Even with this considerable caveat, the possibilities of correlation are clearly demonstrated, and help constrain the range of potential targets for Anthropocene-specific ICS studies.

2. KEY STRATIGRAPHIC MARKERS

The aim – not always achieved – is for GSSPs to have many guiding criteria to support the primary marker (Remane et al. 1996, Smith et al. 2014) to permit both regional and global correlation. This has been the early focus of the AWG, with the description of potentially suitable markers summarised by Waters et al. (2016), whose recommendations this study follows, and as reported by Zalasiewicz et al. (2017c), concludes that the primary marker for the Holocene–Anthropocene boundary should be selected and identified in strata with a mid-20th century age. Such a definition makes the Anthropocene so recent that there are more potential archives available to it than for most, if not all, earlier GSSPs.

ACCEPTED MANUSCRIPT

2.1 Key markers

The lower boundary of a chronostratigraphic unit, at the rank of Stage/Age and above, is defined by a GSSP and is recognized globally by a primary marker within the stratotype section that should be close to or coincident with the GSSP itself. Historically, most chronostratigraphic units use biotic signals, namely the highest or (preferably) lowest occurrence of a single fossil species, as the primary marker (Figure 1). More recent approaches incorporate physico-chemical markers such as magnetic reversals, isotope excursions and cyclostratigraphy, especially for the Cenozoic (Miller and Wright 2017). Although not a requirement, the means for numerically dating the succession is considered a strong site advantage.

Of the 65 GSSPs presently ratified by IUGS, all occur within strata deposited in marine sedimentary environments, with the exception of the Holocene GSSP that is placed within a Greenland ice core (Walker et al. 2009). This reflects the fact that marine fossils have proven better for long-distance correlation than non-marine ones; and more generally that proxy signals are readily preserved and continuously recorded in marine environments. However, a primary marker ideally is traceable globally in marine and non-marine stratigraphic settings, thereby allowing secondary markers to be chosen that will assist correlation in either setting, especially when the primary marker is not detected. These secondary markers should approximate closely to that the stratigraphic position of the primary marker. In an Anthropocene context, the choice of markers should not be to provide an indication of the start of anthropogenically driven effects, but to provide the most pragmatic marker that will allow global correlation of the chosen boundary, being geographically extensive, temporally abrupt and providing a permanent record. Such primary and secondary markers do not need to be symptomatic of the environmental changes across the Holocene–Anthropocene

ACCEPTED MANUSCRIPT

boundary, rather they need to be amenable to widespread correlation in deposits representing different palaeoenvironments. Key signals considered here are mainly anthropogenic in origin, either being entirely novel, such as the production of novel anthropogenic mineral-like compounds, artificial radionuclides, organic and inorganic chemical species, or through perturbations of natural signals associated with, for example, the carbon and nitrogen cycles, and changes to climate proxies or biotic assemblages (Table 2). However, markers of any kind, including ones with little or no human influence (e.g. palaeomagnetic signals or volcanic ash layers) may serve just as well to help correlation. These markers are discussed by Waters et al. (2016), and are summarised below in the context of their likely presence in potential candidate palaeoenvironments.

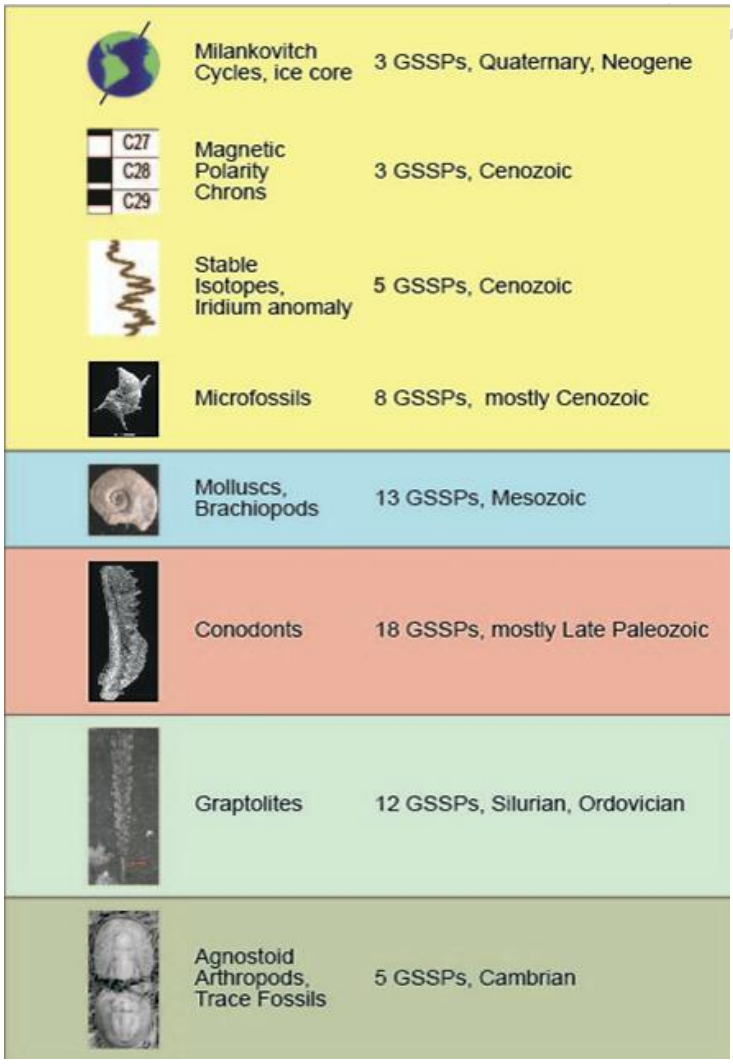

ACCEPTED MANUSCRIPT

Figure 1. Primary and some secondary markers for the 65 GSSPs that have been ratified currently by IUGS. The four in the Cenozoic that deal with stable isotope events (base Eocene, Quaternary, Calabrian and Holocene) and the iridium anomaly (base Paleocene) provide models for choosing markers for the base of the Anthropocene.

2.1.1 Novel materials

Synthetic solids such as metal alloys, glass, carbide abrasives, gemstones, laser crystals, piezoelectric compounds, semiconductors and cement have proliferated in the environment in recent decades (Hazen et al. 2017), being present in novel "metamorphic rocks" such as porcelain, brick and concrete, the latter being the most abundant novel rock on the planet, with over 90% of the ~500 Gt (gigatonnes or 10^{15} grams) produced since the mid-20th century. Complex additives to cement help to chemically and petrographically fingerprint modern concrete (Waters and Zalasiewicz, 2017). These novel anthropogenic mineral-like compounds and rocks often accumulate directly within terrestrial anthropogenic deposits such as landfill sites and road networks. Through subsequent erosion of the widespread human-built landscape, these materials may be reworked and deposited in fluvial, lacustrine, coastal and marine sediments, with a variable time lag between formation and accumulation.

Synthetic organic compounds have become abundant, including plastics that are exceptionally mobile and durable within river and ocean currents. Plastics have, since ~1950 CE, become increasingly widely dispersed, including as abundant microfibres and microbeads, forming signals found extensively in lake, estuarine and marine sediments, even within remote abyssal environments (Zalasiewicz et al. 2016a). Most are the effluents from waste water treatment works and transported through river systems to accumulate in lakes or oceans. The recent recognition of synthetic microfibre fallout accumulations in urban

ACCEPTED MANUSCRIPT

Paris (Dris et al. 2016) raises the possibility of rapid and widespread airborne dispersal across environments.

The first development (in effect first occurrence) and annual production figures of novel anthropogenic mineral-like compounds and organic polymers are known from historical records. However, few studies have investigated them in their stratigraphic context, in order to determine the pattern of their accumulation in sedimentary environments. Matsugama et al. (2017) record the first influx of microplastics into canal sediments in Tokyo in the 1950s, whereas in the Gulf of Thailand a significant increase in abundance occurs in the 1990s; in all cases there is an upward increase in microplastic abundance and polymer types. Because of their novelty, little is known of the longevity and potential fragmentation of plastics in buried sediments. Also of significance in lakes and marine settings is the settling rate within the water column. In the case of microplastic organic polymers (<5 mm diameter) sinking velocities have been estimated as 6–91 mm s^{-1}, which is more rapid than the settling of clay minerals and organic-rich aggregates (Kowalski et al. 2016). Particle density (variable between distinct polymers) and shape, fluid density (with slower settling in saline water), temperature and ingestion by microplankton all can influence settling rates, and these parameters have different effects on different polymers (Kowalski et al. 2016).

Fly ash, the unburned particulates sourced from fossil fuel combustion, includes inorganic ash spheres (IAS), mainly residues from coal burning, and spheroidal carbonaceous particles (SCPs) principally from both coal burning and oil combustion. These particulates are disseminated aerially, and typically show a marked upturn in abundance from about 1950 CE (Oldfield 2014, Rose 2015, Swindles et al. 2015). The upturn in abundance of SCPs should serve as a likely permanent stratigraphic marker for the Anthropocene in lake sediments

ACCEPTED MANUSCRIPT

across all continents. Work is ongoing to assess their likely presence in other environments, such as glacial ice, peat sequences, marine basin sediment and terrestrial anthropogenic deposits such as industrial dumps and landfills. Black carbon (BC), present as char or soot, is generated from both anthropogenic combustion and natural biomass burning (Bond et al. 2007, Han et al. 2017). BC is commonly identified in soil, lacustrine and marine sediments, and glacial ice (Xu et al. 2009).

2.1.2 Geochemical markers

Oxygen and hydrogen isotopes and dust signals are important climate change proxies and hence tools for Quaternary correlation. All three proxies are recognised in glacial ice, within the ice fraction, and complement the air bubble record. Deuterium (^{2}H or D) is an important isotopic tracer for precipitation, and the relationship between δD and δ^{18}O signatures defines a "deuterium excess" marker that is a proxy for sea surface temperature. The deuterium excess ratio is used as the primary marker for the base of the Holocene Series in an ice core GSSP (Walker et al. 2009), where a 2–3‰ decrease in the ratio is associated with a rapid ocean surface temperature decline of 2–4°C. An abrupt dip in δD and deuterium excess reflecting cooling is also seen in a Greenland ice core at 8.2 ka (Walker et al. 2012), and suggested to mark the base of the proposed Middle Holocene Subseries and Northgrippian Stage. Cold stages are commonly associated with increased aeolian dust deposition in ice cores. Decreases in δ^{18}O mark cooling events, and in Greenland ice the overall trend since the Middle to Late Holocene has been of gradual cooling culminating in the Little Ice Age from about 1200 to 1850 CE. The shift to warming induced by increased anthropogenic greenhouse gases emissions is first indicated by a slight change to less negative δ^{18}O values in Greenland ice from ~1850 through to the 1870s CE and again from 1979 to 2007 CE (Masson-Delmotte et al. 2015; see Figure 24 below), although the

ACCEPTED MANUSCRIPT

magnitude of enrichment is small compared with variations across the Pleistocene–Holocene boundary. Warming is also apparent in the Antarctic Peninsula from about 1950 CE, e.g. on James Ross Island (Abram et al. 2013), with lakes on Signy Island from the South Orkney Islands having experienced some of the most rapid air temperature increases of 2°C since the mid-20th century, with concomitant marked responses by lake biota and increased nutrient levels, linked to deglaciation and reductions in lake snow and ice cover (Quayle et al. 2002). Variations in $\delta^{18}O$ are observable in carbonate and phosphate minerals in speleothems, shells, corals, teeth, and bones and also in tree rings. They can be used as a palaeotemperature proxy in marine settings or within terrestrial environments, primarily as a proxy for $\delta^{18}O$ composition in atmospheric precipitation.

About 50% of anthropogenic carbon dioxide emissions, the major product of fossil-fuel combustion, have accumulated in the atmosphere, with the lifetime of much of the atmospheric fossil-fuel-derived CO_2 being ~200 to 2000 years (Archer et al. 2009). The remainder is absorbed approximately equally by land and ocean sinks (Le Quéré et al. 2016). The atmospheric CO_2 record from ~7 ka shows a very slow rise to ~280 ppm by ~1850 CE. Subsequently, the CO_2 concentration shows a marked rate increase (Etheridge et al. 1996, MacFarling-Meure et al. 2006, Rubino et al. 2013), attaining ~310 ppm by 1950 CE and with a further sharp acceleration to its current mean value of >400 ppm, reached in 2015 CE. The rate of increase between 1950 and 2015 CE is ~100 times greater than that of the Late Pleistocene to Early Holocene rise, itself considered rapid in geological terms (Wolff 2014).

Anthropogenic methane emissions arise primarily from agriculture (wet rice cultivation and ruminants), with a smaller fraction from biomass burning and fossil fuel combustion. Some large terrestrial anthropogenic deposits in the form of landfills also emit significant amounts

ACCEPTED MANUSCRIPT

of methane. Unlike CO_2, methane is chemically reactive in the atmosphere, with the dominant sink being oxidation by OH radicals. This process removes about 90% of all emissions of CH_4 each year, or about 9% of the total burden of CH_4 − the atmospheric lifetime is 7–11 years (Ciais et al. 2013). Throughout the Quaternary Period, CH_4 concentrations range from ~400 to 800 ppb, with the higher values marking interglacials. In marked contrast, from 1875 CE there has been a sharp climb to the current levels of ~1800 ppb (Nisbet et al. 2016).

Both CO_2 and CH_4 provide a direct stratigraphic marker where they are preserved within air bubbles in glacial ice, and an indirect record via carbon isotope variations. $\delta^{13}C$ values in CO_2 from ice cores varied by less than 0.4‰ over the duration of the pre-industrial Holocene, with the principal change being a slow enrichment in ^{13}C during the Early Holocene. The subsequent combustion of hydrocarbons, which are depleted in the ^{13}C isotope, has resulted in a sharp reduction in $\delta^{13}C$ values in atmospheric CO_2 of about 2‰ since the late 18th century, with a pronounced inflection at about 1960 CE (Rubino et al. 2013). This Suess effect is recorded in diverse materials, including plants (tree rings), shells, bones, limestones, corals, and in the atmospheric composition of air bubbles trapped in ice, although speleothems are comparatively insensitive to this signal. An abrupt shift towards less negative $\delta^{13}C$ values in atmospheric CH_4 of ~2.5‰ since ~1875 CE in response to these pyrogenic emissions (Ferretti et al. 2005) has been succeeded over the last 12 years by a shift of −0.17‰ of $\delta^{13}C$ in the increasing volume of atmospheric CH_4, attributed to an expansion of tropical wetlands (Nisbet et al. 2016).

Nitrate concentrations have been perturbed mainly through the production of agricultural fertilizers, initially through mined nitrate deposits in the 19th century, but most notably

ACCEPTED MANUSCRIPT

through the industrial production of ammonia from atmospheric nitrogen by the Haber-Bosch process, which started in 1913 CE (Fowler et al. 2013). The nitrate associated with artificial fertilizers shows global airborne distribution. $\delta^{15}N$ values have been acquired from sediment organic matter, commonly from lake deposits, although determinations from anthropogenic deposits, marine anoxic basins, estuaries, deltas, tree rings, and amino acids in corals are also available. Nitrogen compounds and isotopes are not typically recorded in carbonates, including speleothems. Nitrate, total nitrogen oxides (NO_x) and $\delta^{15}N$ values are determined from solid ice in ice cores, providing data at the time of snow accumulation. Both Northern Hemisphere lake sediments (Holtgrieve et al. 2011, Wolfe et al. 2013) and glacial ice (Hastings et al. 2009) show elevated nitrate concentrations and a fall in $\delta^{15}N$, which start towards the end of the 19th century but become appreciably more pronounced during the mid-20th century. A marked increase in NO_x sourced from elevated combustion of hydrocarbons, particularly automobiles and power stations, is also evident in Greenland ice sheets from the mid-20th century (Erisman et al. 2013).

Natural sources of sulphate include volcanic eruptions that produce high-magnitude, short-duration spikes evident in glacial ice over past millennia. There has been an overall trend of increased sulphate content in glacial ice, trees and speleothems since the start of the Industrial Revolution, peaking in the mid- to late-20th century, reflecting patterns of coal consumption; sulphate has widely declined over recent decades, most likely due to legislation requiring the fitting of sulphur scrubbers to power station chimneys to combat acid rain. The signals tend to be associated with local-to-regional industrial changes rather than representing global signals. Stable sulphur isotopes show lower $\delta^{34}S$ ratios in tree rings (e.g. Fairchild et al. 2009, Wynn et al. 2014) and speleothems (e.g. Frisia et al. 2005, Wynn et al. 2010) during the second half of the 20th century.

ACCEPTED MANUSCRIPT

Pure metals such as gold, silver, lead, copper and iron have a long history of extraction (and blending to obtain alloys) to produce tools or ornaments. The early historical mining of these metals provides local and highly diachronous signals evident in lakes, estuaries, peats, sea-floor sediments, and carbonates including corals and speleothems, and they are also present in glacial ice records. The heavy metals are either air-borne as aerosols, dissolved in water, or carried as water-transported particulates. Mercury (Hg) is also transported in gaseous form (RGM – reactive gaseous Hg; GEM – gaseous elemental Hg) (Yang et al. 2010). Within sediments, metal compounds are commonly stabilized by being adsorbed to clay mineral surfaces or organic matter; locally they may be diagenetically mobilized as conditions become reducing with burial, and redeposited in overlying oxidizing environments, thus decreasing their effectiveness as stratigraphic markers. Elevated heavy metal concentrations in tree rings have been suggested as unsuitable for temporal studies of pollution events (Bindler et al. 2004). For most metals and their compounds, the 20th century environmental signals continue to be localised, related to production from local industries. Some metals, such as elemental aluminium and many trace elements, have seen marked upturns in production in the second half of the 20th century as new uses are found for them, and these may be expected to leave signals in sediments. For at least two millennia prior to the Industrial Revolution, Pb concentration in sediments increased and Pb isotope ratios declined as a result of European metallurgy (Renberg et al. 2000). Perhaps the most widespread and abrupt signal is that associated with Pb isotope ratios related to the use of tetraethyl-lead in gasoline from the 1920s, although the isotopic fingerprint reflects the sources of lead used to manufacture this additive, which differ between countries (Reuer and Weiss 2002). Current global atmospheric concentrations of Hg are about two to four times higher than pre-industrial levels as a result of refining ore and burning coal and waste

ACCEPTED MANUSCRIPT

(Lindberg et al. 2007, Yang et al. 2010). Hg has an atmospheric lifetime of 0.75 years so can be dispersed globally before deposition, whereas the larger and more slowly cycling marine reservoir can produce a lagged response of 1 to 2 centuries (Lindberg et al. 2007).

A huge variety of novel organic compounds have been generated and used in industrial processes. Persistent organic pollutants (POPs), those recalcitrant to decomposition, which readily adsorb onto clay and organic particles and are poorly soluble, provide potentially suitable signals. Key potential POP signals include those from organochlorine pesticides (OCPs) such as DDT, aldrin and dieldrin, and various polychlorinated biphenyls (PCBs), along with brominated flame retardants (e.g. polybrominated diphenyl ethers, PBDEs). Most of these have only been generated on industrial scales and released into the environment in notable quantities since the mid-20th century, particularly concentrating in sediments in lakes (Muir and Rose 2005, 2007), estuaries (Vane et al. 2011) and canyons on continental shelf margins (Paull et al. 2006).

Large amounts of anthropogenically-sourced radionuclides have been released by 543 atmospheric nuclear weapons tests, with a total yield of about 440 Mt (i.e. energy released in TNT equivalent), and subsequent fallout (UNSCEAR 2000). Although atmospheric tests and military use began in 1945 CE, it was only with the testing of the large thermonuclear (hydrogen) devices from 1952 CE that fallout was dispersed globally and became recorded in most environments. The signal is almost instantaneous in geological terms, with residence times in the stratosphere of some 15 to 18 months following thermonuclear detonations. Typically, the Pu signal shows an abrupt rise in 1952 CE, a peak in 1963−1964 CE and rapid decline since 1963 CE in response to a Partial Test Ban Treaty, which resulted in most testing moving underground (Waters et al. 2015). Radionuclides that are absent or rare in nature,

ACCEPTED MANUSCRIPT

such as plutonium-239 (^{239}Pu), americium-241 (^{241}Am), caesium-137 (^{137}Cs) and strontium-90 (^{90}Sr) show clear signals in soils, peats, lake and sea-bed deposits, coral and tree rings, and glacial ice. However, the caesium and strontium isotopes have half-lives of about 30 years, so their sedimentary signal is short-lived, while caesium and plutonium may be mobile in anoxic conditions (Jeandel 1981). Additional brief spikes of certain isotopes can be used to aid correlation. For instance, an artificial satellite re-entry in 1964 CE provided a distinctive global ^{238}Pu signal, and, more regionally, the Chernobyl and Fukushima reactor accidents produced spikes in 1986 and 2011 CE, respectively. The common natural radioisotope ^{14}C shows greatly elevated values associated with nuclear tests and provides a further clear and long-lasting signal in most growing organic matter such as wood, bone and carbonates including corals, speleothems and also in glacial ice. ^{239}Pu, because of its longevity (half-life of 24,110 years), is a strong candidate as a primary marker of radionuclide deposition as it will remain detectable for ~100 000 years (Hancock et al. 2014) and beyond as the decay product ^{235}U. Alpha-spectrometry carried out during early studies does not differentiate between ^{239}Pu and ^{240}Pu (itself not an issue, as the combined signal is clearly expressed), but is only applicable where Pu concentrations are high – the detection limit is approximately 0.05 mBq of $^{239+240}$Pu (Hancock et al. 2014). Modern ICP-MS techniques can discriminate between these isotopes, although it is necessary to remove interferences from $^{238}UH^{+}$ and other species, and can be used at low Pu concentrations – the absolute limit of quantification is 0.2 µBq and 0.9 µBq for ^{239}Pu and ^{240}Pu respectively (Lindahl et al. 2011). Other mass spectrometric methods, such as Accelerator Mass Spectrometry (AMS) and Thermal Ionisation Mass Spectrometry (TIMS) also allow the simultaneous determination of ^{239}Pu and ^{240}Pu.

ACCEPTED MANUSCRIPT

2.1.3 Biotic markers

Changes in fossil assemblages are used to demarcate most chronostratigraphic boundaries in the Phanerozoic, mainly through recognition of the lowest stratigraphic occurrence of a fossil taxon, which may approximate to its evolutionary origin, although within any individual stratal section the stratigraphic appearance of a taxon more specifically reflects its local immigration to that place. Such stratigraphic appearances (and commonly disappearances too) provide a widely effective tool for correlation. In the Quaternary Period (and especially for the Anthropocene) the time scales involved are generally too short for many evolutionary appearances and disappearances to have taken place, and so immigration/emigration patterns are widely used for biostratigraphic correlation. Prominent Anthropocene biostratigraphic signals are expressed in recently forming sedimentary deposits by the appearance of unique terrestrial and marine species associations of the neobiota ('invasive species'), the result of human transport of tens of thousands of species around the globe. Recent neobiota include examples among common microplankton such as foraminifera, coccoliths, dinoflagellates and radiolarians in the marine realm, of the kind commonly used as microfossils to recognise stage boundaries in pre-Anthropocene deposits of the Cenozoic (Figure 1). These organisms, as well as macroinvertebrates, such as molluscs, vertebrates and plants (both macroplant remains and pollen) can form useful biostratigraphic tools for correlation because of their geologically preservable hard parts such as skeletons, frustules, shells, or phytoliths.

Human-driven extinctions and local extirpations have become increasingly common over the last 500 years, particularly in island faunas (Ceballos et al. 2015). So far, island floras have been more resilient to extinction than island faunas in spite of the high abundance of introduced plant species in many environments (Ellis et al. 2012), but an accumulating

ACCEPTED MANUSCRIPT

extinction debt is likely (Sax and Gaines 2008). Their provincial nature and low abundances mean that island floras provide regional rather than global stratigraphic markers. Selective breeding of domesticated floras and faunas tends to be associated with rapid changes to morphology, in effect forming distinct morphospecies that can be preserved in sedimentary successions. Moreover, species beneficial to humans, such as domestic maize or chickens, tend to be abundant and geographically widespread. The development of factory farming led to massive increases in amounts of faunal remains of domesticated species being deposited in landfills and other terrestrial stratigraphic contexts from the mid-20th century on.

Another extensive stratigraphic signature over recent centuries, but especially since the mid-20th century, reflects neobiota reaching far beyond their original geographical ranges, through deliberate or accidental human actions. Local arrival of these neobiota is well documented through observation, and is often linked with the extinction or extirpation of local fauna and flora, as observed on Kauai, Hawaii (see section 3.5.5), or among benthic foraminifera preserved in the coastal sedimentary record (McGann et al. 2000, Calvo-Marcilese and Langer 2010).

Biostratigraphic signals may also relate to ecological degradation (Willis et al. 2010, Dearing et al. 2012). In marine environments, a long lead-in of low-level and provincialized ecological degradation gave way to accelerating global change in the early 1950s (Wilkinson et al. 2014). The driver was expansion of industrial pollution, expanding human populations associated with increased raw sewage dispersal offshore, and increased use of fertilisers during agricultural intensification. In Northern Hemisphere lakes, an increase in reactive nitrogen from artificial fertilisers has been well-documented (Holtgrieve et al. 2011, Wolfe et

ACCEPTED MANUSCRIPT

al. 2013), giving rise to increases in primary productivity and marked changes to diatom populations and species assemblages, with surface water acidification as an additional factor. The stratigraphic records collated by Smol (2008) commonly show clear mid-20th century inflections in such lacustrine proxies. Runoff contaminated with these fertilisers has also resulted in seasonally oxygen-starved 'dead zones' in lakes and coastal seas, causing – to take just one example - increases in hypoxia-tolerant benthic foraminifera (Wilkinson et al. 2014). Environmental legislation has locally led to a phase of recovery from pollution stressors in the late-20th and early-21st centuries, but increasingly climate change is imposing pole-ward shifts in species distributions and confounding recovery from acidification (e.g. Battarbee et al. 2014).

2.2 Independent dating techniques

Direct numerical dating of a GSSP is not a prerequisite in the selection of a site, but is beneficial. For the Anthropocene, annual resolution for any proposed boundary section is highly desirable, giving a level of precision not available for any other boundary within the Geological Time Scale. The best time resolution for previous GSSPs is for that of the Holocene, with a 2σ uncertainty of ±99 years (Walker et al. 2009).

Counting annual sedimentary laminae in presently accumulating successions, or annual growth layers in living organisms (that are demonstrably complete), is one means of establishing the numerical age, expressed in years, of an Anthropocene base. The age so determined may be additionally constrained by ^{210}Pb, sourced from the atmosphere or directly from sediments (Noller 2000). This isotope is rapidly scavenged from sea and freshwater onto organic detritus, but is not mobile in the sediment. It has a useful dating range of up to 150 years (the half-life is 22.3 years) with a measurement error of about 10%,

ACCEPTED MANUSCRIPT

and is typically used to determine accumulation rates in organic lake, coastal or marine sediments, peats or glacial ice; it is fixed in living plants and corals, too, and so can determine their growth rates.

Other short-lived radioisotopes include ^{234}Th, with a half-life of 24 days, which can be used to date changes in speleothems and corals over periods as short as 3 months, but it has little value for laminae straddling the Holocene–Anthropocene boundary. Radiocarbon (^{14}C) has a half-life of ~5600 years and has limited use as a chronometer from the mid-20th century, but along with ^{137}Cs (half-life 30 years) and ^{90}Sr (half-life ~28 years), it can help to identify specific episodes, such as the 1963–1964 CE peak in atmospheric nuclear tests (the 'bomb-spike') and the 1986 CE Chernobyl accident recorded in sediments, ice, tree rings and corals.

Anthropogenic materials present possibilities for absolute and relative dating not available in earlier geological successions. For example, the date of manufacture of artefacts (technofossils) found as inclusions in strata can often be ascertained with high resolution through the use of type series, and sometimes the precise date is even stamped, moulded, cast, or indelibly imprinted on objects. Such evidence could be immensely valuable in supplementing more traditional dating methods. More generally, the value of using archaeological techniques for relative dating of stratigraphic sequences of terrestrial anthropogenic ground, in conjunction with geological methods, should be considered.

ACCEPTED MANUSCRIPT

ACCEPTED MANUSCRIPT

Marker / Environment	Annual laminae	Novel materials		Geochemical markers									Biotic markers
		Plastics	Fly ash	$\delta^{18}O$	Deuterium &/or dust	CO_2 & CH_4	$\delta^{13}C$	NO_3^- & $\delta^{15}N$	S & SO_4^{2-}	Heavy metals	Organic com pounds	Radiogenics	Extinctions/ neobiota
Anthropogenic deposits		✓	✓				✓	✓		✓	✓	✓	✓
Marine anoxic basin deposits	✓	✓	✓	✓			✓	✓		✓	✓	✓	✓
Coral bioherms & marine bivalve shells	✓	✓	?	✓			✓	✓		✓	✓	✓	
Estuarine & deltaic deposits	✓	✓	✓	✓			✓	✓		✓	✓	✓	✓
Lake depositss	✓	✓	✓	✓			✓	✓		✓	✓	✓	✓
Peat & peatlands (mires)			✓		✓		✓	✓	✓	✓	✓	✓	✓
Ice	✓		?	✓	✓	✓	✓	✓	✓	✓	✓	✓	
Speleothems	✓			✓					✓	✓	✓	✓	
Tree	✓			✓	✓		✓	✓	✓	✓		✓	

Table 2. Potential palaeoenvironmental archives and facies and their stratigraphic markers for a candidate GSSP. ? – uncertain suitability of the specified signal.

ACCEPTED MANUSCRIPT

3. SUITABILITY OF PALAEOENVIRONMENTAL ARCHIVES FOR HOSTING POTENTIAL GSSP CANDIDATES

There is a wide range of sedimentary and biological records within which a GSSP is feasible. For any candidate section, high-precision dating is needed, if only to provide confidence that there are no missing surfaces in successions that are merely decades to centuries long. Such high-precision dating, potentially to annual resolution, can be achieved in seasonally layered sediments in anoxic marine basins and hypoxic lakes, in glacially influenced or hypersaline lakes and sinking marine deltas, in seasonally layered ice and annual growth layers in corals, bivalves, and in speleothems and trees. Non-layered strata, including anthropogenic deposits and peats provide additional environments in which the Holocene–Anthropocene transition may be observed. In this section these key potential archives are discussed in turn, describing their global extent and continuity, and the arguments for or against their potential for hosting a candidate GSSP. Examples are provided to show how key signals are recorded.

3.1 Anthropogenic deposits

This category includes sedimentary successions that have accumulated through direct human deposition (artificial ground) or by human influence on natural systems (Ford et al. 2014). Artificial ground can show a continuum from entirely natural through to entirely anthropogenic materials, but with the key requirement that they have been deposited through human action. Conversely, few “natural” systems are these days free from human modification (Barnosky et al. 2017), whether via construction of dams influencing sediment flux in fluvial systems (Syvitski and Kettner 2011), or trawler fishing disturbing the upper decimetres of sediments on the continental shelf and slope (Martin et al. 2015).

ACCEPTED MANUSCRIPT

Zalasiewicz et al. (2017b) estimated the spatial extent of human modification of the landscape at about 82 x 10^6 km^2, or about 16% of the total Earth's surface or 55% of the terrestrial land surface, providing many sections that could be investigated as potential GSSPs. Road surfaces alone, with a mass estimated at 1.3% of the physical technosphere (*sensu* Zalasiewicz et al. 2017b), comprise an extensive boundary layer in temperate and tropical climates. Anthropogenic deposits may show remarkably high accumulation rates, locally in excess of one metre per year, and rapidly incorporate novel anthropogenic signatures, which may be lithological, geochemical or biotic. This provides a highly resolvable succession in which artefacts and novel materials can be constrained to decadal resolution (Zalasiewicz et al. 2014a).

A potential Anthropocene Series, which would be defined in a unit of strata, and would represent an equivalent Epoch of geological time, is not synonymous with anthropogenic impact. The lower boundary of anthropogenically-modified deposits (or archaeosphere in an archaeological context) may commonly be a marked unconformity, with the overlying first expression of the archaeosphere often being markedly diachronous over millennia (Edgeworth et al. 2015). Such deposits represent a lithostratigraphic – and when one considers technofossils – also a biostratigraphic unit, but not a chronostratigraphic subdivision with a necessarily isochronous basal boundary. The Anthropocene, if it is to be distinguished within these deposits, requires continuous stratiform accumulation of sediments within which a clear signal can be recognised that can distinguish Anthropocene anthropogenic deposits from underlying Holocene anthropogenic deposits. Although such distinguishing signals can be readily found within these deposits, e.g. novel minerals, aluminium, concrete, plastics, organic compounds (Waters et al. 2016, Zalasiewicz et al. 2016a and references therein), the successions overall are typically marked by numerous

ACCEPTED MANUSCRIPT

internal erosion/hiatus surfaces; anthropogenic deposits are mainly formed by intermittent depositional events, lack simple vertical accretionary patterns, and are commonly disturbed by 'anthroturbation'. The pattern of such complex erosional/non-depositional surfaces is of great value for local correlation, and also for correlation over wider areas where exact synchronicity is not required, but hinders precise regional to global correlation (Edgeworth et al. 2015). The typical stratigraphic incompleteness of these deposits also makes them generally unsuitable for hosting a GSSP. Furthermore, they are also mostly terrestrial (although increasingly they are also becoming a feature of the marine realm), making some of them prone to erosion. However, artificial deposits have potential for direct preservation over geological time scales when located on subsiding environments such as major deltas (see section 3.4) and within subsurface excavations (Zalasiewicz et al. 2014b).

Table 3 summarises the key advantages and disadvantages of using anthropogenic deposits and examples of these extraordinarily diverse successions are provided: the Fresh Kills Landfill (New York), Teufelsberg (Berlin) and in Vienna, all of which are examples of artificial ground; and the Gorrondatxe-Tunelboca beachrock (northern Spain), a naturally formed succession comprising mainly artificial materials (Figure 2).

For:	Against:
• Abundant, mainly terrestrial and notably in urban settings • Comparatively thick; rapid accumulation • Independent dating using ^{210}Pb and ^{14}C and historical and archaeological context • Highly resolvable technofossil stratigraphy • Rapid incorporation of novel materials and geochemical signals	• No annual lamination • Limited extent in oceans • Limited lateral continuity • Highly variable deposition rates • Numerous omission surfaces • Prone to erosion and organic degradation • No guarantee of principle of superposition

Table 3. Reasons for and against using an anthropogenic deposit as a potential host for a GSSP.

ACCEPTED MANUSCRIPT

3.1.1 Fresh Kills Landfill, New York

Fresh Kills Landfill on Staten Island (USA) is a former repository for New York City refuse. Covering some 8.9 million m^2, up to 70 m high, and containing ~150 million tons of municipal waste, it may be the largest human-engineered formation in the world (Melosi 2016). It was opened in 1948 CE (Melosi 2016), with a peak influx of garbage reaching 29,000 tons per day (Nagle 2008) and closed in 2002 CE, the last debris being from the 9/11 event in 2001 CE. The deposit rests upon Holocene estuarine marsh deposits, with few intervening pre-mid-20th century anthropogenic deposits, has complex internal patterns, having accreted laterally as the site expanded, and may even have been overturned in places. Its internal complexity precludes it from hosting a functional GSSP.

3.1.2 Teufelsberg, Berlin

Rubble generated in Berlin during World War II was later redistributed in mounds within the city boundary, the largest being the Teufelsberg. The rubble, including concrete, brick, clinker, rock, fly ash, slag and solid chemical waste, was deposited between 1950 and 1972 CE and is up to 80 m thick, with an area of 1.1 million m^2, and an original rubble volume of 26.2 million m^3 (Mielke 2011, Cocroft and Schofield 2012). The Teufelsberg deposit mainly rests unconformably upon Upper Pleistocene sand and till, and these areas would be unsuitable for hosting a GSSP for that reason. But locally, thin Holocene deposits occur between the two units, and here the placing of a GSSP might be considered. The Teufelsberg comprises a distinct, mappable lithostratigraphic unit with a base approximating to that of the Anthropocene, which also extends lens-like across other rubble heaps of the Berlin area (cf. Zalasiewicz et al. 2016a), and these can be correlated through technofossil and novel material inclusions with other such deposits elsewhere. Similar lens-like post-World War II

ACCEPTED MANUSCRIPT

rubble heaps in Germany occur also at Cologne, Dresden, Frankfurt am Main, Hannover, Leipzig, Stuttgart and Munich, and in England in heavily bombed cities such as Coventry.

3.1.3 Vienna, Austria

In the 19th century, Eduard Suess (1862, 1897) mapped urban strata in Vienna as a geological unit (Schuttdecke), which comprised anthropogenic strata formed during development of the Ringstrasse. The deposits typically range from 4 to 5 m in thickness, locally reaching 10–12 m where infilling the former 17th century city moat, and include brick fragments, broken glass, coins, clay jars, and bones of humans and domestic animals. Subsequently, these artificial deposits extended laterally and aggraded vertically, with the newer Anthropocene materials being of distinctively different composition to those described by Suess. The succession of anthropogenic strata below Vienna dates back to the Neolithic, and has been more or less continuous since Roman times, but many unconformities and much reworking make them typically unsuitable for hosting a GSSP.

3.1.4 Gorrondatxe-Tunelboca beachrock, Spain

The Gorrondatxe-Tunelboca beachrock (Figure 2) comprises 1 million tonnes of sediments accumulated since the 1940s. Its source is the 30 million tonnes of blast furnace waste that was tipped offshore between 1902 and 1995 CE (Irabien et al. 2015). Wave activity transported the waste and it re-sedimented as a beachrock deposit about 1.8 km long and 50 to 100 m wide. The succession comprises up to 7 m of deposits of anthropogenic origin, resting on up to 2.5 m of bioclastic beach sands (Martínez-García et al. 2013). The lowermost high-energy open beach deposit pre-dates the discharges of iron slag and has a distinct foraminiferal assemblage (Figure 2). This is overlain by sands with an anthropogenic component, where the foraminifera decrease upwards in abundance (assemblage 2 of Fig. 2), and then decrease in diversity to become largely monospecific (assemblage 3). The

ACCEPTED MANUSCRIPT

decrease in foraminiferal abundance and diversity coincides with the dumping of the iron foundry deposits offshore. The upper deposits comprise a foreshore succession of cemented conglomerate of furnace bricks, foundry slag with an upper sandy deposit that includes plastics (Zalasiewicz et al. 2016a). Internal erosion surfaces are present throughout, as in any beach deposit. Access to the section is good, the site coinciding with the existing GSSP for the Lutetian Stage (Middle Eocene), while the beachrock deposits are recognised as Geosite 96 of the Basque Region. The supply of anthropogenic materials to the shelf ceased in the 1990s, and the beach deposits have started to be eroded by waves, and so have limited potential for long-term preservation. The presence of internal erosion surfaces, the lack of clear lateral continuity, absence of annually laminated deposition, and poor preservation potential of the site make it unsuitable for hosting a candidate GSSP.

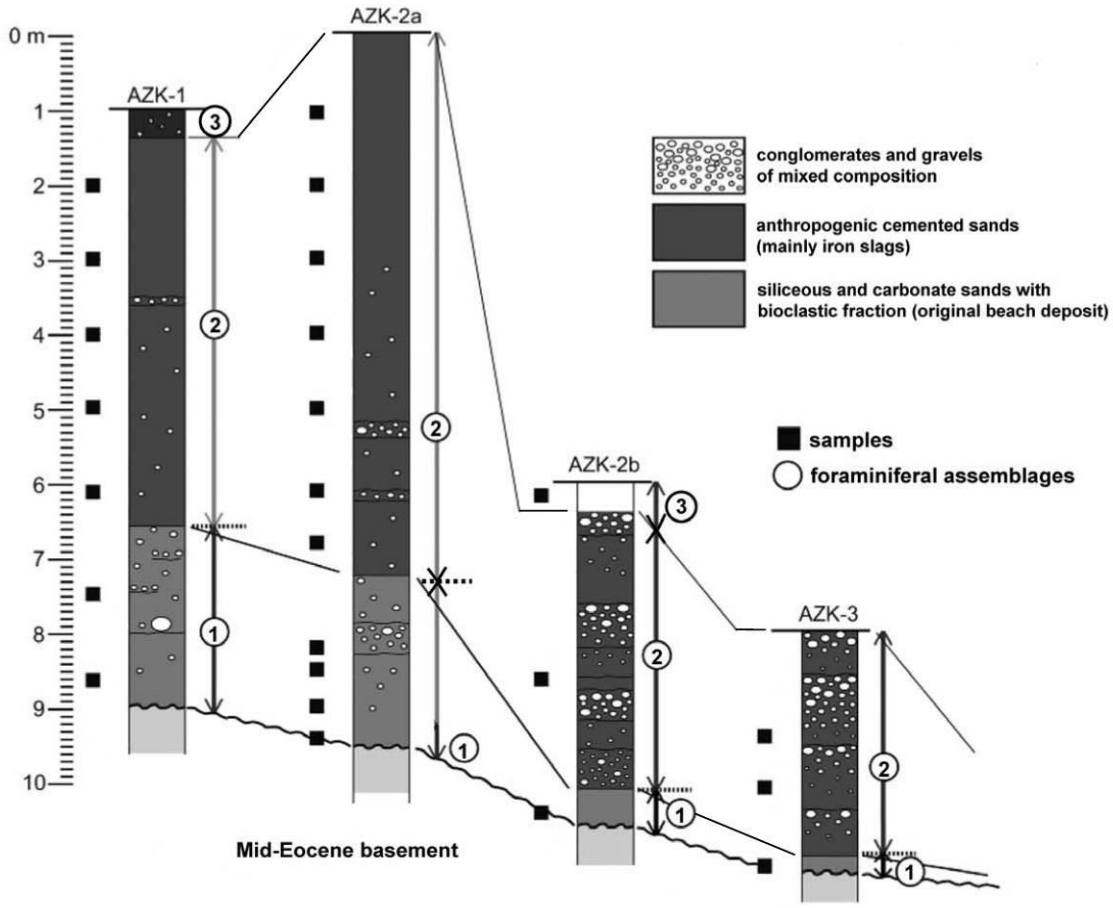

ACCEPTED MANUSCRIPT

Figure 2. Cores through the Gorrondatxe-Tunelboca beachrock, Spain. A natural high-energy open beach sand deposit, pre-dating the discharges of iron slag, is overlain by cemented sandy and coarse beach deposits that are commonly conglomeratic with abundant slag clasts and incorporating littoral foraminifera. Three distinct foraminiferal assemblages are recognised (ranges for assemblages 1, 2 and 3 marked by arrows). Modified from Martínez-García et al. 2013.

3.2 Marine anoxic basin deposits

The oceans where water is >200 m deep comprise about 66% of the Earth's surface, and the sediments that accumulate there might be expected to preserve relatively complete and less disturbed successions compared with those on land or on the continental shelf. However, for deep-ocean deposits to form outcrops on land, rapid rates of uplift are needed and the prospects of such outcrops diminish with increasingly young deposits. Deep marine deposits of the Anthropocene, therefore, almost invariably need to be cored in situ. Cores are not ordinarily used for GSSPs because of their limited material and access, although exceptions were made for the base of the Holocene (Walker et al. 2009), and the proposed base of the Middle Holocene (Walker et al. 2012), both in ice cores. A case might therefore be made for an Anthropocene GSSP in a deep-ocean core. However, deep-ocean deposits often have low sedimentation rates limiting time-stratigraphic resolution, possess few terrestrial fossils, commonly show reduced preservation of calcareous microfossils, and are generally bioturbated, blurring the stratigraphic record in detail. Nevertheless, GSSPs have been located in relatively deep-water facies now preserved in terrestrial cliff sections, as in the Gelasian and Calabrian GSSPs of the Quaternary (Head and Gibbard 2015). Zalasiewicz et al. (2014c) recognised two distinct deep marine systems, the clastic wedges of turbidite fans and contourites that occur adjacent to the continents, and the slowly accumulating deep-sea oozes that lie beyond. In the modern deep ocean, both of these environments may be

ACCEPTED MANUSCRIPT

affected by human activity, directly or indirectly. Anthropogenic modification of river systems, notably through dam construction on major rivers (e.g. Syvitski and Kettner 2011), and trawling on the upper continental slope (e.g. Martin et al. 2015), directly affect sediment supply, as does, indirectly, global warming and resultant rising sea-level. In the abyssal depths the main impacts are: litter, especially plastics (Ivar do Sul and Costa 2014, Zalasiewicz et al. 2016a); organic and inorganic chemical contamination, including radiogenic fallout signals; effects associated with atmospheric CO_2 increase and warming such as variations in pH, dissolved oxygen content and $\delta^{13}C$; and resultant biological changes (Zalasiewicz et al. 2014c, Table 2). Sediment accumulation rates in the deep oceans are typically on the scale of 1–4 mm kyr^{-1} (Tyson and Pearson 1991), with the lowest rates at abyssal depths farther from shore. In such distal settings, the Anthropocene would be sub-millimetric in thickness, with the Holocene represented by just ~10–50 mm.

A suitable marine environment for a GSSP would include rhythmic varves associated with seasonal variation in sediment input that provides exceptionally high temporal resolution (Schimmelmann et al. 2016). For GSSP consideration, such varved successions would need to show little or no disturbance through storm or current activity, bioturbation or trawler fishing, but at the same time be characterised by sufficiently high rates of sedimentation to accumulate an adequate thickness of strata to represent the Anthropocene. Marine anoxic basins appear to be potentially suitable environments, where varve preservation is favoured by oxygen-deficient bottom waters, associated with thermal/or chemical density stratification and enhanced organic accumulation at depth through increased primary productivity in the photic zone, either through coastal upwelling or eutrophication (Schimmelmann et al. 2016).

ACCEPTED MANUSCRIPT

Varved marine anoxic basin successions can be correlated laterally over tens to thousands of kilometres and can record changes to large-scale ocean and atmospheric circulation patterns (Schimmelmann et al. 2016). Marine varved successions are logistically difficult to collect and as a consequence few modern records have received detailed multi-proxy studies including varve counting in coordination with radiometric dating (Schimmelmann et al. 2016).

Marine anoxic/dysoxic basins are mainly semi-enclosed basins where the water mass is isolated from the main shelf, typically below ~100 m and the reach of storm mixing of shelf waters. This can occur in depressions on the continental shelf (e.g. the Santa Barbara and Cariaco basins), in fjords, (e.g. Saanich Inlet and Saguenay Fjord) or in enclosed seas, (e.g. the Black and Baltic seas), but areas with periodic anoxia can also occur on an open shelf (e.g. Middle Atlantic Bight, northern Gulf of Mexico, Namibia, Peru) (Tyson and Pearson 1991, Figure 3), or on a continental slope on which impinges a well-developed anoxic oxygen-minimum zone (southeastern Pacific off Peru, northwestern Arabian Sea).

De-oxygenated dead zones currently occur over ~245,000 km^2 of the coastal oceans (Diaz and Rosenberg 2008), or about 0.7% of the sea floor. The number of these dead zones has approximately doubled each decade since the 1960s (Diaz and Rosenberg 2008). About half of them are the consequence of eutrophication through runoff of fertilisers into the sea, increased primary productivity and enhanced organic flux to the sea bed (Diaz and Rosenberg 2008), and so they tend to occur offshore or downriver from populated areas (Figure 3). Most dead zones are currently seasonal, tending to occur in the summer after spring blooms, when the water is warmest and stratification is strongest (Diaz and Rosenberg 2008). Autumn storms bring a temporary return of benthos, disrupting seabed stratification. Only ~8% of dead zones are persistent (Diaz and Rosenberg 2008), these areas

ACCEPTED MANUSCRIPT

experiencing the least sediment bioturbation, though in open oceans these seem not yet to have developed varves. Sediments of modern dead zones are a local expression of Anthropocene-related conditions, and identifiable by changes in geochemical character and fauna (Diaz and Rosenberg 2008), but they seem unlikely to provide good potential for candidate GSSPs, as they typically rest on the bioturbated deposits of the earlier more consistently oxygenated sea floor.

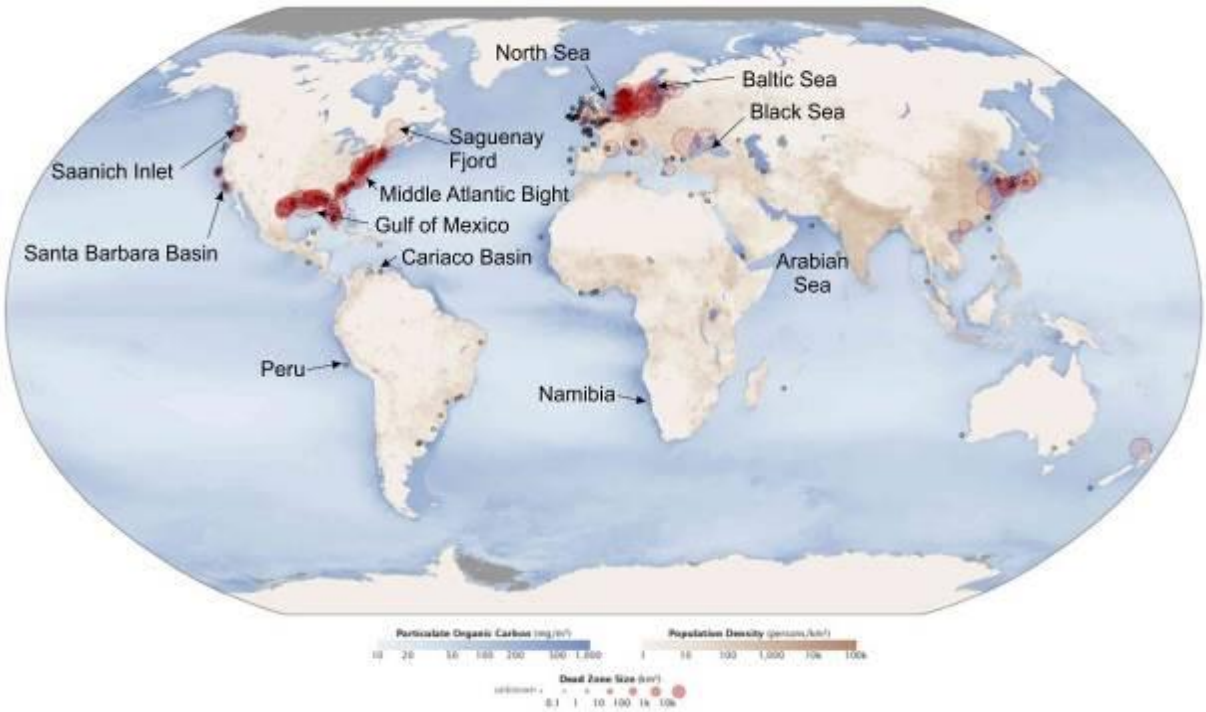

Figure 3. Location of marine dead zones (from NASA Earth Observatory https://earthobservatory.nasa.gov/IOTD/view.php?id=44677; Aquatic Dead Zones generated 17th July 2010). Red circles show the location and size of the dead zones. Black dots show where dead zones of unknown size have been observed. The distribution commonly occurs adjacent to populous land areas (shown by the brown scale), but not to upwelling zones (shown by concentration of particulate organic carbon, in blue scale).

Litter from ships is now seen in most sea floor surveys (Ramirez-Llodra et al. 2011). Clinker, from coal burnt to power steam-ships, was extensively dumped on the sea floor from ~1800

ACCEPTED MANUSCRIPT

to ~1950 CE (Ramirez-Llodra et al. 2011), and may form a useful signal for latest Holocene strata. Much power station fly-ash and clinker has also been dumped at sea, e.g. Blyth power station ash into the North Sea, UK (Bamber 1980). Plastics and aluminium largely date from after 1950 CE, with land-derived microplastic beads and plastic fibres now a near-universal component of low-energy modern marine sediments (Ivar do Sul and Costa 2014, Zalasiewicz et al. 2016a). With about 4.9 billion tons discarded (which is 60% of all plastics produced since 1950) in geologically unstable waste dumps to uncontrolled deposition in terrestrial, aquatic and marine environments (Geyer et al. 2017), the quantity of plastic debris entering the oceans was estimated at 4.8−12.7 million tonnes in 2010 CE (Jambeck et al. 2015) and might strongly increase in the future. However, little work has been done to profile its stratigraphic distribution in marine sediment cores.

Table 4 summarises the key advantages and disadvantages of marine anoxic basin deposits for hosting a potential GSSP. Well-studied examples (explored below) include the Santa Barbara Basin (California), Black Sea, Saanich Inlet (Canada), Saguenay Fjord (Canada) and Cariaco Basin (Venezuela).

For:	Against:
• Undisturbed laterally extensive varves (below storm base) correlatable within basins • Independent ^{210}Pb and ^{14}C dating • Anoxic/dysoxic/hypoxic, no/little benthic bio /anthroturbation • Modification of fluvial input to oceanic basins • Clinker ash from steam-powered ships ~1850-1950 CE; microplastics signal post-1950 CE • Coastal eutrophication since mid-20th century • High organic and clay components scavenge contaminants from water column e.g. metals, radionuclides and POPs • Global radionuclide signal (e.g. ^{239}Pu, ^{14}C)	• Restricted extent (~0.7% of oceans) • Possibility of missing/additional laminae in near-coastal settings due to turbidite events • Thin strata, e.g. last 75 years <20 cm for the for Santa Barbara Basin and 75 cm for Saanich Inlet • Potential decadal time delay for Pu/metal contaminants to reach sea-bed (but settling velocity of ~2000 m yr^{-1} if present as grains, see Kowalski et al. 2016) • Difficult and costly environment to collect samples without disturbance of youngest laminae

ACCEPTED MANUSCRIPT

• Planktonic foraminifera and diatoms as bio/geochemical signals	

Table 4. Reasons for and against using a marine anoxic basin deposit as a potential host for a GSSP.

3.2.1 Santa Barbara Basin, California

The Santa Barbara Basin lies 100 km west of Los Angeles, USA (Figure 3), at depths of up to 590 m. Varves comprise dark terrigenous laminae derived from greater winter river runoff alternating with paler summer bloom laminae with diatoms (mainly *Chaetoceros*), planktonic foraminifera, radiolaria and silicoflagellates (Koide et al. 1975, Field et al. 2006, Barron et al. 2015), reflecting seasonal NW winds that cause upwelling and increase biogenic productivity (Barron et al. 2015). Varves have been dated using ^{210}Pb (Krishnaswami et al. 1973, Koide et al. 1975) and radiocarbon AMS (Schimmelmann et al. 2013). Before 1700 CE some drought years did not produce varves, with intermittent oxygenation events causing bioturbation, but from the 18th century to the present the lamina have been shown to be consistently annual and without gaps (Hendy et al. 2013, Schimmelmann et al. 2013). Strata below the upper ~1 cm are highly anaerobic so there is little bioturbation of the laminae or leaching of Pu (Koide et al. 1975). A distinct 1841 CE bioturbated layer is associated with a flood and turbidite event (Hendy et al. 2013). There are no flood event deposits younger than 1930 CE (Krishnaswami et al. 1973), as dam construction along rivers feeding into the basin began in 1912 CE, limiting sediment supply. Despite this, there has been substantial sediment flux since 1928 CE (Krishnaswami et al. 1973, Figure 4b), with a post-compactional thickness of ~0.5–3 mm per lamina, the diatom ooze lamina component being up to 2 mm thick (Schimmelmann et al. 2016).

The high organic carbon (3–5%) and clay fractions of the sediments scavenge heavy metals, including Pu, from seawater. The $^{239+240}$Pu concentrations initially rise in 1945–1949 CE

ACCEPTED MANUSCRIPT

varves, exceeding background values in the 1950–1954 CE varves (Figure 4a), and continuing to rise into the 1970s (latest data available), with no sign of a distinct 1963−1964 CE bomb spike (Koide et al. 1975), perhaps reflecting the slow settling of Pu in deep water. Radiogenic particles settle only slowly through the water column, at 12.5 m yr^{-1} in the western Pacific (Livingston et al. 2001). But when such particles are bound within marine snow/faecal pellet aggregates they sink more quickly, at an estimated 74−39 m day^{-1} in the Santa Barbara Basin (Alldredge and Gotschalk 1988), allowing rapid transmission to the sea-floor. The continued rise of the Pu signal after the 1963−1964 CE bomb spike likely reflects reworking of terrigenous fallout into the basin (Koide et al. 1975), suggesting the first $^{239+240}Pu$ signal above background, rather than a peak value, as a possible primary marker for the Anthropocene (Zalasiewicz et al. 2015). An ancillary radiogenic signal of ^{238}Pu, sourced from the Snap 9A satellite burnup in 1964 CE, does show a 1964 CE peak (Koide et al. 1975, Figure 4a), suggesting both little mobility of Pu within the sediment and little reworking of that radioisotope.

Heavy metal signals in the basin are complex. A rise in Pb concentrations from 1931 CE (Figure 4c) is due to airborne particulates from leaded gasoline, derived from increased automobile use in Los Angeles, with levelling off from the 1970s representing introduction of unleaded gasoline (Schmidt and Reimers 1991). Cu values increase notably from about 1960 CE, probably industrially sourced via sewage outfalls (Schmidt and Reimers 1991). Reduced anthropogenic input, in the case of Cd since the 1970s, may reflect improved sewage treatment (Schmidt and Reimers 1991).

Among organic geochemical signals, a significant oil spill from a production well in 1969 CE increased Total Organic Carbon (TOC) values, generating a distinctive hydrocarbon signature

ACCEPTED MANUSCRIPT

(Hendy et al. 2015). Polychlorinated biphenyls (PCBs) appeared in the basin sediments about 1945 CE, the DDT pesticide breakdown product DDE [1,1-dichloro-2-2-bis(p-chlorophenyl) ethylene] first appearing ~1952 CE. Concentrations of both show a progressive increase through to 1967 CE (Hom et al. 1974); they may be sourced from sewage outfalls and surface runoff, while DDE can also arrive via atmospheric fallout (Hom et al. 1974).

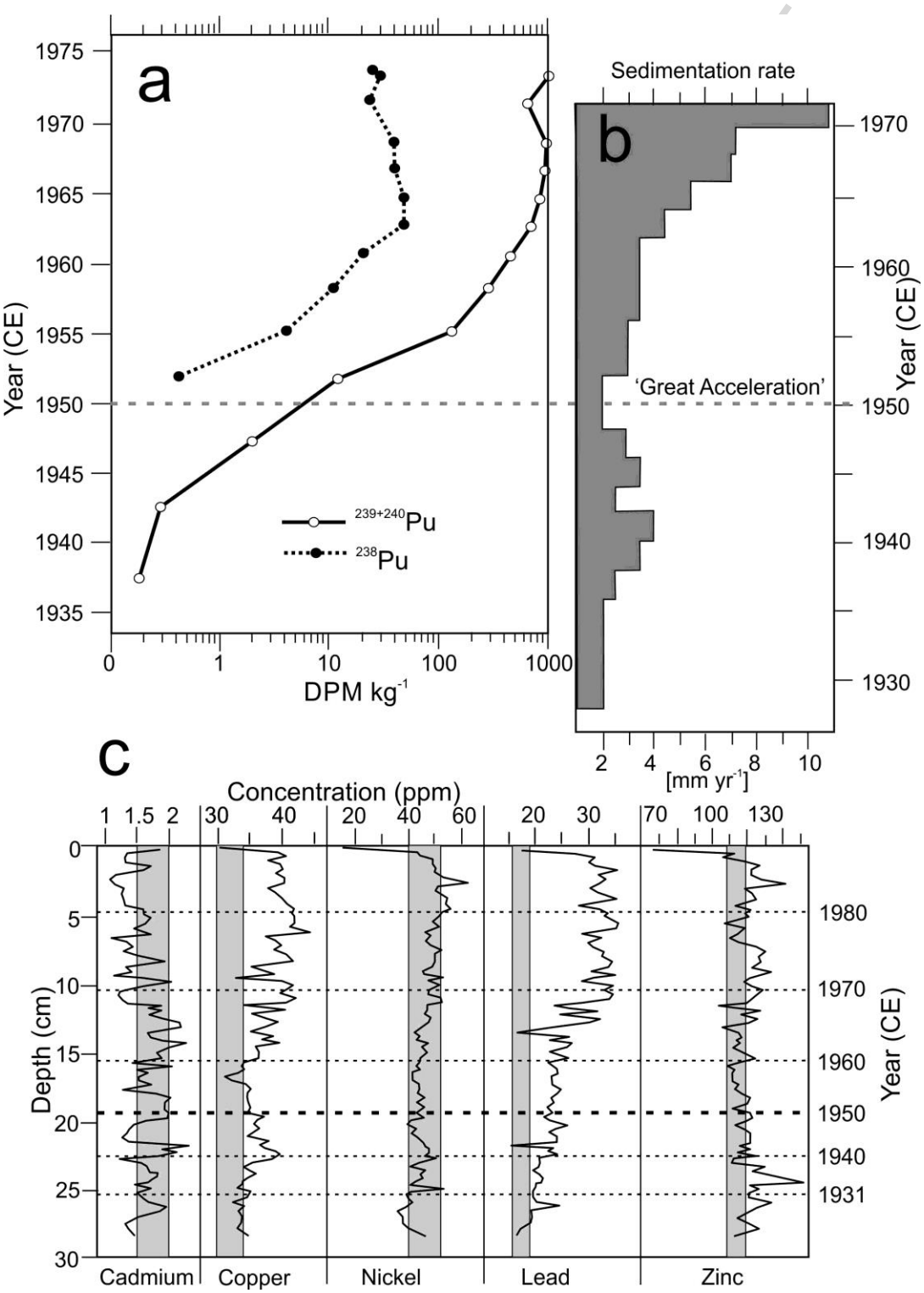

ACCEPTED MANUSCRIPT

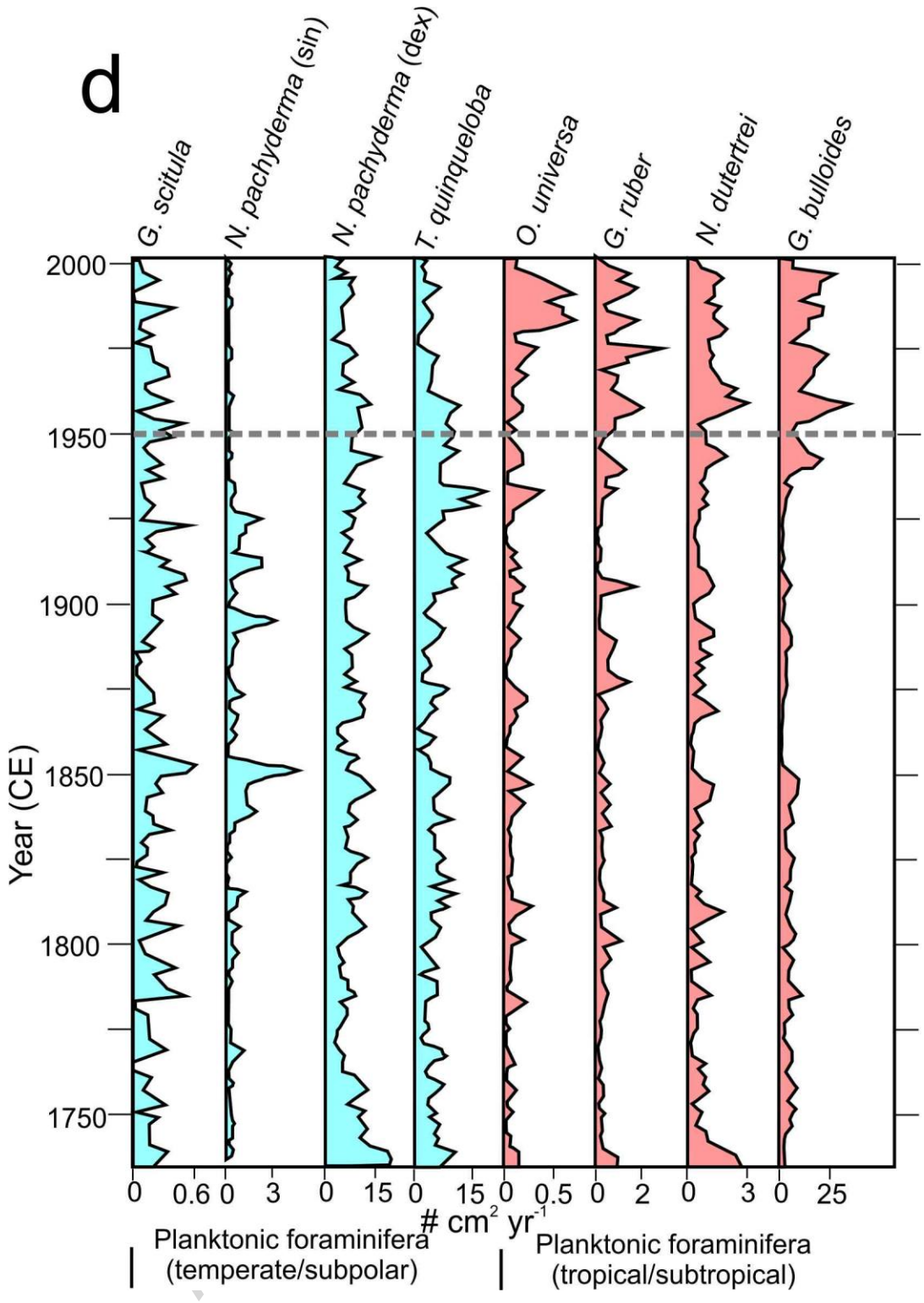

Figure 4. Key signals in marine cores from the Santa Barbara Basin, with a) Pu signal (Koide et al. 1975), b) variations in sedimentation rates (Krishnaswami et al. 1973), c) selected heavy metals (Schmidt and Reimers 1991) and d) planktonic foraminifera (Field et al. 2006).

ACCEPTED MANUSCRIPT

The basin is located close to the boundary between the subarctic and subtropical gyres, the planktonic foraminiferal assemblages reflecting the dominance of one or other of these gyres (Barron et al. 2015). In a 1400-year dataset, decadal-scale fluctuations (the Pacific Decadal Oscillation) dominate, the two assemblages co-varying until 1959 CE (Figure 4d), after which there is increasing abundance of tropical/subtropical species, especially after the mid-1970s (Field et al. 2006). A complementary decrease in temperate/polar species in the late-20th century indicates the penetration of deep warm waters (Field et al. 2006). Evidence of such pronounced warming is not seen earlier in the record, not even during the Medieval Climate Anomaly (Barron et al. 2015). This warming is thought to reflect widespread change in the Northern Pacific in the mid-1970s, with greater cyclonic activity of the Aleutian Low Pressure System and warming in the eastern North Pacific (Field et al. 2006). Observed decreases in algae, zooplankton (which show 80% decline between 1951 and 1993 CE), fish and seabird abundance have also been related to this temperature increase (Roemmich and McGowan 1995).

3.2.2 Black Sea

The Black Sea is an enclosed silled basin with an area of 422,000 km^2 and a maximum depth of 2212 m (Florea et al. 2011). The water column is stratified, with the pycnocline and halocline both occurring at about 75 m depth in the centre of the basin and 200 m at the margins, and marking the boundary between oxygenated water above and euxinic, H_2S-saturated and saline deeper waters below (Arthur et al. 1994, Florea et al. 2011). At the seafloor, there is a topmost gelatinous flocculent surface layer about 2 cm thick overlying a further 2 cm of unlaminated grey/white carbonate-rich sediment (Pilskaln and Pike 2001). The underlying unit (Unit I) is 25–45 cm thick and represents 1633 ± 100 years of sedimentation, based upon varve chronology (Arthur et al. 1994). This unit, present in the

ACCEPTED MANUSCRIPT

deeper parts of the basin, contains varves averaging 0.2 mm thick, consisting of thicker white carbonate-rich summer/autumn laminae with abundant *Emiliania huxleyi* coccoliths alternating with thinner grey clastic-rich laminae deposited from spring and winter river runoff (Arthur et al. 1994, Pilskaln and Pike 2001, Schimmelmann et al. 2016). Black organic-rich laminae with biogenic metal sulphides occur between the carbonate and terrigenous laminae (Pilskaln and Pike 2001, Schimmelmann et al. 2016). The top flocculent layer is thought to be a permanent transition zone that hydraulically sorts particles by density (Pilskaln and Pike 2001).

The varves have been independently dated using ^{210}Pb, ^{137}Cs and ^{14}C AMS, although the latter commonly gives older ages due either to the presence of "dead" carbon in Black Sea sediments or missing varves (Arthur et al. 1994, Pilskaln and Pike 2001, Florea et al. 2011). Although the highest countable varves beneath the flocculent layer date to about 1918 CE (Arthur et al. 1994), Florea et al. (2011) discerned the 1986 CE Chernobyl ^{137}Cs signal at between 5 and 10 mm depth (in samples collected in 2004 CE), which agrees with a ^{210}Pb-dated accumulation rate of 0.49 ± 0.03 mm yr^{-1}. Groups of varves in Unit I have been correlated across the entire deeper basin (Arthur et al. 1994), with no sign of erosion by interbedded cm- to dm-scale fine-grained turbidite layers (Arthur et al. 1994).

3.2.3 Saanich Inlet, Canada

Saanich Inlet is a 24 km long, up to a ~240 m deep, silled fjord in Vancouver Island, Canada, in which the water column shows stratification by density, salinity and temperature, with deep anoxic water containing hydrogen sulphide (Schimmelmann et al. 2016). Bottom water renewal is restricted to brief episodes of coastal upwelling during late summer, with H_2S otherwise present in water as little as 120 m deep (Anderson et al. 1989). Maximum river

ACCEPTED MANUSCRIPT

discharge and minimum salinity occur during summer months (McQuoid and Hobson 1997). Modern sediments include varves in which pale diatomaceous laminae (1.5–17 mm thick), with distinct seasonal assemblages, alternate with terrigenous silty clay laminae (0.5–6 mm thick) deposited in winter (Dean et al. 2001, Dean and Kemp 2004). The varves have been independently dated using ^{210}Pb, ^{137}Cs and ^{14}C (Matsumoto and Wong 1977, McQuoid and Hobson 1997). Laminated intervals during the Holocene are punctuated by massive debris flow event beds (Dean et al. 2001). Laminae dated from 1950 CE have been recognised at a depth of about 75 cm (McQuoid and Hobson 1997).

Biostratigraphic indicators include the invasive diatom *Rhizosolenia setigera*, abundant in autumn blooms (Dean et al. 2001), and introduced in the early 1940s through the arrival of aquaculture species and/or from ship ballast waters, both potential sources increasing in the 1930s and 1940s (McQuoid and Hobson 1997). This invader partly supplanted the species *Thalassiosira gravida* and *Chaetoceros diadema*, which were more abundant prior to the 1930s to 1940s, the assemblages also reflecting increased logging, farming and urbanization, especially from the 1930s (McQuoid and Hobson 1997). Sinking rates of these organisms, when present in aggregates, may reach 50 to 100 m day^{-1} (McQuoid and Hobson 1997 and references therein) meaning that the biotic signal in varves is highly responsive to seasonal changes in abundance in the surface waters. The stratigraphic record shows an abrupt regional climate shift in 1976/1977 CE, with the modern Pacific Decadal Oscillation changing to 22-year periodicity, in contrast to ~15-year periodicity recorded over the previous 2100 years (Dean and Kemp 2004).

Heavy metal residence times in the water column of the inlet are an estimated 0.08 years for ^{210}Pb, 0.07 years for stable Pb, 0.3 years for Cu, 3 years for Cd, and 2 years for Hg

ACCEPTED MANUSCRIPT

(Matsumoto and Wong 1977). This indicates a near-synchronicity of the influx of Pb into the inlet and its subsequent accumulation in the sediments.

3.2.4 Saguenay Fjord, Canada

The Saguenay Fjord, Quebec, Canada, is a submarine valley, 93 km long and 1–6 km wide which links to the St. Lawrence Seaway via a shallow, 20 m deep sill (Gagnon et al. 1997). The fjord comprises two distinct basins with a deeper and larger landward basin up to 275 m deep and a seaward basin up to 250 m deep (Gagnon et al. 1997). The succession is dated with ^{210}Pb and ^{137}Cs (Loring et al. 1983, Smith and Levy 1990). Sediment accumulation rates in the landward basin are 0.2–0.4 cm yr^{-1} (Smith and Walton 1980). The deeper waters are generally saline, well-mixed and oxygenated with the redox boundary present a few centimetres below the sediment surface (Gagnon et al. 1997), but organic-rich effluent from pulp and paper mills produces anoxic, unbioturbated sediments at the head of the fjord (Smith and Levy 1990), making that location more suitable as a potential GSSP target locality.

The Saguenay Fjord has been affected by industrial and municipal waste discharges since the 1930s (Loring et al. 1983, Smith and Levy 1990). Very high Hg concentrations, and significant Zn, Pb, V and Cd contamination are evident in fjord sediments dating from 1948 CE, with peak values in the early 1960s and early 1970s (Loring et al. 1983, Gagnon et al. 1997). Most of the Hg is bound to organic matter (Loring et al. 1983), limiting Hg diffusion through the sediment (Gagnon et al. 1997). The oxidized surface sediments inhibit transfer of Hg to the overlying bottom waters, although surface bioturbation may reduce the efficiency of this barrier (Gagnon et al. 1997). Sustained high Hg values suggest resuspension of the Hg by spring runoff or frequent submarine mass flow events (Gagnon et al. 1997). A time lag of a

ACCEPTED MANUSCRIPT

few months at the head of the fjord and 10–15 years at the seaward end (Loring et al. 1983) makes the Hg signal markedly diachronous.

Polycyclic aromatic hydrocarbon (PAH) concentrations gradually increase in 1926 CE above pre-industrial levels, with dramatic increases in the 1940s after major expansion of aluminium production (Smith and Levy 1990). The PAHs in sediments are mainly scavenged from the water column by organic matter (Smith and Levy 1990).

3.2.5 Cariaco Basin, Venezuela

The Cariaco Basin off Venezuela comprises two euxinic sub-basins of >1400 m depth separated by a 900 m-deep saddle. It contains a stratified water column, with a thermocline and a chemocline between 250 and 375 m deep separating oxic waters above from anoxic waters below (Schimmelmann et al. 2016). The basin has been anoxic since about 12.6 ka BP (Hughen et al. 1996). Euxinic bottom waters are associated with sediments including varves (~0.9–3 mm thick, average 1.3 mm) of pale, biogenic (mainly diatoms) winter/spring laminae rich in planktonic opal, carbonate and organic matter accumulated during arid conditions when upwelling develops, and dark, siliciclastic summer/autumn laminae deposited during times of increased runoff, when there is enhanced input of Saharan dust and reduced upwelling (Hughen et al. 1996, Schimmelmann et al. 2016). Microbioturbation is ubiquitous, but generally only slightly disrupts the laminae (Hughen et al. 1996). The varves have been independently dated using ^{210}Pb, ^{137}Cs and ^{14}C AMS (Hughen et al. 1996). Microturbidites a few mm thick occur throughout, with two distinct turbidites dated to 1897 ± 5 and 1932 ± 4 CE, likely earthquake-triggered, with the older turbidite possibly having eroded a few centimetres of underlying varves (Hughen et al. 1996, Schimmelmann et al. 2016).

ACCEPTED MANUSCRIPT

3.3 Coral bioherms, calcified sponges and marine bivalve shells

Shallow-water coral reefs extend over only about 0.1–0.2% of the oceans, and are limited to the tropics, but they contain a large proportion of marine biotic diversity (Figure 5a). They were first impacted by humans via decreasing diversity of large marine animals beginning around 3.5 ka BP, a trend which accelerated during the Industrial Revolution and especially since 1950 CE (Pandolfi et al. 2003, Hoegh-Guldberg 2014). Widespread bleaching of tropical coral reefs in response to rising sea temperatures started in 1979 CE and has subsequently increased in frequency and severity (Hoegh-Guldberg 2014, Hughes et al. 2017). Other significant stressors, including increased turbidity of marine waters due to increased runoff, rises in pollutants, eutrophication and acidification, and severe overfishing, including the dynamiting of reefs by fishermen, have contributed to a 50% reduction in the abundance of reef-building corals over the past 40–50 years. Over the next several decades, this may lead to the collapse of whole reef systems, as happened during mass extinction events of the geological past (Hoegh-Guldberg 2014).

ACCEPTED MANUSCRIPT

ACCEPTED MANUSCRIPT

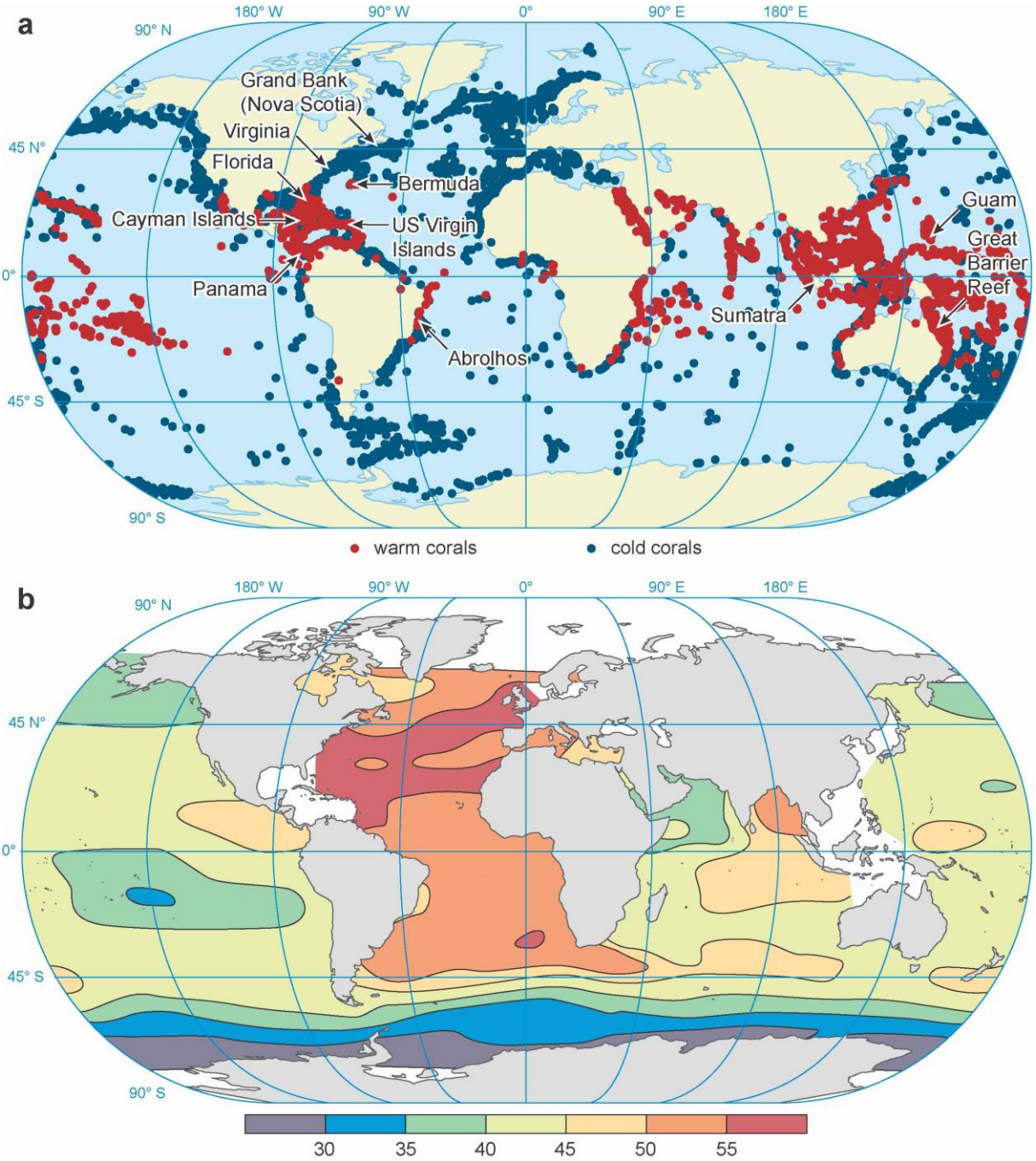

Figure 5. a) Distribution of shallow-water framework-building coral reefs (from NOAA: Where Are Reef Building Corals Found http://oceanservice.noaa.gov/education/tutorial_corals/coral05_distribution.html and cold-water corals (from Freiwald et al. 2017) and b) the inventory of anthropogenic CO_2 (µmol CO_2/kg) in surface waters (from Swart et al. 2010).

Although reef systems as a whole are undergoing significant change, indicating their importance for recognising anthropogenic impacts, individual reefs are complex and non-stratiform. Consequently, it is not a reef as a whole that should be considered as hosting a

ACCEPTED MANUSCRIPT

potential GSSP, but one of the long-lived coral bioherms within it that shows annual growth bands. In the Great Barrier Reef, fluorescent banding reflects seasonal-interannual variations in fluvial discharge of organic compounds (Isdale 1984). The annual laminae can be independently dated using ^{210}Pb and ^{14}C. Key correlatory signals include Pu radionuclide fallout, the ^{13}C Suess effect and uptake of pollutants, in particular heavy metals (Figure 6a).

Cold-water growths of aragonitic scleractinian corals and proteinaceous corals are smaller than the tropical reefs, and occupy a range of latitudes and of water depths – from a few metres to abyssal depths (Figure 5a). Such corals also imprint the Suess effect, radiocarbon and heavy metal signals, and individual cold-water corals can be long-lived. But, those from deep waters contain banding that is not necessarily annual, and ages can only be reliably provided through radiometric dating (Lee et al. 2017). Long-lived bivalves, which also occur in cold waters, also record proxy environmental signals including water temperature and the radiocarbon fallout bomb-spike, though they occupy a smaller depth range (up to ~300 m depth, exceptionally up to 500 m) than cold-water corals.

Calcified sponges (or sclerosponges), found living in water depths up to 145 m, are known to provide good proxy records of water temperature and salinity, secreting their skeletons without some of the vital effects seen in corals and clearly showing the Suess effect on carbon isotopes (Figure 6a). They provide records stretching up to 1000 years, much further back in time than many corals (Swart et al. 1998). However, they are very slow growing (~0.22–0.27 mm yr^{-1}) with living tissue accounting for 3 to 4 years of growth; consequently despite some species showing growth banding, evidence that this is annual is equivocal and ^{14}C- and ^{210}Pb-dating are required to determine ages (Swart et al. 1998). As such, they seem

ACCEPTED MANUSCRIPT

to provide a lower resolution and hence less suitable host for a GSSP than corals or bivalves (see section 3.3.6).

Table 5 summarises the key advantages and disadvantages of using coral laminae in tropical reef bioherms and cold-water corals and bivalve shells for hosting a potential GSSP. Up to now, research on corals has rarely provided multi-proxy signals, so the examples provided below focus on the specific signatures where research has been done.

For:	Against:
• Seasonal growth bands, with large growth rates in shallow-water corals • Independent dating using ^{210}Pb and ^{14}C • Microplastic ingestion in corals, e.g. Great Barrier Reef • Temperature recording ($\delta^{18}O$ and Sr/Ca) in corals and bivalves; bleaching events in corals beginning 1979 CE • $\delta^{13}C$ Suess effect mirrors anthropogenic CO_2 ocean inventory • Shallow water corals with rapid uptake of radionuclides and contaminants • Heavy metal enrichment is coral-species specific and more sensitive than adjacent sediments	• Shallow, warm-water corals limited to tropics; deep-water corals and bivalves provide greater geographical spread • Reefs are complex structures; signal defined on individual coral or bivalve • Deep-water corals are affected by a ~25 year lag in $\Delta^{14}C$ and Pb records compared with shallow-water corals • No GSSP precedent of using living/deceased coral or bivalve

Table 5. Reasons for and against using a coral or bivalve shell as a potential host for a GSSP.

3.3.1 Caribbean ^{13}C Suess effect and heavy metal concentrations

Scleractinian corals mirror changes in the anthropogenic CO_2 inventory of surface oceans (Figure 6a). In a global comparison of rates of change of $\delta^{13}C$ in coral skeletons between 1800 and 2000 CE (Swart et al. 2010), 64% showed a marked decrease from the mid-20th century, attributed to the addition of anthropogenically derived CO_2 (the ^{13}C Suess effect). The decrease was greatest in areas of largest input of anthropogenic CO_2 (Figure 5b) and, in

ACCEPTED MANUSCRIPT

Florida and elsewhere in the Caribbean, from 1960 to 1990 CE, was comparable to the carbon isotopic decrease in atmospheric CO_2 (Swart et al. 2010, Figure 6a). A marked inflection of $\delta^{13}C$ values is seen at about 1955 CE in Atlantic corals and sclerosponges, comparable to the $\delta^{13}C$ inflection seen in Law Dome ice core from the Antarctic (Figure 6a). The rate of change is more variable and less pronounced in the Indian and Pacific oceans (Swart et al. 2010). There is an average air–sea equilibration time of about 1 year for the anthropogenically derived CO_2 (Key et al. 2004), resulting in a minimal signal lag in surface waters. However, anthropogenic CO_2 concentrations decrease with depth, and at about 1000 m water depth the signal is only discernible in the North Atlantic (Key et al. 2004), suggesting either a significant lag or lack of transport to these depths. Shallow-water corals thus provide a more effectively correlatable stable carbon isotope signal than do records from deep marine environments such as deep anoxic basins.

ACCEPTED MANUSCRIPT

ACCEPTED MANUSCRIPT

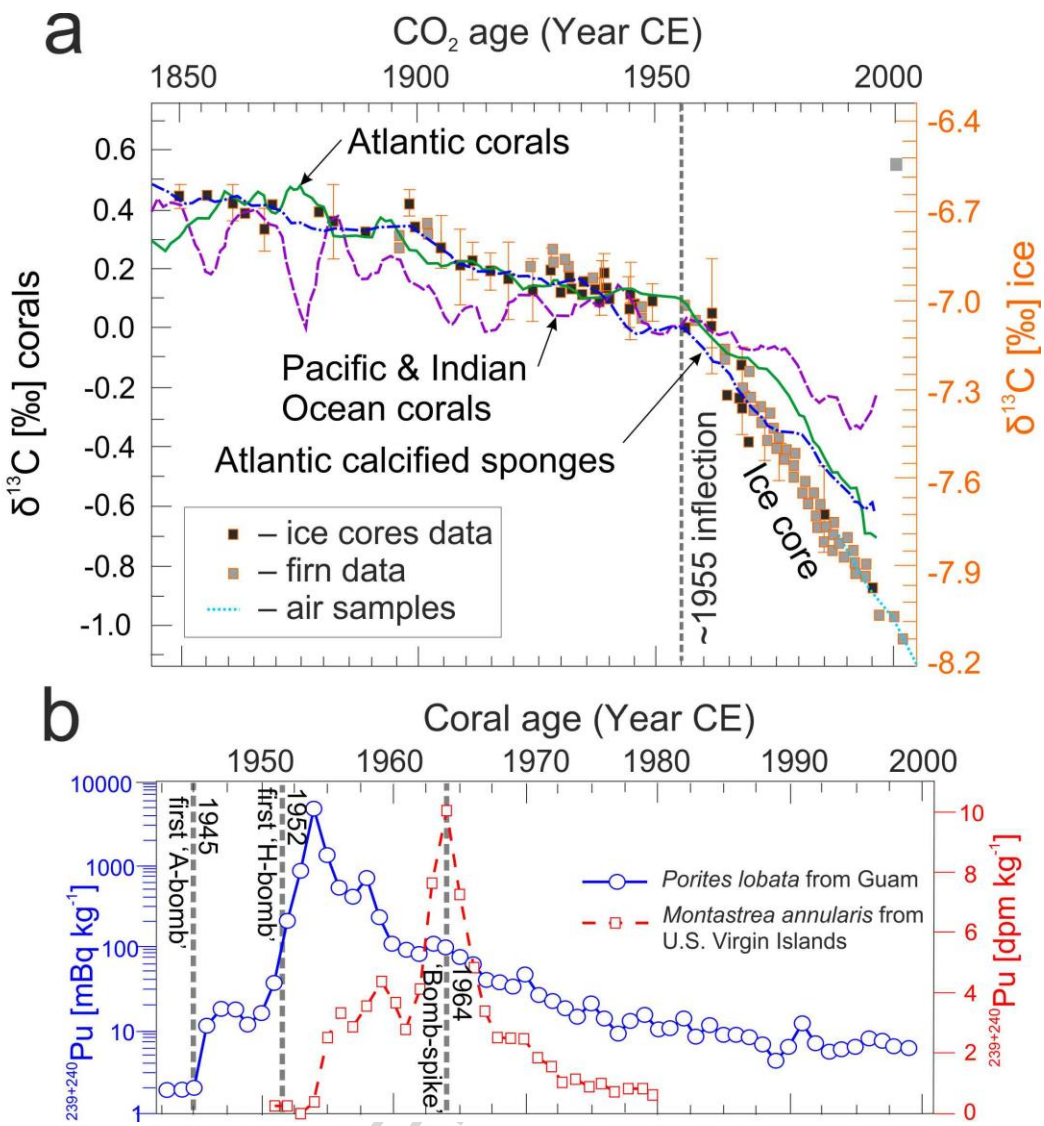

Figure 6. a) Changes in $\delta^{13}C$ with respect to age for corals from the Atlantic and the Pacific/Indian oceans compared to published data from Atlantic calcified sponges, averaged after removing the mean $\delta^{13}C$ value of the coral skeleton from 1900 CE to the present day and shown as a five-year running mean (Swart et al. 2010). This is compared with $\delta^{13}C$ data from Law Dome ice core (Rubino et al. 2013) which show a ~1955 CE inflection; b) $^{240+239}Pu$ concentrations in annual growth bands from *Porites lobata* in Guam (Lindahl et al. 2011) and *Orbicella* (*Montastrea) annularis* in the U.S. Virgin Islands (Benninger and Dodge 1986); dpm kg^{-1} = decays per minute per kilogram; mBq kg^{-1} = millibecquerel per kilogram.

Heavy metal concentrations in Panama tend to be higher in nearshore coral reefs and also in certain species such as *Porites furcata,* and show greater concentrations than in nearby

ACCEPTED MANUSCRIPT

sediments (Berry et al. 2013). Humans have increased the flux of Pb by at least a factor of 10, with rapid and widespread dispersal of Pb into the atmosphere as aerosol particles, and a short residence time of two years within ocean waters (Boyle et al. 2014), which makes Pb potentially suitable as a stratigraphic marker. Of the oceans, the North Atlantic Ocean is most affected by Pb emissions from the Industrial Revolution and subsequently it is this region that has seen most research (Boyle et al. 2014). Corals in Bermuda (Kelly et al. 2009, Figure 7c) show an initial rise of Pb following exploitation of the Upper Mississippi Valley lead-zinc ore in the USA, with an initial peak in lead mining in 1840–1848 CE, followed by a clear increase that began in the late-1940s due to greater consumption of leaded gasoline, peaking in the 1970s following US environmental legislation (the US Clean Air Act of 1970, Boyle et al. 2014). Pb in gasoline from the USA typically has $^{206}Pb/^{207}Pb$ ratios >1.17 as compared to European Pb with ratios <1.15 (Boyle et al. 2014). This is expressed in the Bermuda corals, although the signal is complex, reflecting the different histories of leaded gasoline consumption and legislation in the USA and Europe (Bollhöfer and Rosman 2001). Higher $^{206}Pb/^{207}Pb$ ratios seen in Bermuda until the late-1970s (Figure 7d) are considered sourced from US gasoline, while the markedly lower ratios in the 1980s and 1990s reflect a European source (Kelly et al. 2009). Pb settles only slowly into deep oceanic waters, as seen off Bermuda (Boyle et al. 2014), but this is not a significant factor in contamination of corals at shallow water depths.

The Pb signal shows global heterogeneity. In the Indian Ocean, significant Pb contamination started in the western Sumatra region around the mid-1970s, with increasing Pb/Ca ratios and decreasing $^{206/207}Pb$ and $^{208/207}Pb$ ratios around that time, trends that continue into the 21st century (Lee et al. 2014). Pb emissions from China and SE Asia continue to increase (in

ACCEPTED MANUSCRIPT

contrast to the pattern in areas fringing the North Atlantic), sourced from coal consumption (Boyle et al. 2014).

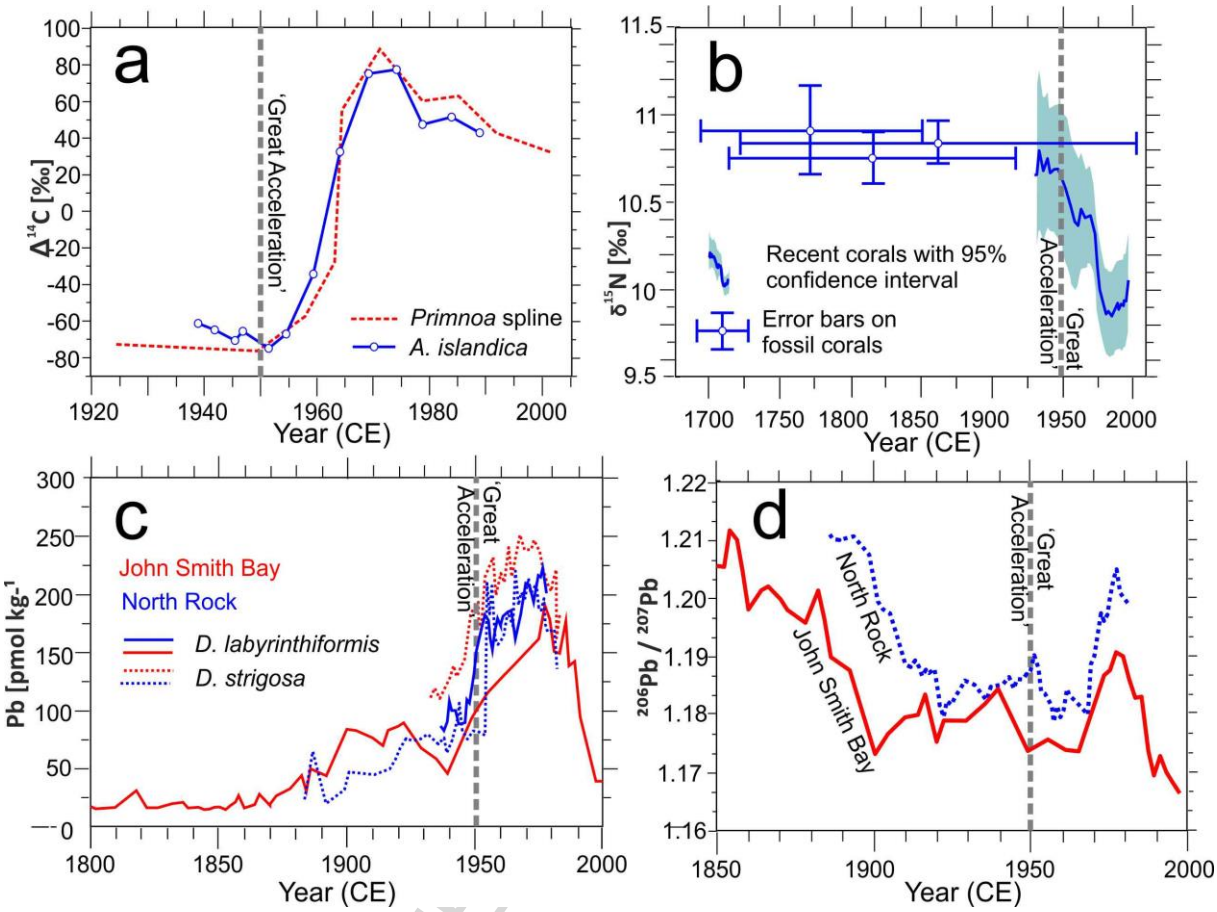

Figure 7. a) Plot of $\Delta^{14}C$ vs age for 7 different colonies of the deep-sea gorgonian coral *Primnoa resedaeformis* with spline fit through the data (Sherwood et al. 2005a), and for the bivalve *Arctica islandica* (Weidman and Jones 1993); b) $\delta^{15}N$-AA depletion in deep-sea gorgonian corals in the NW Atlantic (Sherwood et al. 2011) © (2011) National Academy of Sciences; c) Pb concentration; and d) $^{206}Pb/^{207}Pb$ in Bermuda corals (Kelly et al. 2009).

3.3.2 Guam (Pacific Ocean) .v. Caribbean Pu radionuclide signals

A natural coral archive in *Porites lobata* from Guam Island (NW Pacific Ocean), dated independently using $\delta^{18}O$ cycles to produce a biweekly to monthly chronology between 1787 and 2000 CE, was retrieved in a 273 cm core (Lindahl et al. 2011). Between 1943 and 2000

ACCEPTED MANUSCRIPT

CE the average growth rate was ~15 mm yr^{-1} (Lindahl et al. 2011), significantly higher than most natural accumulation rates in marine and lacustrine basins. From 1943 to 1945 CE, ^{239}Pu (but not ^{240}Pu) was detected in small concentrations (average of 1.96 ± 0.11 mBq kg^{-1}, Figure 6b), though at levels higher than would be expected from an entirely natural source at that time (Lindahl et al. 2011). This suggests some minor mobility of anthropogenic (post-1945 CE) Pu after incorporation into the coral. In 1946 CE, $^{239+240}Pu$ activity concentrations increased by an order of magnitude (11.3 ± 2.4 mBq kg^{-1}, Figure 6b) and continued at low levels until 1951 CE, reflecting fallout from locally tested, low-yield, nuclear devices (Lindahl et al. 2011). A marked bomb-nuclide peak is evident from 1952 to 1960 CE, with an apex in 1954 CE (4540 ± 70 mBq kg^{-1}, Figure 6b), the pattern being closely linked to that of large detonations in the local Pacific Proving Grounds (Lindahl et al. 2011). From 1961 to 1980 CE, there was an exponential decrease of $^{239+240}Pu$ activity, but despite Nuclear Test Ban treaties, residual Pu remains in the sea water and continues to be incorporated into coral growth laminae, such that by 2000 CE levels were comparable to those in 1946 CE (Figure 6b).

The Pu signals seen in a short (30-year) duration record from the coral *Orbicella* (*Montastrea) annularis* in the U.S. Virgin Islands (Benninger and Dodge 1986), reflect a location that is distant from atmospheric nuclear detonations. That study did not analyse coral bands from 1950 CE or earlier, so it is not possible to determine if a pre-1952 CE global fallout signal is present. But it did show clear 1959 and 1964 CE peaks in $^{239+240}Pu$ that closely correspond to global fallout maxima (Benninger and Dodge 1986; Figure 6b herein).

These data illustrate the very high-resolution Pu signal present in coral laminae, with only limited evidence of post-growth mobility of Pu. The example in Guam shows an initial rise in Pu between 1946 and 1951 CE and a peak signal in 1954 CE. Such a signal contrasts with

ACCEPTED MANUSCRIPT

areas distant from testing grounds which show a global Pu fallout pattern (e.g. Waters et al. 2015), with an initial 1959 CE peak and a subsequent higher 1964 CE peak (e.g. Benninger and Dodge 1986). This variability in peak signals suggest the initial rise in global Pu levels would better mark the basal boundary of the Anthropocene than any of the various peak signals (cf. Zalasiewicz et al. 2015). For hosting a potential GSSP, choosing a coral that was distant from nuclear testing grounds would mean that the global atmospheric signal is resolved without local perturbations.

3.3.3 ^{14}C, Pb and $\delta^{15}N$ signals in deep-water Atlantic gorgonian corals

Corals show a ^{14}C bomb-spike that has potential as a marker (Sherwood et al. 2005a; Figure 7a herein). Compared to coral $\Delta^{14}C$ records from Florida in the North Atlantic, the inception of the Brazil (Abrolhos Archipelago) record is delayed by ~1 year during the late 1950s with peak $\Delta^{14}C$ values reached from 1970 to 1972 CE in Florida and at 1974 CE at Abrolhos (Druffel 1996), suggesting an appreciable lag for the bomb ^{14}C to transfer from the main source latitudes in the Northern Hemisphere. There is also a $\Delta^{14}C$ atmosphere–surface ocean equilibration time of approximately 10 years, with some resultant time lag in the signal (Key et al. 2004). However, analysis of growth rings in the deep-water gorgonian coral *Primnoa resedaeformis* at depths of 250–475 m off Nova Scotia (Canada) shows a $\Delta^{14}C$ peak around 1972 CE (Sherwood et al. 2005a; Figure 7a herein), similar to that in shallow water corals in Florida (USA), suggesting rapid transfer of the radiocarbon to such moderate depths via plankton. Overall, a mid-1950s inception of the signal is evident in gorgonian corals from these environments, providing a reasonable proxy for the beginning of the Anthropocene.

ACCEPTED MANUSCRIPT

At much greater depths, $\Delta^{14}C$ records from the coral *Enallopsammia rostrata* from 1410 m depth off Bermuda first show bomb radiocarbon at ~1980 CE (Lee et al. 2017), a delay of some 25 years compared with the atmospheric signal (Lee et al. 2017). In this record, the introduction of anthropogenic lead, evident as an increased Pb/Ca ratio and decreased $^{206}Pb/^{207}Pb$ and $^{208}Pb/^{207}Pb$ ratios, occurs in the 1990s and hence shows a similar 25-year delay, and the signal is significantly smaller compared with that from nearby shallow-water corals (Lee et al. 2017). Given the decade-scale lags for $\Delta^{14}C$ in shallow-water corals, with even greater lags in deep-water corals, Pu is here considered the preferred fallout signal in corals.

Primnoa resedaeformis from Nova Scotia (Canada) to Virginia (USA) records the Suess effect, with $\delta^{13}C$ values decreasing by at least 2‰ since around 1960 CE (Sherwood et al. 2005b). *Primnoa resedaeformis* off Nova Scotia also records a $\delta^{15}N$ signal, considered a proxy for nitrogen source, which is correlated with increasing subtropical versus subpolar slope waters over the 20th century (Sherwood et al. 2011); $\delta^{15}N$ decreased by about 1‰ over this interval, with most of the decline occurring after 1970 CE, coincident with a rise in nitrates (Sherwood et al. 2011). Such coral studies show that the persistence of a warm, nutrient-rich regime since the early 1970s is exceptional in the context of the last ~1800 years (Sherwood et al. 2011, Figure 7b). Coral cores from Dongsha Atoll, western Pacific, show markedly lowered $\delta^{15}N$ values since ~2000 CE in coral skeleton-bound organic matter, probably associated with increased deposition of anthropogenic atmospheric nitrogen (Ren et al. 2017). By contrast, coral studies from some Indo-Pacific reefs affected by untreated sewage outfalls show high $\delta^{15}N$ (and $\delta^{13}C$) signals (Heikoop et al. 2000), indicating the complex behaviour of the nitrogen stratigraphic proxy.

ACCEPTED MANUSCRIPT

3.3.4 Global temperature and pH proxies from corals in the Great Barrier Reef

In the Great Barrier Reef, Australia, annual band thicknesses in corals equate to growth rate, which can be correlated with sea surface temperatures (SSTs) on a time scale of years to centuries (Lough and Barnes 2000). During the bleaching events associated with elevated SSTs of the late 20th century, *Porites* colonies from the Great Barrier Reef showed a decline in linear growth of 13.3% between 1990 and 2005 CE (De'ath et al. 2009), with calcification rates falling by 14.2%. Such changes are unprecedented over at least the last 400 years (De'ath et al. 2009).

Corals in the tropical Pacific region have shown a general decrease of $\delta^{18}O$ values from the late 20th century to the present (Cole 1996). This reflects large-scale warming in the upper layers of the ocean, or a general freshening of these waters, or a combination of both. $\delta^{18}O$ signals in scleractinian coral skeletons have been used as SST proxies in other areas, some as long records (e.g. Colonna et al. 1996), or at very high resolution (e.g. Ahmad et al. 2011). However, $\delta^{18}O$ signals reflect evaporation rates as well as SST, which is why they are frequently used together with other proxies, especially Sr/Ca (e.g. Tierney et al. 2015, Zinke et al. 2016). While some locations show a pronounced temperature increase around 1950 CE (e.g. Hetzinger et al. 2010), coral proxies have also shown that tropical seas might have started to warm as early as the mid-19th century, as an effect of both natural and possibly anthropogenic drivers predating the widely recognized global warming typical of the mid-20th century (Abram et al. 2016). Although temperature reconstructions can be highly refined (DeLong et al. 2016), temperature records from coral skeletons are a mix of local and global factors, and hence better as an ancillary rather than primary marker for defining any potential coral-based GSSP.

ACCEPTED MANUSCRIPT

$\delta^{11}B$ isotopic records in carbonates can provide a proxy for seawater pH. Data from a *Porites* coral in the Great Barrier Reef covering an interval from 1800 to 2004 CE show a recent trend of acidification correlating positively with the $\delta^{13}C$ Suess effect, and negatively with Mg/Ca ratios (a further proxy for SSTs) from 1940 to 2004 CE, indicating a coincident warming (Wei et al. 2009). Pre-industrial boron isotope signals in the coral show 22- and 10-year cycles strongly controlled by the Pacific Decadal Oscillation (Wei et al. 2009). From 1940 to 2004 CE the $\delta^{11}B$ signal indicates a decrease in pH of about 0.2–0.3 U, but with marked annual oscillations of 0.5 U around 1940 and 1998 CE (Wei et al. 2009).

3.3.5 Plastics in the Great Barrier Reef

Macroplastics have become noticeable in coral reefs, through the snagging of fishing nets and as plastic debris generally washed into the oceans. Microplastics are increasingly found both within marine waters and in underlying sediments (Zalasiewicz et al. 2016a). These plastics adsorb heavy metals and organic compounds from water, which can bioaccumulate in worms, fish and seabirds (Ivar do Sul and Costa 2014), and zooplankton (Cole et al. 2013). Microplastic ingestion into scleractinian coral polyps has been recognised recently in the Great Barrier Reef (Hall et al. 2015). Ingestion probably occurs both via microplastic-containing zooplankton and directly from the water. It remains uncertain whether any ingested plastic is transferred into the coral skeleton, as a potentially recognizable feature of future coral growth bands.

3.3.6 North Atlantic marine bivalves

A $\Delta^{14}C$ bomb signal comparable to that in cold-water corals (Figure 7a) was recorded in a long-lived bivalve, the ocean quahog (*Arctica islandica*) collected at a depth of 75 m on Georges Bank off New England, USA (Weidman and Jones 1993), with similar records in haddock otoliths (*Melanogrammus aeglefinus*) from the Grand Banks (Campana 1997). The

ACCEPTED MANUSCRIPT

$\Delta^{14}C$ values measured in these and in the gorgonian coral *P. resedaeformis* (see above) (~ -80 to ~ +80‰) are low compared to those in reef corals from Florida (~ -60 to ~ +160‰) where the stratified subtropical waters have a less diluted bomb signal (Sherwood et al. 2005a). *Arctica islandica* from water depths of 3–80 m across the temperate North Atlantic shows a gradient of increasing amplitude of the radiocarbon bomb-spike from Iceland southwards towards the North Sea (Scourse et al. 2012). All localities show a rapid response to the increase in atmospheric $\Delta^{14}C$ excess, with a lag within the bivalves of as little as 1–2 years, despite the equilibration time between atmosphere and ocean of 7–10 years (Scourse et al. 2012). However, the bivalve data shows a slow response to the decline in the radiocarbon signal, with a diachronous peak that occurs earlier in the south (Scourse et al. 2012).

Annually resolved $\delta^{18}O$ signals recorded in *A. islandica* collected at a water depth of 80 m north of Iceland show gradually increasing values over the period 953–1891 CE (±18 years), after which there is a rapid transition to lower values, with the 20th century represented by values that are significantly lower than at any other time in the last 1000 years (Reynolds et al. 2016).

3.4 Estuarine and deltaic deposits

River estuaries and deltas are present on all continents except Antarctica, forming the transition between the fluvial and marine realms (Figure 8) and representing the zone through which most terrestrial sediments (including those associated with human signals) are transported to the oceans. Estuaries occupy about 10 million km^2 and major deltas 1 million km^2 (Syvitski and Saito 2007). Most modern estuaries and deltas developed during the Early Holocene sea-level rise, with the flooding of river or glacial valleys. Sea level during

ACCEPTED MANUSCRIPT

the Middle and Late Holocene was essentially stable, allowing estuaries to silt up and deltas to build seawards (Zalasiewicz et al. 2014c). In addition, early deforestation and new agricultural practices commonly resulted in increased sediment flux to estuaries and deltas (Syvitski and Kettner 2011). Current and projected absolute sea-level rises are expected to flood both estuarine and deltaic deposits as warming continues to expand ocean water and melt land ice (Giosan et al. 2014). The trapping of sediment behind major dams, constructed on nearly all major rivers in recent decades (Syvitski and Kettner 2011), has greatly reduced sediment flux to the coast since the 1950s (Walling and Fang 2003). This change will leave a clear response as a transgressive, diachronous sequence-stratigraphic system with excellent preservation potential (Poirier et al. 2011). One consequence of decreasing fluvial profiles during sea-level rise is lower rates of erosion in the proximal headwaters, resulting in rivers with slower flow regimes, transporting relatively finer sediments to estuaries and deltas and therefore to coastlines. Where rivers have been dammed, even these sediment loads will not reach the coastal ocean. Many urban centres are located on or close to deltas or estuaries, which may therefore experience substantial anthropogenic influence. Deltas and coastal deposits continue to subside under their own weight, the subsidence now being accentuated by the compaction associated with urban development and with the extraction of groundwater and hydrocarbons (Syvitski and Kettner 2011), while locally drainage has led to the wholesale removal of surface peat layers, further lowering the surface (e.g. Smith et al. 2010) and increasing flooding risk. Twenty four out of the world's 33 major deltas are subsiding, levels of subsidence having reached several metres, as on parts of the Rhine, Nile, Pearl and Yangtze River deltas (Syvitski et al. 2009).

ACCEPTED MANUSCRIPT

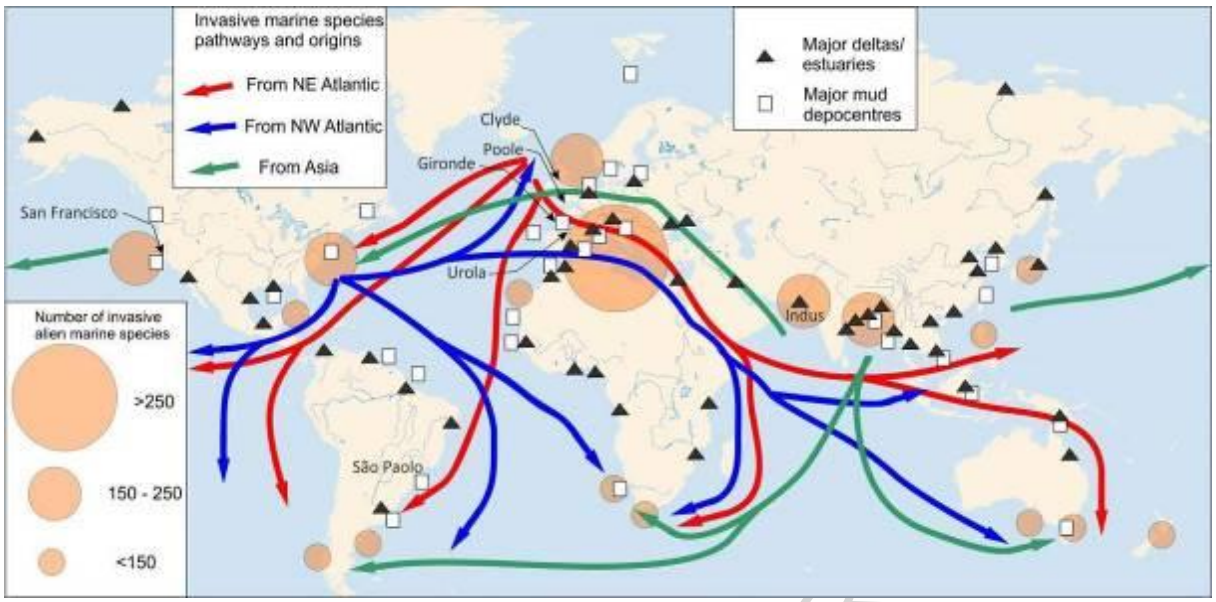

Figure 8. Distribution of deltas and estuaries (from Tessler et al. 2015), major mud depocentres (from Hanebuth et al. 2015) and areas where neobiota amenable to fossilization have recognizably altered coastal ecosystems (from: Major pathways and origins of invasive species infestations in the marine environment In UNEP/GRID-Arendal Maps and Graphics Library http://www.international-marine.com/invasivespecies/PublishingImages/invasive_vectors_001.png).

Mud deposition occurs on the continental shelves in front of major estuarine and deltaic areas (pro-deltas) around the world (Figure 8). They can also form subaqueous deltas disconnected from the source delta, or as scattered mud patches and widespread mud blankets, with a moderate sedimentation rate of 1–5 mm yr^{-1} (Hanebuth et al. 2015). They represent well-resolved palaeoenvironmental accumulations, commonly initiated during early flooding of continental shelves following deglaciation ~14 ky ago (Hanebuth et al. 2015). One example now forming a sink of anthropogenic pollution, including heavy metals and hydrocarbons, lies off the coast of São Paolo State, SE Brazil (Mahiques et al. 2016). Here, the mud deposits originate from many small river inputs and are mixed with coastal sediments. These deposits form a laterally extensive sedimentary succession, where the mid-shelf section at 50−100 m depth is prone to reworking through bioturbation, storms and

ACCEPTED MANUSCRIPT

anthropogenic disturbance, including trawler fishing and sea-bed dredging (Mahiques et al. 2016). Similar shelf mud deposits occur in the Bay of Biscay, in front of the Gironde estuary, SW France (Lesueur et al. 1996), where three mud-patches, totalling 630 km^2, occupy palaeo-valleys at depths of 30–75 m. The rhythmically laminated deposits there, which broadly represent storm layers, accumulated to a thickness of 1.8 m over the last 2000 years and the upper 0.2 m accumulated in <30 years, as shown by ^{14}C and pollen analyses. A marked increase in pollen from *Pinus pinaster* over the last century reflects extensive afforestation (Lesueur et al. 1996).

Estuaries and deltas are particular foci for neobiota (Wilkinson et al. 2014), often associated with marked declines in indigenous species. Widespread translocation of invasive species took place during the 19th and 20th centuries through the establishment of global shipping routes, and resultant transfer of species in ballast water and from hull fouling (Figure 8). Organisms such as diatoms, dinoflagellates, foraminifera and ostracods, are particularly susceptible to transportation in ballast water and hence are likely to produce novel signals within coastal sediments, especially close to major ports (McGann et al. 2000, Calvo-Marcilese and Langer 2010). The International Convention for the Control and Management of Ships' Ballast Water and Sediments, which came into force in September 2017, is aimed at reducing the rate of such biotic transfer.

Aquaculture of fish, shellfish and shrimps has become a growing feature of estuarine settings in the late 20th and early 21st century (Martinez-Porchas and Martinez-Cordova 2012). This has resulted in diverse biotic changes including the displacement of native species, competition for space and food, and the spread of pathogens and parasites, and impacts like these are likely to increase as this kind of fishery develops. In addition, destruction of natural

ACCEPTED MANUSCRIPT

ecosystems, most notably of mangroves along equatorial coastlines, which have seen a 25% decrease in 20 years to 150,000 km^2 in 2000 CE (Martinez-Porchas and Martinez-Cordova 2012), has changed species presence/absence and abundance patterns. Aquaculture can also lead to eutrophication causing phytoplankton blooms, including red tides, the resultant anoxia and increased pathogens killing off benthic organisms (Martinez-Porchas and Martinez-Cordova 2012). The first arrival of many invasive species to local areas is commonly historically documented, but the fossil record of these changes as successive assemblages in recent well-dated sedimentary successions remains poorly studied.

'Bomb spike' calibration and AMS ^{14}C dating have been used to derive a detailed age-depth model for a 1-m long sediment column collected from a salt marsh in Poole Harbour, southern England (Marshall et al. 2007), enabling comparison with chronologies obtained from CRS ^{210}Pb analysis, ^{137}Cs age markers, pollen and spheroidal carbonaceous particles (SCPs). Little or no agreement was found between the ^{14}C 'bomb spike' dates, the ^{210}Pb chronology, and the ^{137}Cs data, the last of these being affected by local (non-fallout) discharges (Marshall et al. 2007). The study showed an acceleration in sedimentation rates during the last 100 years, and indicated that 'bomb spike' ^{14}C calibration dating may often better constrain salt-marsh sedimentation rates than ^{210}Pb dating (Marshall et al. 2007).

Table 6 summarises key advantages and disadvantages of hosting a potential GSSP within estuarine or deltaic deposits, where research has focused on impacts of anthropogenic pollution through geochemical signatures, especially heavy metals and POPs, and on microbiotic content such as foraminifera, diatoms and palynomorphs (Wilkinson et al. 2014). The examples provided below, for the Clyde Estuary (Scotland), Urola Estuary (northern

ACCEPTED MANUSCRIPT

Spain) and Indus Delta (Pakistan), demonstrate a range of signals. For a variety of reasons (Table 6) these types of environment seem unsuitable for hosting a GSSP.

For:	Against:
• May be varved through seasonal variations in sediment flux • Independent dating using ^{210}Pb; ^{14}C more challenging • Radionuclides, no settling delay in water column; clear bomb spike • Micro- and macro-organisms reflect environmental change and commonly preserve as fossils (e.g. foraminifera, diatoms, palynomorphs, molluscs, fish) • Microplastics, direct source from effluents • Heavy metals, close to industrial sources • Persistent organic pollutants signal e.g. chlorinated pesticides, polychlorinated biphenyls • Modification of fluvial input to estuaries related to catchment modification • Samples relatively easy to procure	• Potential of bioturbation • Numerous omission surfaces (natural erosion and anthropogenic dredging) • Limited lateral continuity, but distinct systems may undergo similar histories • Strong modulation of signals by local processes • No GSSP precedent

Table 6. Reasons for and against using an estuarine or deltaic deposit as a potential host for a GSSP.

3.4.1 Clyde Estuary, Scotland (Pb and organic compounds)

Lead concentrations in the Clyde Estuary were initially elevated early in industrial activity, peaking by about 1915 CE, with a prominent decline to historically low concentrations post-1980 CE (Vane et al. 2011, Figure 9a), as heavy industry declined and Pb use in gasoline was phased out. $^{207/206}Pb$ isotope ratios of *Sphagnum* moss collected in Scotland from 1838 CE to the present record variation of atmospheric Pb aerosols (Farmer et al. 2002): a constant pattern during the 19th century until ~1915 CE reflects use of British lead coal-ore and coal-burning (Figure 9a); increased ratios from 1920 CE due to overseas Broken Hill-type Pb

ACCEPTED MANUSCRIPT

additives in gasoline and industrial lead, peaking in the 1980s; and then declining ratios following the banning of lead in gasoline (Vane et al. 2011).

Increased industrialization of the Clyde Estuary in west Scotland has led to elevated levels of sediment-hosted anthropogenic organic chemicals (Vane et al. 2011), including total petroleum hydrocarbons (TPHs), polycyclic aromatic hydrocarbons (PAHs), polychlorinated biphenyls (PCBs) and brominated flame-retardants (polybrominated diphenyl ethers, PBDEs) (Figure 9b). The PAHs are largely sourced from combustion of coal, petroleum or wood with peak concentrations in 1954 CE (Vane et al. 2011, Figure 9b). Increasing petroleum pollution mainly from shipping and petroleum refineries was recorded from about the 1950s by increasing TPH concentrations and a decline in PAHs that reflects decreasing coal use (Vane et al. 2011). This was followed by more modern pollution from the PCBs, which show a prominent onset (1950s), peak (1965–1977 CE) and decline (post-1980s).

The complexity of signals provides a very fine resolution chronometer of pollution in the Clyde Estuary. Although the Pb, TPHs and PAHs provide a local signal, the Pb isotopes and PCBs provide a more widespread and consistent, although not precisely coincident, global signal.

ACCEPTED MANUSCRIPT

ACCEPTED MANUSCRIPT

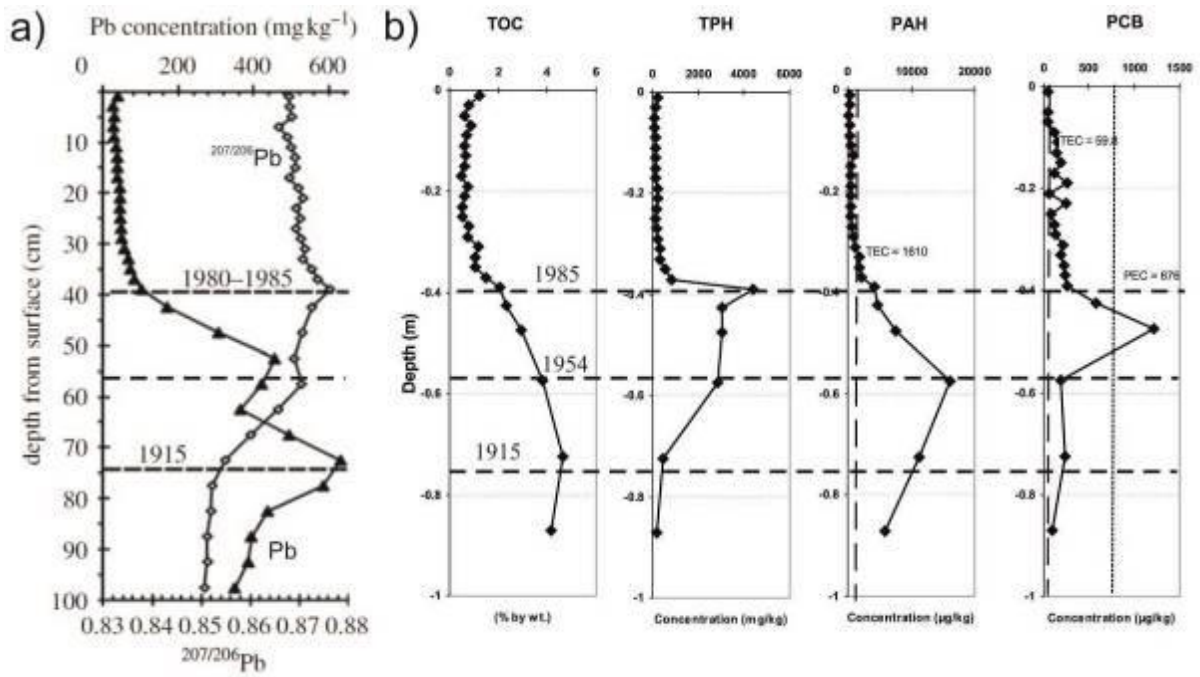

Figure 9. Example of data from a single core from the Clyde Estuary showing a) Pb concentrations and $^{207/206}$Pb isotope ratios, and b) PAH, TPH and PCB organic chemical signatures (Vane et al. 2011). Dates are interpreted.

3.4.2 Urola Estuary, Spain

The lower intertidal part of the Urola estuary (Basque coast, Spain) was studied in a 50 cm core and dated using ^{210}Pb, the basal parts dated using ^{210}Pb to ~1850 CE (Goffard 2016). From the 1960s to the 1980s the rate of sedimentation increased by >60% in response to growing industrial activity, with further increase from the mid-1990s coinciding with nearby dredging. Micropalaeontological analysis of benthic foraminiferal assemblages (FAs) (Goffard 2016) identified three assemblages (Fig. 10) that reflect a local cycle of biological deterioration and reduced diversity followed by recovery. This biostratigraphic succession has been correlated with changes in levels of industrially-derived metals in the sediment, showing that chemical deterioration preceded biological deterioration. Longer-range correlation is provided by: spheroidal carbonaceous particles, which occur mainly in the

ACCEPTED MANUSCRIPT

lower levels; iron spheroids, showing enrichment from the 1960s; and plastic microbeads, which increase from the 1980s (Goffard 2016).

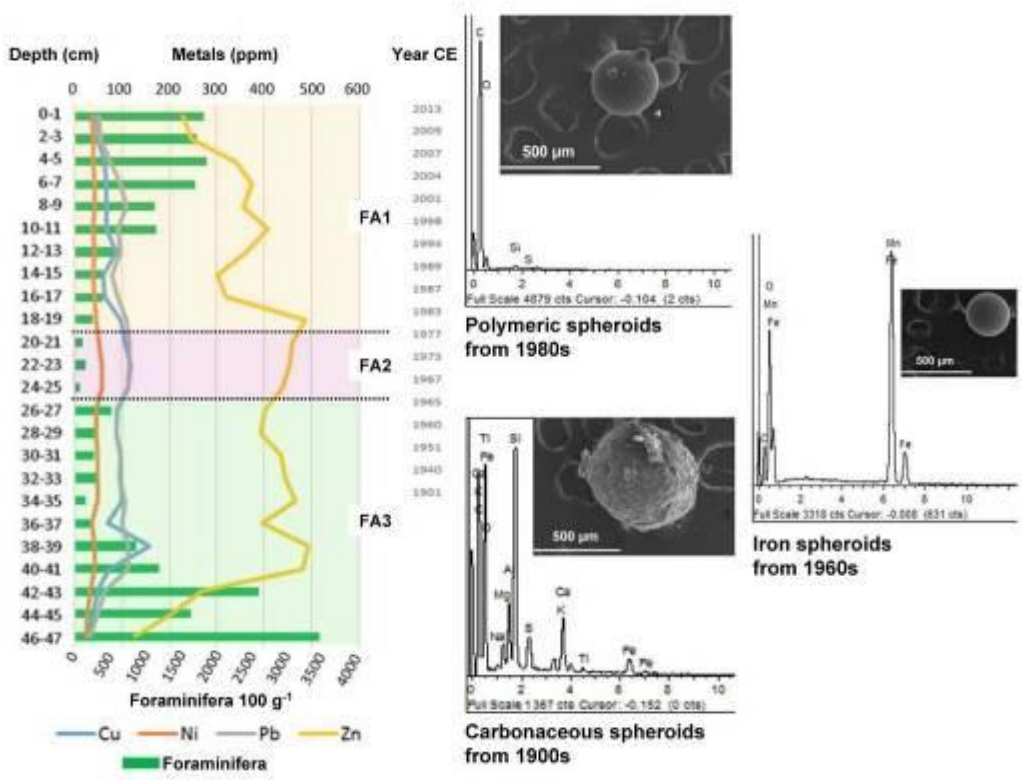

Figure 10. Metal concentrations (Cu, Ni, Pb, Zn) versus foraminiferal density in the Urola estuary (northern Spain). FA1–FA3 represent three distinct foraminiferal assemblages referred to in the text. Modified from Goffard (2016).

3.4.3 San Francisco Bay, USA

San Francisco Bay, with a well-documented history of invasive species (neobiota), is typical of the many coastal ecosystems around the world that are near shipping ports (Figure 8). In a seminal study by Cohen and Carlton (1998), some 234 neobiotic species were recognised, ranging from sponges to mammals. They noted an accelerating trend over 145 years, with about half the invasions occurring since 1960 CE. More recently, studies of shallow sub-tidal

ACCEPTED MANUSCRIPT

sediments in the bay have identified soft-sediment communities dominated by invasive species (Jimenez and Ruiz 2016). The presence of so many neobiotic species in San Francisco Bay suggests the potential for a high-resolution biostratigraphy using species invasions (Figure 11). Building such a stratigraphy would need to resolve the myriad complexities of a sedimentary succession heavily disturbed since the 19th century. Nevertheless, sediment cores with Pleistocene and Holocene micropalaeontology are well known (e.g. Sloan 1992, McGann et al. 2002), providing a pre-human influenced baseline for local coastal assemblages.

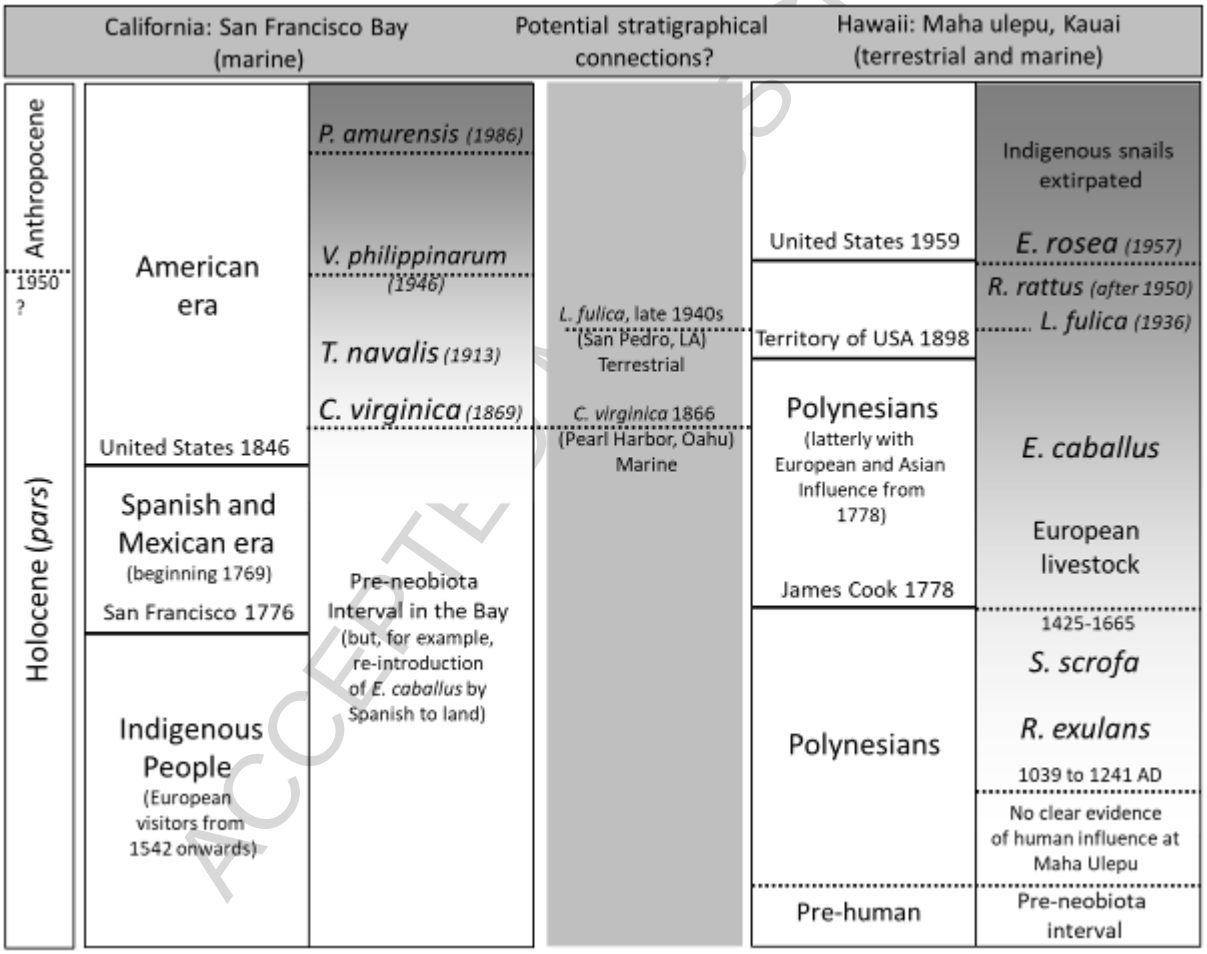

Figure 11. Chronology of selected invasive mollusc species into San Francisco Bay (for dates of invasion see: Carlton et al. 1990; Cohen 2004, 2011; Committee on Nonnative Oysters in the Chesapeake Bay, Fofonoff et al. 2017, National Research Council 2004), and terrestrial invasive species in the Maha'ulepu sinkhole succession of Kauai, Hawaii (Burney et al. 2001). In both successions, cultural human changes are indicated by the left-hand column, and neobiota in the

ACCEPTED MANUSCRIPT

right-hand column. Although the two successions developed nearly 4000 km apart, and in warm temperate and tropical zones respectively, by the mid-19th century some taxa present on the California coast (e.g. the bivalve *Crassostrea virginica*, see DeFelice et al. 2001) were also present in Hawaii, suggesting the possibility of correlation between remote successions.

A focus of such analysis could be bivalves, which are commonly fossilized, widespread and readily recognisable neobiotic species. A biostratigraphic subdivision could begin with a pre-neobiotic interval that is characterised only by indigenous bivalve species, these persisting into the mid-19th century. A subsequent early neobiotic stage (see also Cohen and Carlton 1998) might be characterised by the first appearance of the oyster *Crassostrea virginica*, which entered the Bay in 1869 CE. A native to the Atlantic coast of North America, this species was introduced with the development of oyster fisheries. *Crassostrea virginica* was also introduced into the estuaries of the Hawaiian islands at about the same time (1866 CE), providing a potential biostratigraphic tie with a distant island succession (Figure 11).

The early phase of invasions into San Francisco Bay is followed by increasing indicators of pan-Pacific connections between North America and East Asia, signalled by, for example, the introduction of the East Asian bivalve *Venerupis philippinarum*, first recognised in San Francisco Bay in 1946 CE (Cohen 2011, Figure 11), although there are earlier records elsewhere on the Pacific coast of North America. Locally, this species occurs in abundances of 2000 individuals per m^2, and it has good preservation potential. It has also been widely introduced, from Hawaii (introduced in the 1880s, established by 1918 CE) to Europe. A later colonisation from East Asia was by the Amur Clam *Potamocorbula amurensis*, native to the waters of China, Siberia, Korea and Japan. It was introduced into San Francisco Bay in 1986 CE, likely through ships' ballast water (Figure 11) and then spread widely and rapidly. It now

ACCEPTED MANUSCRIPT

occurs in huge numbers in muddy substrates within the Bay: up to 48,000 individuals have been recorded per m^2 sediment (Cohen 2011).

3.4.4 Indus Delta

The Indus Delta, Pakistan, and its associated river system, is highly managed, with artificial levees, barrages, irrigation canals, upstream reservoir construction and inter-basin water diversions. It has also been affected by watershed deforestation. As a consequence, the river has changed radically, with a current sediment flux of ~13 Mt yr^{-1} to the tidal-dominated delta and its single active distributary, in contrast to the much larger flux >270 Mt yr^{-1} of mainly silt that was transported to the fluvial-dominated delta before these management schemes were implemented. The original delta system comprised 17 channels (which still avulsed naturally) in 1861 CE (Syvitski et al. 2014). Modifications started as early as 1762 CE, although constructed dams were all washed away in a flood in 1826 CE. The modern barrage system was initiated in 1859 CE (Syvitski et al. 2014). With rising sea-levels accompanied by tectonic subsidence, the abandoned distributary channels are being tidally reworked since 1944 CE and the delta has lost 12.7 km^2 yr^{-1} of land and ~69 Mt yr^{-1} of sediment by erosion. The system is highly dynamic due to monsoon-driven floods, storm surges, tsunamis and earthquakes (Syvitski et al. 2014), and hence stratigraphic successions are beginning to emerge as complex backstepping packages of sediment with omission surfaces related to erosive events, in contrast to the pre-1869 CE delta, which was prograding at about 200 m yr^{-1}.

3.5 Lake sediments

The planet has about 117 million lakes greater than 2000 m^2, covering about 3.7% of the ice-free land surface, with the highest concentration and area of lakes at boreal and arctic

ACCEPTED MANUSCRIPT

latitudes between 45°N and 75°N (Verpoorter et al. 2014). The most suitable lake environment for hosting a potential GSSP is one where varves are present. Varves tend to occur in lakes in which a flat bottom profile limits sediment flow, and, ideally, where there is little or no bioturbation, water movement, or gas emission from buried organic material to disturb the laminae (Zolitschka et al. 2015). Many such features are common in glacial lakes, characterized by graded summer silt laminae alternating with winter clays, e.g. Holtgrieve et al. (2011) and Wolfe et al. (2013). Varves can also develop in hypoxic lakes (Figure 12), typically meromictic lakes with stratified water columns in which sediment is introduced through seasonal input of clastic or biogenic material. Saline lakes can develop varves in response to seasonal precipitation of evaporite minerals, within an environment commonly too hostile for benthic life, allowing preservation of the varves; however, these lakes are more likely to periodically dry out, thus tending to miss annual laminae. Lakes are already recognized as suitable locations for hosting a GSSP, having been used as the ancillary GSSP locations for the base of the Holocene (Walker et al. 2009).

Hypoxia has been recorded in sediments of 365 lakes worldwide (Figure 12). Of these, 71 (~20%) show hypoxia developed since the mid-19th century CE, much earlier than the widespread development of hypoxia in coastal zones during the mid-20th century (Jenny et al. 2016). This reflects the sensitivity of lakes to environmental change, where increasing human activities and nutrient release commonly lead to the onset of hypoxia. No correlations were found with changes in precipitation or temperature. There is no evidence for a post-1980s return to well-oxygenated lacustrine conditions in industrialized countries, despite the implementation of restoration programmes (Jenny et al. 2016). Hypoxia notably can change the behaviour of trace elements and radionuclides, by either increasing or reducing their mobility (e.g. Pavin Lake, France; Jeandel 1981).

ACCEPTED MANUSCRIPT

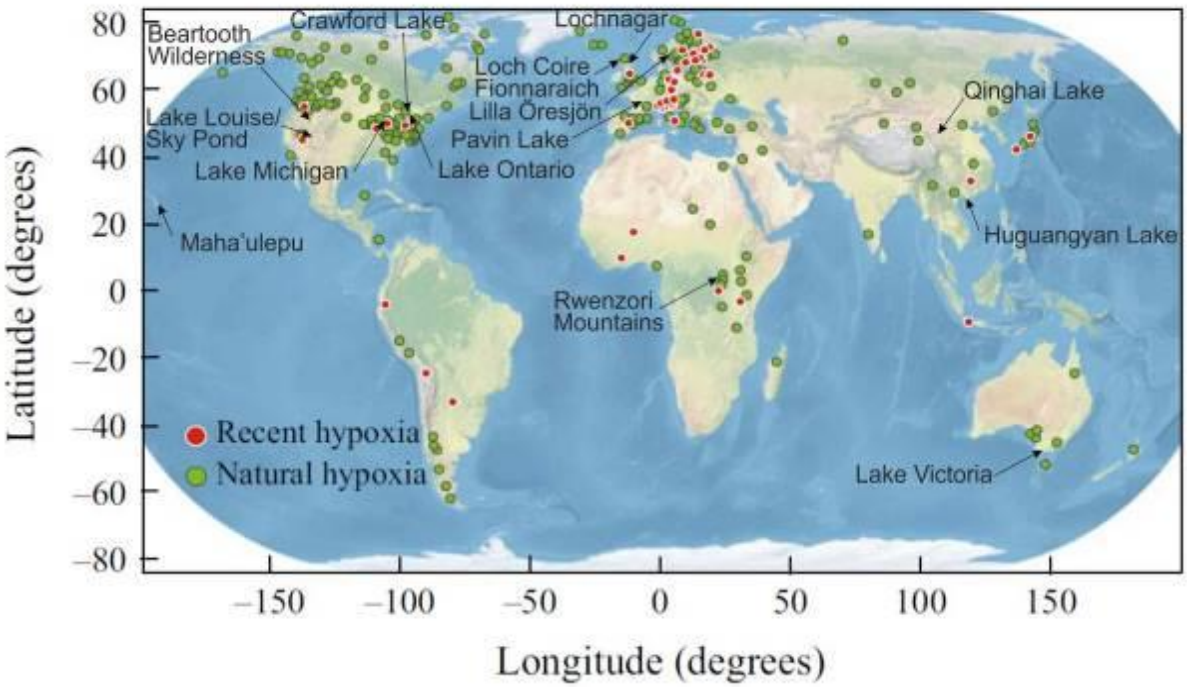

Figure 12. Location of the 365 sites recording lake hypoxia (Jenny et al. 2016). Recent hypoxia records onset of varves after 1700 CE, whereas naturally hypoxic lakes were taken to be those in which laminations persisted for at least 300 years.

The radiogenic fallout signature is commonly well expressed in unbioturbated lake sediments, especially as the mid-latitude Northern Hemisphere peak fallout distributions (Hancock et al. 2014, Waters et al. 2015) coincide with the greatest abundance of hypoxic lakes. Shallow lakes are advantageous in that they show little of the settling delay evident in the anoxic marine basins (see section 3.2). However, they may still be prone to reworking of fallout signals from catchment areas, such that the onset of the signal will probably be unaffected, but the bomb-peak may be broadened although still centred at ~1964 CE. Lake Victoria in Australia is an example of a lake with a large catchment. Despite showing the expected peak of the $^{239+240}$Pu and ^{137}Cs signals in 1964 CE (Figure 13), the Cs peak is broader and the post-1964 CE Pu decline is prolonged because of sedimentation associated with erosion within that catchment.

ACCEPTED MANUSCRIPT

Abundant organic and clay components in lake sediments enable sorption of the main long-lived radiogenic elements (plutonium and radiocarbon). Where plutonium concentrations are relatively high, α-spectroscopy effectively measures the combined activity of ^{239}Pu + ^{240}Pu and also measures ^{238}Pu activity (Figure 13), whereas mass spectrometric (MS) techniques are required where concentrations are low and to measure distinct ^{239}Pu concentrations (Hancock et al. 2014). However, plutonium (and caesium) can be mobilized under anoxic conditions in meromictic lakes, e.g. Pavin Lake, France (Jeandel 1981).

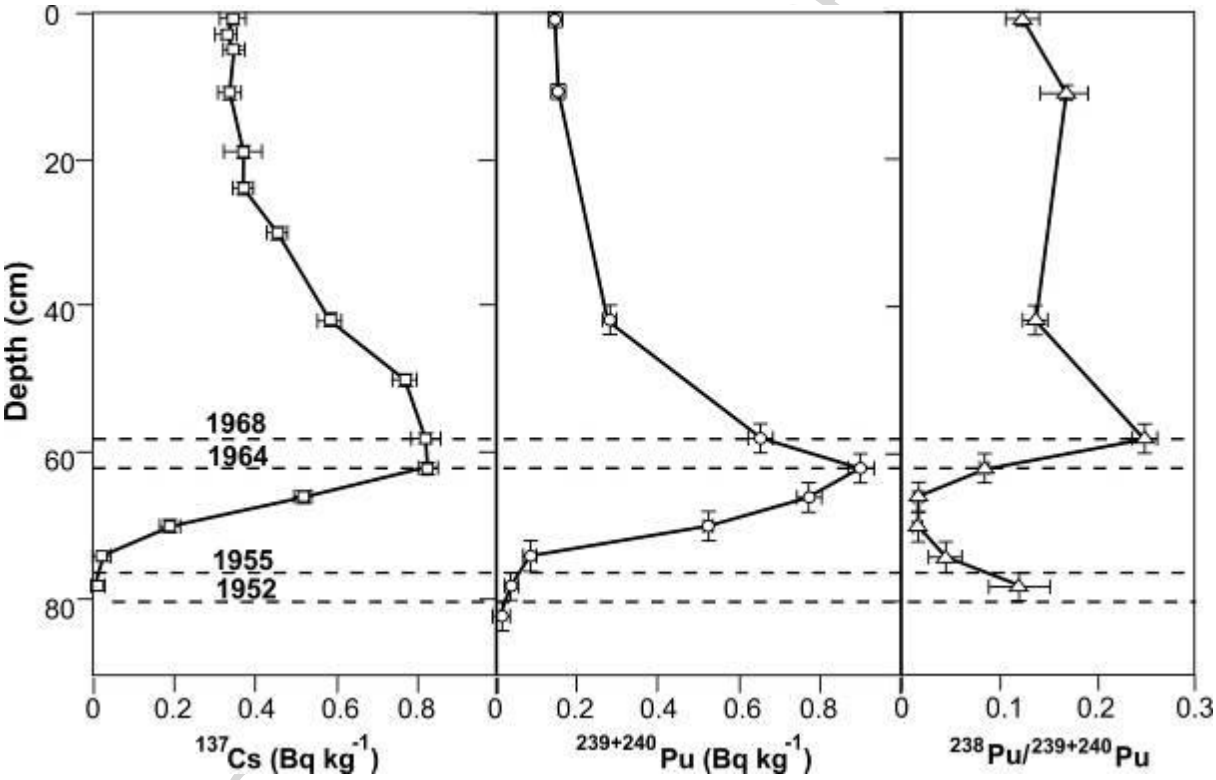

Figure 13. Radiogenic signature from Lake Victoria, Australia (Hancock et al. 2011). Profiles of ^{137}Cs (closed squares), $^{239+240}$Pu (open circles) and ^{238}Pu/$^{239+240}$Pu (triangles).

The atmospheric transfer of reactive nitrogen (Nr) results in the deposition of NH_4^+, HNO_3, and NO_3^- even in remote lakes, as demonstrated in North America and the Arctic regions (Holtgrieve et al. 2011, Wolfe et al. 2013). Stable nitrogen isotope values from lake sediments of those regions show a consistent perturbation of δ^{15}N commencing after 1850

ACCEPTED MANUSCRIPT

CE, typically at 1895 CE ± 10 years (Holtgrieve et al. 2011, Figure 14), but with a faster rate of depletion from 1950 to 1970 CE and after 1980 CE (Wolfe et al. 2013). This depletion is attributed to fossil fuel combustion and the production and use of fertilizers, both with depleted isotopic ratios compared with catchment and preindustrial atmospheric sources (Holtgrieve et al. 2011).

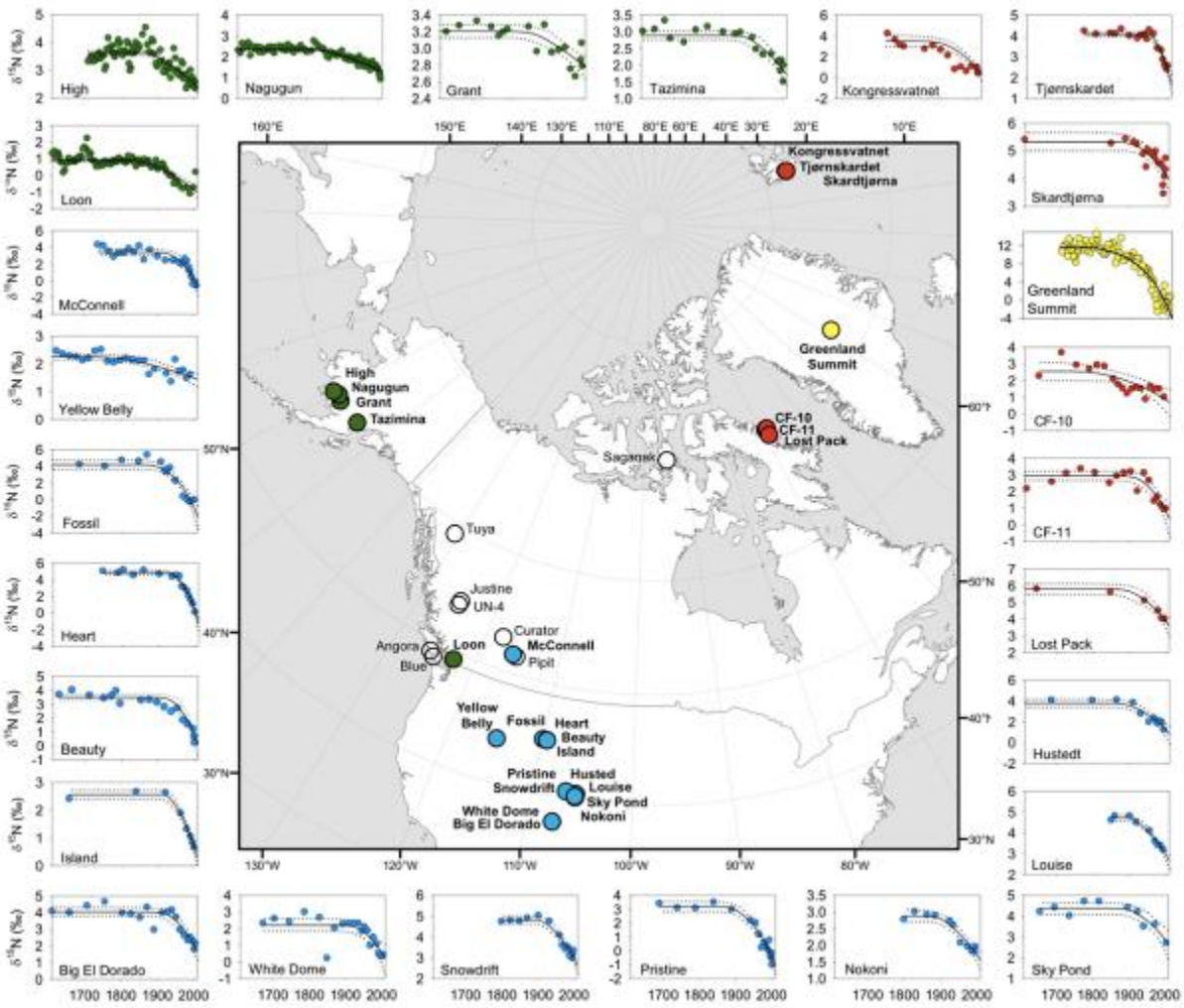

Figure 14. Sediment $\delta^{15}N$ profiles from Northern Hemisphere lakes (from Holtgrieve et al. 2011). Lake ecotypes include: temperate/boreal (green circles), alpine (blue circles), and arctic (red circles), and the Greenland Summit ice core is indicated with a yellow circle. The solid lines are the median posterior fits to the observed data using the most parsimonious model, and the dotted lines are the 2.5 and 97.5% credible limits.

ACCEPTED MANUSCRIPT

Although spheroidal carbonaceous particles (SCPs) are first recorded from strata dating to about 1830 CE, they show a near-synchronous global mid-20th century increase in abundance. This increase was driven by the introduction of fuel-oil combustion, in addition to coal, and coincided with increased abundance of large-scale power plants, with peak abundance in the 1970s to 1990s (Rose 2015). Black carbon, produced from the incomplete combustion of fossil fuels and vegetation, can accumulate in lakes from both atmospheric aerosols and riverine input, and is inert and resistant to degradation (Han et al. 2016). The atmospheric component, generally seen as a smaller size fraction (soot), is more widely transported and hence provides a more regional signal than coarser riverine char (Han et al. 2016). Biomass burning typically produces higher char/soot ratios than fossil fuel combustion, especially motor vehicle emissions (Han et al. 2016). Polycyclic aromatic compounds (PACs) tend to be co-produced with black carbon during hydrocarbon combustion. These can include polycyclic aromatic hydrocarbons (PAHs) and derivatives such as oxygenated PAHs (OPAHs) and azaarenes (nitrogen heterocyclic PAHs, AZAs) (Han et al. 2016). The relationship is demonstrated for Huguangyan Lake, eastern China (section 3.5.4).

Metal concentrations in lake sediments can be affected by variable factors such as the timing of local industrialisation, distinct sources of sediment supplied by river fluxes into the lake, and varying degrees of weathering of the source catchment areas. Anthropogenic Pb deposition in lakes typically shows elevated concentrations in modern sediments in response not only to local industrial sources, but also to regional to global scale Pb atmospheric release. In remote lakes, the supply of anthropogenic Pb is sourced via the atmosphere (e.g. Lake Qinghai, China; Jin et al. 2010), providing a wider and more consistent signal than Pb supplied via river-water influx from nearby industrial sources. In Lake Qinghai, elevated anthropogenic Pb concentrations from the 1960s to at least 2000 CE are considered

ACCEPTED MANUSCRIPT

consistent with other remote Northern Hemisphere lakes (Jin et al. 2010). The lakes of the Rwenzori Mountains of Uganda are distant from direct sources of Pb, and therefore the lake sediments potentially contain reliable archives of long-range atmospheric pollution (Yang et al. 2010). Hg concentrations in these high-altitude lakes show increased Hg burdens from the 1860s, with significantly elevated levels from 1930 ± 6 CE (Yang et al. 2010).

The Great Lakes of North America show widespread microplastic contamination, mainly in surface waters and beach sediments, while plastic pellets have been recorded in bottom sediments of Lake Ontario (Corcoran et al. 2015). Notably, high-density microplastics, including mineral-polyethylene and mineral-polypropylene mixtures, sink to the lake bottom rapidly and have been accumulating since at least 1977 CE (Corcoran et al. 2015). Microplastics tend to concentrate in nearshore sediments, within low-energy environments close to urban and industrial areas at concentrations of up to ~28,000 particles kg^{-1} dry sediment and sediment depths of up to 15 cm (Ballent et al. 2016). Where microplastics are deposited at water depths of <40 m, they are prone to reworking by storm events (Ballent et al. 2016).

Persistent organic pollutants (POPs) are characterised by slow rates of environmental degradation (years to decades), low solubility, high absorption to suspended particles and efficient atmospheric transport. Chlorinated pesticides (e.g. DDT and its degradation products), show a consistent worldwide rise from the 1950s (Muir and Rose 2007), and subsequent decline in the youngest sediments reflecting the US banning of DDT in 1972 CE. Temporal trends of input fluxes of polychlorinated biphenyls (PCBs), and the fire retardants hexabromocyclododecanes (HBCD) and polybrominated diphenyl ethers (PBDEs) in sediment cores from English lakes in urban settings show generally slow rises from ~1960 CE, which

ACCEPTED MANUSCRIPT

are less clearly developed in rural settings. In the case of HBCD, the rise may be delayed by some 35 years (Yang et al. 2016).

Invasive zebra mussels (*Dreissena polymorpha*) and quagga mussels (*Dreissena rostriformis bugensis*) represent novel species introduced into the North American Great Lakes in 1988 and 1989 CE respectively (https://nas.er.usgs.gov/taxgroup/mollusks/ zebramussel/), both originating from southern Russia/Ukraine. As well as providing a novel biogenic signal, they also greatly modify the biotic content of the lakes. The trillions of quagga mussels in Lake Michigan (USA) can filter the equivalent of the entire lake volume in about 1 or 2 days. This has resulted in a shift in diatom composition, with significant reduction in the larger diatom genera, e.g. *Stephanodiscus* and *Aulacoseira*, leaving an impoverished algal community with mainly smaller genera, e.g. *Cyclotella* (Evans et al. 2011). Diatom assemblages in remote Northern Hemisphere lakes commonly show a consistent pattern. Typical Late Holocene benthic diatoms, such as *Staurosira* and *Achnanthidium* show declines concurrent with the rise of planktonic diatoms, first associated with an initially time-transgressive appearance of *Discostella stelligera*, attributed to climate warming (Wolfe et al. 2013). After 1950 CE, the planktonic diatoms *Asterionella formosa* and *Fragilaria crotonensis* became dominant (Saros et al. 2005, Figure 15; Wolfe et al. 2013 suggest 1980 CE). This later change may reflect elevated Nr availability (Wolfe et al. 2013, Figure 14) as well as rising temperatures. A comparable biotic change in the remote oligotrophic Scottish lake of Loch Coire Fionnaraich began in the 19th century following several hundred years of ecological stability (Pla et al. 2009). Changes to diatom (mainly benthic) assemblages were strongly coincident with changes in spheroidal carbonaceous particle concentrations, and may result from atmospheric contamination, possibly Nr enrichment (Pla et al. 2009). Chrysophyte diatom

ACCEPTED MANUSCRIPT

cyst (mainly planktonic) assemblages changed in response to a combination of atmospheric pollution and regional climate warming (Pla et al. 2009).

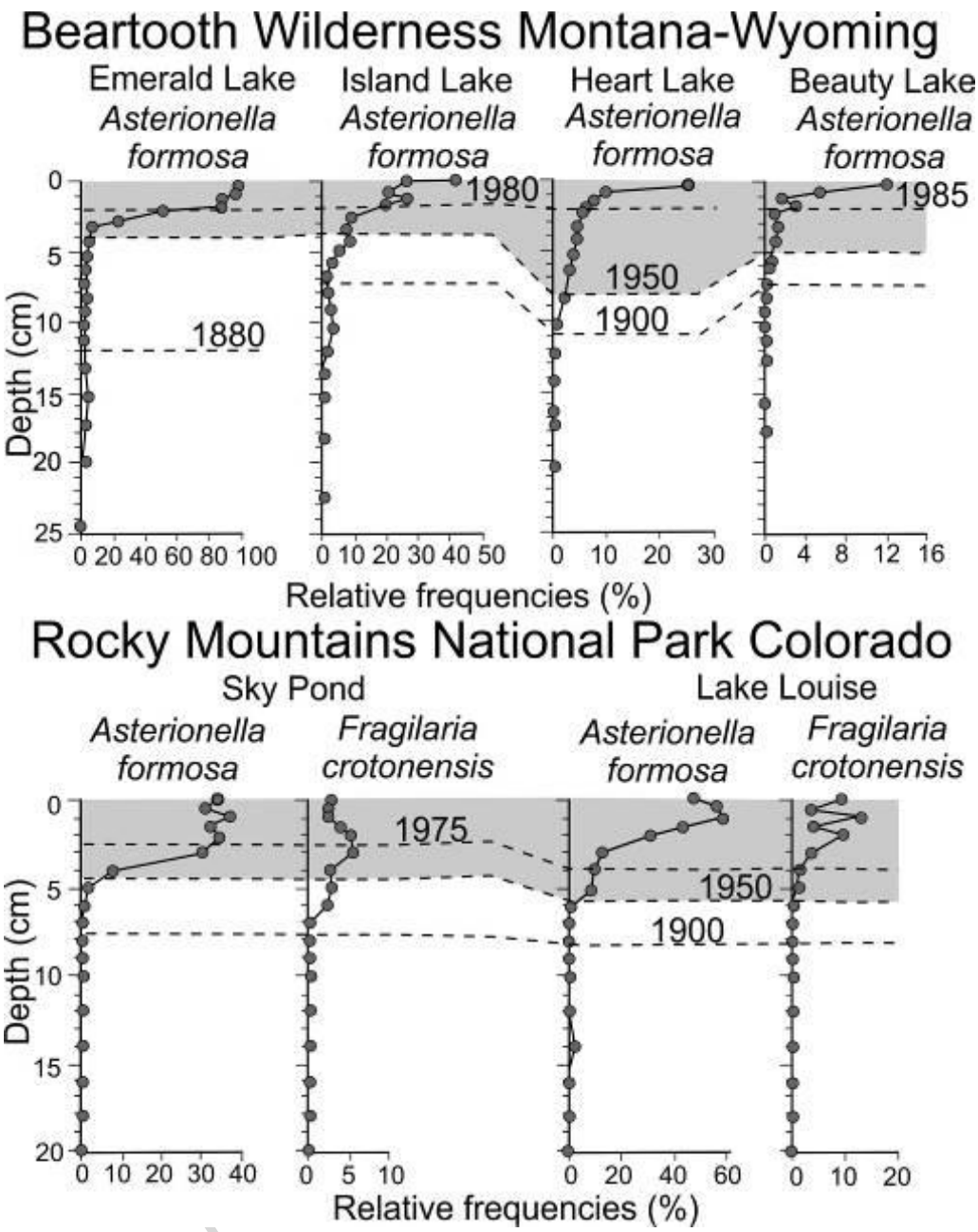

Figure 15. Replacement of Holocene diatom assemblages by *Asterionella formosa* and/or *Fragilaria crotonensis* mainly in lake cores from US high-altitude sites, since ~1950 CE (Saros et al. 2005). Location of lakes shown on Figure 14.

Table 7 summarises the key advantages and disadvantages of having a potential GSSP within lacustrine environments. Varved lake sediments can be strongly influenced by local

ACCEPTED MANUSCRIPT

variations in the geology, hydrology and land use present within catchments, and may be associated with distinct geochemical signals related to input from local industries. Correlation of varved successions within individual lakes may be limited to the extent of the water body, but widespread airborne contaminants, e.g. radiogenic fallout, nitrates, fly ash (Table 2), can show remarkably consistent patterns in lakes across diverse latitudes and be associated across continents. Crawford Lake (Ontario, Canada), Lochnagar (Scotland), Lilla Öresjön (Sweden), Huguangyan Lake (Guangdong, China) and Maha'ulepu Sinkhole (Kauai, Hawaii) are described as examples of potential trans-continental reference sections.

For:	Against:
• May be varved; relatively few omission surfaces • Spatially extensive with regional–global coherent signals • Independent dating using ^{210}Pb and ^{14}C • May be correlatable with tephra stratigraphy • Microplastics and metals with direct source from effluents • Spheroidal carbonaceous particles show global upturn • δ^{15}N marked depletion from mid-20th century • Persistent organic pollutants, e.g. chlorinated pesticides • Radionuclides, no settling delay in water column; clear bomb spike • Microfossils responsive to environmental change e.g. diatoms, ostracods, palynomorphs • Cores relatively easy to procure	• Commonly low sediment accumulation rates (though typically greater than for marine anoxic basins) • Strong modulation of signals by local processes, except for upland or remote lakes • Pu and Cs are mobile under anoxic conditions at the bottom of meromictic lakes • No precedent as GSSP candidate; although 4 of 5 auxiliary stratotypes for the Holocene GSSP are lacustrine

Table 7. Reasons for and against using a lake deposit as a potential host for a GSSP.

ACCEPTED MANUSCRIPT

3.5.1 Crawford Lake, Canada

Crawford Lake (Ontario, Canada) is a small (surface area 2.5 ha), deep (24 m), meromictic lake located close to industrial pollution sources, although it lacks any significant urban development within the lake catchment area. It has a sediment record spanning eight centuries, with a varve chronology dating to 1867 CE and ^{14}C dating for older lamina (Ekdahl et al. 2004). Maize (*Zea mays*) pollen and corn smut spores (*Ustilago maydis*) are irregularly distributed through an interval greater than 200 years, termed the Iroquoian, reflecting sporadic occupation by pre-European indigenous peoples (Ekdahl et al. 2004, 2007, Figure 16). This occupation is associated with increased numbers of the planktonic diatoms *Asterionella formosa, Fragilaria crotonensis* and *Synedra nana*, depleted numbers of *Cyclotella michiganiana*, and the loss of *Cyclotella bodanica*. These changes are attributed to increased nutrient input, which raised lake productivity, causing bottom-water anoxia and altering diatom assemblages (Ekdahl et al. 2004, 2007). Additional stratigraphic proxies record marked changes in the late-19th century (starting 1867 CE) due to introduction of a new agricultural regime by European settlers, and again in the mid- and late-20th century, driven by regional land-use changes of comparable magnitude to the earlier changes by indigenous peoples.

ACCEPTED MANUSCRIPT

ACCEPTED MANUSCRIPT

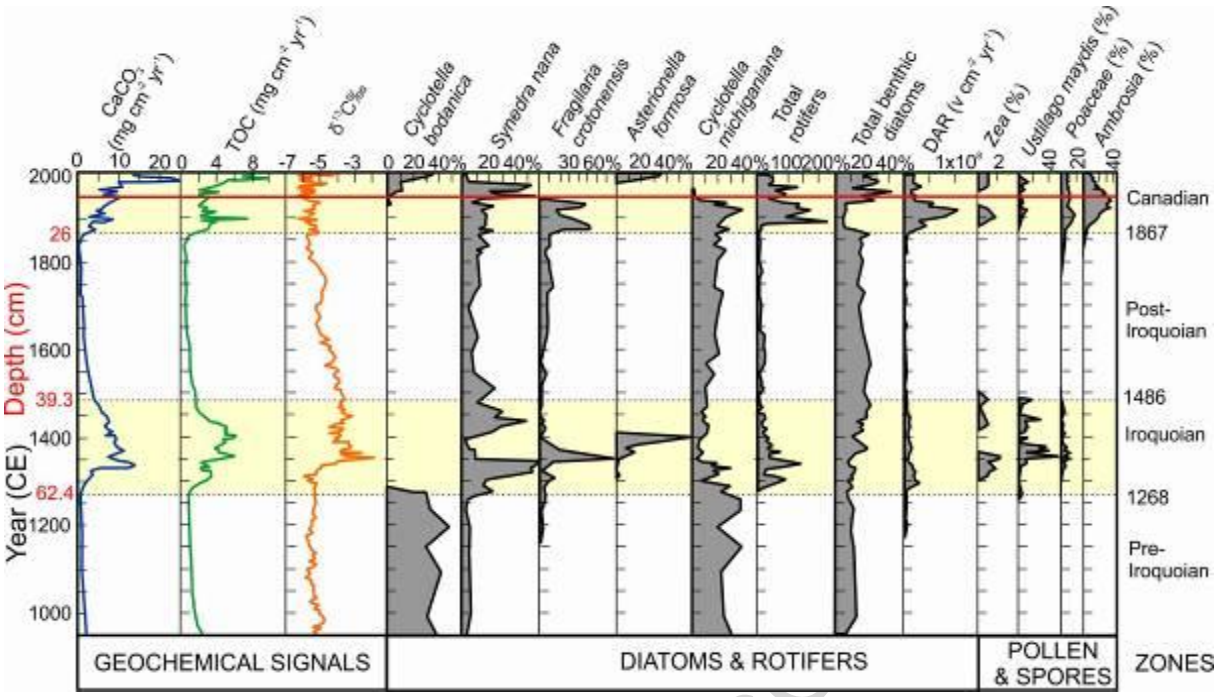

Figure 16. Stratigraphic signals of the last millennium in Crawford Lake, Canada. The horizontal red line near the top is the ~1950 CE level, marked by both lithological and biostratigraphic changes in available data. From Zalasiewicz et al. (2017a), modified after Ekdahl et al. (2004). DAR is diatom accumulation rate.

3.5.2 Lochnagar, Scotland

Lochnagar is a small (surface area 9.8 ha), deep (26.4 m), high altitude (788 m a.s.l) corrie lake in the Grampian Mountains of Scotland. As with many upland and mountain lakes, there are no direct sources of contamination in the catchment so all pollutants are originally from atmospheric deposition. However, the legacy of centuries of atmospheric inputs from industrial sources has resulted in a considerable store in the sparse peat soils which are now being remobilised to constitute a major pollution source to the loch (Yang et al. 2002a).

Lochnagar exhibits a full Holocene record contained within a sedimentary succession <2 m thick. These deposits, neither laminated nor varved but dated by ^{14}C (Dalton et al. 2005), show catchment-driven changes due to the development and degradation of soils (e.g. post-

ACCEPTED MANUSCRIPT

Little Ice Age soil erosion) and human interference on terrestrial vegetation via 'fire management' over the last ~1000 years. Due to the steep morphology of the loch basin, accumulation of sediments varies across the loch with recent accumulations (Rose 2007) being higher than earlier sedimentation rates, as is the case with many European lakes (Rose et al. 2011). Recent sediments are readily dated by ^{210}Pb, independently supported by 1963 CE nuclear weapons testing signals of ^{137}Cs and ^{241}Am and the Chernobyl ^{137}Cs peak in 1986 CE.

The diatom-inferred pH reconstruction for the last 9500 years shows a stable pH of 6.0–6.5 until the 19th century (Monteith et al. 2007) when pH started to decline with the resultant loss of acid-sensitive diatom taxa (*Achnanthes minutissima*, *Achnanthes scotica* and *Fragilaria virescens* var. *exigua*) and an increase in those which are more acid-tolerant (*Achnanthes marginulata* and *Aulacoseira distans* var. *nivalis*) (Battarbee et al. 2014). The pH eventually reached a low of 5.5 in the 1970s before starting to recover in the 1980s, although the trajectory for diatom recovery is not a straightforward reversal (Battarbee et al. 2014). Alongside the 19th century decline in pH were: a) the start of spheroidal carbonaceous particle deposition, which elevated markedly in the mid-20th century (Rose and Yang 2007, Figure 17a); b) increases in the concentrations of trace metals (Figure 17b) such as Pb (from 1860s) and Hg (from the early-20th century), becoming elevated over long-term base-lines (Yang et al. 2002a), and also an increase in Cd, Cu and Zn concentrations (Yang et al. 2002b); and c) a decline in δ^{15}N starting in the late-19th century (Curtis and Simpson 2011, Figure 17c). All of these signals indicate contamination via atmospheric deposition of long-range industrial pollutants.

ACCEPTED MANUSCRIPT

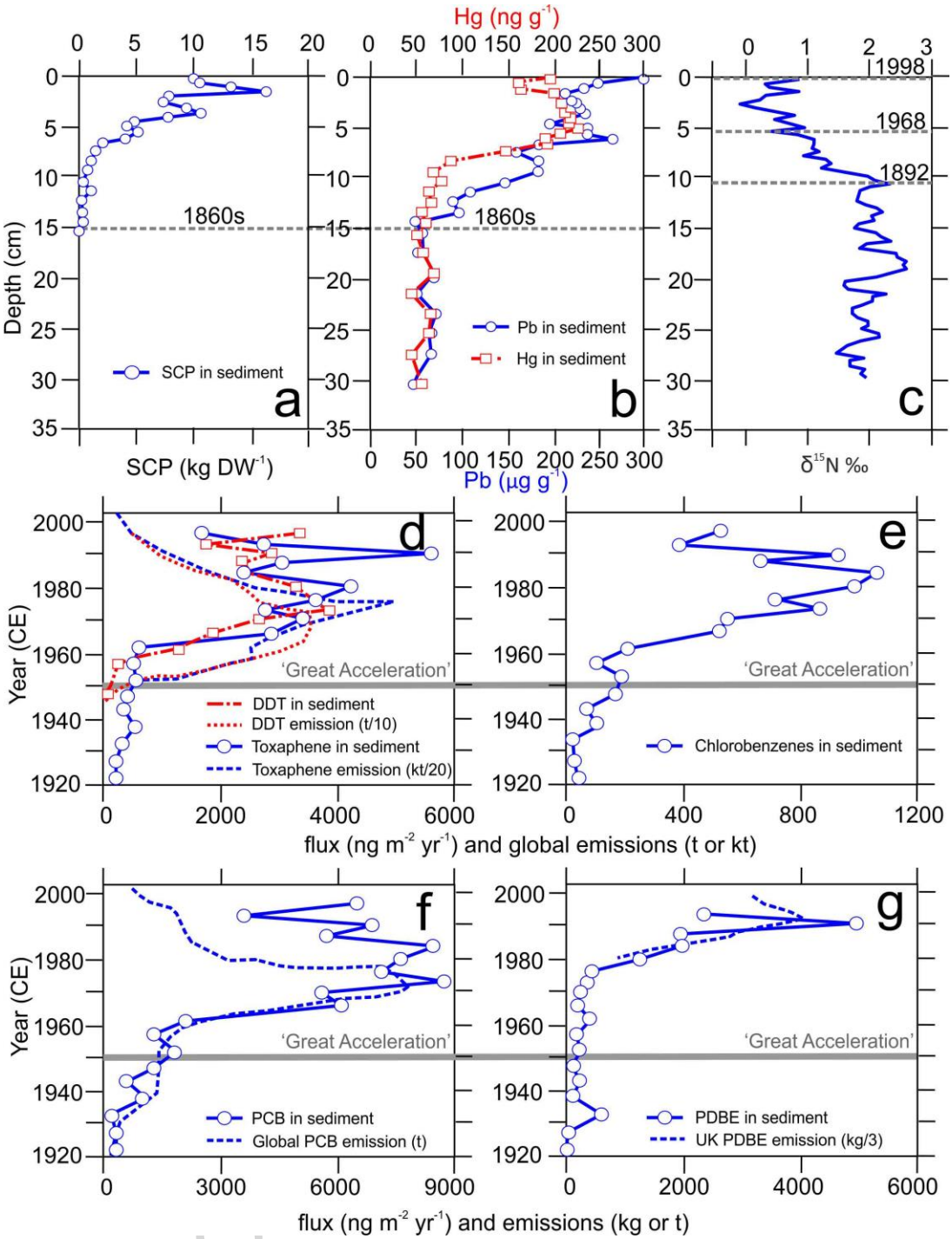

Figure 17. Contamination record in Lochnagar sediments (Scotland) demonstrating appearances as post-mid-20th century markers: (a) Spheroidal carbonaceous particles (SCPs) (from Yang et al. 2002a); (b) Hg and Pb (from Yang et al. 2002a); (c) $\delta^{15}N$ (from Curtis and Simpson 2011); (d) the chlorinated pesticides DDT and toxaphene from core collected in 1997 CE related to emission data (from Muir and Rose 2007); (e) chlorobenzenes (from Muir and Rose 2007); (f) total PCBs related to global emissions (from Muir and Rose 2007); and (g) PDBEs related to UK emissions (from Muir and Rose 2007).

ACCEPTED MANUSCRIPT

Mercury, Pb and SCPs show a further and more significant increase in concentration in the mid-20th century (Figure 17a and b), primarily from fossil-fuel combustion. This period is also accompanied by significant increases in a range of POPs such as organochlorine pesticides, including DDT, although the accumulation in Lochnagar sediments lags about a decade behind emission figures (Muir and Rose 2007, Figure 17d). The organochlorine pesticide toxaphene was never used or produced in the UK (Muir and Rose 2007, Rose et al. 2001), but global emission was greatest in the 1970s with high accumulation rates in Lochnagar sediments in the 1980s and 1990s (Figure 17d). Industrial chemicals including chlorobenzenes and PCBs show elevated values from ~1960 CE and, later, brominated flame retardants such as PBDEs show elevated concentrations from ~1980 CE (Muir and Rose 2007) (Figure 17e–g). The lake sediment records of trace metals and SCPs are matched by records of these same contaminants in the catchment peats of Lochnagar (Yang et al. 2001) with both mid-19th and mid-20th century increases observable.

While the sediment and peat cores of Lochnagar faithfully reflect the temporal trends in contaminant deposition through most of the industrial period, there is evidence that this is not now the case. Temporally-resolved full-basin inventories of Hg and Pb (Yang et al. 2002a) show no decline in inputs to lake sediments in recent decades (Figure 17b) even though emissions of these metals to the atmosphere have declined by 80–90% since the 1970s (NAEI 2017). This 'additional' input of metals can only come from the store of legacy contaminants in catchment soils as a result of increased soil erosion, possibly in part a result of a changing climate. This hypothesis is supported by work at other upland lakes in Scotland for a suite of trace metals and also for SCPs (Rose et al. 2012). The implication of this is that even while upland lake sediments are no longer reliably recording changes in atmospheric

ACCEPTED MANUSCRIPT

deposition (Yang and Smyntek 2014), by being a sink for reworked anthropogenic deposition on land, they are concentrating and temporally extending an anthropogenic signal. This would not affect a mid-20th century GSSP from among such sites.

3.5.3 Lilla Öresjön, Sweden

A lake core from Lilla Öresjön (SW Sweden), a high-sulphate deposition area, records marked physical, chemical and biological trends since 1800 CE (Renberg and Battarbee 1990). Areas of acute lake acidification tend to be associated with atmospheric pollutants including heavy metals, sulphur, fly-ash (spheroidal carbonaceous particles) and PAH, related to fossil-fuel combustion. However, anthropogenic Pb signals have a much longer record in lake sediments in Sweden, initiating 3500 to 4000 years ago, with a small, but clear Roman Pb peak at about 1 CE, a major and unreversed increase at ~1000 CE, markedly elevated levels during the Industrial Revolution, but most prominently after World War II, with peak concentrations at ~1970 CE (Renberg et al. 2000). The record of increased Pb concentration is associated with concomitant declines in the Pb isotope ratio (Renberg et al. 2000).

At Lilla Öresjön atmospheric pollution is evident with an increase in Pb, Zn, and benzo(a)pyrene at about 1900 CE (dated by ^{210}Pb) and a more pronounced increase of these signals along with sulphur and SCPs during the 1960s (Renberg and Battarbee 1990, Figure 18). Heavy metal and sulphur signals peaked in the 1960s and 1970s, and SCPs and PAH in the 1970s. Analysis of diatoms, chrysophytes, cladocerans and pollen show a succession of changes reflecting decreasing lake pH, with a distinct post-mid 20th interval discernable (Figure 18 herein; Renberg and Battarbee 1990).

ACCEPTED MANUSCRIPT

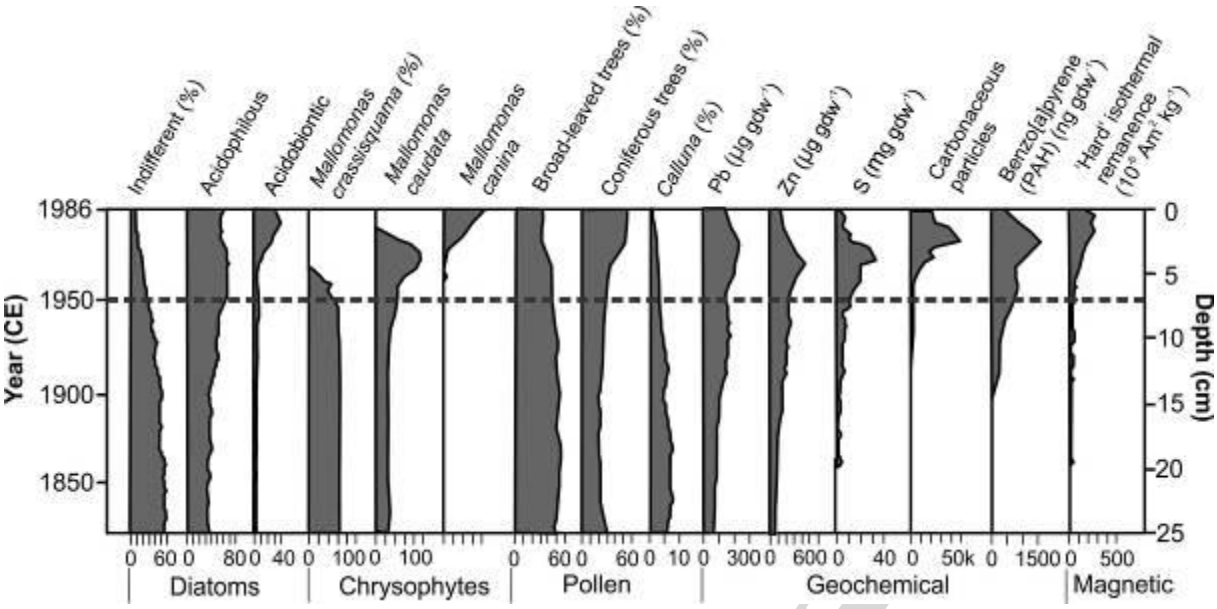

Figure 18. Physical, chemical and biological trends from Lilla Öresjön (SW Sweden), a high-sulphate deposition area (from Renberg and Battarbee 1990).

3.5.4 Huguangyan Maar Lake, Guangdong, China

Huguangyan Lake, eastern China, receives little sediment input from rivers or from soil erosion, hence its records of black carbon (BC) and polycyclic aromatic compounds (PACs) reflect atmospheric deposition (Han et al. 2016). The sediment record covers the past 350 years and has been dated reliably for the last 150 years using ^{210}Pb and ^{137}Cs activities (Han et al. 2016). Concentrations of BC, PAH, oxygenated PAHs (OPAH) and azaarenes (AZAs) increased sharply during the late-1940s to early-1950s, and again in the late-1970s (Han et al. 2016, Figure 19). The BC record peaks from 2004 to 2006 CE, with subsequent rapid decrease, whereas the PAC record has continued to rise (Han et al. 2016).

ACCEPTED MANUSCRIPT

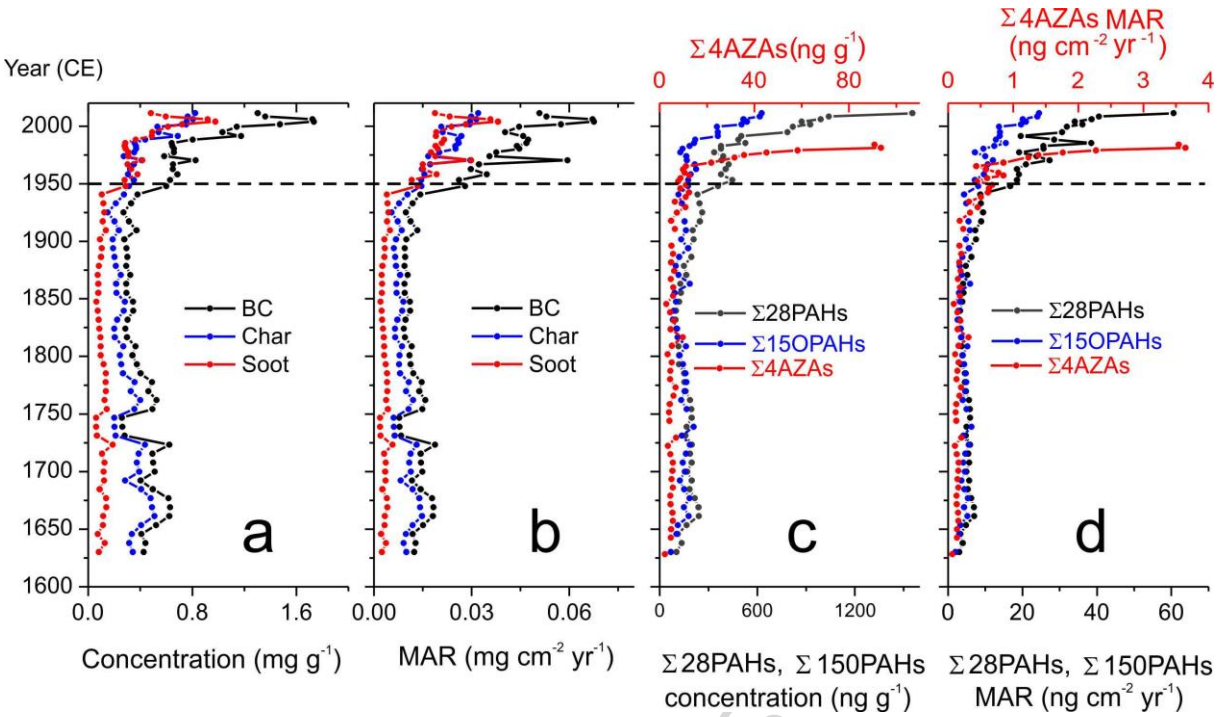

Figure 19. Historical variations of concentrations and mass accumulation rates (MARs) of black carbon (BC), char, and soot, parent-PAHs, oxygenated PAHs (OPAHs), and azaarenes (AZAs) in the Huguangyan Maar Lake (from Han et al. 2016).

The sedimentary record of char, soot, and PACs in this lake reflects the start of the rapid industrialization in China after the 1950s, associated with a change in dominant energy sources from mainly wood burning in the pre-1950s to fossil fuels in the post-1950s (Han et al. 2016).

3.5.5 Maha'ulepu Lake of Kauai, Hawaii

The sedimentary successions of the Maha'ulepu Sinkhole and caves of Kauai, Hawaii (Burney et al. 2001) show a record of extirpation of geographically local taxa and biotic invasions of rats and other fauna. The sinkhole succession extends over the past 9500 years that accumulated in a freshwater to brackish lake, with periodic marine incursions, and which includes diatoms, land snails and bivalves. The diatoms, coupled with ^{14}C dates, provide a

ACCEPTED MANUSCRIPT

detailed stratigraphy for the sinkhole and cave succession, which records step changes in anthropogenic influence through Polynesian and European colonisation of the island.

Human impact in the Maha'ulepu Sinkhole (Figure 11) is first seen as an introduced Pacific rat dated to between 1039 and 1241 CE (Burney et al. 2001). Changes in land snail species indicate the impact firstly of Polynesian and latterly European colonisers and their associated neobiota. Declines in several species coincide with Polynesian activity, whilst all indigenous snail taxa, with the exception of *Cookeconcha* cf. *psaucicostrata*, became extinct during the 19th and early-20th centuries. In the 20th century, *Lissachatina fulica* (in 1936 CE) – the Giant African Snail - and *Euglandina rosea* (in 1957 CE) – the Cannibal Snail of Central America - were introduced (Figure 11). Anecdotal evidence suggests a 20th century extinction for the last indigenous snail population of *C.* cf. *psaucicostrata*. These changes provide a detailed and unfolding biostratigraphical record of human impact on the local biota that is supported by diatom, bird, pollen, and other fossil data (Burney et al. 2001). Furthermore, in the marine succession, neobiotic marine bivalves such as *C. virginica* on Oahu, offer potential for inter-regional correlation (Figure 11).

3.6 Peat and peatlands (mires)

Peatlands (mires) may be defined as wetlands in which at least 40 cm of peat has accumulated; peat is partially-decomposed, sub-fossil plant material containing less than 25% by weight mineral matter (Shotyk 1992). Swamps and fens are "minerotrophic" wetlands, that is, plants growing there receive mineral nutrients primarily from surface waters and groundwaters. Fens are almost always peatlands, but swamps may be either mineral wetlands or peatlands, depending on the thickness of peat accumulation (Shotyk

ACCEPTED MANUSCRIPT

1992). In contrast, the surface layers in bogs are beyond the influence of these waters, and the plants growing there receive their nutrients solely from atmospheric inputs (termed "ombrotrophic"). Because bog plants are fed exclusively by rain and dust, the peats which accumulate in bogs have naturally low concentrations of mineral matter and trace metals, providing low background values against which anthropogenic inputs may be compared. Note that wetlands are not necessarily peatlands, and that most peatlands are not ombrotrophic bogs.

Northern (boreal and subarctic) peatlands are by far the most extensive development of peat, covering some 4 million km^2, whereas the equivalent southern peatlands, mainly in Patagonia, South America cover only 45,000 km^2 (Yu et al. 2010, Figure 20). Tropical peatlands cover an area of ~370,000 km^2 (Yu et al. 2010), the most extensive area being the ~145,000 km^2 of the Congo Basin (Dargie et al. 2017). In the case of the Congo Basin, however, peat was defined as having <35 % mineral matter, and a thickness of >30 cm (Dargie et al. 2017), this differing from the conventional definition cited earlier. Tropical peats mainly occur along major river systems, and in SE Asia are associated with mangrove development along coastal zones (Yu et al. 2010). Peak accumulation rates for these peats are in the Middle Holocene for the tropical peats, Early Holocene for the northern peatlands, and Late Pleistocene for the southern peats (Yu et al. 2010).

ACCEPTED MANUSCRIPT

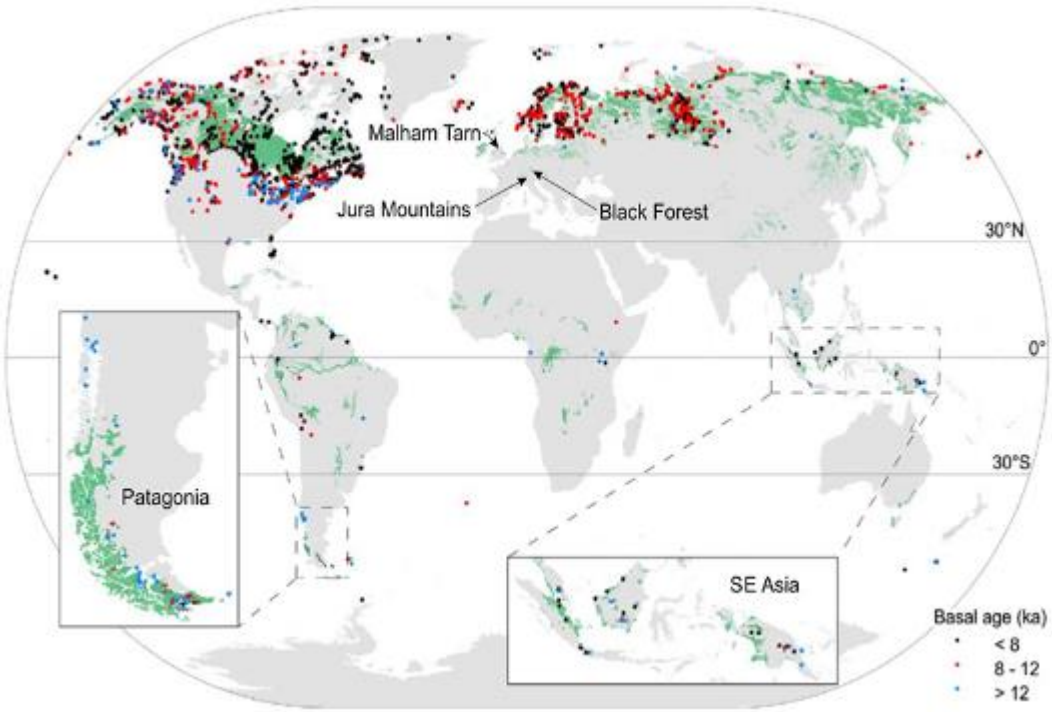

Figure 20. Global map of peatland regions with basal peat ages (black <8 ka, red 8–12 ka, and blue >12 ka) (from Yu et al. 2010).

Surface waters and groundwaters contain carbonate alkalinity from the chemical weathering of carbonate and silicate minerals, so the waters in fens and swamps tend to be neutral to alkaline in pH. Rainwater, on the other hand, contains very little alkalinity. In consequence, the organic acids generated during the decay of organic matter quickly render bog surface waters acidic (pH 4). Bog surface waters are also oligotrophic, so only specialized plant communities are able to thrive. Finally, the depth to water table in bogs will vary seasonally, resulting in redox conditions varying from oxic to anoxic. Seen from this perspective, the peat and corresponding porewaters in bogs represent a complex chemical milieu for the compounds that are continually being supplied by the atmosphere.

As peat accumulates over time, fens and swamps can evolve into bogs, as the surface layers become increasingly removed from the basal mineral sediments and plants gradually

ACCEPTED MANUSCRIPT

become deprived of nutrients. Thus, it is very common to find ombrotrophic bog peats overlying minerotrophic fen and swamp peats (Shotyk 1988). To use peat cores from bogs as archives of atmospheric deposition, it is crucial to clearly distinguish between the ombrotrophic versus minerotrophic sections: this can be done using a broad array of chemical indicators in either the solid or aqueous phases, such as ash or Ca content of the peat, or pH and Ca content of the porewaters (Shotyk 1996).

Peat cores from bogs have been used to study atmospheric change over time using the broad range of parameters listed in Table 8. This list of proxies of environmental change does not imply their fidelity in the peat bog archive. Rather, it should be viewed as an illustration of the broad potential and number of opportunities represented by bogs to study environmental change. While most of these proxies have been impacted by human activities, few provide truly global signals, mainly because of the varying chronology and intensity of anthropogenic emissions throughout the industrial world (mineral dusts, spheroidal particles), biogeochemical transformations within the peatland (N and S compounds) and the size of the host aerosol which is crucial for long-range atmospheric transport (metals and organic contaminants). Radionuclides from nuclear weapons testing are exceptional in that they reached the stratosphere, are found in the sub-micrometre aerosol fraction, and therefore their fallout was dispersed globally (Junge 1963).

ACCEPTED MANUSCRIPT

ACCEPTED MANUSCRIPT

Proxy	Type of environmental change	Example
Plant macrofossils	Climate change, human-induced changes in vegetation caused by impacts to watershed hydrology	Magnan et al. (2014)
Pollen	Landscape evolution in response to climate change, forest clearing and agriculture	Markgraf and Huber (2010)
Soil-derived mineral dusts	Wind erosion of soils due to climate change, or caused by forest clearing for agriculture and soil tillage	Chapman (1964); Vuorela (1983)
Volcanic ash	Natural, episodic inputs that may mask anthropogenic inputs of other inorganic constituents	Zoltai (1989)
Trace elements (Ag, As, Cd, Cr, Cu, Ni, Pb, Sb, Se, Sn, V, Tl, Zn)	Derived mainly from mining, smelting and refining of base metals as well as ferrous metallurgical processing and coal combustion. The chlor-alkali industry was a significant source of atmospheric Hg in the past, and artisanal gold mining is an important source of Hg today	As, Cu, Zn: Küttner et al. (2014); Cr, V; Allan et al. (2014); Hg: Enrico et al. (2016); Pb: Veron et al. (2014); Sb: Rothwell et al. (2010); Sn: Meharg et al. (2012)
Lithophile elements (Al, Sc, Th, Ti, Y and the REE)	Wind erosion of soils due to climate change, or caused by forest clearing for agriculture and soil tillage	Vanneste et al. (2015); Kylander et al. (2016); Pratte et al. (2017)
Platinum group elements (PGE)	From automobile catalytic converters	Rauch et al. (2004, 2010)
Fallout radionuclides (including ^{137}Cs, ^{241}Am; also isotopes of U and Pu)	From atmospheric nuclear weapons testing, plus accidental releases from nuclear reactors	Quinto et al. (2013a, b)
Organic contaminants	Polycyclic aromatic hydrocarbons (PAHs) from both natural (prairie and forest fires) and anthropogenic (fossil fuel combustion, petroleum refining) sources	Zhang et al. (2016)
Organometallic compounds	Tetraethyl-lead and tetramethyl lead, from leaded gasoline	Shotyk et al. (2002)
Nitrogen and sulphur (including stable isotopes)	Atmospheric emissions of nitrogen oxides from fossil fuel combustion; sulphur oxides from this plus sulphide mineral roasting	Wieder et al. (2016a, b)
Spheroidal carbonaceous particles	From fossil fuel combustion	Rose (2015); Swindles et al. (2015)
Inorganic ash spheres	From fossil fuel combustion and nuclear explosions	Fialkiewicz-Kozieł et al. (2016)

ACCEPTED MANUSCRIPT

Table 8. Selected examples of the use of proxies for various types of atmospherically sourced environmental change.

The preservation over time of some of the constituents supplied by the atmosphere may be constrained by the low pH, abundance of complex-forming organic acids, range in redox potentials, and advective flow in response to water table drawdown. The extent of preservation ranges from near-perfect (plant macrofossils are extremely well preserved in anoxic water) to very poor (^{137}Cs is very mobile in ombrotrophic peat, simply because monovalent cations are poorly retained; it is far better retained in minerotrophic peat because of the abundance of phyllosilicates which fix Cs within their siloxane cavities). Some trace metals are very well preserved (e.g. Ti and Zr because of the stability of their host minerals in acidic waters), others not at all (e.g. Mn and Fe which form soluble, mobile cations under anoxic conditions). While there may be hundreds of publications employing bogs as environmental archives, there are remarkably few studies of chemical diagenesis of atmospheric contaminants, and the possible importance of post-depositional migration. Diagenesis of organic contaminants in peat is discussed at length by Thuens et al. (2013), using the example of PAHs, fallout radionuclides using the examples of U and Pu by Quinto et al. (2013a, b), and trace metals using the example of Pb by Shotyk et al. (2016).

Age-dating of peat profiles presents many challenges; peat bogs are not varved, but can have high (annual) growth rates, although these can be very variable. In Switzerland, 1 m peat cores ranged from ~ 1000 to 7000 years of peat accumulation (Shotyk et al. 2000). The most robust age-depth models use a combination of approaches, including ^{14}C (which is physically incorporated within the organic molecules making up the peat) and ^{210}Pb (which is

ACCEPTED MANUSCRIPT

supplied to the peatland surface by the sub-micrometre aerosol fraction and, apparently, becomes adsorbed to the peat).

Table 9 summarises the key advantages and disadvantages of hosting a potential GSSP within peatlands. Examples of geochemical records from peat bogs are provided from the Jura Mountains of Switzerland and Malham Tarn in England.

For:	Against:
• Widely distributed and studied in northern and southern latitudes; extensive deposits in the tropics are beginning to receive attention • Relatively rapid rates of accumulation of organic matter provide reasonable temporal resolution of atmospheric change • Readily amenable to ^{14}C age dating (including the post-1950 CE atmospheric bomb pulse) • Dating of recent peat accumulation (past ~150 years) possible using ^{210}Pb • Ombrotrophic bogs receive inputs directly and exclusively from the atmosphere with no settling delay • Wide variety of indicators of industrial activities are easily measured: soil-derived dust particles, N and S compounds, fallout radionuclides, heavy metals, organic contaminants, spheroidal carbonaceous particles (SCP) and inorganic ash spheres (IAS)	• In many industrialized regions most bogs have been damaged, altered or destroyed due to drainage for agriculture, development, forestry, or exploited for fuel or horticultural peat • Peat accumulation rates vary over time depending on climate, hydrology, fire and inputs of mineral matter from wind erosion of soils, or volcanic ash; they are not varved • ^{210}Pb age dating requires independent confirmation using chronostratigraphic markers including: other fallout radionuclides (such as ^{241}Am), pollen, tephrochronology, or contaminants of known emission history (e.g. DDT) • Pb is immobile in undisturbed peat profiles but can be mobilized by bog water acidification (from acid rain) or peatland drainage (which promotes leaching) • Minerotrophic peatlands are influenced and commonly dominated by aquatic inputs (surface and groundwater). Atmospheric signals may be discernible in minerotrophic systems provided that aquatic inputs are insignificant (e.g. fallout radionuclides) • With acidic bog waters and seasonal variations in water table depth (and therefore varying thickness of the oxic surface layer), each proxy may be subjected to chemical diagenesis; the possible importance of post-depositional migration (or chemical transformation) of each proxy must be evaluated

Table 9. Reasons for and against using a peat deposit as a potential host for a GSSP.

ACCEPTED MANUSCRIPT

3.6.1 Pb, organic contaminants and radionuclide fallout deposition at Etang de la Gruère, Jura Mountains, Switzerland

The protected ombrotrophic *Sphagnum* bog of Etang de la Gruère has the longest record of peat accumulation (6.5 m accumulated in ~15,000 years) in the Northern Hemisphere (Shotyk et al. 1998). Traces of atmospheric lead appear in this Swiss peat bog from 12,370 ^{14}C yr BP (Shotyk et al. 1998). Climate-controlled enhanced Pb fluxes derived from soil dust are recorded with maxima at 10,590 and 8230 ^{14}C yr BP, the latter coinciding with the start of the Middle Holocene (Shotyk et al. 1998). The first anthropogenically-controlled increase in Pb deposition starting at 5320 ^{14}C yr BP is thought to be due to forest clearing and the introduction of agriculture (Shotyk et al. 1998). The first influence of Pb pollution from mining and smelting started at 3000 ^{14}C yr BP and occurs at a depth of 1.4–1.5 m, seen as increased Pb enrichment and decreased ^{206}Pb/^{207}Pb ratios (Shotyk et al. 1998). However, by far the greatest Pb flux occurred in the late 20th century (Figure 21a), reaching 1570 times the background value by 1979 CE (Shotyk et al. 1998), associated with greatly decreased ^{206}Pb/^{207}Pb ratios (Figure 21b). Subsequently, reduced Pb contents and increasing Pb isotope ratios in the later decades of the 20th century appear to record the introduction of unleaded gasoline and a reduction in industrial sources of Pb in the region (Shotyk et al. 1998). The Pb signals in peat at this locality are consistent with Pb levels in the Greenland GRIP ice core over the past 3000 years (Shotyk et al. 1998) and can be compared with the Greenland ACT2 core (Figure 26).

ACCEPTED MANUSCRIPT

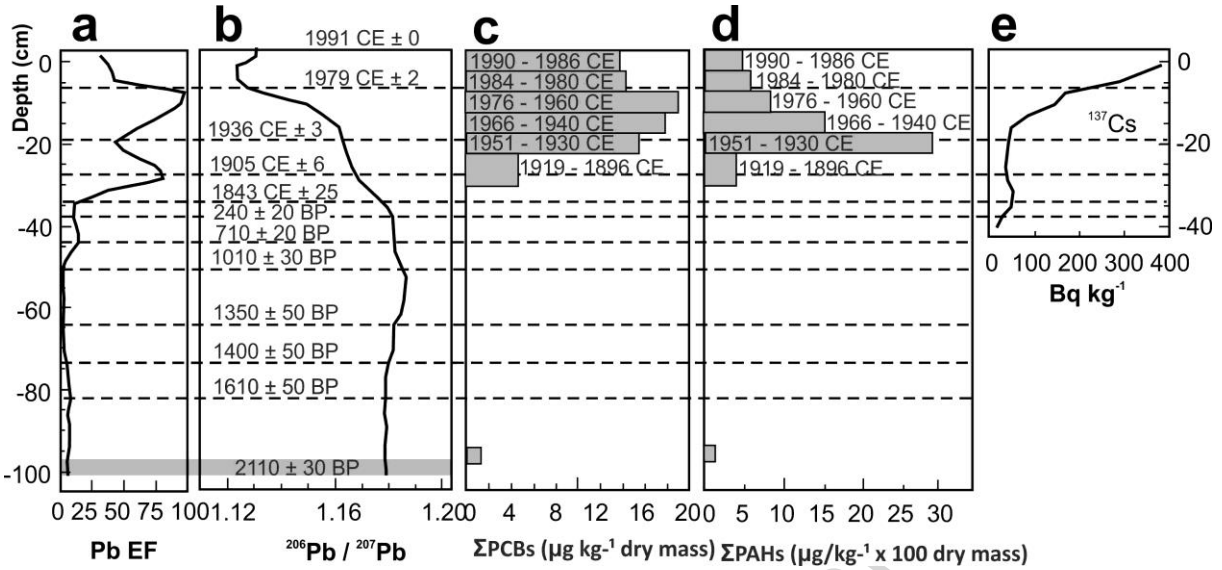

Figure 21. Core from Etang de la Gruère, Switzerland, collected in 1991 CE: a) Pb Enrichment Factor (EF) calculated as the ratio of Pb/Sc in the peats, normalized to the background value (from Shotyk et al. 1998); b) Pb isotopic values (from Shotyk et al. 1998); c) ΣPCBs (from Berset et al. 2001); d) ΣPAHs (from Berset et al. 2001); e) ^{137}Cs (from Appleby et al. 1997). Succession dated using ^{210}Pb to 35 cm depth (Appleby et al. 1997) and ^{14}C yr BP from 35 cm to base (Shotyk et al. 1998).

The highest concentrations of PCBs occurred at a depth of 10–15 cm (dating from 1976 to 1960 CE; Figure 21c) while PAHs reached a maximum at a depth of 20–25 cm (1951 to 1930 CE; Figure 21d), with post-depositional downward migration of these compounds unlikely (Berset et al. 2001). The maximum PAH values coincide with greatest use of coal in Switzerland, after which fuel oil dominated (Berset et al. 2001).

The same core has records of ^{241}Am activity limited to 12–15 cm depth (Appleby et al. 1997), marking the early 1950s to early 1960s bomb-spike. ^{137}Cs activity is at a maximum in the living part of the profile in the upper 3 cm (Appleby et al. 1997; Figure 21e), inferred to be sourced by the Chernobyl disaster of 1986 CE. ^{137}Cs is also recorded below the level of the ^{241}Am signal, probably because it has been remobilized downwards.

ACCEPTED MANUSCRIPT

3.6.2 Spheroidal carbonaceous particles and Pb in Malham Tarn Moss, England

Spheroidal carbonaceous particles (SCPs) first appear in the peat succession adjacent to an upland lake at Malham, England, at a level deposited in the 1850s, but there is a marked increase in their abundance in the 1950s (represented by less than 10 cm of peat), with a peak in the 1970s (Figure 22, Swindles et al. 2015). Atmospheric lead pollution from local industrial activity and additives in petrol, and increased soil erosion (reflected in the Fe and loss-on-ignition data), show comparable upturns in the mid-20th century.

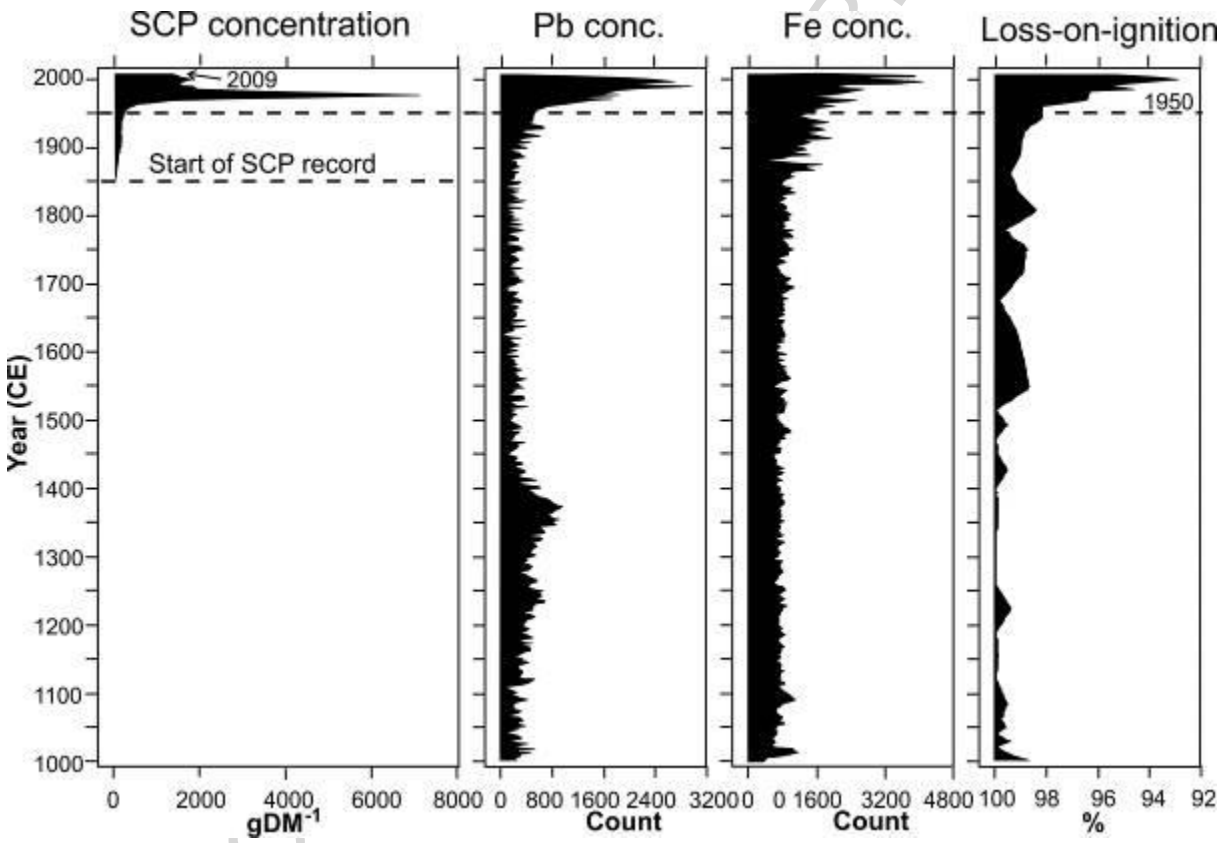

Figure 22. Spheroidal carbonaceous particles (SCPs), lead and iron concentrations from Malham Tarn Moss, England (from Swindles et al. 2015).

ACCEPTED MANUSCRIPT

3.7 Ice

Continental ice sheets including those of Antarctica, covering about 13 million km^2, and Greenland, covering about 1.7 million km^2 (UNEP 2007), are together equivalent to about 9.4% of the total land surface area (Figure 23). Ice from glaciers occurring both marginal to the ice sheets and in high-altitude regions makes up a further ~0.5% of the Earth's land surface, a coverage of 726,800 ± 34,000 km^2 (Pfeffer et al. 2014) (Davies, B. Mapping the World's Glaciers http://www.antarcticglaciers.org/glaciers-and-climate/mapping-worlds-glaciers/ Last updated 22/06/2017). Sea ice fluctuates in extent seasonally and does not form a permanent ice record for consideration as a potential GSSP site. Although ice sheets and glaciers have significant extents, what little permanent ice remains in Africa and Australasia (Figure 23) is rapidly being lost. Alpine glaciers from high altitudes may be suitable as potential GSSPs, but those from lower elevations are prone to significant seasonal melting and potential loss of laminae. Land glaciers in tropical regions are now melting from the top down and losing their younger layers (e.g. in Peru). Within alpine glaciers, unlike on polar ice sheets, meltwater processes can mobilize or remove solutes, attenuating or complicating the environmental signal (Schuster et al. 2002). In contrast, polar land ice is a more permanent record. The Greenland ice sheet shows the effects of greater local contamination from Northern Hemisphere industrial activities, while Antarctic land ice is more pristine.

ACCEPTED MANUSCRIPT

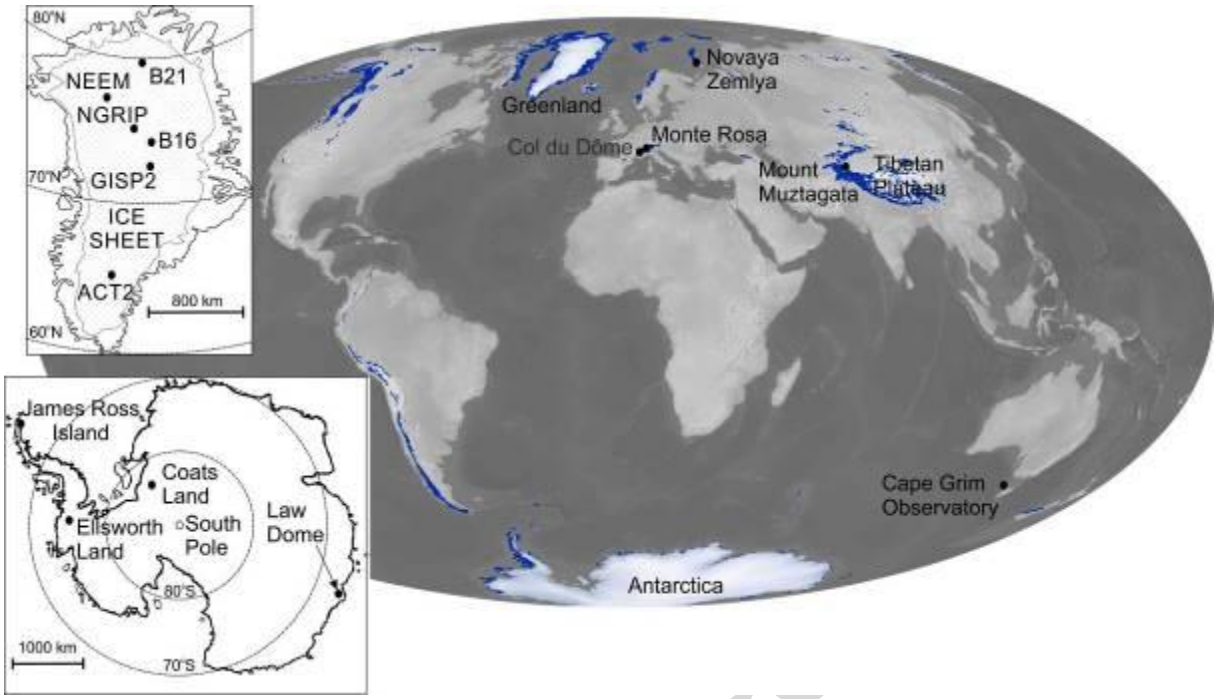

Figure 23. Distribution of ice caps and glaciers (blue) and ice sheets (white) from NASA Earth Observatory Randall Glacier Inventory in 2014 CE http://earthobservatory.nasa.gov/IOTD/view.php?id=83918 (acquired 7th May 2014; produced by Jesse Allen and Robert Simmon). Inset maps showing the main polar drilling sites in Antarctica and Greenland mentioned in the text.

Quaternary stratigraphy is closely linked to climatic variations during the ~2.6 million years of bipolar glaciation. Ice cores provide the best record of climate-related data for up to 800 ka, including isotopic ratios for $\delta^{18}O$ and δD, variations in CO_2 and CH_4 concentrations and dust, and S concentrations related to distinct volcanic events. The use of a Greenland ice core for the Holocene GSSP (Walker et al. 2009) provides a precedent that may be considered for the Anthropocene. Atmospheric CO_2 and CH_4 concentrations and novel compounds such as sulphur hexafluoride SF_6 can be detected in ice-core air bubbles (Wolff 2014). The ice record also captures anthropogenic signals derived from aerosols, including radionuclide signals from nuclear bomb testing (e.g. ^{239}Pu, ^{14}C), unprecedented increases in black carbon (BC) and metals such as Pb from industrial activity and automobile emissions, sulphate especially from coal combustion, and nitrate from fertilisers. These signals occur

ACCEPTED MANUSCRIPT

within annually resolvable laminae, the ages of which are typically determined by counting or from seasonal cycles in $\delta^{18}O$, and then verified using known volcanic eruption signals, which can be identified from electrical conductivity measurements in Greenland (e.g. Masson-Delmotte et al. 2015), and at Law Dome, Antarctica (Etheridge et al. 1996). Silicate dust concentrations in polar snow are exceedingly small, a mean of 2 ppb in Antarctica and 35 ppb in Greenland, with the latter showing no systematic trends over two centuries from 1750 CE (Murozumi et al. 1969).

The upper part of an ice sheet or glacier, which includes the succession that covers the mid-20th century interval, comprises firn (partially compacted snow that is not yet fully ice), where bubbles are not yet closed from connection to the atmosphere. For most signals that are trapped directly in the solid ice this does not represent a problem, but CO_2, CH_4 and N_2O are contained in trapped air bubbles. These air bubbles and their environmental signals are therefore always younger than the enclosing ice, and this effect is significant over the short timescales considered for the Anthropocene. However, recent work shows that the nitrogen isotopes in air bubbles can be used to estimate their ages correctly, enabling direct comparison with ice of the same age (Parrenin et al. 2013). The depth and hence timing of the firn-to-ice transition is dependent upon the accumulation rate, and so sites with rapid accumulation rates are preferable. At the South Pole, where the accumulation rate is only 8 cm yr^{-1} the firn-to-ice transition depth is at about 123 m (Rubino et al. 2013).

Over the past 350 years in East Antarctica, δD proxy values show a long-term warming trend of about 1 ± 0.2 °C, with a marked colder period from 1750 to 1860 CE corresponding to the end of the “Little Ice Age (LIA)” (Ekaykin et al. 2017). This is consistent with James Ross Island and other parts of the Antarctic Peninsula, these areas warming significantly from about

ACCEPTED MANUSCRIPT

1950 CE onwards (Quayle et al. 2002, Abram et al. 2013). In north Greenland, $\delta^{18}O$ shows multi-decadal increasing trends in the late-19th century and since the 1980s, whereas the early-19th century had the lowest signals, associated with the Little Ice Age. Overall, Greenland δD and (laterally variable) $\delta^{18}O$ show no significant variation across the mid-20th century, with the most prominent climatically linked changes occurring about 1850 CE (Masson-Delmotte et al. 2015, Ekaykin et al. 2017, Figure 24 herein).

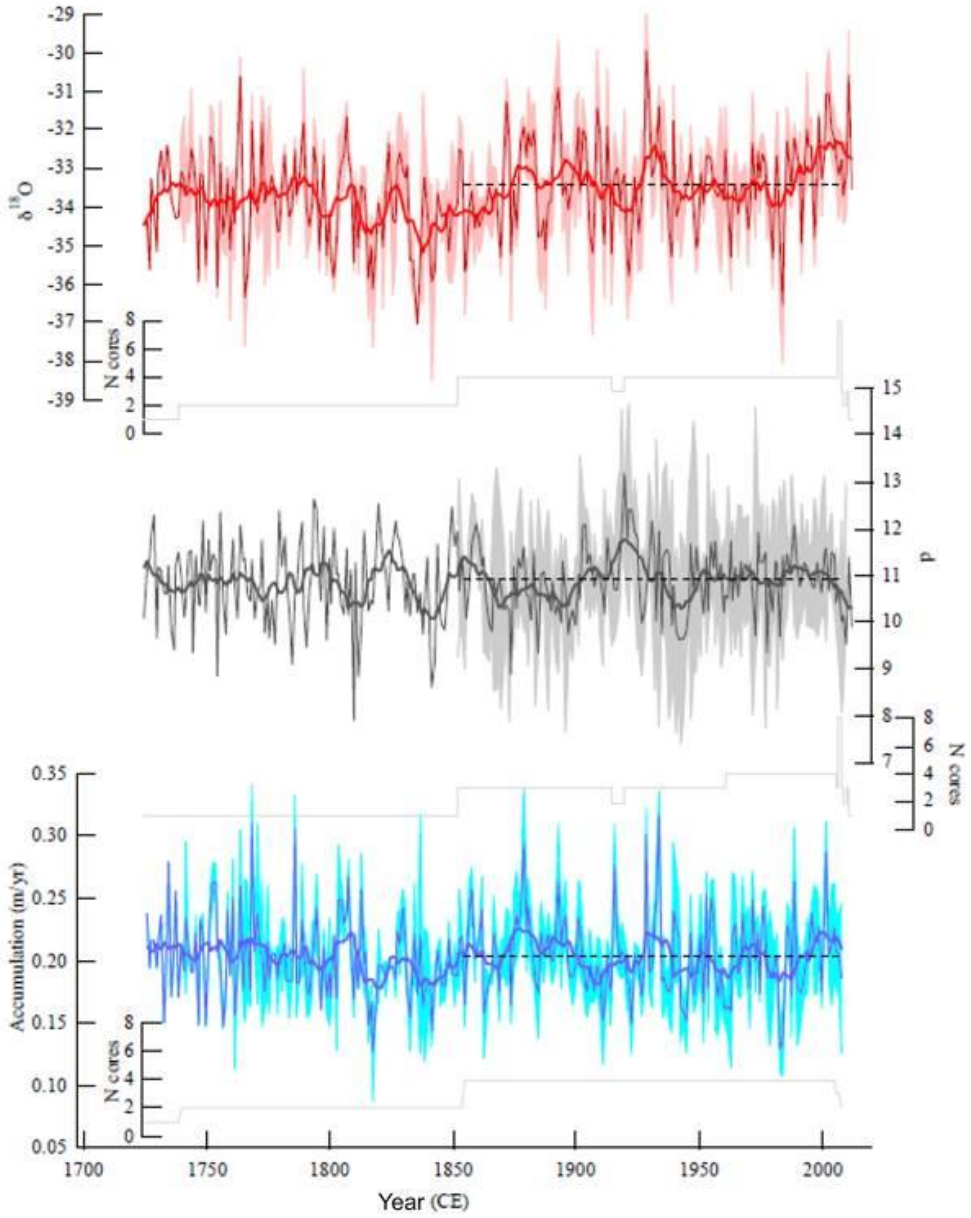

Figure 24. $\delta^{18}O$, δD and accumulation rates for the North Greenland Eemian Ice Drilling site (NEEM) (Masson-Delmotte et al. 2015).

ACCEPTED MANUSCRIPT

One of the main climate-related signals evident in ice sheets is the increase in CO_2 concentration (Figure 25), now 30% above the highest level of the last 800 ka (Wolff 2014), and the $\delta^{13}C$ change to more depleted values, both occurring at about 1960 CE in Law Dome ice core (Rubino et al. 2013) and discussed below. This may reflect the divergence of fossil fuel use (which has accelerated) and land use as independent sources of atmospheric CO_2 and hence of the $\delta^{13}C$ signal (Rubino et al. 2013). CH_4 is now at ~1800 ppb (Figure 25), double the highest level of the last 800 ka (Wolff 2014).

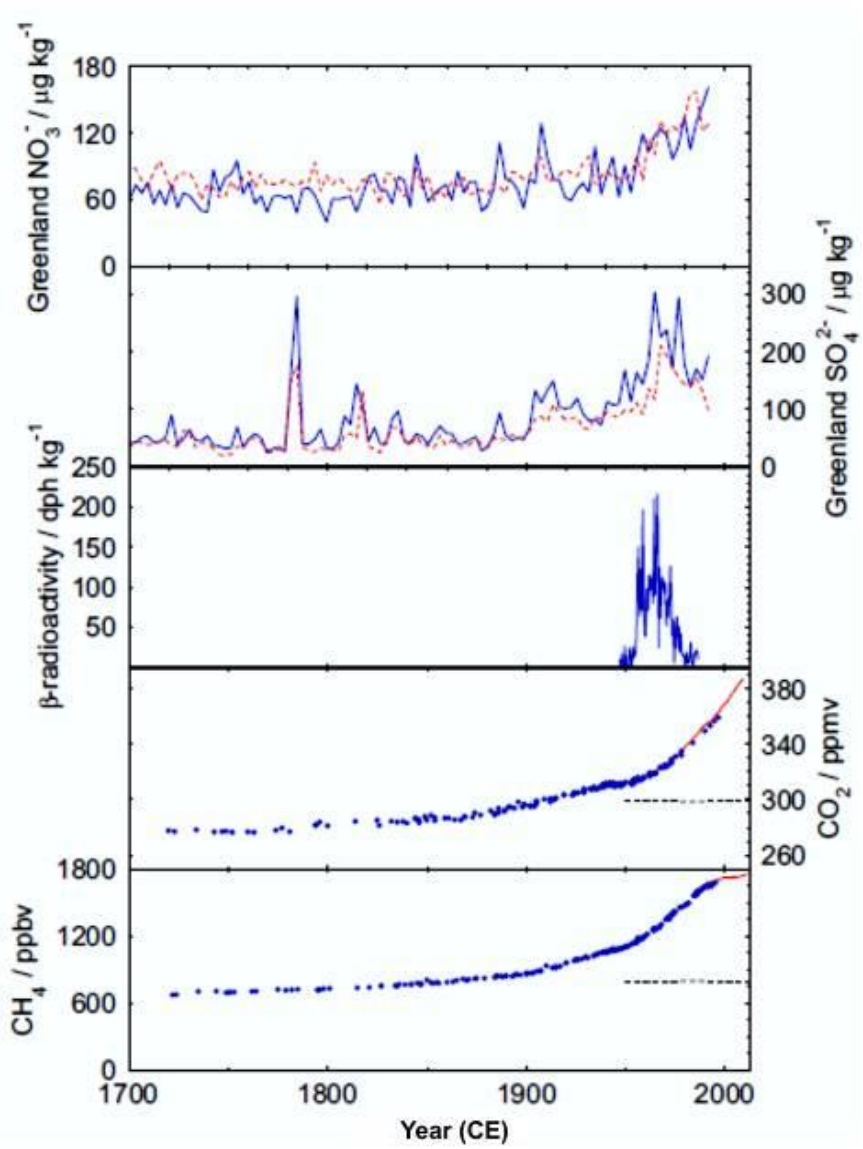

ACCEPTED MANUSCRIPT

Figure 25. Ice core signals since 1700 CE (from Wolff 2014). CH_4 and CO_2 ice-core data (blue dots) are from Law Dome, Antarctica (MacFarling Meure et al. 2006), and recent atmospheric data (red lines) from Mauna Loa (CO_2) and Cape Grim (CH_4) observatories. The horizontal dashed lines are the highest values observed in ice cores of the last 800,000 years prior to the period shown. Beta radioactivity is from Coats Land, Antarctica (Wolff et al. 1999). Sulphate and nitrate are shown for two cores from Greenland: B16 (dashed red) and B21 (solid blue) (Fischer et al. 1998). The 18th- and 19th-century spikes in sulphate are signals of volcanic eruptions.

The most abrupt anthropogenic signal in ice is radioactive fallout from the atmospheric testing of nuclear devices. This is clearly evident in ice core as a marked increase in beta radioactivity initially in 1954 CE and subsequently in 1964 CE to form a bomb-spike peak in 1966 CE (Figure 25), followed by slow decay towards natural background levels (Wolff et al. 1999, Wolff 2014) after testing went underground following the Partial Test Ban Treaty in 1963 CE and essentially ceased following the Comprehensive Test Ban Treaty in 1996 CE (see Waters et al. 2015). The beta radiation is from several radioactive isotopes, some with short half-lives, e.g. ^{90}Sr and tritium. The long-lived radionuclide ^{239}Pu in polar ice has been transferred primarily via the stratosphere, with atmospheric residence times of up to 5 years and with seasonal transfer to the troposphere occurring in late winter and spring in the Northern Hemisphere (Arienzo et al. 2016). The accumulation rate of ^{239}Pu is typically greater in ice, and shows less post-depositional alteration or mixing, than in corals and lake sediments (Arienzo et al. 2016). Analysis for ^{239}Pu using traditional accelerator mass spectrometry (AMS) requires large sample size, typically reducing the resolution to about 3 years (Arienzo et al. 2016). A high-resolution (0.5–1.5 years) ^{239}Pu profile from Monte Rosa on the Italian-Swiss border, using ICP-SFMS, shows an initial peak from 1954–1955 to 1958 CE (Gabrieli et al. 2011). Following a temporary halt of testing in 1959–1960 CE, in which the Pu concentration decreased by half with respect to the 1958 CE peak, in 1961–1962 CE Pu

ACCEPTED MANUSCRIPT

concentrations increased rapidly to a peak in 1963 CE (Gabrieli et al. 2011). Following the Partial Test Ban Treaty, Pu deposition decreased sharply to a minimum in 1967 CE (Gabrieli et al. 2011). The interval 1967–1975 CE is characterized by small irregular Pu smaller peaks likely due to the deposition of Saharan dust contaminated by French nuclear tests of the 1960s, this effect diminishing after 1975 CE (Gabrieli et al. 2011). Arctic ice typically has a higher ^{239}Pu activity (differing by about a factor of three) than Antarctic ice (Arienzo et al. 2016) and, despite the first significant atmospheric thermonuclear detonations occurring in 1952 CE, the first detection of ^{239}Pu in polar ice was in 1953 CE (Arienzo et al. 2016). The post-moratorium ^{239}Pu bomb-spike (peak signal) occurs in the 1962 CE ice laminae in the Arctic, but is not strongly resolved in the Antarctic, mainly because the principal testing occurred in Novaya Zemlya (northern Russia), and little of this fallout crossed into the Southern Hemisphere (Arienzo et al. 2016).

Ice cores provide the most straightforward archives of sulphur, both as a record of global volcanic events (Schuster et al. 2002), but also in documenting the long-range effects of pollution unaffected by the local pollution seen in tree rings and speleothems (Fairchild et al. 2009). In Greenland ice, sulphate (SO_4^{2-}) concentrations increased markedly from 1900 to 1920 CE and 1940 to 1980 CE (Figures 24 and 25), and by 1980 CE concentrations were a factor of 2–5 above pre-industrial peak values (Fischer et al. 1998), but did not exceed concentrations linked to large volcanic eruptions or during the Last Glacial Maximum (Wolff 2014). In central Asia, in ice on Mount Muztagata (China), the steep rise in sulphate concentrations that started after the mid-1970s and decreased in the 1990s is associated with changes in industrial activity (Zhao et al. 2011). No equivalent signature is recorded in Antarctic ice, which is more remote from the main sources of sulphate pollution (Wolff 2014).

ACCEPTED MANUSCRIPT

N_2O, a greenhouse gas, has an atmospheric lifetime of about 120 years, so any changes recorded in ice cores reflect global changes, thought to mainly reflect increased application of agricultural fertilizers (Wolff 2013). N_2O concentrations recorded in air bubbles within the ice have risen by about 20% in the last 200 years (see Law Dome example below) and are at levels higher than recorded for the last 800 ka (Wolff 2013). In contrast, ammonium (NH_4^+), mainly deposited as aerosol, and nitrate (NO_3^-), deposited as an aerosol or as nitric acid, have much shorter atmospheric residence times, and changes in their concentrations reflect local changes in source areas (Wolff 2013). Mid-latitude glaciers, such as Mount Muztagata in China, show an approximately three-fold increase in ammonium concentrations between 1960 and 1990 CE, probably as a consequence of agricultural emissions (Zhao et al. 2011). However, there is no significant recent trend at either pole (Wolff 2013). Whereas ammonium is permanently fixed in the snow, nitrate can be re-emitted back to the atmosphere (Fischer et al. 1998, Wolff 2013). Increased nitrate concentrations evident in the Northern Hemisphere (Figure 25) are mainly due to NO_x emissions from fossil fuel combustion (Wolff 2013, 2014), including automobiles and coal-fired power stations. In Greenland ice the main phase of nitrate increase, which has risen by a factor of 2–3, occurred from 1950 to 1980 CE (Fischer et al. 1998, Wolff 2013); by 1980 CE levels were higher than over the past 100 kyr (Wolff 2014). In the French Alps, at the Col du Dôme, high snow accumulation rates allow distinction between summer and winter snow, with higher summer nitrate values showing a fivefold increase during the 20th century, most markedly between 1960 and 1980 CE and sourced by emissions within 1000 km of the glacier (Preunkert et al. 2003). However, nitrate does not provide a consistent global signal. In central Asia, at Mount Muztagata, the steep rise in nitrate concentrations, which increased

ACCEPTED MANUSCRIPT

by a factor of two, started after the late-1970s and had already peaked by 2000 CE (Zhao et al. 2011), whereas no significant increase occurs then in Antarctic ice (Wolff 2013).

A shallow (100 m) GISP2 ice core from Summit (Greenland), ranging in age from 1718 to 2006 CE, shows a clear decreasing $\delta^{15}N$ trend in atmospheric nitrate, from pre-industrial values around 11 to -1‰ in the early 21st century (Hastings et al. 2009). The $\delta^{15}N$ trend began about 1850 CE, whereas the increase in nitrate from the same core rises in about 1890 CE (Hastings et al. 2009). The greatest rate of change in $\delta^{15}N$ occurred from 1950 to 1980 CE, coincident with a rapid rise in fossil fuel emissions (Hastings et al. 2009).

During pre-industrial times, about half the lead in the troposphere was associated with soil dust and half with volcanic gases (Patterson and Settle 1987). Pb, As, Sb, Bi, Cu, and Zn enrichments in Arctic ice cores started at around 3300–3000 yr BP, with an additional significant Roman phase (Hong et al. 1994, Krachler et al. 2008, 2009). Further increases of Pb, Tl, and Cd in response to the Industrial Revolution are more significant, with elevated concentrations from the 1860s, accelerated concentrations from 1887 to 1889 CE and peaks in the early 20th century (Tl in 1911–1915 CE, Cd in 1906 CE, Pb in 1915 CE) (McConnell and Edwards 2008, Figure 26). This early peak is considered to reflect increased coal burning in North America and Europe (McConnell and Edwards 2008). However, the greatest rises in Pb concentrations are from the 1950s, peaking in the 1960s, associated with emissions of Pb used in alkyl-leaded gasoline (Murozumi et al. 1969, Boutron et al. 1991, McConnell and Edwards 2008). Tl shows no equivalent mid-20th century peak, whereas Cd has a 1946 CE peak concentration (Figure 26). At its peak, Pb levels in Greenland ice were above Holocene background levels by a factor of 200 and exceeded concentrations seen during the last glacial maximum (Murozumi et al. 1969); in Antarctic ice they were a factor of five above

ACCEPTED MANUSCRIPT

pre-Industrial levels (Patterson and Settle 1987, Wolff and Suttie 1994). Use of lead additives in gasoline became limited in the USA and other Northern Hemisphere countries from about 1970 CE, and concentrations decreased in Greenland by a factor of 7.5 between 1970 and 1990 CE, with Cd (Figure 26) and Zn sourced from industrial processes showing a decrease by a factor of 2.5 over the same interval (Boutron et al. 1991, McConnell and Edwards 2008). In Antarctica, by 1920 CE anthropogenic Pb (mainly from metal processing) dominated concentrations that were 2 to 4 times higher than pre-Industrial levels (Wolff and Suttie 1994). Lower concentrations in the 1930s to mid-1940s are followed by a marked upturn in concentrations by a factor of >2 from 1950 to 1980 CE, with subsequent decline (Wolff and Suttie 1994). The first use of unleaded gasoline in many Southern Hemisphere countries started as late as the 1980s and 1990s (Wolff and Suttie 1994). Because most combustion of gasoline occurred in the Northern Hemisphere, it is in Greenland that the rise and subsequent fall of Pb signals is greatest. Lead aerosols have a 10-day residence time in the atmosphere resulting in little inter-hemispheric interchange (Patterson and Settle 1987).

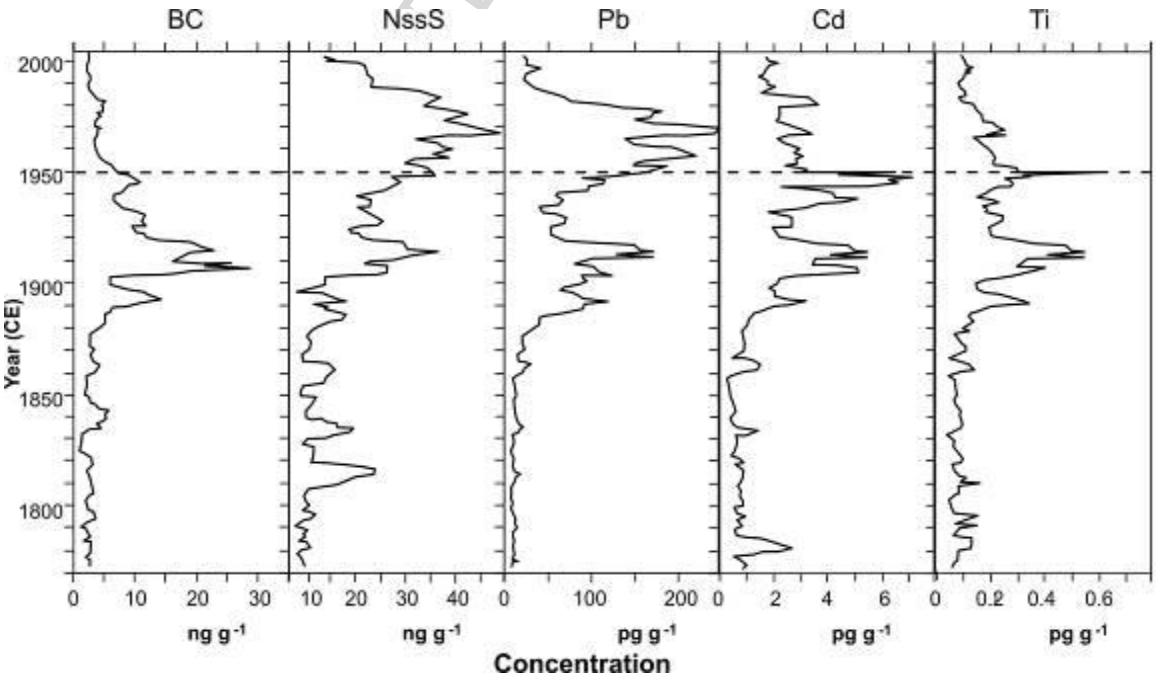

ACCEPTED MANUSCRIPT

Figure 26. Concentrations (5-year running means) in Greenland ACT2 ice core from 1772 to 2003 CE of sulphur (NssS), thallium (TI), cadmium (Cd) and lead (Pb), compared to black carbon (BC), from McConnell and Edwards (2008). Sulphur peaks in 1817 and 1883 CE relate to the Tambora and Krakatoa volcanic eruptions, respectively. © (2008) National Academy of Sciences, U.S.A.

Atmospheric Hg contamination in a glacier in Wyoming (USA) from ~1720 to 1993 CE shows a twenty-fold increase from pre-1840 CE levels to a ~1984 CE peak (Schuster et al. 2002). Early spikes include both volcanic sources from Tambora (1815 CE) and Krakatoa (1883 CE), showing cross-hemispheric transfer of Hg, and an anthropogenic source with a double peak and elevated values from ~1850 to 1884 CE associated with the California Gold Rush in western USA (Schuster et al. 2002).

In Greenland, black carbon is attributed by McConnell and Edwards (2008) as: Preindustrial (1772–1860 CE), coal-dominated industrial (1860–1940 CE), and oil-dominated industrial (1940–2003 CE), with peak concentrations in the first decade of the 20th century (Figure 26). However, peak combustion of coal is later in Asia. Black carbon and organic carbon concentrations in Tibetan ice cores show a marked high during the 1950s and 1960s, attributed to the inflows of industrial emissions, mainly from Europe, with a decline during the 1970s and 1980s (Xu et al. 2009). Glaciers in the southern part of the plateau show black and organic carbon increases after the 1990s, from a southern source (Xu et al. 2009). Increased black carbon on glacial ice reduces surface reflectivity and increases melting (Xu et al. 2009), potentially causing significant hiatuses in modern laminae.

Microplastics have been reported in Arctic sea-ice (Obbard et al. 2014) from contaminated surface sea-water that has been frozen. However, there is no record of microplastics in polar

ACCEPTED MANUSCRIPT

continental ice sheets or glaciers. The potential for airborne transfer of microfibres (Dris et al. 2016) suggests that microplastic fallout in glacial ice might occur, especially where glaciers are close to urban areas.

Table 10 summarises the key advantages and disadvantages of having a potential GSSP within glacial ice, as is the case for the base of the Holocene. The Law Dome ice core from Antarctica has a high-resolution multi-proxy record for the last 1000–2000 years and shows many characteristics that make it suitable for hosting a potential GSSP. Other similarly suitable ice cores are available elsewhere in both Antarctica and Greenland (Figure 23), although many of the sites are unsuitable because the rate of accumulation is too low (e.g. Dome C, Antarctica).

For:	Against:
• Annual layers, high resolution • Extensive distribution, but only Greenland and Antarctic ice sheets likely to persist • Independent dating using ^{210}Pb, but not ^{14}C • Major volcanic eruption events provide clear S spikes • SO_4^{2-} clear spike starts mid-20th century, but diachronous • NO_3^- increase and $\delta^{15}N$ depletion from ~1950 CE • Increased lead accumulation from 1950s, especially from gasoline source • Increased Zn, Cd, and Cu concentrations • Radionuclides, clearly resolved bomb spike • Holocene GSSP precedent in Greenland	• Surficial laminae (recent decades) are more prone to melting by global warming than deeper laminae (Holocene), especially in alpine glaciers and coastal ice sheets • Alpine glaciers melting at rapid rate • Lag between age of ice and younger age of air bubbles (100 years in Greenland, possibly up to 1000 years in Antarctica) • δD and $\delta^{18}O$ no significant variation across mid-20th century • Increased dust flux not consistently evident • Mid-20th century increased CO_2 and CH_4 concentrations and $\delta^{13}C$ depletion signal not fixed in air bubbles • Core difficult/expensive to procure and to store safely

Table 10. Reasons for and against using an ice core as a potential host for a GSSP.

ACCEPTED MANUSCRIPT

3.7.1 Law Dome Ice Core, East Antarctica

A high-precision 1000–2000 year history of CO_2, CH_4, N_2O and $\delta^{13}C$ has been acquired from the Law Dome site in East Antarctica (Etheridge et al. 1996, Francey et al. 1999, Ferretti et al. 2005, MacFarling Meure et al. 2006, Rubino et al. 2013). As regards hosting a potential GSSP site, the high snow accumulation rates, low temperatures, and small quantities of impurities at Law Dome make this record particularly suitable, especially for recognising a high-resolution $\delta^{13}C$ signal (Rubino et al. 2013). The Law Dome site comprises three cores drilled between 1987 and 1993 CE, (Etheridge et al. 1996, Rubino et al. 2013), dated by counting annual layers in oxygen isotope ratios ($\delta^{18}0$), ice electroconductivity measurements and hydrogen peroxide (H_20_2) concentrations (Etheridge et al. 1996), with a gas-age/ice-age difference of between ~31 and ~55 years for CO_2 (Rubino et al. 2013).

Between 1000 and 1600 CE, the CO_2 concentration varies between 278 and 284 ppm (Figure 27a), and between 1000 and 1500 CE, the $\delta^{13}C$ values remained constant at about -6.55‰ (Rubino et al. 2013). The brief decrease in concentration of CO_2 in the Law Dome ice core around 1600 CE (Etheridge et al. 1996, MacFarling Meure et al. 2006) was used by Lewis and Maslin (2015) as their "Orbis Event" which they regarded as sufficiently important to be a candidate for defining the beginning of the Anthropocene. Analysis of changes in atmospheric carbonyl sulphide concentration, which is linked to changes in gross primary production of terrestrial ecosystems, shows that temperature change, rather than vegetation re-growth, was the main cause of the increased terrestrial storage and hence drop in atmospheric CO_2 around 1600 CE (Rubino et al. 2016). After a recovery, CO_2 maintained comparatively low concentrations and elevated $\delta^{13}C$ through to 1750 CE (Rubino et al. 2013). Over the past 200 years, atmospheric CO_2 concentrations at Law Dome have increased by 29% (MacFarling Meure et al. 2006). Following the Industrial Revolution,

ACCEPTED MANUSCRIPT

Rubino et al. (2013) show two inflexion points in the 20th century $\delta^{13}C$ signal: from 1915 CE, and from 1955 CE. There is stabilization of atmospheric CO_2 concentrations at 310–312 ppm from ~1940 to 1955 CE (Figure 25) (MacFarling Meure et al. 2006). The subsequent increase appears to coincide with increase in fossil fuel use at about 1950 CE (Rubino et al. 2013). The Francey et al. (1999) high-precision record of atmospheric $\delta^{13}C$ based on Antarctic ice cores shows two straight segments: one between 1850 and 1961 CE, and a steeper segment between 1962 and 1980 CE.

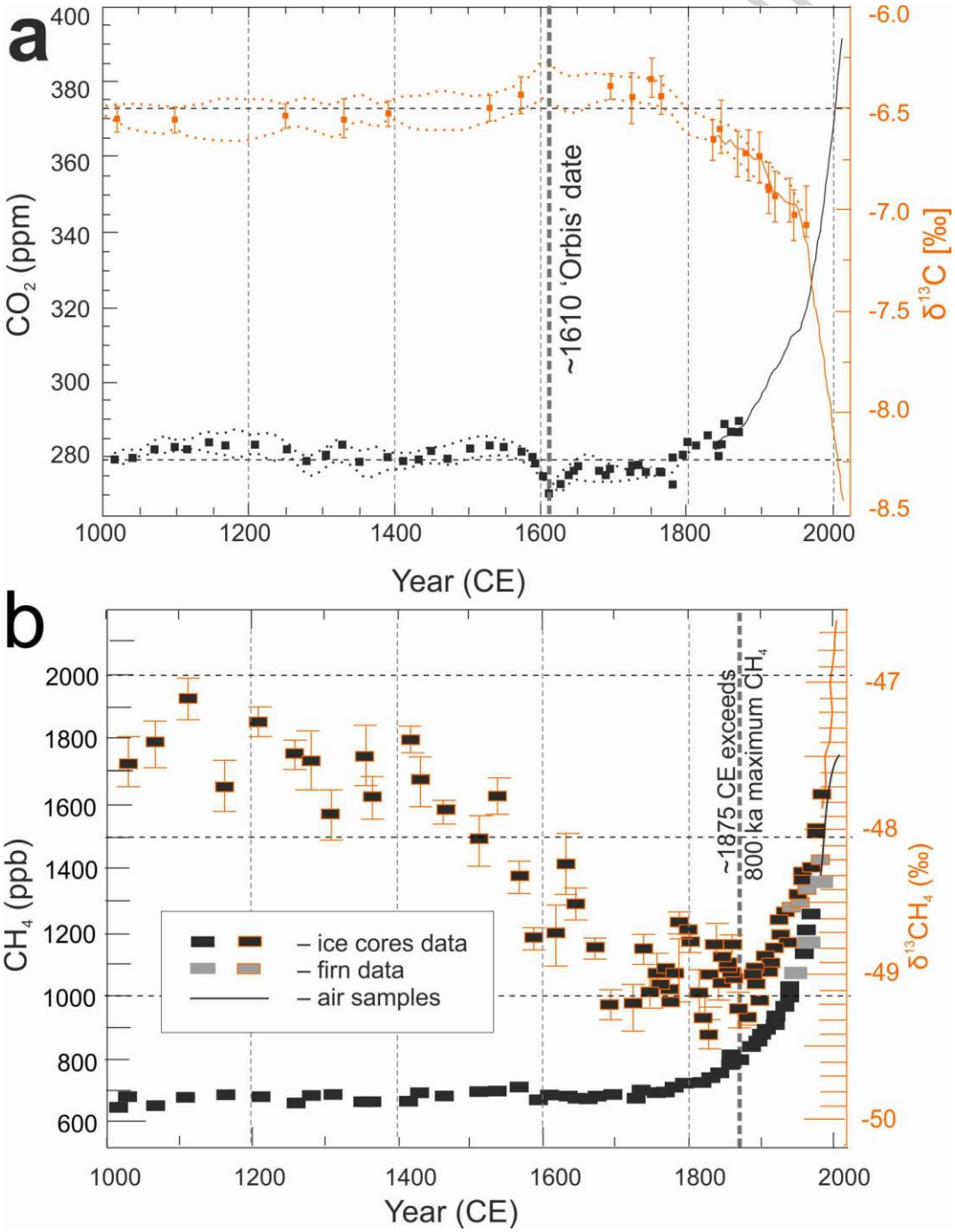

ACCEPTED MANUSCRIPT

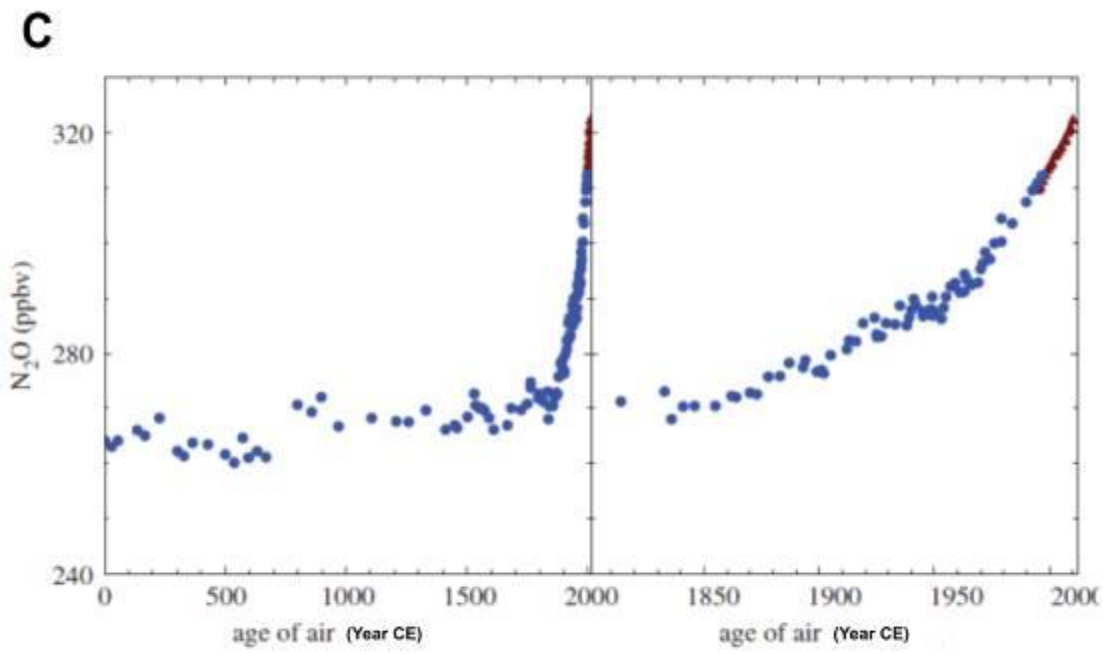

Figure 27. a) Law Dome ice core and firn records for CO_2 concentration and $\delta^{13}C$ for atmospheric CO_2 for the past 1000 years (from Rubino et al. 2013); b) Law Dome ice core and firn records for CH_4 concentration and $\delta^{13}C$ for atmospheric CH_4 for the past 1000 years (from Ferretti et al. 2005); c) N_2O concentrations in the Law Dome ice core over the past 2000 years and 200 years (Wolff 2013).

The Law Dome ice core records also show atmospheric methane (CH_4) concentrations ranging from 590 to 760 parts per billion (ppb) through much of the Holocene, up to 1700 CE, with as little as ~55 ppb difference from 1000 to 1700 CE (Ferretti et al. 2005). This is followed by an unprecedented increase to 1700 ppb by 2004 CE (Ferretti et al. 2005, Figure 27a), an increase of 150% over 200 years (MacFarling Meure et al. 2006). Growth rates in CH_4 decreased during ~1940–1955 CE (MacFarling Meure et al. 2006). The $\delta^{13}C$ curve for CH_4 shows a marked decrease of ~2‰ from ~1000 to 1700 CE, perhaps in response to reduced biomass burning, and a subsequent abrupt rise from ~1875 CE to the present value of ~-47‰, reflecting increasing pyrogenic emissions (Ferretti et al. 2005, Figure 27a).

ACCEPTED MANUSCRIPT

Over the past 200 years, atmospheric N_2O concentrations at Law Dome increased by 21% (MacFarling Meure et al. 2006). N_2O concentrations ranged from 260 to 270 ppb between 1 and 1850 CE, followed by a steady rise to 290 ppb by 1950 CE, from when there was a rapid rise to 320 ppb by 2000 CE (Wolff 2013, Figure 27b). The $\delta^{15}N$ signal in firn ice at Law Dome is more scattered than would be expected, most probably due to random analytical noise (Rubino et al. 2013).

3.8 Speleothems

Annually laminated calcareous speleothems (typically stalagmites) occur within natural cave systems, typical of karst environments, or within artificial tunnels where either the adjacent bedrock or the degradation of mortar in concrete linings of the tunnel contributes the calcium carbonate. Karst landscapes occur across extensive parts of Eurasia, Australasia and the Americas, in total about 10% of the Earth's land mass (Figure 28). There is precedent in using speleothems for the location of a GSSP, as Walker et al. (2012) used a stalagmite from Mawmluh Cave, India, as the proposed GSSP for the Upper Holocene Subseries (= proposed Meghalayan Stage) at 4.2 ka.

In addition to lamina counting, the age of older speleothems is typically determined by ^{234}U-^{230}Th dating, although this is unsuitable for carbonates precipitated over the past century. Independent dating using ^{210}Pb–^{226}Ra has been undertaken at a few locations (e.g. by Condomines and Rihs 2006 at St. Nectaire, France, and Bonotto et al. 2012 at Santana Cave in Brazil). Radiocarbon has quite commonly been used to confirm an age model from annual laminae, but does not provide annually resolved dates. If Pu is chosen as a primary tool for

ACCEPTED MANUSCRIPT

correlation, the lack of Pu isotope determination would rule out a speleothem as GSSP for the Anthropocene (Fairchild 2017), but one could be chosen as an auxiliary site.

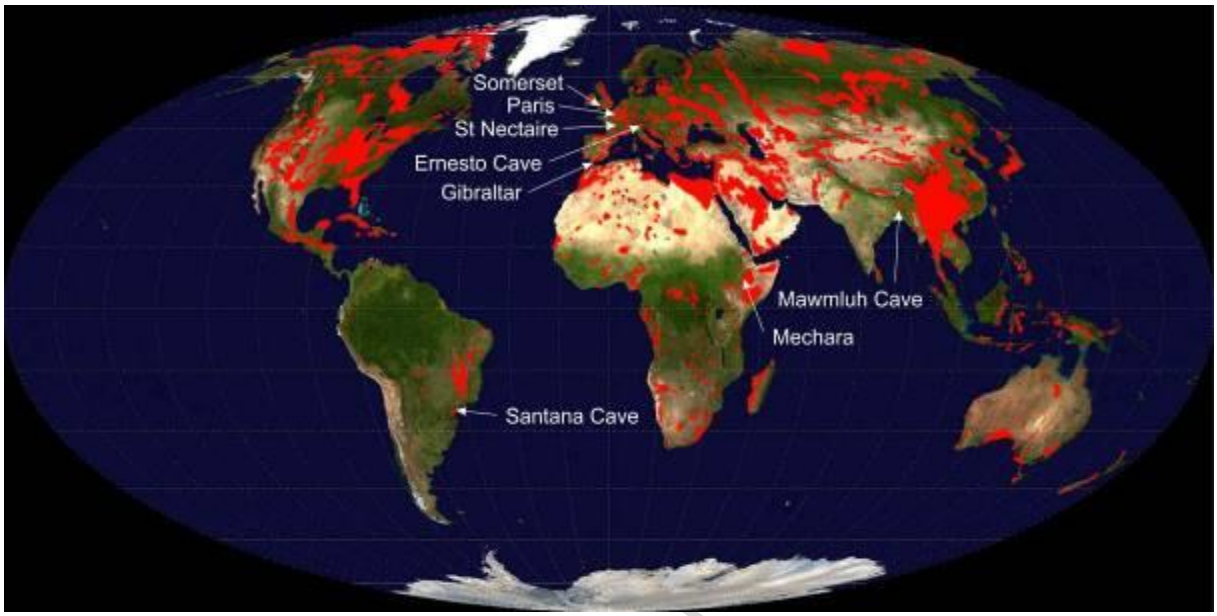

Figure 28. Extent of carbonate outcrops present across global land mass by Ulrichstill https://commons.wikimedia.org/w/index.php?curid=9412430 Created 6th February 2010. Karst landscapes and speleothems occur within these regions, and locations mentioned in the text are indicated.

Natural speleothem growth is typically slow, on the order of tens to hundreds of micrometres per year. In contrast, speleothems related to hyperalkaline groundwaters, commonly from anthropogenic sources, can grow at a rate of 10 mm per year (Baker et al. 1998), hence potentially permitting fine-scale resolution of environmental changes, although the chemistry will be strongly kinetically modified (Hartland et al. 2014, Newton et al. 2015). ^{210}Pb dating of stalactites in Santana Cave (Brazil) shows a longitudinal growth rate of 1.3 mm yr^{-1} and lateral rate of 0.01 mm yr^{-1} (Bonotto et al. 2012). A study of hydrothermal

ACCEPTED MANUSCRIPT

stalagmites at St Nectaire (France) using $^{210}Pb/^{226}Ra$ ratios showed growth rates varying from 5.3 ± 0.5 mm to 2.6 ± 0.2 mm yr^{-1} (Condomines and Rihs 2006).

Speleothems record changing environmental conditions in the atmosphere, soil and ecosystem through geochemical signals transmitted from the ground surface, through rock, to the subterranean void. The processes of speleothem formation and their chemistry are detailed by Fairchild and Baker (2012), and their relevance to recognition of Anthropocene signals is given in Fairchild and Frisia (2014) and Fairchild (2017). Principal signals that may be used to recognise a potential Holocene–Anthropocene boundary (Table 2) include shifts in atmospheric ^{14}C and sulphur (sulphate concentration and $\delta^{34}S$), which relate to global-scale changes to atmospheric chemistry (Fairchild and Frisia 2014, Figure 29). Local signals include: 1) variations in growth rates of laminae and $\delta^{18}O$ which relate to air temperature and humidity, 2) $\delta^{13}C$ as an indicator of deforestation and/or introduction of C4 plants, 3) development of biomarkers such as a reduction in the ratio of C_{27}/C_{31} n-alkanes and increase in n-alkanols as observed at Mechara (Ethiopia) reflecting the local introduction of agriculture about 1935 CE (Blyth et al. 2016), and 4) shifts in trace elements and isotope ratios (Fairchild 2017). Although of local source and probably diachronous in nature, such signals may link to global patterns of environmental change and so contribute to characterising a potential GSSP site. For example, Pb anomalies have been recorded in speleothems in Somerset, UK near mines active in pre-Roman, Roman and mediaeval times (McFarlane et al. 2013). Sulphur pollution from coal combustion increased during the Industrial Revolution and culminated in peak S concentrations and depleted $\delta^{34}S$ values in the mid- to late-20th century in developed countries (Wynn et al. 2010, Figure 29d). However, speleothems are insensitive to the significant increases in atmospheric CO_2 concentrations and depletion in $\delta^{13}C$ over the past century (Fairchild and Frisia 2014).

ACCEPTED MANUSCRIPT

Changes in the nitrogen cycle via N abundance or isotopic fractionation related to fertiliser use have not been investigated in speleothems (Fairchild 2017). Phosphorus is strongly modulated by seasonal vegetational die-back and changed infiltration rates (Fairchild and Frisia 2014) rather than by fertiliser application.

Transport of solutes via plants, soil and rock commonly results in signals being variably attenuated and delayed (Fairchild and Frisia 2014, Fairchild 2017). For example, speleothems in SW France and Gibraltar show ^{14}C concentrations with differing degrees of attenuation and delay of the peak signal, but the initial rise was consistent at 1958 CE and coincides with changes in atmospheric concentrations (Fairchild and Frisia 2014). The timing of onset of the ^{14}C rise in speleothems is typically within 1–2 years of the atmospheric change (Genty and Massault 1999).

Table 11 summarises the key advantages and disadvantages of such a potential GSSP for the Anthropocene. As examples, the Ernesto Cave in Italy has multi-proxy studies of speleothem laminae within a natural cave system, but urban speleothems may show greater tuning to modified anthropogenic signals.

For:	Against:
• Annual lamination • Undisturbed locations • Independent ^{14}C markers • S, $\delta^{34}S$, ^{14}C reflect atmospheric composition, but modified by soil-ecosystem • Solid samples easier to handle than unconsolidated sediment • Precedent of Mawmluh Cave, India, for the proposed Upper Holocene GSSP	• The atmospheric Suess effect on $\delta^{13}C$ is smaller than fractionation effects in the soil-ecosystem so an inflection corresponding to atmospheric change is not normally present • Although S, $\delta^{34}S$, ^{14}C may show initial rise as atmosphere changes, the peak is delayed because of storage in soil/ecosystem • Changes in trace pollutant metals (e.g. Pb, Zn, REE) are strongly linked to organic matter from soil and increases tend to reflect soil disturbance/deforestation effects • Not able to reliably detect signals usable elsewhere, e.g. Pu, anthropogenic detritus

ACCEPTED MANUSCRIPT

Table 11. Reasons for and against using a speleothem as a potential host for a GSSP.

3.8.1 Ernesto Cave, Italy

Ernesto Cave, northern Italy, closely studied for >20 years, has supplied various proxy data series from annually-laminated speleothems independently dated using U-Th series (Frisia et al. 2003). These show a strong annual signal of fluorescent laminae associated with a range of colloid-transported elements (Fairchild and Frisia 2014). A pronounced change is recognised since about 1840 CE, from open and impurity-rich crystals within relatively thin laminae to thicker laminae of clean calcite (Figure 29a), representing higher growth rates, closely correlated with temperature increases (Frisia et al. 2003, Fairchild and Frisia 2014) associated with the local ending of the Little Ice Age. This pattern broadly coincides with the initial increase in sulphate concentrations within speleothems in this cave at about 1880 CE (Frisia et al. 2005), associated with the initiation of atmospheric pollution in response to the Industrial Revolution.

No appreciable change in stable isotopes has occurred across the mid-20th century (Figure 29b), the most significant change in $\delta^{13}C$ being a marked positive excursion at ~1840 CE (Scholz et al. 2012).

ACCEPTED MANUSCRIPT

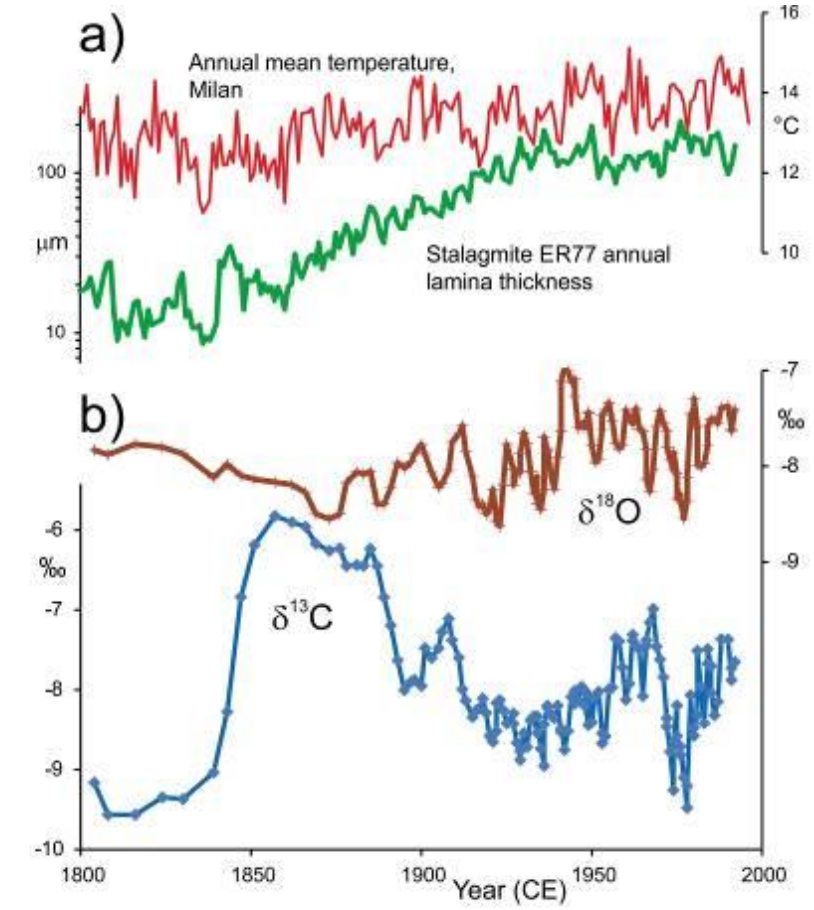
a)
Annual mean temperature, Milan
Stalagmite ER77 annual lamina thickness
µm
°C
b)
δ18O
δ13C
‰
Year (CE)

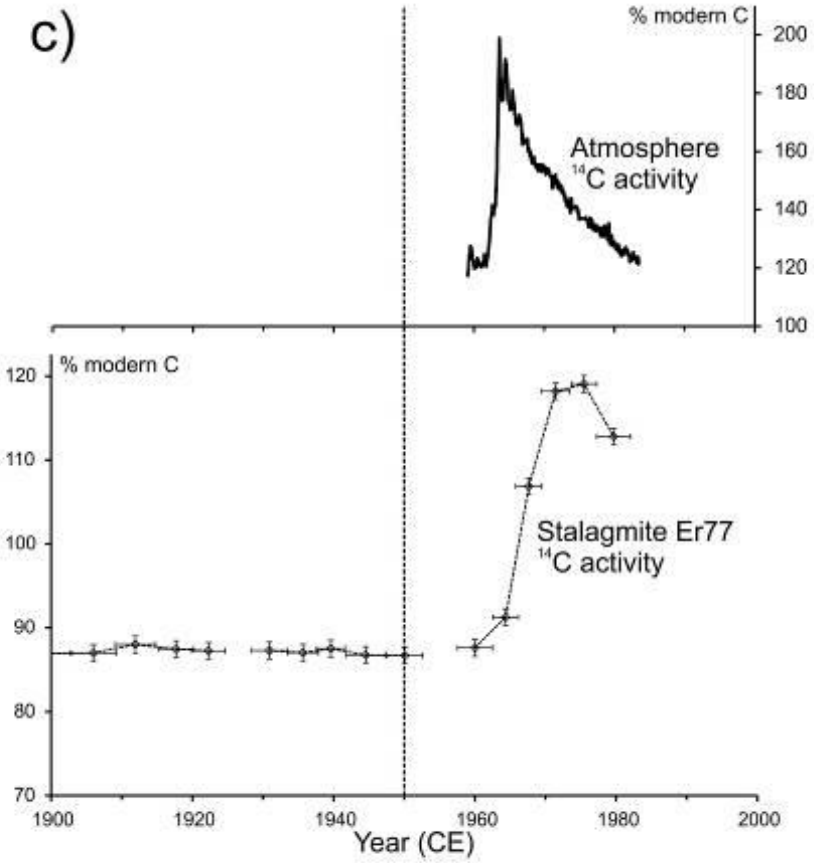
c)
% modern C
Atmosphere 14C activity
Stalagmite Er77 14C activity
Year (CE)

ACCEPTED MANUSCRIPT

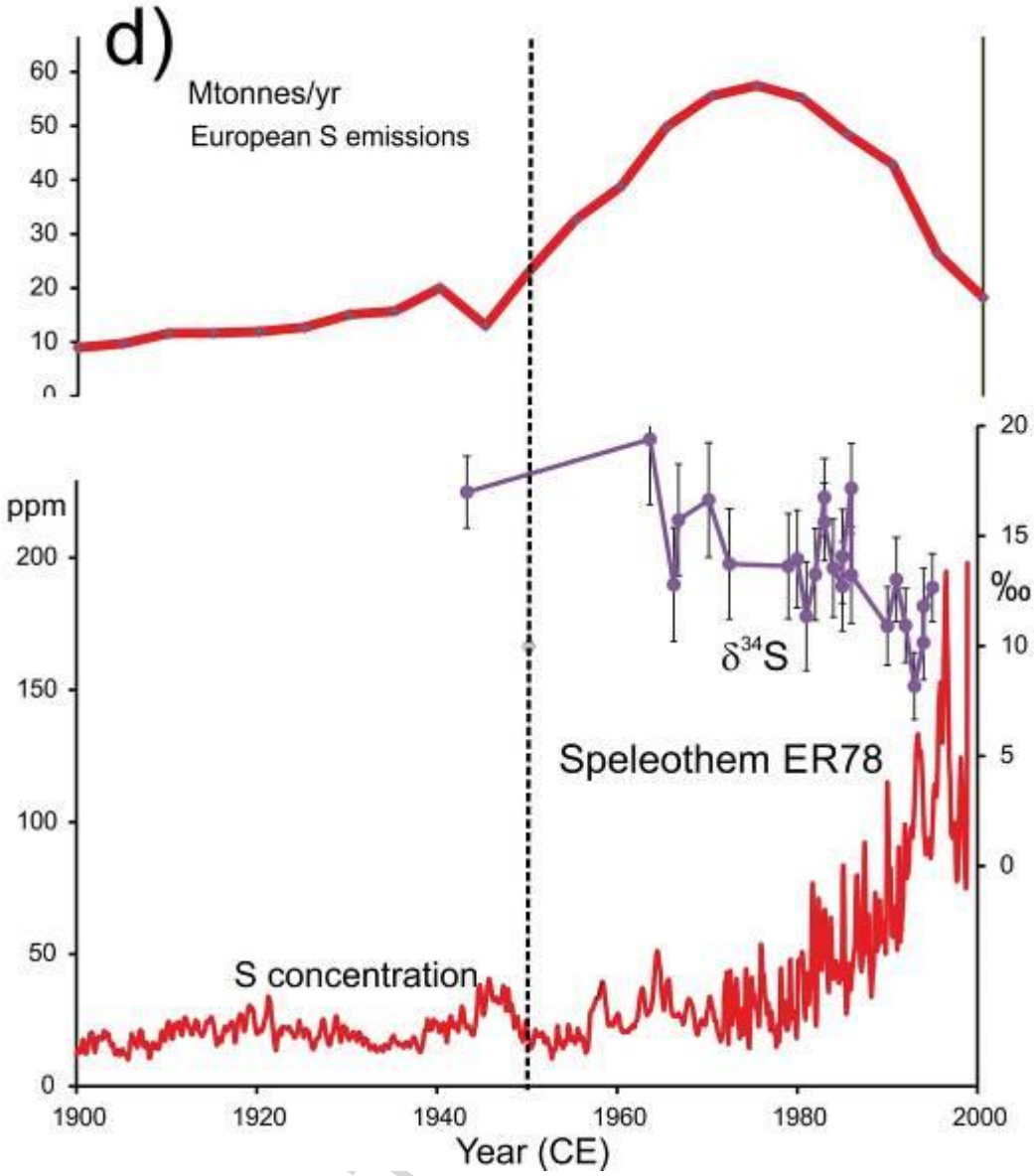

Figure 29. Ernesto Cave, Italy: a) Age model based on lamina counting related to local mean air temperature (Frisia et al. 2003); b) $\delta^{18}O$ and $\delta^{13}C$ profiles (Scholz et al. 2012); c) Radiocarbon profile and comparable European atmospheric emissions (Fohlmeister et al. 2011); d) S concentration and $\delta^{34}S$ (Frisia et al. 2005, Wynn et al. 2010).

The ^{14}C bomb-spike has been recorded from the cave (Figure 29c), but with a decade lag compared with atmospheric signals (Fohlmeister et al. 2011). Records of sulphur loading and lowering of $\delta^{34}S$ in both speleothem and tree rings show a similar lag in the speleothems of about 15–20 years (Figure 29c), such that in 2000 CE the speleothem was still recording peak atmospheric loading (Wynn et al. 2010, 2014) that was locally experienced in the 1980s

ACCEPTED MANUSCRIPT

(Fohlmeister et al. 2011), but which is now declining (Borsato et al. 2015). Trace element concentrations increased greatly during the early-20th century, a time of deforestation in the area (Borsato et al. 2007).

3.8.2 Urban speleothem, Paris

Rises in several trace metals and rare earth elements are found in urban speleothems in an underground aqueduct beneath Paris that have grown over 300 years with a record of two laminae per year, independently dated using U-Th series (Pons-Branchu et al. 2015). Two distinct phases of heavy metal pollution are recognised: a) 18th century metal contamination resulting from use of urban waste (night soil) as fertilizer; and b) since 1900 CE elevated Pb, Mn, V, Cu, Cd and Al concentrations, attributed to urbanisation, with a more marked increase since 1960–1970 CE (Pons-Branchu et al. 2015). $^{206}Pb/^{207}Pb$ isotope ratios show no consistent pattern in these speleothems. The dominant value of 1.181 ± 0.003, is typical of values associated with lead from northern Europe (Pons-Branchu et al. 2015), though one speleothem showed a change after the mid-19th century, suggesting a new contribution from coal burning or from Pb from Spain. Pb ratios typical of leaded gasoline are not discriminated (Pons-Branchu et al. 2015).

3.9 Trees

Forest coverage in 2005 CE was about 39 million km^2, or ~30% of the world's land area (FAO 2006) and there are an estimated 3 trillion trees (Crowther et al. 2015). Forests are extensive on all continents except Antarctica, and include the boreal forests of North America and Eurasia and tropical forests of South America, central Africa and south-east Asia (Figure 30). Tropical trees from aseasonal tropical regions lack reliable annual rings, so trees from

ACCEPTED MANUSCRIPT

temperate or boreal environments would be most suitable for a GSSP as the tree rings themselves can provide a precise annually-resolved chronology.

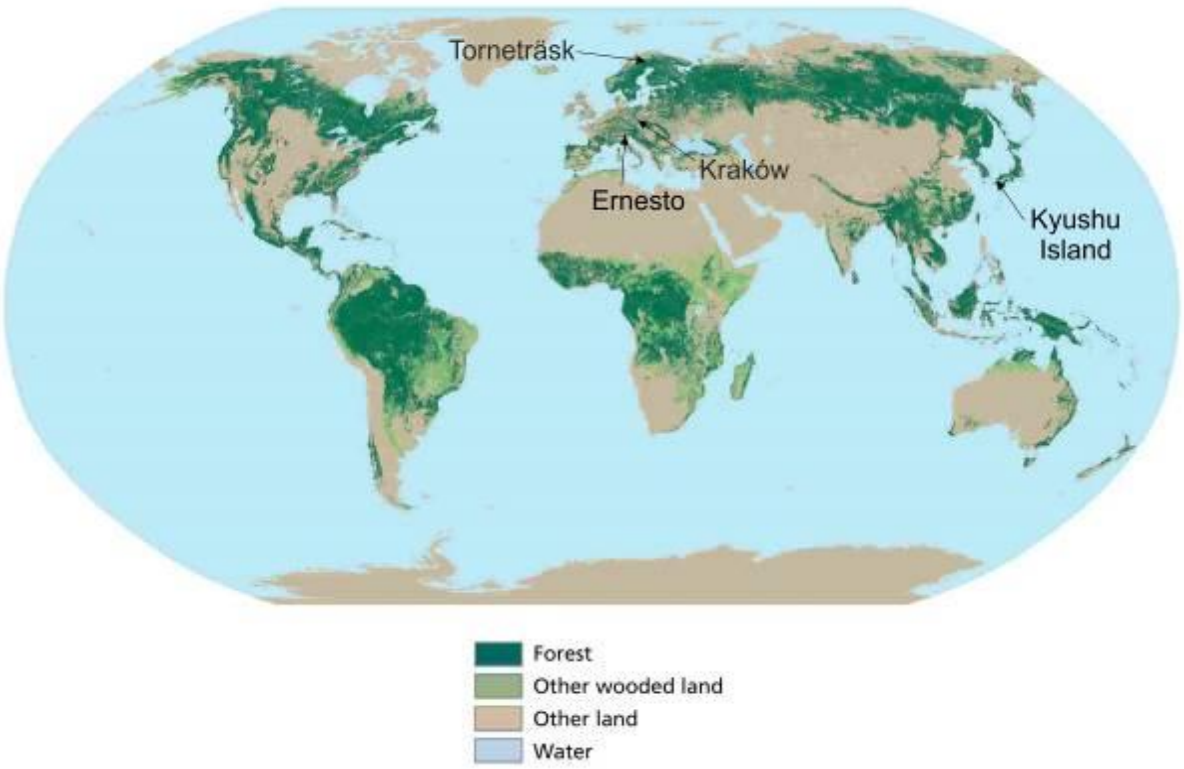

Figure 30. Forest map of the world with key locations mentioned in the text. © (2006)FAO.]

ACCEPTED

Tree rings provide a perfect annually-resolved chronology, and within this an annually resolved archive of environmental change, most notably palaeoclimate, at local to global scales. This signal can be evident in the physical properties of the tree ring (width, density, reflectance) or chemical indicators such as the stable isotopic ratios of carbon (sourced from atmospheric CO_2), and hydrogen and oxygen (sourced from precipitation, soil or ground water) (Fritts 1976, Speer 2010, McCarroll and Loader 2004). In many species, the tree rings may be further divided into early wood (formed during the spring) and late wood (formed during the summer, primarily from photosynthates fixed during the growth year). Rings from living trees can provide environmental information spanning both the mid-20th century putative boundary for the Anthropocene and the late-18th century transition from pre-

ACCEPTED MANUSCRIPT

industrial times through the development of the Industrial Revolution. Similar records can also be found in preserved dead trees that accumulated in bogs or lakes, and also in building timbers. Where trees co-existed in time they will co-record a shared environmental signal that may therefore be cross-dated to assign chronology or to provide independent replication between trees or across study regions.

Table 12 summarises the key advantages and disadvantages of having a potential GSSP within tree rings. Proxy signals associated with palaeoclimate, stable carbon isotopes, sulphur concentrations and isotopic ratios, radiocarbon fallout and heavy metal concentrations are discussed below.

For:	Against:
• Global expression and distribution; widespread terrestrial extent • Bi-annual layers • Precise dating through dendrochronology • Independent ^{14}C dating possible • Environmental signals preserved in deadwood • $\delta^{18}O$ and δD: record source water, which contains a climate signal • $\delta^{13}C$ is highly sensitive to the Suess effect on atmospheric CO_2 • Sulphur and $\delta^{34}S$ signal commencing mid-20th century • ^{14}C bomb spike clearly defined • High potential for independent replication • Tangible, stable and archivable	• Growth ring width may not be suitable for picking mid-20th century climate signal (due to local effects or 'divergence') • Complex record of local signals in physical and chemical proxies • $\delta^{13}C$ can be affected by local modifications • Heavy metal concentrations may be unsuitable proxy for pollution events due to radial mobility • No precedent of using a living/deceased organism for GSSP

Table 12. Reasons for and against using a tree as a potential host for a GSSP.

ACCEPTED MANUSCRIPT

3.9.1 Tree rings and palaeoclimate signals

Dendrochronology relies upon the counting and statistical synchronisation of annual changes in tree ring widths, and their assignment to a calendrical or relative timescale. This is possible because the variability in tree growth driving this signal is related to regional climatic changes. Trees growing at the same time in history, and experiencing a similar climate history, will in the absence of external disturbances yield similar patterns of wide and narrow growth rings that may be cross-dated by dendrochronology to develop a precise timescale. Due to the physical increase in the diameter of a tree as it grows, tree-rings show a characteristic decline in width with increasing tree age (size). Where a climatic signal is to be extracted from the ring width data, statistical techniques are required to remove this growth or age-related trend. This statistical processing may cause climate signals of frequency longer or equal to the age-span of the tree to be lost, reducing the value of tree-ring widths in recording long-term climate change (Cook et al. 1995, Esper et al. 2002). However, this effect can be significantly reduced/removed by using more complex detrending protocols and numerous multi-centennial records of temperature changes from 800 to 1990 CE have been determined from high-elevation and high-latitude locations across the Northern Hemisphere using Regional Curve-based Standardization techniques (Esper et al. 2002, Melvin and Briffa 2008). These data contain evidence for a Northern Hemisphere Medieval Climatic Anomaly (MCA) between about 900 and 1200 CE, and for below average temperatures typical of the Little Ice Age (LIA) from 1200 to 1850 CE, and for warming since 1850 CE comparable in scale to that of the MCA (Wilson et al. 2016, Esper et al. 2002, Figure 31a).

The suitability of using tree rings to establish the temperature profile post-1950 CE has been questioned due to a conspicuous increase in the statistical uncertainty in reconstructions

ACCEPTED MANUSCRIPT

after 1975 CE, which may reflect an anomalous reduction in growth performance at some high northern latitude conifer sites, but is also often coincident with a decrease in the replication of the composite record (Esper et al. 2002). This “divergence” between growth-based reconstructions and observed climate has been the subject of significant attention by dendroclimatologists and many potential causes, from unbalanced replication and signal processing effects to changes in seasonality and CO_2 fertilisation, have been considered (D’Arrigo et al. 2007). Whilst this may reduce current confidence in the use of ringwidth-based reconstructions to define climatic changes attributed to the start of the Anthropocene, maximum late wood density appears to be less impacted upon by such divergence issues and density-based reconstructions of past climate remain some of the best records of past climatic variability currently available to climate scientists. There are few palaeoclimate proxies other than tree-rings capable of providing the same precisely dated, annually-resolved palaeoclimate reconstructions with the same capacity for independent verification through replication, capable of being objectively calibrated against instrumental observations and independently verified.

ACCEPTED MANUSCRIPT

ACCEPTED MANUSCRIPT

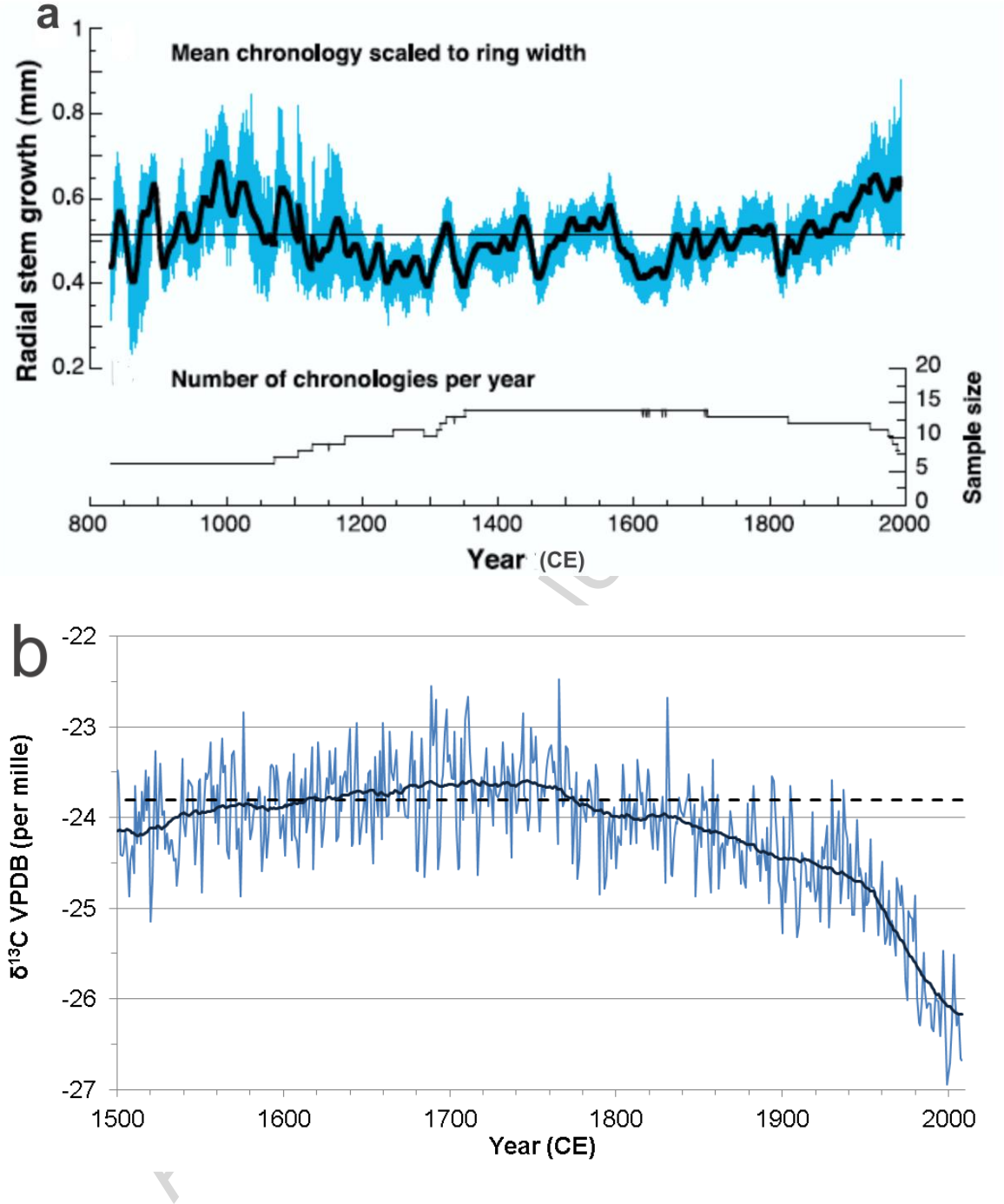

Figure 31. a) The 20-year smoothed Northern Hemisphere extratropics reconstruction of radial stem productivity in high elevation and high latitude forest environments since 800 CE (black) and two-tailed 95% bootstrap confidence intervals (blue) (from Esper et al. 2002); b) $\delta^{13}C$ variability from Loader et al. (2013a) for the period 1500–2008 CE measured in tree-ring cellulose for a composite tree ring stable isotope chronology developed using *Pinus sylvestris* trees from northern Fennoscandia. Fine line represents annually-resolved $\delta^{13}C$ variability, thick solid line presents the

ACCEPTED MANUSCRIPT

annual data smoothed with a centrally-weighted 51-year moving average. Dashed line represents the mean $\delta^{13}C$ value for the "pre-industrial" period 1500–1799 CE. Mean annual replication for the record is >13 trees. Analytical precision σ_{n-1} = 0.12 per mille n=951 which compares favourably with the analytical precision of the method typically reported (σ_{n-1} = 0.10 n=10) (Boettger et al. 2007, McCarroll and Loader 2004, Loader et al. 2013a).

3.9.2 Stable carbon isotopic signal

Stable isotope variability in tree rings appears to be less affected by non-climatic age-related tendencies (Young et al. 2011). Long-term trends of stable carbon isotopic data in tree rings may therefore mark the start of the Anthropocene in the tree ring archive. The stable carbon isotopes in tree rings record primarily the stable isotopic composition of the source CO_2 sampled by the tree during photosynthesis. This signal is further imprinted upon by the tree's physiological response to climatic change (the balance between stomatal conductance and photosynthetic rate), photosynthetic and respirative processes (Farquhar et al. 1982, McCarroll and Loader 2004, and references therein). Inter-annually, $\delta^{13}C$ values will vary in response to changes in irradiance, soil moisture, precipitation and relative humidity and this has allowed the tree rings to be used as a record of past climate variability. As a biological system, tree ring stable carbon isotopic ratios will also vary depending upon the species of tree (angiosperm versus gymnosperm) and their individual environmental history. In addition, factors such as leaf morphology, ecological amplitude, pollution, forest management history, disturbance and nutrient availability, can all influence the resulting tree ring isotopic record, but at all times, the basic physiological response of the tree will remain the same. This natural inter-tree variability has been characterised in resampling experiments (Loader et al. 2013b), and although extreme cases have been reported (Li et al.

ACCEPTED MANUSCRIPT

2005), natural intra-site variability falls within reasonable limits defined by current analytical uncertainties.

When viewed over a long (centennial-millennial) timescale, trees have the capacity to record and contextualise the unprecedented anthropogenic changes in atmospheric $\delta^{13}C$ associated with global industrialisation and land-use change. By combining records from different geographical regions, location-specific year-to-year climatic variability and the effect of random disturbances may be reduced to yield a regionally relevant record of carbon isotopic variability in atmospheric CO_2. A reduction of atmospheric $\delta^{13}C$ values by ~2‰ has occurred since the start of the global Industrial Revolution ~1820 CE (the $\delta^{13}C$ Suess effect), which is among the dates proposed as a start for the Anthropocene (Figure 31b). This effect is observed in tree rings worldwide and is also clearly observable in ringless trees from the aseasonal tropics (Loader et al. 2011).

The $\delta^{13}C$ Suess effect is commonly removed in tree ring carbon isotope series through mathematical detrending without loss of low-frequency climatic information (McCarroll and Loader 2004). This makes the data suitable for numerical calibration against instrumental climate data, but prevents its use as an arbiter of atmospheric $\delta^{13}C$ changes. To assess the potential base of the Anthropocene using $\delta^{13}C$ changes, raw carbon isotope data are required.

A further consideration when assessing the candidature of tree ring $\delta^{13}C$ as a marker for the Anthropocene is the influence of increased atmospheric CO_2 concentration on photosynthesis. This “fertilisation” or “greening” effect has been widely reported and in the context of stable carbon isotopic variability is seen as a change in the intrinsic water-use

ACCEPTED MANUSCRIPT

efficiency of the tree (Seibt et al. 2008, Saurer et al. 2014, Frank et al. 2015). Methods have been developed to quantify and to correct for this effect, which will vary from tree to tree (Treydte et al. 2009, McCarroll et al. 2009). Several studies have also identified a limit to the degree to which trees can adapt to higher atmospheric CO_2 concentrations. This "fertilisation" effect does not negate the use of $\delta^{13}C$ as a potential marker, but it should be taken into consideration.

A large-scale/global composite of global carbon isotope time-series from tree rings could help locate the boundary of the Anthropocene, as individual records are affected by local climate, forest disturbance, or the local impact of atmospheric pollution on stomatal conductance and disease (McCarroll and Loader 2004 and references therein, Bukata and Kyser 2007, Treydte et al. 2007, 2009, Loader et al. 2013b, Boettger et al. 2014, Saurer et al. 2014, Frank et al. 2015), all of which could potentially obscure the true expression of the global $\delta^{13}C$ Suess effect in tree rings. Nevertheless, the change in tree ring carbon isotopic values resulting from global industrialisation is far greater than anything observed in the tree ring isotope record during the last 1100 years. The combination of a temporally stable proxy preserved within a precisely constrained chronology for the tree rings represents an opportunity to constrain a boundary to the Anthropocene.

3.9.3 Sulphur concentrations and isotopic ratios

Bulk analyses of the conifer *Abies alba* from near the Ernesto cave site, NE Italy, show that S concentrations within annual rings reflect atmospheric SO_2 pollution (Figure 32b), with significantly higher values in the second half of the 20th century (Fairchild et al. 2009). Both the trees and the nearby stalagmite record the overall increasing trend in the 20th century, from the 1960s onwards, with the trees showing a more immediate (earlier) response to the

ACCEPTED MANUSCRIPT

high S emissions of the 1960s and 1970s (Fairchild et al. 2009, Wynn et al. 2014). The *Abies* samples show considerable noise, including variation between individual trees (Fairchild et al. 2009). Furthermore, the S is mainly sourced from soil-waters rather than directly from the atmosphere, and the S is stored both in soil and biomass, which means that the original atmospheric signal is necessarily modified (Fairchild et al. 2009). These trees also show a trend in $\delta^{34}S$ towards lighter isotopes in recent rings, with pre-industrial values of +7.5‰ and modern values of +0.7‰, with no significant signature corresponding to the mid-20th century (Wynn et al. 2014, Figure 32b).

$\delta^{34}S$ is potentially a useful chronological proxy for past atmospheric S pollution, particularly as there is limited fractionation during incorporation into the tree (Kawamura et al. 2006). Three conifers studied from Kyushu Island, Japan provide a significant record from 1945 CE, where a dominant organically-bound sulphur (OBS) fraction and a minor water-soluble sulphur (WSS) fraction were discriminated (Kawamura et al. 2006). These showed a general increase, then decrease, in the second part of the 20th century, with higher values and a greater range seen in urban as compared with rural areas. Increased atmospheric S emissions from petroleum combustion with negative $\delta^{34}S$ values were mainly sourced from the Middle East since the 1950s, until legislation was introduced in 1968 CE. There is a ~5 year delay in $\delta^{34}S_{OBS}$ tree ring values compared with maximum atmospheric S concentrations, probably reflecting the time taken for sulphur deposited in soil to mobilise to the roots, and for the metabolism of sulphur after absorption (Kawamura et al. 2006).

ACCEPTED MANUSCRIPT

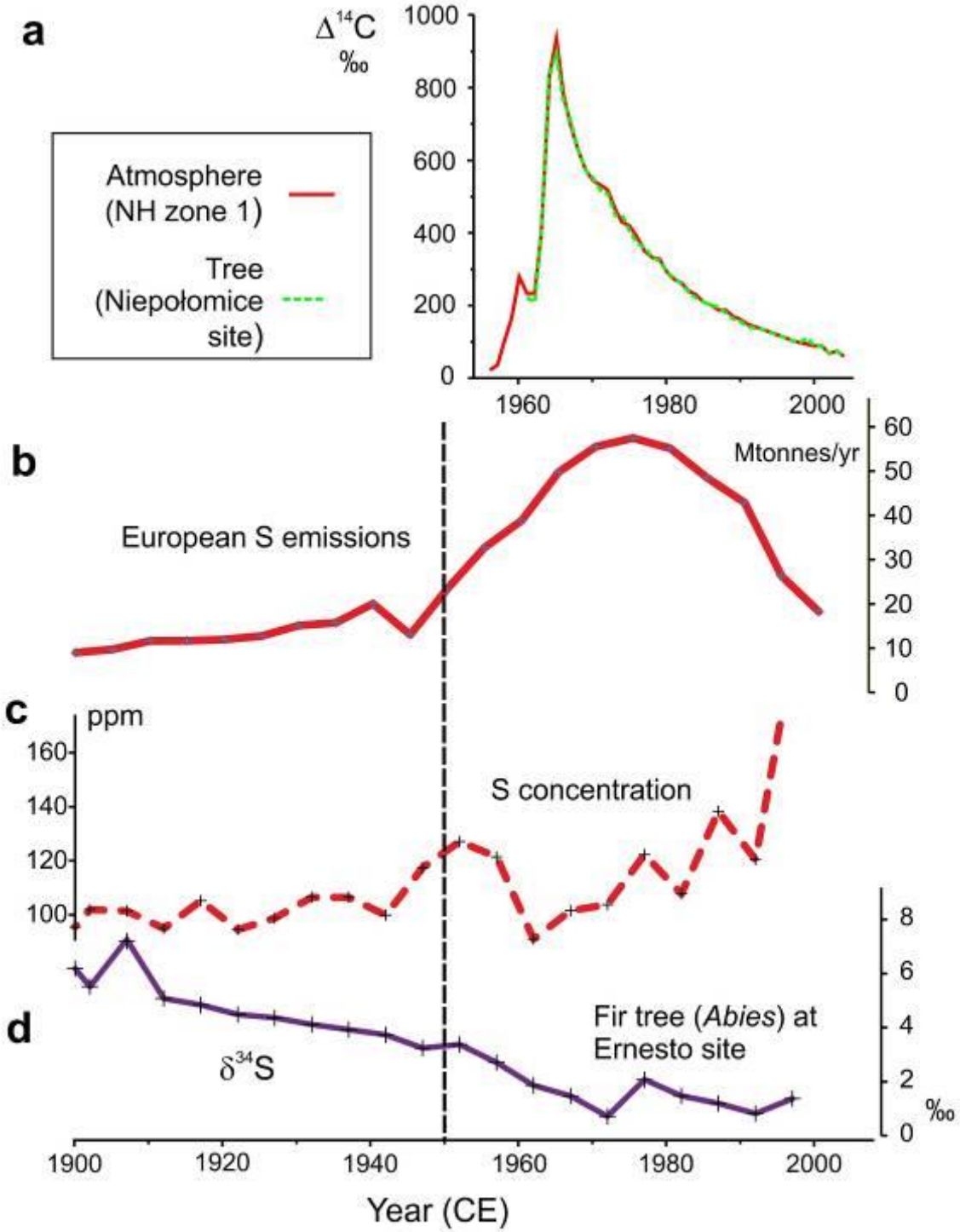

Figure 32. a) Tree rings (*Pinus sylvestris*) samples from 1960 to 2003 CE at Niepołomice (Poland) showing changes of radiocarbon concentration (from Rakowski et al. 2013) compared with Northern Hemisphere (Zone 1) atmospheric values (from Hua and Barbetti 2004); b) European S emissions; c) S concentrations; and d) $\delta^{34}S$ in *Abies alba* from NE Italy compared with European S emissions (Wynn et al. 2014).

ACCEPTED MANUSCRIPT

3.9.4 The radiocarbon bomb spike and heavy metal concentrations

Atmospheric $\Delta^{14}C$ decreased by about 20.0‰ between 1890 and 1950 CE in response to the Suess effect of adding low-activity fossil carbon, punctuated by a marked bomb spike in response to nuclear weapons testing, peaking in ~1963 CE that led to a level two times higher than that of pre-1850 CE times (Rakowski et al. 2013). Annual rings of a pine tree (*Pinus sylvestris*) taken in the Niepołomice area, near Kraków, Poland from 1960 to 2003 CE show a clear $\Delta^{14}C$ bomb-spike in 1964 CE (Rakowski et al. 2013, Figure 32a). A suitable GSSP candidate should have a data set of both $\Delta^{14}C$ and $\delta^{13}C$ extending back to pre-industrial times; the data in the tree analysed by Rakowski et al. (2013) began close to the peak bomb-spike interval, so lack an adequate record of the transition across a potential Holocene–Anthropocene boundary. $^{239+240}Pu$ records in tree rings are less studied, but the distribution of Pu in tree rings and in lake sediment cores seems to show similar trends (Mahara and Kudo 1995) suggesting Pu as a potentially suitable signal.

Historical changes in trace metal levels can be recognised in some tree ring records, although there may well be a time lag between metal deposition and the passage through soils and root system. Element concentrations in tree rings for a given year may differ markedly between trees from a single location (Watmough 1999). Studies on the sugar maple (*Acer saccharum*) suggest that there is both a rapid uptake of trace metals (e.g. Cu, Ni, Cr, Zn, Cd, Co and As) and a minimal lateral movement between rings (Watmough 1999), although radial movement of trace elements has been reported in other studies (Hietz et al. 2014).

ACCEPTED MANUSCRIPT

4 Summary

Many of the signals described above are highly resolved, widespread and correlatable. Notably, heavy metals, $\delta^{13}C$ and radiogenic fallout signals tend to be recorded in most environments that might conceivably be suitable for hosting a GSSP (Table 2). Other airborne signals, such as fly ash, nitrates and $\delta^{15}N$, and to a lesser extent sulphur and sulphates, CO_2 and CH_4 concentrations and $\delta^{18}O$ occur in many environments and provide additional means of correlation. Biotic assemblages have been demonstrated to respond rapidly to local environmental changes and can provide useful secondary and local markers, but seem on current evidence unlikely to provide a globally correlatable and synchronous marker that is as temporally well-resolved as $\delta^{13}C$ and radiogenic fallout or other airborne signals.

These more nearly synchronous and widespread signals, combined with the possibility of directly dating successions by such means as lamina counting, show that a well-chosen GSSP level might be precisely dated to the nearest year (or season) and might be correlated to other well-studied high-resolution sections with a resolution of a year or a few years. In less well-studied sections, or those lacking annual lamination, use of the very wide range of available proxy signals should still be able to provide correlative resolution of a few to several years, sufficient to widely locate a practically effective Holocene–Anthropocene boundary, even in apparently unpromising geological settings. For instance, Smith et al. (2016) identified what would be regarded as an Anthropocene succession of sub-ice shelf deposits at Pine Island in West Antarctica, by identifying bomb-derived plutonium within the deposits.

The location of such a Holocene–Anthropocene boundary within relatively recent successions – of the last few centuries – we regard as having use beyond the formal value of

ACCEPTED MANUSCRIPT

the establishment of chronostratigraphic divisions. An extensive, variably interconnected suite of physical, chemical and biological changes to the Earth System has been taking place, some local, some global, many of which leave stratigraphically detectable traces. These include phenomena such as the spread of various kinds of industrially related pollutants and their biotic effects, changes to the atmosphere and hence to the Earth's radiative properties, a complex pattern of species extinctions, extirpations and invasions, and the emergence and evolution of technological systems on a planetary scale. For practical analysis of these changes – many of which are ongoing, or accelerating – placing them in an effective framework of space and time is a prerequisite. We suggest that a chronostratigraphic Holocene–Anthropocene boundary could make a significant contribution to this analytical process, not least in that this time interval is emerging as a critical transition in the geological history of this planet (e.g. Steffen et al. 2016). The survey we provide here suggests that such a boundary would be workable in practice, across the range of the environments we survey here and likely more widely. Table 13 surveys the range of chemostratigraphic signals recorded here and provides their onset and peak date for key environments. This shows the wide range of potential proxies that could be used to mark a mid-20th century boundary.

ACCEPTED MANUSCRIPT

ACCEPTED MANUSCRIPT

Environment \ Marker	Black Carbon	Fly ash	Lead	PCBs	Pesticides (DDT)	NO_3^-	$\delta^{15}N$	Sulphur	SO_4^{2-}	CO_2	CH_4	$\delta^{13}C$	$\delta^{18}O$	D &/or dust	^{239}Pu	^{14}C
Marine anoxic basins (1)	?	?	1965 (1970s)	1945 (1967)	1952 (1967)	?	x	x	x	x	x	?	?	x	1950-54 (1970s)	?
Coral bioherms & marine bivalves (2) (3)	?	?	Late 1940s (1970s) (2)	?	x	~1970 (3)	~1950 (3)	x	x	x	x	1955 (2)	~1950 (2)	x	1952 (1964) (2)	1958 (1972) (3)
Estuaries/ Deltas (4) (5)	?	1900s (5)	(1915) (4)	1950s (1965-1977) (4)	?	?	x	x	x	x	x	?	?	x	?	?
Lakes (6) (7) (8) (9) (10)	1940s-1950s (2004-6) (8)	~1950 (1970-1990)	1960s (Post-2000) (8)	~1960 (9)	1950s (9)	?	~1950 (7)	~1950 (10)	x	x	x	?	?	x	~1955 (1964) (6)	?
Peat & peat-lands (11) (12)	x	1950s (1970s) (11)	1810 (1979) (12)	(1960-1976) (12)	x	x	x	x	x	x	x	?	x	x	x	x
Ice (13) (14)	~1880 (~1910) (14)	?	~1940 (~1970) (14)	?	?	~1950 (14)	~1950 (1980) (14)	~1940 (~1970) (14)	~1940 (14)	~1950 (13)	~1950 (13)	1955 (13)	1980s (2010) (14)	~1850 (13)	1953 (1962) (13)	1954 (1966) (13)
Speleothems (15)	x	x	?	?	?	?	?	1980 (2000)	1880 (15)	x	x	~1840 (1860)	1875 (1940)	x	x	~1965 (~1975)
Trees (16) (17) (18)	x	x	?	?	?	?	1945 (18)	1960s (15)	?	x	x	1940 (1750) (16)	?	1960	?	1956 (1964) (17)

ACCEPTED MANUSCRIPT

Table 13. Summary of key mid-20th century proxy signals and potential palaeoenvironments for a GSSP. The initial date represents the marked onset of the signal; the peak signal is shown in brackets. Key signals and environments are shown in boxes. Reference numbers relate to main geographical locations mentioned in the text: (1) Santa Barbara, USA; (2) Caribbean; (3) Nova Scotia, Canada; (4) Clyde Estuary, Scotland; (5) Urola Estuary, Spain; (6) Lake Victoria, Australia; (7) North America; (8) China; (9) Lochnagar, Scotland; (10) Lilla Öresjön, Sweden; (11) Northern England; (12) Switzerland; (13) Antarctica; (14) Greenland; (15) Ernesto Cave, Italy; (16) Fenno-Scandinavia; (17) Poland; (18) Ontario, Canada.

With regard to the environments most suitable for seeking a candidate GSSP, we offer the following guidance:

- Anthropogenic deposits are common in terrestrial environments. They may be relatively thick (up to tens of metres), contain signals that closely reflect human influence, and are readily datable, particularly using technofossils. They tend to lack lateral continuity, may contain omission surfaces, are not annually laminated, and may lack 'preservability', all of which are likely to discount many such deposits as hosts for primary or auxiliary GSSP candidates. However, much the same criticisms also apply to many Holocene deposits. Suitable potential GSSP candidates may well exist within anthropogenic deposits, or perhaps at the interface between anthropogenic and non-anthropogenic strata, although none have yet been identified or described. More work is required in this area of investigation.

- Marine anoxic basins tend to display undisturbed annually resolved laminae that can be independently dated. The radionuclide fallout signal may show some smearing due to processes affecting the settling of radioisotopes through the water column, which can inhibit development of a sharp bomb spike. Even so, the early 1950s start of the signal (Table 13) is

ACCEPTED MANUSCRIPT

typically robust. In these environments, heavy metals including Pb, organic compounds, such as PCBs and pesticides (Table 13), microplastics and biotic signals, including planktonic foraminifera and diatoms (and their stable isotope patterns), tend to be controlled by local environmental variations. Although they broadly display changes in the mid- to late-20th century, the onset of their signal can vary by decades between regions. Low sedimentation rates may reduce the thickness of Anthropocene strata to a few centimetres. Even so, the signals of change may still be clearly resolved and laterally extensive. This environment has potential for hosting an Anthropocene GSSP, provided that the fallout signal, especially ^{239}Pu, is not significantly smeared by slow settling rates or by bioturbation.

- Coral growth bands can exhibit very-high resolution records, which, along with rapid growth rates commonly exceeding sediment accumulation rates, provide a potentially suitable medium for hosting a GSSP. The onset of the ^{239}Pu signal is particularly robust as an early 1950s marker (Table 13), with no concerns about the influence of settling rates through the water column; peak signals are more variable between localities. However, reefs that are distal to nuclear detonation test sites might be more suitable so as to more clearly show the global pattern, rather than including some residues of the early, pre-1952 CE tests that only left a local signal. The Caribbean, Red Sea, western and northern Indian Ocean are distant from the main testing grounds (Waters et al. 2015) and are more likely to most clearly show the global atmospheric signal. Radiocarbon tends to have latitudinal diachroneity and shows a delayed signal in shallow-water corals of about a decade compared with atmospheric ^{14}C and the ^{239}Pu signal (Table 13), with increased lags also associated with greater water depth of coral growth. The decline of δ^{13}C in corals is most marked in Atlantic corals from 1957 CE (Table 13), with the accumulation rate being more variable and of much smaller magnitude in the Indian and Pacific oceans. δ^{15}N values are complex, related to source areas of ocean

ACCEPTED MANUSCRIPT

currents and types of anthropogenic sources. Heavy metals can be concentrated within certain species of coral, but they tend to record only local contamination events. Temperature records are a mix of local and global factors and a single core would probably not be suitable as a GSSP. If corals are to be considered as a potential host for a GSSP, examples from the Caribbean, using ^{239}Pu as the primary signal, may be most suitable.

- Estuaries and deltas are typically responsive to anthropogenic influence, whether biotic change in response to environmental modifications and widespread introduction of neobiota, changes to sediment flux through alteration of catchment erosion rates or impounding sediments through dam construction, or through contamination by fly ash, heavy metals such as Pb, organic chemicals such as PCBs (Table 13), or microplastics. These environments, while offering good potential for hosting a candidate GSSP, may suffer from strong modulation by local influences, a lack of lateral continuity, and the common presence of omission surfaces.

- Lakes, despite being laterally disconnected, are found across large parts of the planet and, although commonly strongly modulated by local processes, also display numerous globally coherent signals. As with estuaries and deltas, lakes tend to be responsive to anthropogenic influence, resulting in a spectrum of highly resolved signals, including black carbon, fly ash, organic compounds, δ^{15}N, S and ^{239}Pu which provide potential 1950s markers (Table 13). Despite the Anthropocene successions being typically thin, shallow perennial lakes are advantageous for hosting a potential GSSP given that settling rates of radiogenic fallout and heavy metals will be minimal and at the same time there should be few omission surfaces. The latter issue limits the suitability of many arid saline lakes, but numerous Northern Hemisphere meromictic lakes could host suitable candidate GSSP or auxiliary

ACCEPTED MANUSCRIPT

sections. Lake sediments have been accepted as hosts for global auxiliary stratotypes for the base of the Holocene.

- Ombrotrophic peat bogs provide widespread local archives that faithfully record aerosol distribution from local, regional and global sources. The range of potential suitable signals are diverse (Table 8), with fly ash providing the most robust 1950s marker (Table 13). The behaviour of trace elements may be influenced by changing redox conditions and has to be carefully documented. As there is no varved sedimentation, and as some signals such as the Pu bomb spike show redistribution effects, hosting a primary GSSP in peat bogs seems not appropriate, but this environment may provide a useful auxiliary GSSP section.

- Glacial ice provides a broad spectrum of annually resolvable atmospheric signals including radionuclides, $\delta^{18}O$, sulphates, nitrates, $\delta^{15}N$, Pb and other metals, and so may provide a suitable mid-20th century marker (Table 13). Given the precedent of locating the Holocene GSSP in glacial ice, there is a strong argument for locating in an ice sheet at least an auxiliary stratotype GSSP section for the base of the Anthropocene, not least to show how its signals contrast with those at the base of the Holocene. A significant issue for the temporal resolution required for the Anthropocene is the significant time lag between the age of the ice and the included air bubbles. This lag affects CO_2, CH_4, $\delta^{13}C$ and N_2O values, which are consistently younger than the enclosing ice. This effect is most pronounced where snow accumulation is slowest, so is typically more of an issue in Antarctica than Greenland. Even so, it has been recently demonstrated that the age of air bubbles can be matched to that of the associated ice through the use of nitrogen isotopes (Parrenin et al. 2013), which may circumvent what until recently appeared to be a significant problem. Slowly accumulating Antarctic ice tends to show only the more global signals, whereas Greenland

ACCEPTED MANUSCRIPT

ice can reveal many regional Northern Hemisphere influences. Nevertheless, Antarctic coastal ice cores do accumulate at high rates (e.g. Law Dome) and may provide an appropriate GSSP candidate section. Care would have to be taken to locate such a prospective GSSP in a region where the danger of calving of significant areas of ice from ice shelves and ice loss due to global climate change is less imminent, given the shallow depths at which the signal would be evident. Ellsworth Land, at the base of the Antarctic Peninsula might provide a suitable location, since the observed increase in snow accumulation there during the late 20th century is unprecedented in the context of the past 300 years (Thomas et al. 2015).

- Speleothems suffer from modulation of environmental signals by the soil ecosystem, making the interpretation of signal variation complex. Sulphur loading, the depletion of $\delta^{34}S$ and the ^{14}C (but importantly not ^{239}Pu) bomb-spike can be clearly resolved in speleothems, with an onset close to the atmospheric signal, although the peak tends to show a decadal-scale lag (Table 13). These environments also tend to lack mid-20th century $\delta^{13}C$, $\delta^{18}O$ and heavy metal shifts as potential environmental markers.

- Tree rings, compared with speleothems, are more responsive to and provide a clearer archive of changing atmospheric chemistries. They benefit from a global distribution and are capable of precise calendrical dating through dendrochronology without reliance upon external dating methods. Stable carbon isotopes provide the strongest “candidate” measure from tree rings as they have been demonstrated to record worldwide the change in atmospheric $\delta^{13}C$ since the onset of global industrialisation. Such a uniformly expressed, well-characterised ~1940 CE departure (Table 13) has not been observed in the older tree-ring record, and the co-recorded chronology enables this trend to be clearly recognised.

ACCEPTED MANUSCRIPT

Sulphur loading and depletion of $\delta^{34}S$ is evident in developed countries, starting in the 1960s, with enrichment of excess ^{14}C from the early 1950s to a 1964 CE peak (Table 13), but this signal is a terrestrial marker only. Although certainly widespread, tree-ring signals can be influenced by complex local environmental processes, yet these may be resolved through a capacity for large-scale independent replication. There is no precedent for using a living or deceased organism (such as a tree) as the host for a GSSP, but as an archive containing a signal of atmospheric carbon isotope variability and precise timescale there are close parallels to the use of the North Greenland ice core (NGRIP) for establishing the base of the Holocene.

To summarize, the information provided here is a first overall appraisal of suitable palaeoenvironments as regards their overall potentials for hosting an Anthropocene GSSP and a range of auxiliary sections. Clearly, many candidates that are geologically suitable exist, and are found in a range of different depositional settings. The review presented here is a critical prelude to help guide the necessary next steps, which involve selecting a small number of maximally suitable sites from the most appropriate geological facies, and subjecting them to multi-proxy analysis in order to assess changes in stratigraphically-relevant proxies from pre-industrial times through to the present.

ACCEPTED MANUSCRIPT

5 Conclusions

- Many widespread, correlatable, and highly resolved signals could be used as the primary marker and as secondary markers for the base of an Anthropocene Series. $\delta^{13}C$ and radionuclide fallout signals are applicable across most environments. The latter provides the most abrupt signal, with a marked upturn in abundance of

ACCEPTED MANUSCRIPT

radioisotopes of ^{239}Pu or ^{14}C, in 1952 and 1954 CE respectively, appearing to provide a consistent horizon for correlation, whereas the peak 'bomb-signals' appear diachronous.

- Varved deposits, such as those accumulating in marine anoxic basins, meromictic lakes, and estuaries and deltas, along with layers in glacial ice and growth rings, such as developed in corals, marine bivalves, speleothems and trees, represent those palaeoenvironments yielding highest resolution 'stratigraphy' at annual or even seasonal scale, and are hence preferred targets for searching for a likely GSSP section. The use of lamina or layer counting to determine ages can be verified, precisely in the case of tree rings, or radiometrically via ^{210}Pb (marine anoxic basins, corals and bivalves, lakes, ice) and ^{14}C (marine anoxic basins, corals and bivalves, lakes, speleothems and trees) dating.
- Ombrotrophic peat bogs and some anthropogenic deposits provide clear expression of numerous key stratigraphical markers and can show high stratal accumulation rates, but lack the annual lamination seen in other environments.
- Preservation of continuous laminated successions without missing 'strata' is essential. Estuaries and deltas are prone to missing laminae through erosive events, ice laminae from high-altitude glaciers through melting events, and speleothems through periods of aridity.
- Time lags between signal generation and recording within varves or laminae on decadal scales represents a significant correlatory problem in speleothems.
- A lag between the age of ice and the younger age of air bubbles within the ice limits the potential use of atmospheric CO_2 and CH_4 signals from ice cores, but close examination of sites of rapid accumulation on the Antarctic Peninsula may be

ACCEPTED MANUSCRIPT

suitable, as well as sites in other coastal regions (Law Dome in Antarctica), or in Greenland).

- Deep marine environments can display a significant settling delay that affects radioisotopes and heavy metal signals, though this effect mainly delays the peak signal rather than onset. Except for some marine anoxic basins and perhaps cold-water corals, the rates of sedimentation are too low and the rates of bioturbation are too high for the development of suitable sections for a GSSP.
- Proximity to the source of signals can result in local discrepancies in the timing of their initial onset within successions. In the search for a GSSP, there is advantage in looking at locations that are distant from such perturbations and provide a global signal, e.g. Antarctica for glacial ice, or the Caribbean for corals.
- Overall, the range of high-resolution stratigraphic proxy signals, and the varied and widespread nature of the palaeoenvironments where they can be systematically preserved in strata, suggests that there is excellent potential for locating an effective candidate Anthropocene GSSP together with auxiliary stratotypes.

Acknowledgements

Lisa Barber is thanked for the drafting of Figure 5. This paper is a contribution of the Anthropocene Working Group (AWG), a constituent working group of the Subcommission on Quaternary Stratigraphy of the International Commission on Stratigraphy. Lucy Edwards and Jim Rose are thanked for their helpful reviews of the original manuscript.

Declaration of Interest

The AWG receives no direct funding to carry out its research, and the authors declare no competing financial interests.

ACCEPTED MANUSCRIPT

References

Abram, N.J., Mulvaney, R., Wolff, E.W., Triest, J., Kipfstuhl, S., Trusel, L.D., Vimeux, F, Fleet, L., Arrowsmith, C. 2013. Acceleration of snow melt in an Antarctic Peninsula ice core during the twentieth century. Nature Geoscience, v. 6, 404–411.

Abram, N.J., McGregor, H.V., Tierney, J.E., Evans, M.N., McKay, N.P., Kaufman, D.S. & the PAGES 2k Consortium, 2016, Early onset of industrial-era warming across the oceans and continents. Nature, v. 536, 411–418.

Ahmad, S.M., Padmakumari, V.M., Raza, W., 2011. High-resolution carbon and oxygen isotope records from scleractinian (*Porites*) coral of Lakshadweep Archipelago, Quaternary International, v. 238, 107–114.

Allan, M., Le Roux, G., De Vleeschouwer, F., Bindler, R., Blaauw, M., Piotrowska, N., Sikorski, J., Fagel, N., 2013. High-resolution reconstruction of atmospheric deposition of trace metals and metalloids since AD 1400 recorded by ombrotrophic peat cores in Hautes-Fagnes, Belgium. Environmental Pollution, v. 178, 381–394.

Alldredge, A.L., Gotschalk, C. 1988. In situ settling behavior of marine snow. Limnology and Oceanography, v. 33(3). 339−351.

Anderson, R.F., LeHuray, A.P., Fleisher, M.Q., Murray, J.W., 1989. Uranium deposition in Saanich Inlet sediments, Vancouver Island. Geochimica et Cosmochimica Acta, v. 53, 2205−2213.

Appleby, P.G., Shotyk, W., Fankhauser, A., 1997. 210Pb age dating of three peat cores in the Jura Mountains, Switzerland. Water Air and Soil Pollution, v. 100 (3/4), 223−231.

Archer, D., Eby, M., Brovkin, V., Ridgwell, A., Long Cao, Mikolajewicz, U., Caldeira, K., Matsumoto, K., Munhoven, G., Montenegro, A., Tokos, K., 2009. Atmospheric lifetime of fossil fuel carbon dioxide. Annual Review of Earth and Planetary Science, v.37, 117–34.

Arienzo, M.M., McConnell, J.R., Chellman, N., Criscitiello, A.S., Curran, M., Fritzsche, D., Kipfstuhl, S., Mulvaney, R., Nolan, M., Opel, T., Sigl, M., Steffensen, J.P., 2016. A method for continuous

ACCEPTED MANUSCRIPT

^{239}Pu determinations in Arctic and Antarctic ice cores. Environmental Science and Technology, v. 50 (13), 7066–7073.

Arthur, M.A., Dean, W.E., Neff, E.D., Hay, B.J., King, J., Jones, G., 1994. Varve calibrated records of carbonate and organic carbon accumulation over the last 2000 years in the Black Sea. Glob. Biogeochem. Cycles, v. 8, 195–217.

Baker, A., Genty, D., Dreybrodt, W. Barnes, W.L., Mockler, N.J., Grapes, J., 1998. Testing theoretically predicted stalagmite growth rate with recent annually laminated samples: Implications for past stalagmite deposition. Geochimica et Cosmochimica Acta, v. 62(3), 393–404.

Ballent, A., Corcoran, P.L., Madden, O., Helm, P.A., Longstaff, F.J., 2016. Sources and sinks of microplastics in Canadian Lake Ontario nearshore, tributary and beach sediments. Marine Pollution Bulletin, v .110, 383–395.

Bamber, R.N., 1980. Properties of fly ash as a marine sediment. Marine Pollution Bulletin, v. 11, 323–326.

Barnosky, A.D., Hadly, E.A, Gonzalez, P., Head, J., Polly, P.D., Lawing, A.M., Eronen, J.T., Ackerly, D.D., Alex, K., Biber, E., Blois, J., Brashares, J., Ceballos, G., Davis, E., Dietl, G.P., Dirzo, R., Doremus, H., Fortelius, M., Greene, H.W., Hellmann, J., Hickler, T., Jackson, S.T., Kemp, M., Koch, P.L,. Kremen, C., Lindsey, E.L., Looy, C., Marshall, C.R., Mendenhall, C., Mulch, A., Mychajliw, A.M., Nowak, C., Ramakrishnan, U., Schnitzler, J., Das Shrestha, K., Solari, K., Stegner, L., Stegner, M.A., Stenseth, N.C., Wake, M.H., Zhibin Zhang, 2017. Merging paleobiology with conservation biology to guide the future of terrestrial ecosystems. Science, v. 355(6325), eaah4787

Barron, J.A., Bukry, D., Hendy, I.L., 2015, High-resolution paleoclimatology of the Santa Barbara Basin during the Medieval Climate Anomaly and early Little Ice Age based on diatom and silicoflagellate assemblages in Kasten core SPR0901-02KC, Quaternary International, v. 387, 13–22.

ACCEPTED MANUSCRIPT

Battarbee, R.W., Simpson, G.L., Shilland, E.M., Flower, R.J., Kreiser, A., Yang, H., Clarke, G., 2014. Recovery of UK lakes from acidification: An assessment using combined palaeoecological and contemporary diatom assemblage data. Ecological Indicators, v. 37, 365–380.

Benninger L.K., Dodge R.E., 1986, Fallout plutonium and natural radionuclides in annual bands of the coral *Montastrea annularis*, St. Croix, U.S. Virgin Islands, Geochimica Cosmochimica Acta, v. 50, 2785–2797.

Berry, K.L.E., Seemann, J., Dellwig, O., Struck, U., Wild, C., Leinfelder, R.R., 2013. Sources and spatial distribution of heavy metals in scleractinian coral tissues and sediments from the Bocas del Toro Archipelago, Panama. Environmental Monitoring and Assessment, v. 185, 9089–9099.

Berset, J.-D., Kuehne, P., Shotyk, W., 2001. Concentrations and distribution of some polychlorinated biphenyls (PCBs) and polycyclic aromatic hydrocarbons (PAHs) in an ombrotrophic peat bog profile of Switzerland. Science of the Total Environment, v. 267, 76–85.

Bindler, R., Renberg, I., Klaminder, J., Emteryd, O., 2004. Tree rings as Pb pollution archives? A comparison of 206 Pb/207 Pb isotope ratios in pine and other environmental media. Science of the Total Environment, v. 319(1), 173–183.

Blyth, A.J., Hartland, A., Baker, A. 2016. Organic proxies in speleothems: New developments, advantages and limitations. Quaternary Science Reviews, v. 149, 1–17.

Boettger, T., Haupt, M., Knöller, K., Weise, S.M., Waterhouse, J.S., Rinne, K.T., Loader, N.J., Sonninen, E., Jungner, H., Masson-Delmotte, V., Stievenard, M., Guillemin, M.-T., Pierre, M., Pazdur, A., Leuenberger, M., Filot, M., Saurer, M., Reynolds, C.E., Helle, G., Schleser, G.H., 2007. Wood cellulose preparation methods and mass spectrometric analyses of $\delta^{13}C$, $\delta^{18}O$, and nonexchangeable $\delta^{2}H$ values in cellulose, sugar, and starch: An interlaboratory comparison. Analytical Chemistry, v. 79, 4603–4612.

Boettger, T., Haupt, M., Friedrich, M, Waterhouse, J.S., 2014. Reduced climate sensitivity of carbon, oxygen and hydrogen stable isotope ratios in tree-ring cellulose of silver fir (*Abies alba* Mill.) influenced by background SO_2 in Franconia (Germany, Central Europe). Environmental Pollution, v. 185, 281–294.

ACCEPTED MANUSCRIPT

Bollhöfer, A., Rosman, K.J.R. 2001. Isotopic source signatures for atmospheric lead: the Northern Hemisphere. *Geochimica et Cosmochimica Acta*, v. *65*(11), 1727–1740.

Bond, T.C., Bhardwaj, E., Dong, R., Jogani, R., Jung, S.K., Roden, C., Streets, D.G., Trautmann, N.M. 2007. Historical emissions of black and organic carbon aerosol from energy-related combustion, 1850–2000. Global Biogeochem Cycles, v. 21(2). DOI: 10.1029/2006GB002840.

Bonotto, D.M., Karmann, I., Baskaran, M.M., 2012. Growth rates in modern speleothems from Santana Cave, Brazil, by the ^{210}Pb-method. Radiation Measurements, v. 47, 168–177.

Borsato, A., Frisia, S., Fairchild, I. J., Somogyi, A., Susini, J., 2007. Trace element distribution in annual stalagmite laminae mapped by micrometer-resolution X-ray fluorescence: implications for incorporation of environmentally significant species. Geochimica et Cosmochimica Acta, v.71, 1494–1512.

Borsato, A., Frisia, S., Wynn, P., Fairchild, I.J., Miorandi, R., 2015. Sulphate concentration in cave dripwater and speleothems: long-term trends and overview of its significance as proxy of environmental processes and climate forcing. Quaternary Science Reviews, v. 127, 48–60.

Boutron, C.F., Görlach, U., Candelone, J.-P., Bolshov, M. A., Delmas, R.J., 1991. Decrease in anthropogenic lead, cadmium and zinc in Greenland snows since the late 1960s. Nature, v. 353, 153–156.

Boyle, E.A., Lee, J.-M., Echegoyen, Y., Noble, A. Moos, S. Carrasco, G. Zhao, N., Kayser, R., Zhang, J. Gamo, T. Obata, H., Norisuye, K., 2014. Anthropogenic lead emissions in the ocean: The evolving global experiment, Oceanography, v. 27(1), 69–75.

Brown, A.G., Tooth, S., Bullard, J.E., Thomas, D.S.G., Chiverrell, R.C., Plater, A.J., Murton, J., Thorndycraft, V.R., Tarolli, P., Rose, J., Wainwright, J., Downs, P., Aalto, R., 2017. The Geomorphology of the Anthropocene: Emergence, Status and Implications. Earth Surface Processes and Landforms, v. 42, 71–90.

Bukata, A.R., Kyser T.K., 2007. Carbon and nitrogen isotope variations in tree-rings as records of perturbations in regional carbon and nitrogen cycles. Environmental Science and Technology, v. 41 (4), 1331–1338.

ACCEPTED MANUSCRIPT

Burney, D.A., & 11 others, 2001. Fossil evidence for a diverse biota from Kaua'i and its transformation since human arrival. Ecological Monographs, v. 7, 615–641.

Calvo-Marcilese, L., Langer, M.R., 2010. Breaching biogeographic barriers: the invasion of *Haynesina germanica* (Foraminifera, Protista) in the Bahía Blanca estuary, Argentina. Biological Invasions, v. 12, 3299–3306.

Campana, S.E., 1997. Use of radiocarbon from nuclear fallout as a dated marker in the otoliths of haddock *Melanogrammus aeglefinus*. Marine Ecology Progress Series, v. 150, 49–56.

Carlton, J.T., Thompson, J.K., Schemel, L.E., Nichols, F.H., 1990. Remarkable invasion of San Francisco Bay (California, USA) by the Asian clam *Potamocorbula amurensis*. Marine Ecology Progress Series, v. 66, 81–94.

Ceballos, G., Ehrlich, P.R., Barnosky, A.D., García, A., Pringle, R.M., Palmer, T.M., 2015. Accelerated modern human–induced species losses: Entering the sixth mass extinction. Science Advances, v. 1(5), e1400253, DOI: 10.1126/sciadv.1400253.

Chapman, S.B., 1964. The ecology of Coom Rigg Moss, Northumberland, II. The chemistry of peat profiles and the development of the bog system. Journal of Ecology, v. 52, 315–321.

Ciais, P., Sabine, C., Bala, G., Bopp, L., Brovkin, V., Canadell, J., Chhabra, A., DeFries, R., Galloway, J., Heimann, M., Jones, C., Le Quéré, C., Myneni , R.B., Piao, S., Thornton, P., 2013. Carbon and Other Biogeochemical Cycles. In: Climate Change 2013: The Physical Science Basis. Contribution of Working Group I to the Fifth Assessment Report of the Intergovernmental Panel on Climate Change [Stocker, T.F., D. Qin, G.-K. Plattner, M. Tignor, S.K. Allen, J. Boschung, A. Nauels, Y. Xia, V. Bex and P.M. Midgley (eds.)]. Cambridge University Press, Cambridge, United Kingdom and New York, NY, USA, pp. 465–570. doi:10.1017/CBO9781107415324.015.

Cocroft W., Schofield, G. 2012. The Secret Hill: Cold War Archaeology of the Teufelsberg. British Archaeology, v. 126, 38–43.

Cohen, A.N., 2004. Invasions in the sea. Park Science, v. 22, 37–41.

ACCEPTED MANUSCRIPT

Cohen, A.N., 2011. The Exotics Guide: Non-native Marine Species of the North American Pacific Coast. Center for Research on Aquatic Bioinvasions, Richmond, CA, and San Francisco Estuary Institute, Oakland, CA. Revised September 2011. http://www.exoticsguide.org

Cohen, A.N., Carlton, J.T., 1998. Accelerating invasion rate in a highly invaded estuary. Science, v. 279, 555–557.

Cole, J.E., 1996, Coral records of climate change: understanding past variability in the Tropical Ocean-Atmosphere, *In:* Jones, P. D., Bradley, R. S. and Jouzel, J. (eds.) Climatic Fluctuations and Forcing: Mechanisms of the Last 2000 Years, (Springer, Berlin), pp. 333–355.

Cole, M., Lindeque, P., Fileman, E., Halsband, C., Goodhead, R., Moger, J., Galloway, T.S., 2013, Microplastic Ingestion by Zooplankton, Environ. Sci. Technol., v. 47, 6646–6655.

Colonna, M., Casanova, J., Dullo, W.-C., Camoin, G., 1996. Sea-level changes and $\delta^{18}O$ record for the past 34,000 yr from Mayotte Reef, Indian Ocean. Quaternary Research, v. 46, 335–339.

Committee on Nonnative Oysters in the Chesapeake Bay, National Research Council. 2004. Nonnative Oysters in the Chesapeake Bay. 344 pp.

Condomines, M., Rihs, S., 2006. First ^{226}Ra–^{210}Pb dating of a young speleothem. Earth and Planetary Science Letters, v. 250, 4–10.

Cook, E.R., Briffa, K.R., Meko, D.M., Graybill, D.A., Funkhouser, G., 1995. The 'segment length curse' in long tree-ring chronology development for palæoclimatic studies. The Holocene, v. 5 229–237.

Corcoran, P.L., Norris, T., Ceccanese, T., Walzak, M.J., Helm, P.A., Marvin, C.H., 2015. Hidden plastics of Lake Ontario: Canada and their potential preservation in the sediment record. Environmental Pollution, v. 204, 17–25.

Crowther, T.W., Glick, H.B., Covey, K.R., Bettigole, C., Maynard, D.S., Thomas, S.M., Smith, J.R., Hintler, G., Duguid, M.C., Amatulli, G., Tuanmu, M.-N., Jetz, W., Salas, C., Stam, C., Piotto, D., Tavani, R., Green, S., Bruce, G., Williams, S.J., Wiser, S.K., Huber, M.O., Hengeveld, G.M., Nabuurs, G.-J., Tikhonova, E., Borchardt, P., Li, C.-F., Powrie, L.W., Fischer, M., Hemp, A., Homeier, J., Cho, P., Vibrans, A.C., Umunay, P.M., Piao, S.L., Rowe, C.W., Ashton, M.S., Crane,

ACCEPTED MANUSCRIPT

P.R., Bradford, M.A., 2015. Mapping tree density at a global scale. Nature, v. 515, 201 [doi: 10.1038/nature 14967]

Crutzen, P.J., Stoermer, E.F., 2000. The Anthropocene, Global Change Newsletters, v. 41, 17–18.

Curtis, C.J. and Simpson, G.L. (Eds.) (2011). Freshwater Umbrella – the effects of nitrogen deposition on freshwaters in the UK. Report to DEFRA under contract AQ0803. ECRC Research Report No 152. University College London, UK. 204 pp.

Dalton, C., Birks, H.J.B., Brooks, S.J., Cameron, N.G., Evershed, R.P., Peglar, S.M., Scott, J.A., Thompson, R., 2005. A multi-proxy study of lake-development in response to catchment changes during the Holocene at Lochnagar, north-east Scotland. Palaeogeography, Palaeoclimatology, Palaeoecology, v. 221(3-4), 175–201.

Dargie, G.C., Lewis, S.L., Lawson, I.T., Mitchard, E.T., Page, S.E., Bocko, Y.E., Ifo, S.A., 2017. Age, extent and carbon storage of the central Congo Basin peatland complex. Nature, v. 542, 86–90.

D'Arrigo, R., Wilson, R., Liepert, B., Cherubini, P., 2007. On the 'divergence problem' in northern forests: a review of the tree-ring evidence and possible causes. Global Planetary Change, v. 60(3–4), 289–305.

Dean, J.M., Kemp, A.E.S., 2004. A 2100 year BP record of the Pacific Decadal Oscillation, El Niño Southern Oscillation and Quasi-Biennial Oscillation in marine production and fluvial input from Saanich Inlet, British Columbia. Palaeogeography, Palaeoclimatology, Palaeoecology, v. 213, 207– 229.

Dean, J.M., Kemp, A.E.S., Pearce, R.B., 2001. Palaeo-flux records from electron microscope studies of Holocene laminated sediments, Saanich Inlet, British Columbia. Marine Geology, v. 174, 139–158.

Dearing, J.A., Xiangdong Yang, Xuhui Dong, Enlou Zhang, Xu Chen, Langdon, P.G., Ke Zhang, Weiguo Zhang, Dawson, T.P., 2012. Extending the timescale and range of ecosystem services through paleoenvironmental analyses, exemplified in the lower Yangtze basin. Proceedings of the National Academy of Science, U.S.A., v. 109, E1111–E1120.

ACCEPTED MANUSCRIPT

De'ath, G., Lough, J.M., Fabricius, K.E., 2009. Declining coral calcification on the Great Barrier Reef. Science, v. 323, 116–119.

DeFelice, R.C., Eldredge, L.G., Carlton, J.T., 2001. Nonindigenous invertebrates. In: Eldredge, L.G. & Smith, C.M. (eds). A guidebook of introduced marine species in Hawaii. Bishop Museum Technical Report 21.

DeLong, K.L., Maupin, C.R., Flannery, J.A., Quinn, T.M., Shen, C.-C., 2016. Refining temperature reconstructions with the Atlantic coral Siderastrea siderea, Palaeogeography, Palaeoclimatology, Palaeoecology, v. 462, 1–15.

Diaz, R.J., Rosenberg, R., 2008, Spreading Dead Zones and Consequences for Marine Ecosystems, *Science*, v. 321, 926–929.

Dris, R., Gasperi, J., Saad, M., Mirande, C., Tassin, B., 2016. Synthetic fibers in atmospheric fallout: A source of microplastics in the environment? Marine Pollution Bulletin, v. 104, 290–293.

Druffel, E.R.M., 1996. Post-bomb radiocarbon records of surface corals from the tropical Atlantic Ocean. Radiocarbon, v. 38(3), 563–572.

Edgeworth, M., Richter D. deB., Waters, C.N., Haff, P., Neal, C., Price, S.J., 2015. Diachronous beginnings of the Anthropocene: The lower bounding surface of anthropogenic deposits, Anthropocene Review, v. 2(1), 1–26.

Ekaykin, A.A., Vladimirova, D.O., Lipenkov, V.Y., Masson-Delmotte, V., 2017. Climatic variability in Princess Elizabeth Land (East Antarctica) over the last 350 years, Climate of the Past Discussions, 13(1), 61–71..

Ekdahl, E.J., Teranes, J.L., Guilderson, T.P., Turton, C.L., McAndrews, J.H., Wittkop, C.A., Stoermer, E.F., 2004. Prehistorical record of cultural eutrophication from Crawford Lake, Canada, Geology, v. 32, 745–748.

Ekdahl, E.J., Teranes, J.L., Wittkop, C.A., Stoermer, E.F., Reavie, E.D., Smol, J.P., 2007. Diatom assemblage response to Iroquoian and Euro-Canadian eutrophication of Crawford Lake, Ontario, Canada, Journal of Paleolimnology, v. 37, 233–246.

ACCEPTED MANUSCRIPT

Ellis, E.C., Antill, E.C., Kreft, H., 2012. All is not loss: Plant biodiversity in the Anthropocene. PLoS ONE, v. 7(1), e30535. doi:10.1371/journal.pone.0030535

Enrico, M., Le Roux, G., Marusczak, N., Heimbürger, L., Claustres, A., Fu, X., Sun, R., Sonke, J.E., 2016. Atmospheric mercury transfer to peat bogs dominated by gaseous elemental mercury dry deposition. Environmental Science & Technology, v. 50, 2405–2412.

Erisman, J.W., Galloway, J.N., Seitzinger, S., Bleeker, A., Dise, N.B., Petrescu, A.M.R., Leach, A.M., de Vries, W., 2013. Consequences of human modification of the global nitrogen cycle. Philosophical Transactions of the Royal Society B, v. 368: 20130116.

Esper, J., Cook, E.R., Schweingruber, F.H., 2002. Low-frequency signals in long tree ring chronologies for reconstructing past temperature variability. Science, v. 295, 2250–2253.

Etheridge, D.M., Steele, L.P., Langenfelds, R.L., Francey, R.J., Barnola, J.M., Morgan, V.I., 1996. Natural and anthropogenic changes in atmospheric CO_2 over the last 1000 years from air in Antarctic ice and firn. J. Geophys. Res., v. 101(D2), 4115–4128.

Evans, M.A., Fahnenstiel, G., Scavia, D., 2011. Incidental Oligotrophication of North American Great Lakes. Environmental Science & Technology, v. 45(8), 3297–3303.

Fairchild, I.J., 2017. Geochemical records in Speleothems. *In:* Elias, S. (ed.) Encyclopedia of the Anthropocene, Elsevier Reference Modules. DOI10.1016/B978-0-12-409548-9.10006-5.

Fairchild, I.J., Baker, A., 2012. Speleothem Science. From Process to Past Environment. Wiley-Blackwell, Chichester.

Fairchild, I.J., Frisia, S., 2014. Definition of the Anthropocene: a view from the underworld. In: Waters, C., Zalasiewicz, J., Williams, M., Ellis, M.A., and Snelling A. (eds.) A Stratigraphical Basis for the Anthropocene. Geological Society Special Publication, v. 395, 239–254.

Fairchild, I.J., Loader, N.J., Wynn, P.M., Frisia, S., Thomas, P.A., Lageard, J.G.A., De Momi, A., Hartland, A., Borsato, A., La Porta, N., Susini, J., 2009. Sulfur fixation in wood mapped by synchrotron X-ray studies: implications for environmental archives, Environmental Science and Technology, v. 43, 1310–1315.

ACCEPTED MANUSCRIPT

FAO (Food and Agriculture Organization of the United Nations) (2006). Global Forest Resources Assessment 2005: Progress towards sustainable forest management. FAO Forestry Paper 147. Published January 2006.

Farmer, J.G., Eades, L.J., Atkins, H., Chamberlain, D.F., 2002, Historical trends in the lead isotopic composition of archival Sphagnum mosses from Scotland (1838–2000). Environmental Science & Technology, v. 36, 152–157.

Farquhar, G.D., O'Leary, M.H., Berry, J.A., 1982 On the relationship between carbon dioxide discrimination and the intercellular carbon dioxide concentration in leaves. Australian Journal of Plant Physiology, v. 9, 121–137.

Ferretti, D.F., Miller, J.B., White, J.W.C., Etheridge, D.M., Lassey, K.R., Lowe, D.C., MacFarling Meure, C., Dreier, M.F., Trudinger, C.M., van Ommen, D., 2005. Unexpected changes to the global methane budget over the last 2,000 years. Science, v. 309, 1714–1717.

Fiałkiewicz-Kozieł, B., Smieja-Król, B., Frontasyeva, M., Słowiński, M., Marcisz, K., Lapshina, E., Gilbert, D., Buttler, A., Jassey, V E J., Kaliszan, Laggoun-Défarge, K.F., Kołaczek, P. Lamentowicz, M., 2016. Anthropogenic- and natural sources of dust in peatland during the Anthropocene. Scientific Reports, v. 6, 38731. DOI: 10.1038/srep38731.

Field, D.B., Baumgartner, T.R., Charles, C.D., Ferreira-Bartrina, V., Ohman, M.D., 2006. Planktonic foraminifera of the California Current reflect 20th-century warming. Science, v. 311, 63−66.

Fischer, H., Wagenbach, D., Kipfstuhl, J. 1998. Sulfate and nitrate firn concentrations on the Greenland ice sheet. 2. Temporal anthropogenic deposition changes. Journal of Geophysical Research, v. 103, 21 935–21 942.

Florea, N., Cristache, C., Oaie, G., Duliu, O.G., 2011. Concordant ^{210}Pb and ^{137}Cs ages of black sea anoxic unconsolidated sediments. Geochronometria, v. 38, 101–106.

Fofonoff, P.W., Ruiz, G.M., Steves, B., Simkanin, C., Carlton, J.T. 2017. National Exotic Marine and Estuarine Species Information System. http://invasions.si.edu/nemesis/.

Fohlmeister, J., Kromer, B., Mangini, A., 2011. The influence of soil organic matter age spectrum on the reconstruction of atmospheric ^{14}C levels via stalagmites, Radiocarbon, v. 53, 99–115.

ACCEPTED MANUSCRIPT

Ford, J.R., Price, S.J., Cooper, A.H., Waters, C.N., 2014, An assessment of lithostratigraphy for anthropogenic deposits, *In*: Waters, C.N., Zalasiewicz, J., Williams, M., Ellis, M.A., and Snelling A. (eds.) A Stratigraphical Basis for the Anthropocene. Geological Society, London, Special Publications v. 395, 55–89.

Fowler D, Coyle M, Skiba U., Sutton, M.A., Cape, J.N., Reis, S., Sheppard, L.J., 2013. The global nitrogen cycle in the 21st century. Philosophical Transactions of the Royal Society B, v. 368(1621), 1–13.

Francey, R.J., Allison, C.E., Etheridge, D.M., Trudinger, C.M., Enting, I.G., Leuenberger, M., Langenfelds, R.L., Michel, E., Steele, L.P., 1999. A 1000-year high precision record of δ13C in atmospheric CO_2. Tellus, v. 51B, 170–193.

Frank, D.C., Poulter, B., Saurer, M., Esper, J., Huntingford, C., Helle, G., Treydte, K., Zimmermann, N.E., Schleser, G.H., Ahlström, A., Ciais, P., Friedlingstein, P., Levis, S., Lomas, M., Sitch, S., Viovy, N., Andreu-Hayles, L., Bednarz, Z., Berninger, F., Boettger, T., D'Alessandro, C.M., Daux, V., Filot, M., Grabner, M., Gutierrez, E., Haupt, M., Hilasvuori, E., Jungner, H., Kalela-Brundin, M., Krapiec, M., Leuenberger, M., Loader, N.J., Marah, H., Masson-Delmotte, V., Pazdur, A., Pawelczyk, S., Pierre, M., Planells, O., Pukiene, R., Reynolds-Henne, C.E., Rinne, K.T., Saracino, A., Sonninen, E., Stievenard, M., Switsur, V.R., Szczepanek, M., Szychowska-Krapiec, E., Todaro, L., Waterhouse, J.S., Weigl, M., 2015. Water-use efficiency and transpiration across European forests during the Anthropocene. Nature Climate Change, v.5, 579–583.

Freiwald, A., Rogers, A., Hall-Spencer, J., Guinotte, J.M., Davies, A.J., Yesson, C., Martin, C.S., Weatherdon, L.V., 2017. Global distribution of cold-water corals (version 3.0). Second update to the dataset in Freiwald, A., Fosså, J.H., Grehan, A., Koslow, T., Roberts, J.M. (2004) Cold-water coral reefs: out of sight – no longer out of mind. Biodiversity Series 22. Cambridge (UK): UNEP World Conservation Monitoring Centre. 86 pp. URL: http://data.unep-wcmc.org/datasets/3

ACCEPTED MANUSCRIPT

Frisia, S., Borsato, A., Preto, N., McDermott, F., 2003, Late Holocene annual growth in three Alpine stalagmites records the influence of solar activity and the North Atlantic Oscillation on winter climate, Earth and Planetary Science Letters, v. 216, 411–424.

Frisia, S., Borsato, A., Fairchild, I. J., Susini, J., 2005. Variations in atmospheric sulphate recorded in stalagmites by synchrotron micro-XRF and XANES analyses. Earth and Planetary Science Letters, v.235, 729–740.

Fritts, H.C., 1976. Tree Rings and Climate. Academic Press, USA

Gabrieli, J., Cozzi, G. Vallelonga, P., Schwikowski, M., Sigl, M., Eickenberg, J., Wacker, L., Boutron, C., Gäggeler, H., Cescon, P., Barbante, C., 2011. Contamination of Alpine snow and ice at Colle Gnifetti, Swiss/Italian Alps, from nuclear weapons tests. Atmospheric Environment, v. 45, 587–593.

Gagnon, C., Pelletier, É., Mucci, A., 1997. Behaviour of anthropogenic mercury in coastal marine sediments. Marine Chemistry, v. 59, 159–176.

Genty, D., Massault, M., 1999. Carbon transfer dynamics from bomb-^{14}C and ^{13}C time series of a laminated stalagmite from SW France: modelling and comparison with other stalagmite records. Geochimica et Cosmochimica Acta, v. 63, 1537–1548.

Geyer, R., Jambeck, J.R. Lavender Law, K. 2017. Production, use, and fate of all plastics ever made. Science Advances, v. 3, e1700782. DOI: 10.1126/sciadv.1700782

Giosan, L., Syvitski, J., Constantinescu, S., Day, J., 2014, Climate Change: Protect the world's deltas. Nature, v. 516, 31–33.

Goffard, A., 2016. Registro geológico del impacto humano en el estuario del Urola (Geoparque de la Costa Vasca) durante el Antropoceno. CKQ Estudios de Cuaternario, v. 6, 43–60.

Gradstein, F.M., Ogg, J.G, Schmitz, M., Ogg, G. (eds) A Geological Time Scale 2012. Elsevier, 1144 pp.

Grudd, H., 2008. Torneträsk tree-ring width and density AD 500–2004: A test of climatic sensitivity and a new 1500-year reconstruction of north Fennoscandian summers. Climate Dynamics, v. 31, 843–857.

ACCEPTED MANUSCRIPT

Hall, N.M, Berry, K.L.E., Rintoul, L., Hoogenboom, M.O., 2015. Microplastic ingestion by scleractinian corals, Marine Biology, v. 162, 725–732.

Han, Y.M., Wei, C., Huang, R.J., Bandowe, B.A.M., Ho, S.S.H., Cao, J.J., Jin, Z.D., Xu, B.Q., Gao, S.P., Tie, X.X., An, Z.S., Wilcke, W. 2016. Reconstruction of atmospheric soot history in inland regions from lake sediments over the past 150 years. Scientific Reports, v. 6, 19151.

Han, Y.M., An, Z.S. and Cao, J.J., 2017. The Anthropocene—A potential stratigraphic definition based on black carbon, char, and soot records. Encyclopedia of the Anthropocene. DOI:10.1016/B978-0-12-409548-9.10001-6.

Hancock, G.J., Leslie, C., Everett, S.E., Tims, S.G., Brunskill, G.J., and Haese, R., 2011, Plutonium as a chronomarker in Australian and New Zealand sediments: a comparison with ^{137}Cs, Journal of Environmental Radioactivity, v. 102, 919–929.

Hancock, G.J., Tims, S.G., Fifield, L.K., Webster, I.T., 2014. The release and persistence of radioactive Anthropogenic nuclides. In: Waters, C.N., Zalasiewicz, J., Williams, M., Ellis, M.A., Snelling, A. (eds) A Stratigraphical Basis for the Anthropocene. Geological Society, London, Special Publications, v. 395, 265–281.

Hanebuth, T.J.J., Lantzsch, H., Nizou, J., 2015. Mud depocenters on continental shelves—appearance, initiation times, and growth dynamics. Geo-Marine Letters, v. 35(6), 487–503.

Hartland, A., Fairchild, I.J., Müller, W., Domínguez-Villar, D., 2014. Preservation of colloid-metal complexes in a modern hyperalkaline stalagmite: implications for speleothem trace element geochemistry. Geochimica et Cosmochimica Acta, v. 128, 29–43.

Hastings, M.G., Jarvis, J.C., Steig, E.J., 2009. Anthropogenic impacts on nitrogen isotopes of ice-core nitrate. Science, v. 324, 1288.

Hazen, R.M., Grew, E.S., Origlieri, M.J., Downs, R.T., 2017. On the mineralogy of the "Anthropocene Epoch". American Mineralogist, v. 102, 596–611.

Head, M.J., Gibbard, P.L., 2015. Formal subdivision of the Quaternary System/Period: Past, present, and future. Quaternary International, v. 383, 4–35.

ACCEPTED MANUSCRIPT

Heikoop, J.M., Risk, M.J, Lazier, A.V., Edinger, E.N., Jompa, J., Limmon, G.V., Dunn, J.J., Browne, D.R., Schwarcz, H.P., 2000. Nitrogen-15 signals of anthropogenic nutrient loading in reef corals. Marine Pollution Bulletin, v. 40(7), 628–636.

Hendy, I.L., Dunn, L., Schimmelmann, A., Pak D.K., 2013. Resolving varve and radiocarbon chronology differences during the last 2000 years in the Santa Barbara Basin sedimentary record, California. Quaternary International, v. 310, 155–168.

Hendy, I.L., Napier, T.J., Schimmelmann, A., 2015. From extreme rainfall to drought: 250 years of annually resolved sediment deposition in Santa Barbara Basin, California. Quaternary International, v. 387, 3–12.

Hetzinger, S., Pfeiffer, M., Dullo, W.-C., Garbe-Schönberg, D., Halfar, J., 2010. Rapid 20th century warming in the Caribbean and impact of remote forcing on climate in the northern tropical Atlantic as recorded in a Guadeloupe coral. Palaeogeography, Palaeoclimatology, Palaeoecology, v. 296, 111–124.

Hietz, P., Horsky, M., Prohaska, T., Lang, I., Grabner, M., 2015. High-resolution densitometry and elemental analysis of tropical wood. Trees, v. 29, 487–497.

Hoegh-Guldberg, O., 2014. Coral reefs in the Anthropocene: persistence or the end of the line? *In:* Waters, C.N., Zalasiewicz, J., Williams, M., Ellis, M.A., and Snelling A. (eds.) A Stratigraphical Basis for the Anthropocene. Geological Society, London, Special Publications, v. 395, 167–183.

Holtgrieve, G.W., Schindler, D.E., Hobbs, W.O., Leavitt, P.R., Ward, E.J., Bunting, L., Chen, G., Finney, B.P., Gregory-Eaves, I., Holmgren, S., Lisac, M.J., Lisi, P.J., Nydick, K., Rogers, L.A., Saros, J.E., Selbie, D.T., Shapley, M.D., Walsh, P.B., Wolfe, A.P., 2011. A Coherent Signature of Anthropogenic Nitrogen Deposition to Remote Watersheds of the Northern Hemisphere, Science, v. 334, 1545–1548.

Hom, W., Risebrough, R.W., Soutar, A., Young, D.R., 1974. Deposition of DDE and Polychlorinated Biphenyls in Dated Sediments of the Santa Barbara Basin. Science, v. 184 (4142), 1197-1199.

ACCEPTED MANUSCRIPT

Hong, S., Candelone, J.P., Patterson, C.C., Boutron, C.F., 1994. Greenland ice evidences of hemispheric pollution for lead two millennia ago by Greek and Roman civilizations. Science, v. 265, 1841–1843.

Hua, Q., Barbetti, M., 2004. Review of tropospheric bomb ^{14}C data for carbon cycle modeling and age calibration purposes. Radiocarbon, v. 46(3) 1273–1298.

Hughen, K.A., Overpeck, J.T., Peterson, L.C., Anderson, R.F., 1996. The nature of varved sedimentation in the Cariaco Basin, Venezuela, and its palaeoclimatic significance. In: Kemp, A.E.S. (Ed.), Palaeoclimatology and palaeoceanography from laminated sediments. Geol. Soc. London Spec. Pub., v. 116, 171–183.

Hughes, T.P. and 45 others, 2017. Global warming and recurrent mass bleaching of corals. Nature, v. 543, 373–377.

Irabien, M.J. García-Artola, A., Cearreta, A., Leorri, E., 2015. Chemostratigraphic and lithostratigraphic signatures of the Anthropocene in estuarine areas from the eastern Cantabrian coast (N. Spain), Quaternary International, v. 364, 196–205.

Isdale, P., 1984. Fluorescent bands in massive coral record centuries of coastal rainfall, Nature, v. 310, 578–579.

Ivar do Sul, J.A., Costa, M.F., 2014. The present and future of microplastic pollution in the marine environment, Environmental Pollution, v. 185, p. 352–364.

Jambeck, J.R., Geyer, R., Wilcox, C., Siegler, T.R., Perryman, M., Andrady, A., Narayan, R, Law, K.L., 2015. Plastic waste inputs from land into the ocean. Science, v. 347, 768–771.

Jeandel C., 1981. Comportement du Plutonium dans les mileux naturels (Lacustre, Fluvial et Estuarien). Thèse 3° Cycle, Université de Paris VII, 280 p.

Jenny, J-P, Francus, P., Normandeau, A., Lapointe, F., Perga, M-E., Ojala, A., Schimmelmann, A., Zolitschka, B., 2016, Global spread of hypoxia in freshwater ecosystems during the last three centuries is caused by rising local human pressure Global Change Biology, v. 22, 1481–1489.

Jimenez, H., Ruiz, G.M., 2016. Contribution of non-native species to soft-sediment marine

ACCEPTED MANUSCRIPT

community structure of San Francisco Bay, California. Biological Invasions, v. 18 (7), 2007–2016.

Jin, Z., Han, Y., Chen, L., 2010. Past atmospheric Pb deposition in Lake Qinghai, northeastern Tibetan Plateau. Journal of Paleolimnology, v. 43, 551–563.

Junge, C.E., 1963. Air Chemistry and Radioactivity. Academic Press, New York, 382pp.

Kawamura, H., Matusoka, N., Momoshima, N., Koike, M., Takashima, T., 2006. Isotopic evidence in tree rings for historical changes in atmospheric sulfur sources. Environ. Sci. Technol., v. 40, 5750–5754.

Kelly, A.E., Reuer, M.K. Goodkin, N.F., Boyle, E.A., 2009. Lead concentrations and isotopes in corals and water near Bermuda, 1780–2000. Earth and Planetary Science Letters, v. 283, 93–100. http://dx.doi.org/10.1016/j.epsl.2009.03.045.

Key, R.M., Kozyr, A., Sabine, C.L., Lee, K., Wanninkhof, R., Bullister, J.L., Feely, R.A., Millero, F.J., Mordy, C., Peng, T.-H., 2004. A global ocean carbon climatology: Results from Global Data Analysis Project (GLODAP), Global Biogeochem. Cycles, v. 18, GB4031, doi:10.1029/2004GB002247.

Koide, M., Griffin, J.J., Goldberg, E.D., 1975. Records of Plutonium Fallout in Marine and Terrestrial Samples, Journal of Geophysical Research, v. 80, 4153–4162.

Kowalski, N., Reichardt, A.M., Waniek, J.J., 2016. Sinking rates of microplastics and potential implications of their alteration by physical, biological, and chemical factors. Marine Pollution Bulletin, v. 109, 310–319.

Krachler, M., Zheng, J., Fisher, D., Shotyk, W., 2008. Atmospheric Sb in the Arctic during the past 16,000 years: Responses to climate change and human impacts, Global Biogeochemical Cycles, v. 22, GB1015. doi:10.1029/2007GB002998

Krachler, M., Zheng, J., Fisher, D., Shotyk, W., 2009, Global atmospheric As and Bi contamination preserved in 3000 year old Arctic ice, Global Biogeochemical Cycles. v. 23, GB3011.

ACCEPTED MANUSCRIPT

Krishnaswami, S., Lal, D., Amin, B.S., Soutar, A., 1973, Geochronological studies in Santa Barbara Basin: 55Fe as a unique tracer for particulate settling, Limnology and Oceanography, v. 18 (5), 763–770.

Küttner, A., Mighall, T.M., De Vleeschouwer, F., Mauquoy, D., Martínez Cortizas, A., Foster, I.D.L., Krupp, E.A., 2014. 3300-year atmospheric metal contamination record from Raeburn Flow raised bog, south west Scotland. Journal of Archaeological Science, v. 44, 1–11.

Kylander, M.E., Martínez-Cortizas, A., Bindler, R., Greenwood, S.L., Mörth, C.-M., Rauch, S., 2016. Potentials and problems of building detailed dust records using peat archives: An example from Store Mosse (the "Great Bog"), Sweden. Geochimica Cosmochimica Acta, v. 190, 156–174.

Lee, J-M., Boyle, E.A., Nurhati, I.S., Pfeiffer, M., Meltzner, A.J., Suwargadi, B., 2014. Coral-based history of lead and lead isotopes of the surface Indian Ocean since the mid-20th century. Earth and Planetary Science Letters, v. 398, 37–47.

Lee, J-M., Eltgroth, S.F., Boyle, E.A., Adkins, J.F., 2017. The transfer of bomb radiocarbon and anthropogenic lead to the deep North Atlantic Ocean observed from a deep sea coral. Earth and Planetary Science Letters, v. 458, 223–232.

Le Quéré, C., Andrew, R.M., Canadell, J.G., Sitch, S., Korsbakken, J.I., Peters, G.P., Manning, A.C., Boden, T.A., Tans, P.P., Houghton, R.A., Keeling, R.F., Alin, S., Andrews, O.D., Anthoni, P., Barbero, L., Bopp, L., Chevallier, F., Chini, L.P., Ciais, P., Currie, K., Delire, C., Doney, S.C. Friedlingstein, P., Gkritzalis, T., Harris, I., Hauck, J., Haverd, V., Hoppema, M., Klein Goldewijk, K., Jain, A.K., Kato, E., Körtzinger, A., Landschützer, P., Lefèvre, N., Lenton, A. Lienert, S., Lombardozzi, D., Melton, J.R., Metzl, N., Millero, F., Monteiro, P.M.S., Munro, D.R., Nabel, J.M.S., Nakaoka, S-I., O'Brien, K., Olsen, A., Omar, A.M., Ono, Pierrot, T.D.,Poulter, B., Rödenbeck, C., Salisbury, J., Schuster, U., Schwinger, J., Séférian, R., Skjelvan, I., Stocker, B.D., Sutton, A.J., Takahashi, T., Tian, H., Tilbrook, B., van der Laan-Luijkx, I.T., van der Werf, G.R., Viovy, N., Walker, A.P., Wiltshire, A.J. and Zaehle, S. (2016) Global Carbon Budget 2016. Earth System. Science Data, v. 8, 605–649.

ACCEPTED MANUSCRIPT

Lesueur, P., Tastet, J.P., Marambat, L., 1996. Shelf mud fields formation within historical times: examples from offshore the Gironde estuary, France. Continental Shelf Research, v. 16(14), 1849–1870.

Lewis, S.L., Maslin, M.A., 2015. Defining the Anthropocene, Nature, v. 519, 171–180.

Lindahl, P., Asami, R., Iryu, Y., Worsfold, P., Keith-Roach, M, Choi, M.-S., 2011. Sources of plutonium to the tropical Northwest Pacific Ocean (1943–1999) identified using a natural coral archive, Geochemica et Cosmochimica Acta, v. 75, 1346–1356.

Lindberg, S., Bullock, R., Ebinghaus, R., Engstrom, D., Xinbin, Feng, Fitzgerald, W., Pirrone, N., Prestbo, E., Seigneur, C., 2007. A synthesis of progress and uncertainties in attributing the sources of mercury in deposition. Ambio, v. 36(1), 19–32.

Livingston, H.D., Povinec, P.P., Ito, T., Togawa, O.., 2001. The behaviour of plutonium in the Pacific Ocean. In: Kudo A (ed.) Radioactivity in the Environment. Volume 1, Plutonium in the Environment. Amsterdam: Elsevier, pp. 267–292.

Loader, N.J., Walsh, R.P.D, Robertson, I., Bidin, K., Ong, R.C., Reynolds, G., McCarroll, D., Gagen, M., Young, G.H.F.., 2011. Recent trends in the intrinsic water-use efficiency of ringless rainforest trees in Borneo. Philosophical Transactions of the Royal Society B, v. 366, 3330–3339.

Loader, N.J., Young, G.H.F., Grudd, H., McCarroll, D., 2013a. Stable carbon isotopes from Torneträsk, northern Sweden provide a millennial length reconstruction of summer sunshine and its relationship to Arctic circulation. Quaternary Science Reviews, v. 62, 97–113.

Loader, N.J., Young, G.H.F., McCarroll, D., Wilson. R.J.S., 2013b. Quantifying uncertainty in isotope dendroclimatology. The Holocene, v. 23, 1221 – 1226. 10.1177/0959683613486945

Lough, J.M., Barnes, D.J., 2000. Environmental controls on growth of the massive coral *Porites*, Journal of Experimental Marine Biology and Ecology, v. 245 (2), 225–243.

Loring, D.H., Rantala, R.T.T., Smith, J.N., 1983. Response time of Saguenay Fjord sediments to metal contamination. In: Hallberg, R. (ed.) Environtal Biogeochemistry Ecological Bulletins (Stockholm) v. 35, 59–72.

ACCEPTED MANUSCRIPT

MacFarling Meure, C., Etheridge, D. E., Trudinger, C., Steele, P., Langenfelds, R., van Ommen, T., Smith, A., Elkins, J., 2006. Law Dome CO_2, CH_4 and N_2O ice core records extended to 2000 years BP, Geophys. Res. Lett., v. 33(14), L14810, doi:10.1029/2006GL026152.

McCarroll, D., Loader, N.J., 2004. Stable isotopes in tree rings. Quaternary Science Reviews, v. 23, 771–801.

McCarroll, D., Gagen, M.H., Loader, N.J., Robertson, I., Anchukaitis, K.J., Los, S., Young, G.H.F., Jalkanen, R., Kirchhefer, A., Waterhouse, J.S., 2009. Correction of tree ring stable carbon isotope chronologies for changes in the carbon dioxide content of the atmosphere. Geochimica et Cosmochimica Acta, v. 73, 1539–1547.

McConnell, J.R., Edwards, R., 2008. Coal burning leaves toxic heavy metal legacy in the Arctic. Proceedings of the National Academy of Sciences, v. 105(34), 12140–12144.

McFarlane, D. A., Lundberg, J., Neff, H., 2013. A speleothem record of early British and Roman mining at Charterhouse, Mendip, England. Archaeometry http://dx.doi.org/10.1111/arcm.12025

McGann, M., Sloan, D., Cohen, A.N., 2000. Invasion by a Japanese marine microorganism in western North America. Hydrobiologia, v. 421, 25–30.

McGann, M., Sloan, D., Wan, E., 2002. Biostratigraphy beneath central San Francisco Bay along the San Francisco-Oakland Bay Bridge transect. pp. 11–28 in: Crustal structure of the coastal and marine San Francisco Bay region, California.

McQuoid, M.R., Hobson, L.A., 1997. A 91-year record of seasonal and inter-annual variability of diatoms from laminated sediments in Saanich Inlet, British Columbia. J. Plankton. Res., v. 19(1), 173–194.

Magnan, G., Garneau, M., Payette, S., 2014. Holocene development of maritime ombrotrophic peatlands of the St. Lawrence North Shore in eastern Canada. Quaternary Research, v. 82 (1), 96–106.

Mahara, Y., Kudo, A., 1995. Plutonium released by the Nagasaki A-bomb: mobility in the environment. Applied Radiation and Isotopes, v. 46(11), 1191–1201.

ACCEPTED MANUSCRIPT

Mahiques, M.M., Hanebuth, T.J.J., Martins, C.C., Montoya-Montes, Alcántara-Carrió, J., Figueira, R.C.L, Bícego, M.C., 2016. Mud depocentres on the continental shelf: a neglected sink for anthropogenic contaminants from the coastal zone. Environmental Earth Sciences, v. 75(44). doi: 10.1007/s12665-015-4782-z.

Markgraf, V., Huber, U.M., 2010. Late and postglacial vegetation and fire history in Southern Patagonia and Tierra del Fuego. Palaeogeography Palaeoclimatology Palaeoecology, v. 297, 351–366.

Marshall, W.A., Gehrels, W.R., Garnett, M.H., Freeman, S.P.H.T., Maden, C., Xu, S., 2007. The use of 'bomb pike' calibration and high-precision AMS ^{14}C analyses to date salt marsh sediments deposited during the last three centuries. Quaternary Research, v. 68, 325–337.

Martin J., Puig, P., Palanques, A., Giamportone, A., 2015. Commercial bottom trawling as a driver of sediment dynamics and deep seascape evolution in the Anthropocene, Anthropocene, v. 7, 1–15.

Martínez-García, B., Pascual, A., Baceta, J.I., Murelaga, X., 2013. Estudio de los foraminíferos bentónicos del "beach-rock" de Azkorri (Getxo, Bizkaia). Geogaceta, v. 53, 29–32.

Martinez-Porchas, M., Martinez-Cordova, L.R., 2012. World Aquaculture: Environmental Impacts and Troubleshooting Alternatives. The Scientific World Journal, v. 2012, Article ID 389623, 9 p. doi:10.1100/2012/389623

Masson-Delmotte, V., Steen-Larsen, H.C., Ortega, P., Swingedouw, D., Popp, T., Vinther, B.M., Oerter, H., Sveinbjornsdottir, A.E., Gudlaugsdottir, H., Box, J.E., Falourd, S., Fettweis, X., Gallée, H., Garnier, E., Gkinis, V., Jouzel, J., Landais, A., Minster, B., Paradis, N., Orsi, A., Risi, C., Werner M., White, J.W.C., 2015. Recent changes in north-west Greenland climate documented by NEEM shallow ice core data and simulations, and implications for past-temperature reconstructions. The Cryosphere, v. 9, 1481–1504.

Matsuguma, Y., Takada, H., Kumata, H, Kanke, H., Sakurai, S., Suzuki, T., Itoh, M., Okazaki, Y., Boonyatumanond, R., Zakaria, M.P., Weerts, S., Newman, B., 2017. Microplastics in sediment

ACCEPTED MANUSCRIPT

cores from Asia and Africa as indicators of temporal trends in plastic pollution. Archives of Environmental Contamination and Toxicology, v. 73, 230–239.

Matsumoto, E., Wong, C.S., 1977. Heavy metal sedimentation in Saanich Inlet measured with ^{210}Pb technique. J. Geophys. Res., v. 82, 5477–5482..

Meharg, A.A., Edwards, K.J., Schofield, J.E., Raab, A., Feldmann, J., Moran, A., Bryant, C.L., Thornton, B., Dawson, J.J.-C., 2012. First comprehensive peat depositional records for tin, lead and copper associated with the antiquity of Europe's largest cassiterite deposits. Journal of Archaeological Science, v. 39, 717–727.

Melosi, M.V., 2016. Fresh Kills: The Making and Unmaking of a Wastescape, *in* Mauch, C. (ed.), Out of Sight, Out of Mind: The Politics and Culture of Waste. RCC Perspectives: Transformations in Environment and Society, v. 1, 59–65.

Melvin, T.M., Briffa, K.R., 2008. A ''signal-free'' approach to dendroclimatic standardisation. Dendrochronologia, v. 26, 71–86.

Mielke, H.-J., 2011. Wald und Politik: Die unendliche Geschichte des Berliner Teufelsberges. 48 pp, Berlin, (Projekte-Verlag Cornelius GmbH).

Miller, K.G., Wright, J.D., 2017. Success and failure in Cenozoic global correlations using golden spikes: A geochemical and magnetostratigraphic perspective. Episodes, v. 40, 8–21.

Monteith, D.T., Evans, C.D., Dalton, C., 2007. Acidification of Lochnagar and prospects for recovery. In: Rose, N.L. (ed.). Lochnagar: The natural history of a mountain lake. Developments in Paleoenvironmental Research, v. 12, 317–344. Springer, Dordrecht.

Muir, D.C.G., Rose, N.L., 2005. Lake sediments as records of Arctic and Antarctic pollution. In: Pienitz, R., Douglas, M.S.V., Smol, J.P. (eds.) Long-term Environmental Change in Arctic and Antarctic Lakes. Developments in Paleoenvironmental Research, v. 8, 209–239. Kluwer Academic Publishers, Dordrecht, The Netherlands.

Muir, D.C.G., Rose, N.L., 2007. Persistent organic pollutants in the sediments of Lochnagar. *In* Rose, N.L. (ed.), Lochnagar: The Natural History of a Mountain Lake, Developments in Paleoenvironmental Research, v. 12, 375–402. Springer, Dordrecht.

ACCEPTED MANUSCRIPT

Murozumi, M., Chow, T.J., Patterson, C.C., 1969. Geochemical concentrations of pollutant lead aerosols, terrestrial dusts and sea salts in Greenland and Antarctic snow data. Geochimica et Cosmochimica Acta, v. 33, 1247–1294.

Nagle, R., 2008. To love a Landfill. The History and Future of Fresh Kills, *in* France, R.L. (ed.) Handbook of Regenerative and Landscape Design. CRC Press, Boca Raton, p. 3–16.

National Atmospheric Emissions Inventory (NAEI), 2017. Overview of air pollutants. http://naei.defra.gov.uk/overview/ap-overview Accessed 12th April 2017

Newton, K.E., Fairchild, I.J., Gunn, J., 2015. Rates of calcite precipitation from hyperalkaline waters, Poole's Cavern, Derbyshire. Cave and Karst Science, v. 42, 116–124.

Nisbet, E.G., Dlugokencky, E.J., Manning, M.R., Lowry, D., Fisher, R.E., France, J.L., Michel, S.E., Miller, J.B., White, J.W.C., Vaughn, B., Bousquet, P., Pyle, J.A., Warwick, N.J., Cain, M., Brownlow, R., Zazzeri, G., Lanoisellé, M., Manning, A.C., Gloor, E., Worthy, D.E.J., Brunke, E.-G., Labuschagne, C., Wolff, E.W., Ganesan A.L., 2016. Rising atmospheric methane: 2007–2014 growth and isotopic shift. Global Biogeochemical Cycles, v. 30, 1356–1370.

Noller, J.S., 2000. Lead-210 Geochronology, Quaternary Geochronology: Methods and Applications, AGU Reference Shelf 4.

Obbard, R.W., Sadri, S. Wong, Y.Q., Khitun, A.A. Baker, I., Thompson, R.C., 2014, Global warming releases microplastic legacy frozen in Arctic Sea ice, Earth's Future, v. 2, 315–320.

Oldfield, F., 2014. Can the magnetic signatures from inorganic fly ash be used to mark the onset of the Anthropocene? Anthropocene Review, v. 2(1), 3–13.

Pandolfi, J.M., Bradbury, R.H., Sala, E., Hughes, T.P., Bjorndal, K.A., Cooke, R.G., McArdle, D., McClenachan, L., Newman, M.J., Paredes, G., Warner, R.R., 2003. Global trajectories of the long-term decline of coral reef ecosystems. Science, v. 301(5635), 955–958.

Parrenin, F., Masson-Delmotte, V., Köhler, P., Raynaud, D., Paillard, D., Schwander, J., Barbante, C., Landais, A., Wegner, A., Jouzel, J., 2013. Synchronous change of atmospheric CO_2 and Antarctic temperature during the last deglacial warming. Science, v. 339, 1060–1063.

ACCEPTED MANUSCRIPT

Patterson, C.C., Settle, D.M., 1987. Review of data on eolian fluxes of industrial and natural lead to the lands and seas in remote regions on a global scale. Mar. Chem., v. 22, 137–162.

Paull, C.K., Ussler III, W., Mitts, P.J., Caress, D.W., West, G.J., 2006. Discordant ^{14}C-stratigraphies in upper Monterey Canyon: A signal of anthropogenic disturbance. Marine Geology. v. 233, 21–36.

Pfeffer, W.T., Arendt, A.A., Bliss, A., Bolch, T., 2014. The Randolph Glacier Inventory: a globally complete inventory of glaciers. Journal of Glaciology, v. 60(221), 537–552.

Pilskaln, C.H., Pike, J., 2001. Formation of Holocene sedimentary laminae in the Black Sea and the role of the benthic flocculent layer. Paleoceanography, v. 16, 1–19. http://dx.doi.org/10.1029/1999PA000469.

Pla, S., Monteith, D., Flower, R., Rose, N., 2009. The recent palaeolimnology of a remote Scottish loch with special reference to the relative impacts of regional warming and atmospheric contamination. Freshwater Biology, v. 54, 505–523.

Poirier, C., Chaumillon, E., Arnaud, F., 2011. Siltation of river-influenced coastal environments: Respective impact of late Holocene land use and high-frequency climate changes, Marine Geology, v. 290, 51–62.

Pons-Branchu, E., Ayrault, S., Roy-Barman, M., Bordier, L., Borst, W., Branchu, P., Douville, E., Dumont, E., 2015. Three centuries of heavy metal pollution in Paris (France) recorded by urban spelelothems. Science of the Total Environment, v. 518-519, 85–96.

Pratte, S., Garneau, M., De Vleeschouwer, F., 2017. Late-Holocene atmospheric dust deposition in eastern Canada. The Holocene, v. 27, 12–25.

Preunkert S, Wagenbach D, Legrand M., 2003. A seasonally resolved alpine ice core record of nitrate: comparison with anthropogenic inventories and estimation of preindustrial emissions of NO in Europe. J. Geophys. Res., v. 108, 4861. doi:10.1029/2003JD003475.

Quayle, W.C., Peck, L.S., Peat, H., Ellis-Evans, J.C., Harrigan, P.R., 2002. Extreme responses to climate change in Antarctic lakes. Science, v. 295, 645.

ACCEPTED MANUSCRIPT

Quinto, F., Hrnecek, E., Krachler, M., Shotyk, W., Steier, P., Winkler, S.R., 2013a. Determination of ^{239}Pu, ^{240}Pu, ^{241}Pu and ^{242}Pu at femtogram and attogram levels - evidence for the migration of fallout plutonium in an ombrotrophic peat bog profile. Environmental Science Processes and Impacts, v. 15(4), 839–847.

Quinto, F., Hrnecek, E., Krachler, M., Shotyk, W, Steier, P., Winkler, S.R., 2013b. Measurements of ^{236}U in ancient and modern peat samples and implications for post depositional migration of fallout radionuclides. Environmental Sciemce & Technology, v. 47, 5243–5250.

Rakowski, A.Z., Nadeau, M-J, Nakamura, T., Pazdur, A., Pawełczyk, S., Piotrowska, N., 2013. Radiocarbon method in environmental monitoring of CO_2 emission. Nuclear Instruments and Methods in Physics Research B, v. 294, 503–507.

Ramirez-Llodra, E., Tyler, P.A., Baker, M.C., Bergstad, O.A., Clark, M.R., Escobar, E., Levin, L.A. Menot, L., Rowden, A.A., Smith, C.R., Van Dover, C.L., 2011. Man and the Last Great Wilderness: Human Impact on the Deep Sea. Plos One, v. 6(8), e22588, 1–25.

Rauch, S., Hemond, H.F, and Peucker-Ehrenbrink, B., 2004. Source characterisation of atmospheric platinum group element deposition into an ombrotrophic peat bog. Journal of Environmental Monitoring, v. 6, 335–343.

Rauch, S., Peucker-Ehrenbrink, B., Kylander, M., Weiss, D.J., Martinez-Cortizas, A., Heslop, D., Olid, C, Mighall, T.M. and Hemond, H.F., 2010. Anthropogenic Forcings on the Surficial Osmium Cycle Environmental Science & Technology, v. 44, 881–887.

Remane, J., Bassett, M.G., Cowie, J.W., Gohrbandt, K.H., Lane, H.R., Michelsen, O., Wang, N., with the cooperation of members of ICS, 1996. Revised guidelines for the establishment of global chronostratigraphic standards by the International Commision on Stratigraphy (ICS). Episodes, v. 19, 77–81.

Remane, J., 1997. Foreword: chronostratigraphic standards: how are they defined and when should they be changed? Quaternary International, v. 40, 3–4.

Remane, J., 2003. Chronostratigraphic correlations: their importance for the definition of geochronologic units, Palaeogeography, Palaeoclimatology, Palaeoecology, v. 196, 7–18.

ACCEPTED MANUSCRIPT

Renberg, I., Battarbee, R.W., 1990. The SWAP Palaeolimnology Programme: A synthesis. In Mason, B.J (ed) The Surface Waters Acidification Programme. Cambridge University Press, Cambridge, 281–300.

Renberg, I., Brännvall, M-L., Bindler, R., Emteryd, O., 2000. Atmospheric lead pollution history during four millennia (2000 BC to 2000 AD) in Sweden. Ambio, v. 29(3), 150–156.

Ren, H., Chen, Y-C., Wang, X.T., Wong, G.T.F., Cohen, A.L., DeCarlo, T.M., Weigand, M.A., Mii, H-S., Sigman, D.M., 2017. Atmospheric deposition of anthropogenic nitrogen has become a major nitrogen source in the South China Sea. Science, v. 356, 749–752.

Reuer, M.K. and Weiss, D.J. 2002, Anthropogenic lead dynamics in the terrestrial and marine environment. Philosophical Transactions of the Royal Society London A, v. 360, 2889–2904.

Reynolds, D.J., Scourse, J.D., Halloran, P.R., Nederbragt, A.J., Wanamaker, A.D., Butler, P.G., Richardson, C.A. Heinemeier, J., Eiríksson, J., Knudsen, K.L., Hall, I.R., 2016. Annually resolved North Atlantic marine climate over the last millennium. Nature Communications, v. 7, 13502. doi: 10.1038/ncomms13502.

Roemmich, D., McGowan, J., 1995. Climatic warming and the decline of zooplankton in the California Current, Science, v. 267, 1324.

Rose, N.L., 2007. The sediments of Lochnagar: Distribution, accumulation and composition. In: Rose, N.L. (ed.). Lochnagar: The natural history of a mountain lake. Developments in Paleoenvironmental Research, v. 12, 155–175. Springer, Dordrecht.

Rose, N.L., 2015. Spheroidal carbonaceous fly ash particles provide a globally synchronous stratigraphic marker for the Anthropocene, Environmental Science and Technology, v. 49(7), 4155–4162.

Rose, N.L., Yang, H., 2007. Temporal and spatial patterns of spheroidal carbonaceous particles (SCPs) in sediments, soils and deposition at Lochnagar. In: Rose, N.L. (ed.). Lochnagar: The natural history of a mountain lake. Developments in Paleoenvironmental Research, v. 12, 403–423. Springer, Dordrecht.

ACCEPTED MANUSCRIPT

Rose, N.L., Backus, S., Karlsson, H., Muir, D.C.G., 2001. An historical record of toxaphene and its congeners in a remote lake in western Europe. Environmental Science & Technology, v. 35(7), 1312–1319.

Rose, N.L., Morley, D., Appleby, P.G., Battarbee, R.W., Alliksaar, T., Guilizzoni, P., Jeppesen, E., Korhola, A., Punning, J.M., 2011. Sediment accumulation rates in European lakes since AD1850: trends, reference conditions and exceedence. Journal of Paleolimnology, v. 45, 447–468.

Rose, N.L., Yang, H., Turner, S.D., Simpson, G.L., 2012. An assessment of the mechanisms for the transfer of lead and mercury from atmospherically contaminated organic soils to lake sediments with particular reference to Scotland, UK. Geochimica et Cosmochimica Acta, v. 82, 113–135.

Rothwell, J.J., Taylor, K.G., Chenery, S.R.N., Cundy, A.B., Evans, M.G., Allott, T.E.H., 2010. Storage and behavior of As, Sb, Pb, and Cu in ombrotrophic peat bogs under contrasting water table conditions. Environtal Science & Technology, v. 44, 8497–8502.

Rubino, M., Etheridge, D.M. Trudinger, C.M. Allison, C.E. Battle, M.O. Langenfelds, R.L. Steele, L.P. Curran, M. Bender, M. White, J.W.C., Jenk, T.M. Blunier, T., Francey., R.J., 2013. A revised 1000 year atmospheric $\delta^{13}C$-CO_2 record from Law Dome and South Pole, Antarctica. Journal of Geophysical Research Atmospheres, v. 118, 8482–8499.

Rubino, M., Etheridge, D.M., Trudinger, C.M., Allison, C.E., Rayner, P.J., Enting, I., Mulvaney, R., Steele, L.P., Langenfelds, R.L., Sturges, W.T., Curran, M.A.J., Smith, A.M., 2016. Low atmospheric CO_2 levels during the Little Ice Age due to cooling-induced terrestrial uptake. Nature Geoscience v. 9, 691–694.

Saros, J.E., Michel, T.J., Interlandi, S.J., Wolfe, A.P., 2005. Resource requirements of *Asterionella formosa* and *Fragilaria crotonensis* in oligotrophic alpine lakes: implications for recent phytoplankton community reorganizations. Canadian Journal of Fisheries and Aquatic Sciences, v. 62(7), 1681–1689.

ACCEPTED MANUSCRIPT

Saurer, M., Spahni, R., Frank, D.C., Joos, F., Leuenberger, M., Loader, N.J., McCarroll, D., Gagen, M., Poulter, B., Siegwolf, R.T.W., Andreu-Hayles, L., Boettger, T., Liñán, I.D., Fairchild, I.J., Friedrich, M., Gutierrez, E., Haupt, M., Hilasvuori, E., Heinrich, I., Helle, G., Grudd, H., Jalkanen, R., Levanič, T., Linderholm, H.W., Robertson, I., Sonninen, E., Treydte, K., Waterhouse, J.S., Woodley, E.J., Wynn, P.M., Young, G.H.F., 2014. Spatial variability and temporal trends in water-use efficiency of European forests. Global Change Biology, v. 20, 3700–3712.

Sax, D.F., Gaines, S.D., 2008. Species invasions and extinction: the future of native biodiversity on islands. Proceedings of the National Academy of Sciences, v. 105, Supplement 1, 11490–11497.

Schimmelmann, A., Hendy, I.L., Dunn, L., Pak D.K., Lange, C.B., 2013. Revised ~2000-year chronostratigraphy of partially varved marine sediment in Santa Barbara Basin, California, GFF, v. 135(3–4), 258–264.

Schimmelmann, A., Lange, C.B., Schieber, J., Francus, P., Ojala, A.E.K., Zolitschka, B., 2016. Varves in marine sediments: A review. Earth-Science Reviews, v. 159, 215–246.

Schmidt, H., Reimers, C.E., 1991. The Recent History of Trace Metal Accumulation in the Santa Barbara Basin, Southern California Borderland, Estuarine, Coastal and Shelf Science, v. 33, 485–500.

Scholz, D., Frisia, S., Borsato, A., Spötl, C., Fohlmeister, J., Mudelsee, M., Miorandi, R., Mangini, A., 2012. Holocene climate variability in north-eastern Italy: potential influence of the NAO and solar activity recorded by speleothem data. Climate of the Past, v. 8, 1367–1383.

Schuster, P.F., Krabbenhoft, D.P., Naftz, D.L., Cecil, L.D., Olson, M.L., De Wild, J.F., Susong, D.D., Green, J.R., Abbott, M.L., 2002. Atmospheric mercury deposition during the last 270 years: A glacial ice core record of natural and anthropogenic sources. Environmental Science & Technology, v. 36(11), 2303–2310.

Scourse, J.D., Wanamaker Jr, A.D., Weidman, C., Heinemeier, J., Reimer, P.J., Butler, P.G., Witbaard, R., Richardson, C.A., 2012. The marine radiocarbon bomb pulse across the temperate north

ACCEPTED MANUSCRIPT

Atlantic: a compilation of $\Delta^{14}C$ time histories from *Arctica Islandica* growth increments. Radiocarbon, v. 54(2), 165–186.

Seibt, U., Rajabi, A., Griffiths, H., Berry, J.A., 2008. Carbon isotopes and water use efficiency: sense and sensitivity. Oecologia, v. 155, 441–454.

Sherwood, O.A., Scott, D.B., Risk, M.J., Guilderson, T.P. 2005a. Radiocarbon evidence for annual growth rings in a deep sea octocoral (*Primnoa resedaeformis*). Marine Ecology Progress Series, v. 301, 129–134.

Sherwood, O.A., Heikoop, J.M., Scott, D.B., Risk, M.J., Guilderson, T.P., McKinney, R.A., 2005b. Stable isotopic composition of deep-sea gorgonian corals *Primnoa* spp.: a new archive of surface processes. Marine Ecology Progress Series, v. 301, 135–148.

Sherwood, O.A., Lehmann, M.F., Schubert, C.J., Scott, D.B., McCarthy, M.D., 2011. Nutrient regime shift in the western North Atlantic indicated by compound-specific $\delta^{15}N$ of deep-sea gorgonian corals, PNAS, v. 108(3), 1011–1015.

Shotyk, W., 1988. Review of the inorganic geochemistry of peats and peatland waters. Earth-Science Reviews, v. 25(2), 95–176.

Shotyk, W., 1992. Organic soils. Ch. 13 in Martini, I.P. and Chesworth, W. (eds.) Weathering, Soils, and Paleosols. Elsevier, Amsterdam, 203–224.

Shotyk, W., 1996. Peat bog archives of atmospheric metal deposition: Geochemical assessment of peat profiles, natural variations in metal concentrations, and metal enrichment factors. Environmental Reviews, v. 4(2), 149–183.

Shotyk, W., Weiss, D., Appleby, P.G., Cheburkin, A.K., Frei, R., Gloor, M., Kramers, J.D., Reese, S., van der Knaap, W.O., 1998. History of atmospheric lead deposition since 12,370 14C yr BP from a peat bog, Jura Mountains, Switzerland. Science, v. 281, 1635–1640. http://dx.doi.org/10.1126/science.281.5383.1635.

Shotyk, W., Blaser, P., Grünig, A., Cheburkin, A.K., 2000. A new approach for quantifying cumulative, anthropogenic, atmospheric lead deposition using peat cores from bogs: Pb in eight Swiss peat bog profiles. Science of the Total Environment, v. 249, 281–295.

ACCEPTED MANUSCRIPT

Shotyk, W., Weiss, D., Heisterkamp, M., Cheburkin, A.K., Adams, F.C., 2002. A new peat bog record of atmospheric lead pollution in Switzerland: Pb concentrations, enrichment factors, isotopic composition, and organolead species Environmental Science and Technology, v. 36(18), 3893–3900.

Shotyk, W., Appleby, P.G., Bicalho, B., Davies, L, Froese, D., Grant-Weaver, I., Krachler, M., Magnan, G., Mullan-Boudreau, G., Noernberg, T., Pelletier, R., Shannon, B, van Bellen, S., and Zaccone, C., 2016. Peat bogs in northern Alberta, Canada reveal decades of declining atmospheric Pb contamination. Geophysical Research Letters, v. 43, 9964–9974.

Sloan, D., 1992. The Yerba Buena mud: record of the last-interglacial predecessor of San Francisco Bay, California. GSA Bulletin, v. 104, 716–727.

Smith, A.G. Barry, T., Bown, P., Cope, J., Gale, A., Gibbard, P., Gregory, J., Hounslow, M., Kemp, D., Knox, R., Marshall, J., Oates, M., Rawson, P., Waters, C., 2014. GSSPs, global stratigraphy and correlation, in Smith, D.G., Bailey, R.J., Burgess, P.M., and Fraser, A.J. eds., Strata and Time: Probing the Gaps in Our Understanding. Geological Society, London, Special Publications, v. 404, 37–67.

Smith, D.M., Zalasiewicz, J.A., Williams, M., Wilkinson, I., Redding, M., Begg, C., 2010. Holocene drainage of the English Fenland: roddons and their environmental significance. Proceedings of the Geologists' Association, v. 121, 256–269.

Smith, J.A., Andersen, T.J., Shortt, M., Gaffney, A.M., Truffer, M., Stanton, T.P., Bindschadler, R., Dutrieux, P., Jenkins, A., Hillenbrand, C.-D., Ehrmann, W., Corr, H.F.J., Farley, N., Crowhurst, S., Vaughan, D.G. 2016. Sub-ice-shelf sediments record twentieth century retreat of Pine Island Glacier. Nature, v. 541, 77–80.

Smith, J.N., Levy, E.M., 1990. Geochronology for Polycyclic Aromatic Hydrocarbon contamination in sediments of the Saguenay Fjord. Environ. Sci. Technol., v. 24, 874–879.

Smith, J.N., Walton, A., 1980. Sediment accumulation rates and geochronolgies measured in the Saguenay Fiord using the Pb-210 dating method. Geochimica et Cosmochimica Acta, v. 46, 941–954.

ACCEPTED MANUSCRIPT

Smol, J.P., 2008. Pollution of lakes and rivers: A palaeoenvironmental perspective (2nd Ed.). Wiley-Blackwell, 396 pp.

Speer, J.H., 2010. Fundamentals of Tree-Ring Research. The University of Arizona Press. USA.

Steffen, W., Leinfelder, R., Zalasiewicz, J., Waters, C.N., Williams, M., Summerhayes, C., Barnosky, A.D., Cearreta, A., Crutzen, P.J., Edgeworth, M., Ellis, E.C., Fairchild, I.J., Gałuszka, A., Grinevald, J., Haywood, A., Ivar Do Sul, J., Jeandel, C., McNeill, J.R., Odada, E., Oreskes, N., Revkin, A., Richter, D. DeB., Syvitski, J., Vidas, D., Wagreich, M., Wing, S.L., Wolfe, A.P., Schellnhuber, H.J., 2016. Stratigraphic and Earth System approaches in defining the Anthropocene. Earth's Future, v. 8, 324–345.

Suess, E., 1862. Der Boden der Stadt Wien nach seiner Bildungsweise, Beschaffenheit und seinen Beziehungen zum Bürgerlichen Leben. Eine geologische Studie von Eduard Suess. Wilhelm Braumüller, 326 pp.

Suess, E., 1897. Der Boden der Stadt Wien und sein Relief. Geschichte der Stadt Wien, Bd. 1, 26 pp. (Herausgegeben vom Alterthumsvereine zu Wien).

Swart, P.K., Rubenstone, J.L., Charles, C., Reitner, J. 1998. Sclerosponges: a new proxy indicator of climate. National Oceanic and Atmospheric Administration (NOAA), Climate and Global Change Program, Special Report, v. 12, 21 pp.

Swart, P.K., Greer, L., Rosenheim, B.E., Moses, C.S., Waite, A.J., Winter, A., Dodge, R.E., Helmle, K., 2010. The ^{13}C Suess effect in scleractinian corals mirror changes in the anthropogenic CO_2 inventory of the surface oceans, Geophysical Research Letters, v. 37, L05604.

Swindles, G. T., Watson, E., Turner, T. E., Galloway, J. M., Hadlari, T., Wheeler, J., Bacon, K. L., 2015. Spheroidal carbonaceous particles are a defining stratigraphic marker for the Anthropocene. Scientific Reports, v. 5(10264). doi:10.1038/srep10264.

Syvitski, J.P.M., Kettner, A., 2011. Sediment flux and the Anthropocene, Philosophical Transactions of the Royal Society A, v. 369, 1938, 957–975.

ACCEPTED MANUSCRIPT

Syvitski, J.P.M., Kettner, A.J., Overeem, I., Hutton, E.W.H., Hannon, M.T., Brakenridge, G.R., Day, J., Vörösmarty, C., Saito. Y., Giosan, L., Nicholls, R.J., 2009. Sinking deltas due to human activities. Nature Geoscience, v. 2, 681–686.

Syvitski, J.P.M., Kettner, A.J., Overeem, I., Giosan, L., Brakenridge, G.R., Hannon, M., Bilham, R., 2014. Anthropocene metamorphosis of the Indus Delta and lower floodplain, Anthropocene, v. 3, 24–35.

Syvitski, J.P.M., Saito, Y., 2007. Morphodynamics of deltas under the influence of Humans. Global and Planetary Changes, v. 57, 261–182.

Tessler, Z.D., Vörösmarty, C.J., Grossberg, M., Gladkova, I. Aizenman, H., Syvitski, J.P.M., Foufoula-Georgiou, E., 2015. Profiling risk and sustainability in coastal deltas of the world, Science, v. 349 (6248), 638–643.

Thomas, E.R., Hosking, J.S., Tuckwell, R.R., Warren, R.A., and Ludlow, E.C., 2015. Twentieth century increase in snowfall in coastal West Antarctica, Geophysical Research Letters, v. 42, 9387–9393. doi:10.1002/2015GL065750.

Thuens, S., Blodau, C., Radke, M., 2013. How suitable are peat cores to study historical deposition of PAHs? Science of the Total Environment, v. 450-451, 271–279.

Tierney, J.E., Abram, N.J., Anchukaitis, K.J., Evans, M.N., Giry, C., Kilbourne, J.H., Saenger, C.P., Wu, H.C., Zinke, J., 2015. Tropical sea surface temperatures for the past four centuries reconstructed from coral archives. Paleoceanography, v. 30, 226–252.

Treydte, K., Frank, D., Esper, J., Andreu, L., Bednarz, Z., Berninger, F., Boettger, T., D'Alessandro, C.M., Etien, N., Filot, M., Grabner, M., Guillemin, M.T., Gutierrez, E., Haupt, M., Helle, G., Hilasvuori, E., Jungner, H., Kalela-Brundin, M., Krapiec, M., Leuenberger, M., Loader, N.J., Masson-Delmotte, V., Pazdur, A., Pawelczyk, S., Pierre, M., Planells, O., Pukiene, R., Reynolds-Henne, C.E., Rinne, K.T., Saracino, A., Saurer, M., Sonninen, E., Stievenard, M., Switsur, V.R., Szczepanek, M., Szychowska-Krapiec, E., Todaro, L., Waterhouse, J.S., Weigl, M., Schleser, G.H., 2007. Signal strength and climate calibration of a European tree-ring isotope network. Geophysical Research Letters, v. 34, L24302. doi:10.1029/2007GL031106.

ACCEPTED MANUSCRIPT

Treydte, K.S., Frank, D.C., Saurer, M., Helle, G., Schleser, G.H., Esper, J., 2009. Impact of climate and CO_2 on a millennium-long tree-ring carbon isotope record. Geochim. Cosmochim. Acta, v. 73, 4635–4647.

Tyson, R.V., Pearson, T.H., 1991, Modern and ancient continental shelf anoxia: an overview *in* Tyson, R.V., and Pearson, T.H. (eds.) Modern and Ancient Continental ShelfAnoxia, Geological Society Special Publication, v. 58, 1–24.

UNEP, 2007. Global glacier changes: facts and figures. World Glacier Monitoring Service, pp.88.

UNSCEAR (United Nations Scientific Committee on the Effects of Atomic Radiation) (2000) Sources and Effects of Ionizing Radiation, 2000 Report, Volume 1. New York: United Nations. Available at: http://www.unscear.org/unscear/en/publications/2000_1.html

Vane, C.H., Chenery, S.R., Harrison, I., Kim, A.W. Moss-Hayes, V., Jones, D.G., 2011. Chemical signatures of the Anthropocene in the Clyde estuary, UK: sediment-hosted Pb, $^{207/206}$Pb, total petroleum hydrocarbon, polyaromatic hydrocarbon and polychlorinated biphenyl pollution records, Philosophical Transactions of the Royal Society A, v. 369, 1085–1111.

Vanneste, H., Vleeschouwer, F. De, Martínez-Cortizas, A., von Scheffer, C., Piotrowska, N., Coronato, A., Le Roux, G., 2015. Late-glacial elevated dust deposition linked to westerly wind shifts in southern South America. Scientific Reports, v. 5, 11670. DOI:10.1038/srep11670.

Veron, A., Novak, M., Brizova, E., Stepanova, M., 2014. Environmental imprints of climate changes and anthropogenic activities in the Ore Mountains of Bohemia (Central Europe) since 13 cal. kyr BP. The Holocene, v. 24, 919–931.

Verpoorter, C., Kutser, T., Seekell D.A., Transvik, L.J., 2014. A global inventory of lakes based on high-resolution satellite imagery, Geophysical Research Letter, v. 41, 6396–6402.

Vuorela, I., 1983. Field erosion by wind as indicated by fluctuations in the ash content of Sphagnum peat. Bulletin of the Geological Society of Finland, v. 55, 25–33.

Walker, M., Johnsen, S., Rasmussen, S.O., Popp, T., Steffensen, J.-P., Gibbard, P., Hoek, W., Lowe, J., Andrews, J., Björck, S., Cwynar, L.C., Hughen, K., Kershaw, P., Kromer, B., Litt, T., Lowe, D.J., Nakagawa, T., Newnham, R., Schwander, J., 2009. Formal definition and dating of the GSSP

ACCEPTED MANUSCRIPT

(Global Stratotype Section and Point) for the base of the Holocene using the Greenland NGRIP ice core, and selected auxiliary records, Journal of Quaternary Science, v. 24, 3–17.

Walker, M.J.C., Berkelhammer, M., Björck, S., Cwynar, L.C., Fisher, D.A., Long, A.J. Lowe, J.J., Newnham, R.M., Rasmussen, S.O., Weiss, H., 2012. Formal subdivision of the Holocene Series/Epoch: a Discussion Paper by a Working Group of INTIMATE (Integration of ice-core, marine and terrestrial records) and the Subcommission on Quaternary Stratigraphy (International Commission on Stratigraphy). Journal of Quaternary Science, V. 27, 649–659.

Walling, D.E., Fang, D., 2003. Recent trends in the suspended sediment loads of the world's rivers. Global Planetary Change, v. 39, 111–126.

Waters, C.N., Zalasiewicz, J., 2017. Concrete: the most abundant novel rock type of the Anthropocene. In: Encyclopedia of the Anthropocene, D. DellaSala (Editor). Elsevier.

Waters, C.N., Syvitski, J.P.M., Gałuszka, A. Hancock, G.J., Zalasiewicz, J., Cearreta, A., Grinevald, J., Jeandel, C., McNeill, J.R., Summerhayes, C., Barnosky, A., 2015. Can nuclear weapons fallout mark the beginning of the Anthropocene Epoch? Bulletin of the Atomic Scientists, v. 71, 46–57.

Waters, C.N., Zalasiewicz J., Summerhayes C., Barnosky, A.D., Poirier, C., Gałuszka, A., Cearreta, A., Edgeworth, M., Ellis, E.C., Ellis, M., Jeandel, C., Leinfelder, R., McNeill, J.R., Richter, D. deB., Steffen, W., Syvitski, J., Vidas, D., Wagreich, M., Williams, M., An Zhisheng, Grinevald, J., Odada, E., Oreskes, N., Wolfe, A.P., 2016. The Anthropocene is functionally and stratigraphically distinct from the Holocene, Science, v. 351, 137, http://dx.doi.org/10.1126/science.aad2622.

Watmough, S.A., 1999. Monitoring historical changes in soil and atmospheric trace metal levels by dendrochemical analysis. Environmental Pollution, v. 106, 391–403.

Wei, G., McCulloch, M.T., Mortimer, G., Deng, W., Xie, L., 2009. Evidence for ocean acidification in the Great Barrier Reef of Australia. Geochimica et Cosmochimica Acta, v. 73, 2332–2346.

Weidman, C.R., Jones, G.A., 1993. A shell-derived time history of bomb ^{14}C on Georges Bank and its Labrador Sea implications. Journal of Geophysical Research, v. 98(C8), 14577–14588.

ACCEPTED MANUSCRIPT

Wieder, R.K., Vile, M.A., Scott, K.D., Albright, C.M., McMillen, K.J., Vitt, D.H., Fenn, M.E., 2016. Differential effects of high atmospheric N and S deposition on bog plant/lichen tissue and porewater chemistry across the Athabasca oil sands region. Environmental Science & Technology, v. 50, 12630–12640.

Wilkinson, I.P., Poirier, C, Head, M.J., Sayer, C.D., Tibby, J., 2014. Microbiotic signatures of the Anthropocene in marginal marine and freshwater palaeoenvironments, *in* Waters, C.N., Zalasiewicz, J.A., Williams, M., Ellis, M.A., Snelling, A.M. eds., A Stratigraphical Basis for the Anthropocene. Geological Society, London, Special Publications, v. 395, 185–219.

Willis, K.J., Bailey, R.M., Bhagwat, S.A., Birks, H.J.B., 2010. Biodiversity baselines, thresholds and resilience: Testing predictions and assumptions using palaeoecological data. Trends in Ecology and Evolution, v. 25, 583–591.

Wilson, R. Anchukaitis, K., Briffa, K.R., Büntgen, U., Cook, E., D'Arrigo, R., Davi, N., Esper, J., Frank, D., Gunnarson, B., Hegerl, G., Helama, S., Klesse, S., Krusic, P.J., Linderholm, H.W., Myglan, V., Osborn, T.J., Rydval, M., Zorita., E., 2016. Last millennium northern hemisphere summer temperatures from tree rings: Part I: The long term context. Quaternary Science Reviews, v.134, 1–18.

Wolfe, A.P., Hobbs, W.O., Birks, H.H., Briner, J.P., Holmgren, S.U., Ingólfsson, Ó., Kaushal, S.S., Miller, G.H., Pagani, M., Saros, J.E., Vinebrooke, R.D., 2013. Stratigraphic expressions of the Holocene–Anthropocene transition revealed in sediments from remote lakes. Earth Science Reviews, v. 116, 17–34.

Wolff, E.W., 2013. Ice sheets and nitrogen. Philosophical Transactions of the Royal Society B, v. 368, 20130127. http://dx.doi.org/10.1098/rstb.2013.0127.

Wolff, E.W., 2014. Ice Sheets and the Anthropocene, *in* Waters, C.N., Zalasiewicz, J.A., Williams, M., Ellis, M.A., and Snelling, A.M. eds., A Stratigraphical Basis for the Anthropocene. Geological Society, London, Special Publications, v. 395, 255–263.

Wolff, E.W., Suttie, E.D. 1994. Antarctic snow record of southern hemisphere lead pollution. Geophysical Research Letters, v. 21, 781–784.

ACCEPTED MANUSCRIPT

Wolff, E.W., Suttie, E.D., Peel, D.A. 1999. Antarctic snow record of cadmium, copper, and zinc content during the twentieth century. Atmospheric Environment, v. 33, 1535–1541.

Wynn, P.M., Fairchild, I.J. Frisia, S., Spötl, C., Baker, A., Borsato., A., 2010. High-resolution sulphur isotope analysis of speleothem carbonate by secondary ionisation mass spectrometry. Chemical Geology, v. 271, 101–107.

Wynn, P.M., Loader, N.J., Fairchild, I.J., 2014. Interrogating trees for isotopic archives of atmospheric sulphur deposition and comparison to speleothem records. Environmental Pollution, v. 187, 98–105.

Xu, B.Q., Cao, J., Hansen, J, Yao, T., Joswia, D.R., Wang, N., Wu, G., Wang, M., Zhao, H., Yang, W., Liu, X, He, J., 2009. Black soot and the survival of Tibetan glaciers, Proceedings of the National Academy of Sciences (U.S.A.), v. 106(52), 22,114–22,118.

Yang, C., Rose, N.L., Turner, S.D., Yang, H., Goldsmith, B., Losada, S., Barber, J.L., Harrad, S.., 2016. Hexabromocyclododecanes, polybrominated diphenyl ethers, and polychlorinated biphenyls in radiometrically dated sediment cores from English lakes, ~ 1950–present. Science of the Total Environment, v. 541, 721–728.

Yang, H., Smyntek, P.M., 2014. Use of the mercury record in Red Tarn sediments to reveal air pollution history and the implications of catchment erosion. Environmental Science: Processes and Impacts, v. 16, 2554–2563.

Yang, H., Rose, N.L., Boyle, J.F., Battarbee, R.W., 2001. Storage and distribution of trace metals and spheroidal carbonaceous particles (SCPs) from atmospheric deposition in the catchment peats of Lochnagar, Scotland. Environmental Pollution, v. 115(2), 231–238.

Yang, H., Rose, N.L., Battarbee, R.W., Boyle, J.F., 2002a. Mercury and lead budgets for Lochnagar, a Scottish mountain lake and its catchment. Environmental Science & Technology, v. 36(7), 1383–1388.

Yang, H., Rose, N.L., Battarbee, R.W., 2002b. Distribution of some trace metals in Lochnagar, a Scottish mountain lake ecosystem and its catchment. Science of the Total Environment, v. 285, 197–208.

ACCEPTED MANUSCRIPT

Yang, H., Engstrom, D.R., Rose, N.L., 2010. Recent changes in atmospheric mercury deposition recorded in the sediments of remote equatorial lakes in the Rwenzori Mountains, Uganda. Environmental Science & Technology, v. 44, 6570–6575.

Young, G.H.F., Demmler, J.C., Gunnarson, B.E., Kirchhefer, A.J., Loader, N.J., McCarroll, D., 2011. Age trends in tree-ring growth and isotopic archives: A case study of *Pinus sylvestris L.* from northwestern Norway. Global Biogeochemical Cycles, v. 25, GB2020. doi:10.1029/2010GB003913.

Yu, Z., Loisel, J., Brosseau, D.P., Beilman, D.W., 2010. Global peatland dynamics since the Last Glacial Maximum. Geophysical Research Letters, v. 37, L13402. doi:10.1029/2010GL043584.

Zaccone C., Cocozza, C., Cheburkin, A.K., Shotyk, W., Miano, T.M., 2007. Enrichment and depletion of major and trace elements, and radionuclides in ombrotrophic raw peat and corresponding humic acids. Geoderma, v. 141, 235–246.

Zalasiewicz, J., Williams, M., Waters, C.N., Barnosky, A.D., Haff, P., 2014a. The technofossil record of humans, Anthropocene Review, v. 1, 34–43.

Zalasiewicz, J., Waters, C.N., Williams, M., 2014b. Human bioturbation, and the subterranean landscape of the Anthropocene. Anthropocene, v. 6, 3–9.

Zalasiewicz, J., Williams, M., Waters, C.N., 2014c. Can an Anthropocene Series be defined and recognized? *In:* Waters, C.N., Zalasiewicz, J.A., Williams, M, Ellis, M.A., and Snelling, A.M. (eds.) A stratigraphical basis for the Anthropocene. Geological Society, London, Special Publication, v. 395, 39–54.

Zalasiewicz, J., Waters, C.N., Barnosky, A.D., Cearreta, A., Edgeworth, M., Ellis, E.C., Gałuszka, A., Gibbard, P.L., Grinevald, J., Hajdas, I., Ivar do Sul, J.A., Jeandel, C., Leinfelder, R., McNeill, J.R., Poirier, C., Revkin, A., Richter, D. deB., Steffen, W., Summerhayes, C., Syvitski, J.P.M., Vidas, D., Wagreich, M., Williams, M., Wolfe, A.P., 2015. Colonization of the Americas, 'Little Ice Age' climate, and bomb-produced carbon: Their role in defining the Anthropocene. The Anthropocene Review, v. 2, 117–127.

ACCEPTED MANUSCRIPT

Zalasiewicz, J. Waters, C.N., Ivar do Sul, J., Corcoran, P.L., Barnosky, A.D., Cearreta, A., Edgeworth, M., Galuszka, A., Jeandel, C., Leinfelder, R., McNeill, J.R., Steffen, W., Summerhayes, C., Wagreich, M., Williams, M., Wolfe, A.P., Yonan, Y., 2016a. The geological cycle of plastics and their use as a stratigraphic indicator of the Anthropocene, Anthropocene, v. 13, 4–17.

Zalasiewicz, J., Waters, C.N., Wolfe, A.P., Barnosky, A.D., Cearreta, A., Edgeworth, M., Ellis, E.C., Fairchild, I.J., Gradstein, F.M., Grinevald, J., Haff, P., Head, M.J., Ivar do Sul, J.A., Jeandel, C., Leinfelder, R., McNeill, J.R., Oreskes, N., Poirier, C., Revkin, A., Richter, D. deB., Steffen, W., Summerhayes, C., Syvitski, J.P.M., Vidas, D., Wagreich, M., Wing, S., Williams, M., 2017a. Making the case for a formal Anthropocene Epoch: an analysis of ongoing critiques. Newsletters on Stratigraphy, v. 50, 205–226.

Zalasiewicz, J., Williams, M., Waters, C., Barnosky, T., Palmesino, J., Rönnskog, A.-S., Edgeworth, M., Neal, C., Cearreta, A., Ellis, E.C., Grinevald, J., Haff, P., Ivar do Sul, J., Jeandel, C., Leinfelder, R., McNeill, J.R., Odada, E., Oreskes, N., Price, S.J., Revkin, A., Steffen, W., Summerhayes, C., Vidas, D., Wing, S., Wolfe, A.P., 2017b. Scale and diversity of the physical technosphere: a geological perspective, The Anthropocene Review, v. 4, 9–22.

Zalasiewicz, J., Waters, C.N., Summerhayes, C., Wolfe, A.P., Barnosky, A.D., Cearreta, A., Crutzen, P., Ellis, E.C., Fairchild, I.J., Gałuszka, A., Haff, P., Hajdas, I., Head, M.J., Ivar do Sul, J., Jeandel, C., Leinfelder, R., McNeill, J.R., Neal, C., Odada, E., Oreskes, N., Steffen, W., Syvitski, J.P.M., Wagreich, M., Williams, M., 2017c. The Working Group on the 'Anthropocene': Summary of evidence and recommendations 2016. Anthropocene, v.19, 55–60.

Zhang, Y., Shotyk, W., Zaccone, C., Noernberg, T., Pelletier, R., Bicalho, B., Froese, D.G., Davies, L., Martin, J.W., 2016. Airborne petcoke dust is amajor source of polycyclic aromatic hydrocarbons in the Athabasca oil sands region. Environmental Science & Technology, v. 50, 1711–1720.

Zhao, H, Xu, B, Yao, T, Tian, L, Li, Z., 2011. Records of sulfate and nitrate in an ice core from Mount Muztagata, central Asia. Journal of Geophysical Research, v. 116, D13304. doi:10.1029/2011jd015735

ACCEPTED MANUSCRIPT

Zinke, J., Reuning, L., Pfeiffer, M., Wassenburg. J.A., Hardman, E., Jhangeer-Khan, R., Davies, G.R., Ng, C.K.G., Kroon, D., 2016. A sea surface temperature reconstruction for the southern Indian Ocean trade wind belt from corals in Rodrigues Island (19◦ S, 63◦ E), Biogeosciences, v. 13, 5827–5847.

Zolitschka, B., Francus, P., Ojala, A.E.K., Schimmelmann, A., 2015. Varves in lake sediments – a review. Quat. Sci. Rev., v. 117, 1–41.

Zoltai, S.C., 1989. Late Quarternary volcanic ash in the peatlands of central Alberta. Canadian Journal of Earth Sciences, v.26, 207–214.

ACCEPTED MANUSCRIPT